



Novel Miniature Microwave Quasi-Elliptical Function Bandpass Filters with Wideband Harmonic Suppression

Muhammad Riaz

BSc (EE), BSc (ECE), MSc (TACNE)

A thesis submitted in partial fulfilment
of the requirements of London Metropolitan University
for the degree of Doctor of Philosophy

Centre for Communications Technology & Mathematics
School of Computing & Digital Media

© London Metropolitan University
September 2017

Abstract

Filters are integral components in all wireless communication systems, and their function is to permit predefined band of frequencies into the system and reject all other signals. The ever-growing demand in the use of the radio frequency (RF) spectrum for new applications has resulted in the need for high performance microwave filters with strict requirements on both in-band and out-of-band characteristics. High selectivity, high rejection, low loss and extremely wide spurious-free performance are required for both transmitter and receiver channels. In addition, these devices need to be highly compact, easy to integrate within transceivers and should be amenable to low cost manufacturing. High selectivity is essential to enable the guard band between adjacent channels to be reduced thus improving the efficiency of the RF spectrum and hence increasing the capacity of the system. A low insertion-loss, high return-loss and small group-delay in the passband are necessary to minimize signal degradation. A wide stopband is necessary to suppress spurious passbands outside the filter's bandwidth that may allow spurious emissions from modulation process (harmonic, parasitic, intermodulation and frequency conversion products) and interfere with other systems. The EMC Directive 89/336/EEC mandates that all electronic equipment must comply with the applicable EN specification for EMI

This thesis presents the research work that has resulted in the development of innovative and compact microstrip bandpass filters that fulfil the above stringent requirements for wireless communication systems. In fact, the proposed highly compact planar microstrip filters provide an alternative solution for existing and next generation of wireless communications systems. In particular, the proposed filters exhibit a low-loss and quasi-elliptic function response that is normally only possible with filter designs using waveguides and high temperature superconductors. The selectivity of the filters has been improved by inserting a pair of transmission zeros between the passband edges, and implementing notched rejection bands in the filter's frequency response to widen its stopband performance. The filter structures have been analysed theoretically and modelled by using Keysight Technologies' Advanced Design System (ADS™) and Momentum® software.

The dissertation is essentially composed of four main sections. In the first section, several compact and quasi-elliptic function bandpass filter structures are proposed and theoretically analysed. Selectivity and stopband performance of these filters is enhanced by loading the input and output feed-lines with inductive stubs that introduce transmission zeros at specified frequencies in the filter's frequency response. This technique is shown to provide a sharp 3-dB roll-off and steep selectivity skirt with high out-of-band rejection over a wide

frequency span. In addition, the 3-dB fractional bandwidth of the filters is shown to be controllable by manipulating the filter's geometric parameters.

Traditional microwave bandpass filters are designed using quarter-wavelength distributed transmission-line resonators that are either end-coupled or side-coupled. The sharpness of the filter response is determined by the number of resonators employed which degrades the filter's passband loss performance. This results in a filter with a significantly larger footprint which precludes miniaturization. To circumvent these drawbacks the second section describes the development of a novel and compact wideband bandpass filter with the desired characteristics. The quasi-elliptic function filter comprises open-loop resonators that are coupled to each other using a stub loaded resonator. The proposed filter is shown to achieve a wideband 3-dB fractional bandwidth of 23% with much better loss performance, sharp skirt selectivity and very wide rejection bandwidth.

The third section describes the investigation of novel ultra-wideband (UWB) microstrip bandpass filter designs. Parametric study enabled the optimization of the filter's performance which was verified through practical measurements. The proposed filters meet the stringent characteristics required by modern communications systems, i.e. the filters are highly compact and miniature even when fabricated on a low dielectric constant substrate, possess a sharp quasi-elliptic function bandpass response with low passband insertion-loss, and ultra-wide stopband performance.

With the rapid development of multi-band operation in modern and next generation wireless communication systems, there is a great demand for single frequency discriminating devices that can operate over multiple frequency bands to facilitate miniaturization. These multi-band bandpass filters need to be physically small, have low insertion-loss, high return-loss, and excellent selectivity. In the fourth section two miniature microstrip dual-band and triple-band bandpass filter designs are explored. A detailed parametric study was conducted to fully understand how the geometric parameters of the filters affected their performance. The optimized filters were fabricated and measured to validate their performance.

Acknowledgements

First, I would like to thank Almighty Allah for his countless blessings upon me. It's a great pleasure to acknowledge my sincere and deepest gratitude to my respected supervisor, Professor Bal Virdee for his much-needed kind guidance and support to keep me motivated in an academic and personal capacity throughout my doctoral work. He always spared his busy time generously for me whenever I needed him for discussion and his kind advice. I would also like to thank my second supervisor Professor Hassan Kazemian for his valuable support and assistance throughout my research work. I would like to convey my appreciation and thanks to Dr Saeed Taghizadeh for his much-needed help on several occasions for PCB fabrication.

Finely, I would like to dedicate my work to my wife and children for their unconditional and continuous support, help, sacrifice and patience. I sincerely appreciate my brothers and sisters for their continuous support and help during my studies.

Author's Declaration

I declare that all the material contained in this thesis is my own work.

Table of Contents

I.	Introduction	
1.0	Background	1
1.1	Research Objectives	2
1.2	Research Methodology	3
1.3	Thesis Structure	4
1.4	References	5
II.	Overview on Microwave Filters	
2.0	Microwave Filters for Radio Communications	6
2.1	References	9
III.	Compact and Miniaturized Wideband Bandpass Filters	
3.0	Introduction	12
3.1	Theoretical Analysis of Stub Notch Filter	13
3.2	ABCD Matrix Model of the Notch Filter	15
3.3	Coupled Double Open-Loop Ring Resonator Bandpass Filter	17
3.4	Selectivity and Stopband Performance Enhancement	20
3.5	Ring Resonator Bandpass Filter with Interdigital Coupled Feed-line	25
3.6	Summary	36
3.7	References	36
IV.	Compact Microstrip Bandpass Filter with Wideband Spurious Suppression	
4.0	Introduction	37
4.1	Transmission-line Coupling Schemes	37
4.1.1	Electric Coupling	38
4.1.2	Magnetic Coupling	40
4.1.3	Mixed Coupling	42
4.2	Electrically coupled Bandpass Filter Structure	44

4.3	Wideband Bandpass Filter with Coupled Feed-line Sections	60
4.4	Summary	72
4.5	References	72
V.	Compact Wide Stopband Bandpass Filter Using Stub Loaded Half-Wavelength Resonators	
5.0	Introduction	74
5.1	Even and Odd Mode Analysis of Stub Loaded Resonator	74
5.1.1	Even Mode Analysis	74
5.1.2	Odd Mode Analysis	79
5.2	Wideband Filter Structure	80
5.3	Summary	94
5.4	References	94
VI.	Design of Miniaturized UWB Bandpass Filter for Sharp Rejection Skirts and very wide Stopband Performance	
6.0	Introduction	95
6.1	Proposed Multiple Mode Resonator Design	98
6.1.1	Parameter Analysis and Measured Results	102
6.1.2	Simulation Results and Discussion	104
6.2	Wideband BPF Design	112
6.2.1	Simulation Results and Discussion	114
6.3	Summary	121
6.4	References	122
VII.	Design of Novel Dual and Triple Band Filters Based on Stub Loaded Resonators	
7.0	Introduction	123
7.1	Analysis of Stub Loaded Resonators	126
7.1.1	Dual Bandpass Filter Design	128
7.1.2	Simulation Results and Discussion	130
7.2	Design of Triple-Band Bandpass Filter	143

7.2.1	Simulation Results and Discussion	146
7.3	Summary	164
7.4	References	165
VIII.	Conclusion and Future Work	
8.0	Conclusion	166
8.1	Future Work	168
8.2	Papers produced on the Research work	170

List of Figures

Figure 2.1	Block diagram of a communication payload of a typical satellite	7
Figure 2.2	Simplified block diagram of RF front-end of cellular base-station	7
Figure 3.1	Graph of Cut-off frequency (3-dB)	13
Figure 3.2	Single stub notch filter	14
Figure 3.3	ABCD matrix representation of the single stub notch filter	16
Figure 3.4	Configuration of the filter using two hairpin resonators with asymmetric tapping feed-lines	17
Figure 3.5	Compact version of the filter using two open-loop ring resonators with asymmetric tapping feed lines	20
Figure 3.6	Proposed bandpass filter with multiple transmission zeros	21
Figure 3.7	Transmission and reflection-coefficient response of the proposed filter without spiral feed line	22
Figure 3.8	Transmission and reflection-coefficient response of the proposed filter with spiral loaded feed line	23
Figure 3.9	Effect of resonator separation on the transmission zeros, centre frequency and loss performance as a function of resonator separation	23
Figure 3.10	Frequency response of the proposed filter as a function of inter-resonator coupling gap	24
Figure 3.11	Frequency response of proposed filter as a function of resonator width	25
Figure 3.12	Effect of resonator separation on the transmission zeros, centre frequency and loss performance as a function of resonator width	25
Figure 3.13	Configuration of filter with two interdigital coupled feed-line	26
Figure 3.14	Transmission and reflection-coefficient response of the interdigital coupled feed-line BPF	26
Figure 3.15	Group delay response of the proposed bandpass filter	27
Figure 3.16	Wide band frequency response of the proposed highly selective and very wide stopband bandpass filter	27

Figure 3.17	(a) Configuration of the filter with three finger interdigital coupled feed-line, and (b) photograph of the filter.	28
Figure 3.18	S-parameter simulation response of the proposed filter	28
Figure 3.19	Measured response (a) (narrow band view) (b) (wideband view).	29
Figure 3.20	Frequency response of the filter as a function of length L_{b3}	30
Figure 3.21	Frequency response of the filter as a function of resonator length l_4	30
Figure 3.22	Frequency response of the filter as a function of resonators length l_2 and l_3 , where the lower transmission zero is controlled by l_3 and the upper zero by l_2	31
Figure 3.23	Effect on filter's insertion loss as a function of coupled feed-line length	32
Figure 3.24	Effect on the filter's out-of-band rejection and loss performance as a function of coupled feed-line length	32
Figure 3.25	Frequency response of filter as a function of coupled feed-line length L_{b3}	33
Figure 3.26	Effect on filter's insertion loss as a function of coupled feed-line width	33
Figure 3.27	Effect on the filter's out-of-band rejection as a function of the coupled feed-line width	34
Figure 3.28	Frequency response of filter as a function of coupled feed-line width	34
Figure 3.29	Frequency response of the optimized filter	35
Figure 3.30	Frequency response of the narrowest 3-dB fractional bandwidth	35
Figure 4.1	Transmission-line coupling configuration schemes, (a) electric coupling, (b) magnetic coupling, and (c) mixed coupling	38
Figure 4.2	(a) Equivalent lumped element model of electrical coupling, and (b) simplified equivalent circuit	40
Figure 4.3	(a) Equivalent lumped element model of magnetic coupling, and (b) simplified equivalent circuit	41
Figure 4.4	(a) Network representation of coupled resonator with mixed coupling, and (b) simplified equivalent circuit	43
Figure 4.5	(a) Layout of proposed bandpass filter with loaded inductive lines, and (b) Photograph of the implemented filter.	45

Figure 4.6	Simulated S-parameter response of the proposed bandpass filter (a) without spirals (b) with spirals	45
Figure 4.7	Measured performance (a) (narrowband view) (b) (wideband view)	46
Figure 4.8	Effect of inter-resonator coupling gap on the centre frequency and loss performance of the filter.	47
Figure 4.9	Effect of the inter-resonator coupling gap on the out-of-band rejection level of the filter.	47
Figure 4.10	Frequency response of the proposed filter as a function of inter-resonator coupling gap	47
Figure 4.11	Effect of coupling length on the filter's passband transmission zeros, centre frequency, and insertion-loss	48
Figure 4.12	Effect of coupling length on the out-of-band rejection level	49
Figure 4.13	Frequency response of the proposed filter as a function of coupled resonator length	50
Figure 4.14	Effect of spiral stub location (L_{x2}) on the passband transmission zeros, centre frequency and loss performance	51
Figure 4.15	Effect of spiral stub location (L_{x2}) on the out-of-band rejection	51
Figure 4.16	Frequency response of the proposed filter as a function of spiral stub location (L_{x2})	52
Figure 4.17	Effect of the inter-spiral loading gap (L_{y2}) on the passband transmission zeros, centre frequency and loss performance	52
Figure 4.18	Effect of feed line length on band rejection level as a function of (L_{y2})	53
Figure 4.19	Frequency response of proposed filter as a function of inter-spiral gap	53
Figure 4.20	Effect of coupled resonator width on passband transmission zeros, centre frequency, and loss performance	54
Figure 4.21	Frequency response of the proposed filter as a function of coupled resonator width (W_b)	54
Figure 4.22	Frequency response of the proposed filter as a function of coupling space between spirals shaped inductive lines (S_2)	55
Figure 4.23	Effect of coupling space between spirals shaped inductive lines on passband transmission zeros	56
Figure 4.24	Effect of resonator length (l_d) on passband transmission zeros	56

Figure 4.25	Effect of coupled resonator length on passband transmission zeros and centre frequency.	57
Figure 4.26	Effect of resonator length (l_1) on passband transmission zeros and centre frequency	58
Figure 4.27	Effect of coupled resonator length (l_1) on passband transmission zeros, centre frequency	58
Figure 4.28	Effect of resonator length (l_2) on passband transmission zero	59
Figure 4.29	Effect of coupled resonator length on passband transmission zero	59
Figure 4.30	Configuration of the interdigital coupled feed-line microwave bandpass filter	61
Figure 4.31	Transmission and reflection-coefficient response of the proposed filter	61
Figure 4.32	Photograph and configuration of the three finger interdigital coupled feed-line bandpass filter	62
Figure 4.33	(a) Simulated S-parameter response of the proposed filter without stub loaded resonators, (b) simulated S-parameter response with stub loaded resonators	63
Figure 4.34	(a) Measured S-parameter response (narrowband view), and (b) measured S-parameter response (wideband performance)	64
Figure 4.35	Effect of open stub length on the filter's transmission zeros, centre frequency, and insertion-loss performance	65
Figure 4.36	Frequency response of the filter in Fig. 4.31 as a function of open stub length	65
Figure 4.37	Frequency response of the filter in Fig. 4.32 as a function of interdigital feed-line coupling gap	66
Figure 4.38	Effect on centre frequency and loss by interdigital feed-line coupling gap	66
Figure 4.39	Effect on out-of-band rejection level as a function of interdigital feed-line coupling gap	67
Figure 4.40	Frequency response of the filter as a function of resonator coupling gap (S_4)	68
Figure 4.41	Frequency response of the filter as a function of interdigital feed-line coupling length	68
Figure 4.42	Transmission and reflection-coefficient response of the optimized filter	69
Figure 4.43	Transmission and reflection-coefficient response of the narrowest 3-dB fractional bandwidth	69

Figure 4.44	Frequency response of the filter as a function of resonator length (l_6)	70
Figure 4.45	Effect on transmission zeros as a function of resonator length (l_6)	70
Figure 4.46	Frequency response of the filter as a function of resonator length (l_5)	71
Figure 4.47	Effect on transmission zeros as a function of resonator length (l_5)	71
Figure 5.1	(a) Structure of the stub-loaded resonator, (b) even-mode equivalent circuit, and (c) odd-mode equivalent circuit model	75
Figure 5.2	Normalized resonator length against microstrip-line length (in degrees) as a function of impedance ratio	76
Figure 5.3	Normalized length as a function of impedance ratio	78
Figure 5.4	Ratio of lowest spurious frequencies $f_{SA} (\lambda_g/4)$ and $f_{SB} (\lambda_g/2)$ to fundamental frequency (f_0)	79
Figure 5.5	Odd-mode equivalent circuit model	80
Figure 5.6	(a) Configuration of the three finger interdigital coupled feed-line bandpass filter using stub loading resonator, and (b) photograph of the filter	81
Figure 5.7	Simulated frequency response of the stub loaded resonator filter	81
Figure 5.8	Measured response of stub loaded resonator filter	82
Figure 5.9	Wide stopband performance of the stub loaded resonator filter with -20 dB attenuation	82
Figure 5.10	Group-delay response of the stub loaded resonator filter	83
Figure 5.11	Frequency response of the filter as a function of low impedance section length L_{b2}	83
Figure 5.12	Effect of low impedance section length L_{b2} on insertion-loss performance	84
Figure 5.13	Effect of low impedance section length L_{b2} on out-of-band rejection level	84
Figure 5.14	Frequency response of the proposed filter as a function of inter-resonator coupling gap.	85
Figure 5.15	Frequency response of filter as a function of resonator separation L_6	85

Figure 5.16	Effect of resonator separation L_6 on the centre frequency, loss performance and transmission zeros	86
Figure 5.17	Effect of resonator coupling length (L_5) on the centre frequency and transmission zeros	87
Figure 5.18	Frequency response of the proposed filter as a function of resonator coupling length (L_5)	87
Figure 5.19	Frequency response of the proposed filter as a function of feed-line coupling gap (S_3)	88
Figure 5.20	Frequency response of the proposed filter as a function of the open stub length (L_a)	89
Figure 5.21	Effect of open stub length (L_a) on (a) lower transmission zero (b) lower out of band rejection level	89
Figure 5.22	Frequency response of the proposed filter as a function of the open stub length (L_{a1})	90
Figure 5.23	Effect of open stub length (L_{a1}) on (a) upper transmission zero (b) upper out of band rejection level.	91
Figure 5.24	Frequency response of the proposed filter as a function of length (L_{b3})	92
Figure 5.25	Effect of length (L_{b3}) on out of band rejection levels	92
Figure 5.26	Frequency response of the proposed filter as a function of coupled length	93
Figure 5.27	Frequency response of the proposed filter as a function of width (W_{a1})	94
Figure 6.1	Simulated insertion-loss response of UWB filter proposed in reference	96
Figure 6.2	Measured and simulated S-parameter and group delay response of UWB filter proposed in reference	97
Figure 6.3	Simulated and measured frequency responses of proposed UWB bandpass filter [6]	97
Figure 6.4	Structure of the proposed UWB quasi-elliptical bandpass filter.	98
Figure 6.5	Configuration of basic MMR structure. Parallel open-circuit stubs are indicated in dotted lines.	99
Figure 6.6	Equivalent circuit model of the MMR structure, (a) even-mode circuit, and (b) odd-mode circuit model.	99
Figure 6.7	Normalized frequency of resonance modes as a function of impedance ratio	101

Figure 6.8	Separation of the resonance mode frequencies as a function of impedance ratio.	102
Figure 6.9	Photograph of the proposed fabricated UWB BPF	103
Figure 6.10	Simulated and measured insertion-loss and return-loss response of the UWB BPF, (a) close-up view, and (b) wideband view.	103
Figure 6.11	Group-delay response of UWB BPF	104
Figure 6.12	Frequency response of the filter as a function of resonator width.	105
Figure 6.13	Effect on the filter's upper transmission zero, first odd resonant frequency as a function of resonator width.	105
Figure 6.14	Frequency response of filter as a function of stub loaded resonator width	106
Figure 6.15	Effect on the filter's lower and upper transmission zeros and third even resonant frequency as a function of stub loaded resonator width	106
Figure 6.16	Frequency response of the filter as a function of stub loaded resonator length	107
Figure 6.17	Effect on the filter's lower and upper transmission zeros and first and third resonant frequencies as a function of stub loaded resonator length	107
Figure 6.18	Frequency response of the filter as a function of horizontal resonator length.	108
Figure 6.19	Effect on the filter's second odd and third even resonant frequencies as a function of resonator length	109
Figure 6.20	Frequency response of the filter as a function of interdigital feed-line coupling length	110
Figure 6.21	Effect on the filter's first and second odd and second even resonant frequencies as a function of interdigital feed-line coupling length	110
Figure 6.22	Frequency response of the filter as a function of resonator length (L_4)	111
Figure 6.23	Effect on the resonant frequency f_{odd2} as a function of resonator length (L_4)	111
Figure 6.24	(a) Configuration of the three finger interdigital coupled feed-line wideband bandpass filter, and (b) photograph of the fabricated filter	112

Figure 6.25	Simulated and measured results of the wideband bandpass filter	113
Figure 6.26	Frequency response of UWBF under weak coupling	114
Figure 6.27	Group-delay response of the wideband Bandpass Filter	114
Figure 6.28	Frequency response of the filter as a function of resonator length (L_7)	115
Figure 6.29	Effect on the filter's transmission zeros and resonant frequencies as a function of resonator length (L_7)	115
Figure 6.30	Frequency response of the filter as a function of interdigital feed-line coupling length (L_2)	116
Figure 6.31	Effect on the filter's resonant frequencies as a function of interdigital feed-line coupling length	116
Figure 6.32	Frequency response of filter as a function of resonator separation (L_4)	117
Figure 6.33	Effect of resonator separation (L_4) on resonant frequencies and transmission zeros.	118
Figure 6.34	Frequency response of proposed filter as a function of coupled length (L_6)	119
Figure 6.35	Effect of (L_6) on resonant frequencies and transmission zeros.	119
Figure 6.36	Frequency response of the proposed filter as a function of length (L_5)	120
Figure 6.37	Effect of length (L_5) on resonant frequencies and transmission zero.	120
Figure 6.38	Frequency response of the proposed filter as a function of open stub length (L_a)	121
Figure 7.1	Simulated and measured results of fabricated dual and tri-BPF. The inset is the photographs of fabricated dual and tri-BPF	124
Figure 7.2	Simulated and measured results of Filter	125
Figure 7.3	(a) Configuration of the dual-band bandpass filter using stub loaded resonator, and (b) structure of the stub-loaded resonator	126

Figure 7.4	(a) Solution of resonance frequency ratio of higher order modes relative to the fundamental frequency as a function of θ_1 and k for a stub length of 120° , and (b) Resonance frequency and k for a stub length of 120° , and (b) Resonance frequency ratio as a function of θ_1 ratio as a function of for different stub lengths.	128
Figure 7.5	Transmission and reflection-coefficient response of the proposed dual band bandpass filter	129
Figure 7.6	Photograph three finger interdigital coupled feed-line dual band bandpass filter	129
Figure 7.7	Transmission and reflection-coefficient response of the proposed dual band bandpass filter	130
Figure 7.8	Frequency response of the filter as a function of open stub length (L_a)	131
Figure 7.9	Effect on the filter's first and second transmission zeros and second even resonant frequency as a function of open stub length (L_a)	131
Figure 7.10	Frequency response of the filter as a function of open stub length (L_{a1})	132
Figure 7.11	Effect on the filter transmission zeros, even and odd resonant frequencies as a function of open stub length (L_{a1})	133
Figure 7.12	Frequency response of the filter as a function of resonator length (L_5)	134
Figure 7.13	Effect on the filter transmission zeros and even and odd resonant frequencies as a function of resonator length (L_5)	134
Figure 7.14	Frequency response of the filter as a function of resonator length (L_8)	135
Figure 7.15	Effect on the filter transmission zeros and even and odd resonant frequencies as a function of resonator length (L_8)	135
Figure 7.16	Frequency response of the filter as a function of resonator length (L_7)	136
Figure 7.17	Effect on the filter transmission zeros and even and odd resonant frequencies as a function of resonator length (L_7)	137
Figure 7.18	Frequency response of the proposed filter as a function of coupled length (L_{b3})	137
Figure 7.19	Frequency response of the filter as a function of resonator width (W_a)	138

Figure 7.20	Effect on filter transmission zeros as a function of resonator width (W_a)	138
Figure 7.21	Frequency response of the filter as a function of resonator length (L_9)	139
Figure 7.22	Effect on the filter first even mode frequency as a function of resonator length (L_9)	140
Figure 7.23	Frequency response of the filter as a function of resonator width (W_{a2})	141
Figure 7.24	Effect on the filter first even mode frequency as a function of resonator width (W_{a2})	141
Figure 7.25	Frequency response of the filter as a function of resonator length (L_6)	142
Figure 7.26	Effect on the filter transmission zero, even and odd resonant frequencies as a function of resonator length (L_6)	143
Figure 7.27	(a) Configuration of the three finger interdigital coupled feed-line triple-band filter using stub loaded resonator, and (b) photograph of the implemented filter.	144
Figure 7.28	Transmission and reflection-coefficient response of the proposed triple-bandpass filter	145
Figure 7.29	Frequency response of the filter as a function of resonator length (L_{b3})	146
Figure 7.30	Effect on the filter return losses as a function of resonator length (L_{b3})	146
Figure 7.31	Frequency response of the filter as a function of resonator width (W_{a4})	147
Figure 7.32	Effect on the filter return losses as a function of resonator width (W_{a4})	148
Figure 7.33	Effect on the filter centre frequency and transmission zero as a function of resonator width (W_{a4})	148
Figure 7.34	Frequency response of the filter as a function of resonator length (L_a)	149
Figure 7.35	Effect on the filter return loss as a function of resonator length (L_a)	149
Figure 7.36	Effect on the filter transmission zeros and centre frequency as a function of resonator length (L_a)	150
Figure 7.37	Frequency response of the filter as a function of resonator length (L_{10})	151

Figure 7.38	Effect on the filter transmission zeros and centre frequencies as a function of resonator length (L_{10})	151
Figure 7.39	Effect on the filter return losses as a function of resonator length (L_{10})	152
Figure 7.40	Frequency response of the filter as a function of resonator length (L_5)	153
Figure 7.41	Effect on the filter transmission zeros and centre frequencies as a function of resonator length (L_5)	153
Figure 7.42	Effect on the filter return losses as a function of resonator length (L_5)	154
Figure 7.43	Frequency response of the filter as a function of resonator length (L_6)	155
Figure 7.44	Effect on the filter transmission zeros and centre frequencies as a function of resonator length (L_6)	155
Figure 7.45	Effect on the filter return losses as a function of resonator length (L_6)	156
Figure 7.46	Frequency response of the filter as a function of resonator length (L_9)	157
Figure 7.47	Effect on the filter transmission zero and centre frequency as a function of resonator length (L_9)	157
Figure 7.48	Effect on the filter return losses as a function of resonator length (L_9)	158
Figure 7.49	Frequency response of the filter as a function of resonator length (L_8)	159
Figure 7.50	Effect on the filter return loss as a function of resonator length (L_8)	159
Figure 7.51	Effect on filter resonant frequency as a function of resonator length (L_8)	160
Figure 7.52	Frequency response of the filter as a function of resonator length (L_3)	161
Figure 7.53	Effect on the filter transmission zeros and centre frequencies as a function of resonator length (L_3)	161
Figure 7.54	Effect on the filter return losses as a function of resonator length (L_3)	162
Figure 7.55	Frequency response of the filter as a function of resonator length (L_2)	163

Figure 7.56	Effect on the filter transmission zeros and centre frequencies as a function of resonator length (L_2)	163
Figure 7.57	Effect on the filter return losses as a function of resonator length (L_2)	164

List of Tables

Table 3.1	Effect of resonator separation on the transmission zeros, centre frequency and loss performance.	22
Table 3.2	Effect of resonator width on the transmission zeros, centre frequency and loss performance.	24
Table 3.3	Effect of coupled feed-line length on the characteristics of the filter.	31
Table 3.4	Effect of coupled feed-line width on the characteristics of the filter.	34
Table 4.1	Effect of inter-resonator coupling on the centre frequency, loss, out-of-band rejection level, 3-dB bandwidth and fractional bandwidth performance.	48
Table 4.2	Effect of coupling length on the passband transmission zeros, centre frequency, loss and out-of-band rejection level performance.	49
Table 4.3	The effect of the spiral load location on the passband transmission zeros, centre frequency, loss and out-of-band rejection performance	50
Table 4.4	Effect of the inter-spiral loading gap (L_{y2}) on the passband transmission zeros, centre frequency, loss and out-of-band rejection level performance	52
Table 4.5	Effect of coupled resonators width on the transmission zeros, bandpass rejection level, centre frequency and loss performance	54
Table 4.6	Effect of coupling space between spiral shaped inductive lines on transmission zeros	55
Table 4.7	Effect of resonator length (l_4) on the passband transmission zeros and centre frequency	57
Table 4.8	Effect of resonator length (l_1) on filter passband transmission zero	58
Table 4.9	Effect of resonator length (l_2) on the passband transmission zero	60
Table 4.10	Effect of open stub length on the transmission zeros, centre frequency and loss performance	65
Table 4.11	Effect of coupling space between coupled feed lines on the centre frequency, bandpass rejection level and loss performance.	67
Table 4.12	Effect of resonator length (l_6) on the passband transmission zero	70

Table 5.1	Effect of low impedance section length (L_{b2}) on the filter's centre frequency, loss performance and band rejection level.	84
Table 5.2	Effect of resonator separation length (L_6) on the transmission zeros, centre frequency and loss performance.	86
Table 5.3	Effect of resonator coupling length (L_5) on the transmission zeros and centre frequency.	87
Table 5.4	Effect of open stub length on lower transmission zero and lower out of band rejection level	90
Table 5.5	Effect of open stub length on upper transmission zero and upper out of band rejection level.	90
Table 5.6	Effect of coupled feed lines length on bandpass rejection levels	93
Table 6.1	Effect of resonator width on upper transmission zero and resonant frequency	114
Table 6.2	Effect of stub loaded resonator width on lower and upper transmission zeros and third even resonant frequency	106
Table 6.3	Effect of stub loaded resonator length on lower and upper transmission zeros and first third even resonant frequencies	108
Table 6.4	Effect of horizontal resonator length on second odd and third even resonant frequencies	109
Table 6.5	Effect of interdigital feed-line coupling length on odd and even resonant frequencies	110
Table 6.6	Effect of resonator length (L_4) on resonant mode	112
Table 6.7	Effect of resonator length (L_7) on transmission zeros and resonant frequencies.	115
Table 6.8	Effect of interdigital feed-line coupling length (L_2) on resonant frequencies.	117
Table 6.9	Effect of resonator separation length (L_4) on the transmission zeros and resonant frequencies	118
Table 6.10	Effect of resonator coupled length (L_6) on the transmission zeros and resonant frequencies.	119
Table 6.11	Effect of resonator length (L_5) on transmission zero and resonant modes.	121
Table 7.1	Effect of stub length on first and second transmission zeros and second even resonant frequency	132

Table 7.2	Effect of open stub length on second and third transmission zeros and first and second odd resonant frequencies.	133
Table 7.3	Effect of resonator length (L_5) on transmission zeros, even and odd resonant frequencies.	134
Table 7.4	Effect of resonator length (L_8) on transmission zeros, even and odd resonant frequencies	136
Table 7.5	Effect of resonator length (L_7) on transmission zeros, even and odd resonant frequencies	137
Table 7.6	Effect of resonator width (W_a) on transmission zeros.	139
Table 7.7	Effect of resonator length (L_9) on first even resonant mode.	140
Table 7.8	Effect of resonator width (W_{a2}) on first even mode frequency	141
Table 7.9	Effect of resonator length (L_6) on transmission zero, even and odd resonant frequencies	142
Table 7.10	Comparison between this work and recently published dual band BPF'S	143
Table 7.11	Effect of coupled length (L_{b3}) on return losses	147
Table 7.12	Effect of resonator width (W_{a4}) on return loss, transmission zero and centre frequency.	148
Table 7.13	Effect of resonator length (L_a) on return loss, transmission zeros and centre frequency	150
Table 7.14	Effect of resonator length (L_{10}) on return losses, transmission zeros and centre frequencies	152
Table 7.15	Effect of resonator length (L_5) on return losses, transmission zeros and centre frequencies	154
Table 7.16	Effect of resonator length (L_6) on return losses, transmission zeros and centre frequencies	156
Table 7.17	Effect of resonator length (L_9) on return losses, transmission zero and centre frequency	158
Table 7.18	Effect of resonator length (L_8) on transmission zero and centre frequency	160
Table 7.19	Effect of resonator length (L_3) on return losses, transmission zero and centre frequencies	162
Table 7.20	Effect of resonator length (L_2) on return losses, transmission zero and centre frequencies	164

List of Abbreviations

ABCD	Transfer matrix
BPF	Bandpass filter
CDMA	Code division multiple access
CQ	Cascaded quadruplet
CT	Cascaded trisection
dB	Decibel
DGS	Defected ground structure
EBG	Electromagnetic bandgap
EMC	Electromagnetic compatibility
EMI	Electromagnetic interference
FBW	Fractional bandwidth
f_{tz}	Transmission zero
GHz	Gigahertz
GSM	Global system for mobile communication
IL	Insertion-loss
kHz	Kilohertz
LTCC	Low-temperature cofired ceramic
MEMS	Microelectromechanical systems
MHz	Megahertz
MMIC	Monolithic microwave integrated circuits
RF	Radio frequency
RL	Return-loss
SIR	Stepped impedance resonator
SLR	Stub loaded resonator
TE	Transverse electric waves
TEM	Transverse electromagnetic mode
TM	Transverse magnetic waves
UWB	Ultra-wideband
WiMAX	Worldwide Interoperability for Microwave Access
WLAN	Wireless local area network

Introduction

1.0 Background

The RF/microwave filter is a component which provides frequency selectivity in wireless communications systems such as mobile and satellite communications, radar, electronic warfare, and remote sensing systems. These devices are employed to separate and combine or select and reject signals at various frequencies [1]-[5]. With the emergence of new ultra-wideband (UWB) communication systems and the development of 5G mobile technology, the demand for the frequency spectrum is getting greater. 5G is expected to support significantly faster mobile broadband speeds and increasingly extensive mobile data usage - as well as to enable the full potential of the Internet of Things. From virtual reality and autonomous cars, to the industrial internet and smart cities, 5G will be at the heart of the future of communications [6]. However, the frequency spectrum is a finite resource which is very expensive and is highly congested especially between 1-6 GHz. Hence, new and emerging wireless systems therefore impose strict requirements from microwave filters in terms of small insertion-loss, large return-loss for good impedance matching with interconnecting components, and high frequency-selectivity to prevent interference. A highly frequency-selective filter enables the guard band between each channel to be reduced which increases the system capacity, i.e. accommodate more channels. Low insertion-loss is a critical requirement in transmitter and receiver filters as it improves the transmitter's power efficiency, reduces thermal load, and enhances the receiver's noise-figure [7]. Also, small group-delay and amplitude variation of the filter in the passband are required for minimum signal degradation. In addition to that, these devices need to be accompanied with very small physical size and integration.

Another reason for the need for high performance RF/microwave filters is because power amplifiers used in transmitters are notorious in producing out-of-band intermodulation products and harmonics due to their non-linear characteristics. These spurious signals must be filtered to prevent leakage into the receiver and to satisfy regulatory requirements on out-of-band radiation. Therefore, the transmit filter must have a high level of attenuation in the received band. Furthermore, the transmit filter must have low passband insertion-loss to satisfy efficiency requirements. Similarly, receiver must be protected by the filter with high attenuation in the transmit band to isolate the high-power transmitter. This filter must have low passband insertion-loss to preserve system sensitivity. This means in applications such as cellular base-stations the filters must achieve a

remarkable performance in terms of very low-loss within the passband, high frequency-selectivity, and to reject the unwanted frequency signals near the passband [3].

RF/microwave filters are also classified by technology used for the filter realization into active and passive filters. Active filters are realized by using active elements such as transistors, diodes and amplifiers, in addition to the passive components. These filters are simple to realize, they provide gain, high quality factor, and can be easily integrated with the other system components. However, due to the active elements used in the filter, the filter requires a power supply, which may increase the complexity of the system. Moreover, the internal feedback is required, that may increase the sensitivity of the filter [8].

Passive filters are realized by using passive elements such as capacitors and inductors. This kind of filters has many advantages over active filters, they are more stable than the active filters, do not need power supply, and less expensive. In this research work the filters will be passive and will not employ any passive lumped elements, thus making the design and manufacture less complex and inexpensive.

While system complexity is on the rise, system size has continued to shrink thanks to breakthroughs such as on chip integration. This approach however proves less effective with filters operating especially in the RF or microwave frequencies mainly due to two reasons [5]. Firstly, it is incredibly difficult to realize lumped elements with sufficient accuracy especially at microwave frequencies due to parasitic effects. Integrating planar distributed filters into an IC may seem to be a solution. However, since the size of a distributed filter is directly proportional to its operating wavelength, this approach may only work on a small minority of filters, where the operating frequencies allow filters to physically fit into an IC. Secondly, the quality-factor of a distributed resonator is proportional to its physical size. Therefore, distributed filters suffer from severe losses which may easily impair system performance. Therefore, to better meet the more stringent requirements posed by modern communication systems, it is essential to develop advanced filter configurations that can be easily fabricated and integrated with other electronic systems, while keeping low loss, excellent stopband performance, high selectivity and low group-delay.

1.1 Research Objectives

The aim and objective of this research are to investigate novel resonant structure(s) that fulfil the increasing demand in satellite/mobile telecommunication systems for high performance microwave filters. In particular, the microwave bandpass filters with characteristics of narrowband / wideband / UWB should have the following salient features:

- Low insertion-loss
- High return-loss
- High frequency-selectivity
- High out-of-band isolation
- Low group-delay
- Light weight
- Low cost

1.2 Research Methodology

The current work will initially begin with a literature search of various microwave filters, methods of theoretically characterizing them, current concepts that can improve insertion-loss performance of microstrip circuits, and techniques of suppressing spurious responses while preserving the bandwidth of filter. Several novel microstrip resonant structures will then be developed and investigated. This will require analysis using advanced simulation tools such as Advance Design System (ADS™), Momentum® and CST Microwave Studio®, to determine a suitable structure(s) that have the potential to fulfil the desired characteristics. ADS™ by Agilent Technologies is a state-of-the-art computer aided engineering package that provides an environment for the simulation and design of RF and microwave circuits as well as the simulation of complete wireless communications system. It has a simple GUI and elegant data display interface to a powerful simulation engine. Momentum® is a EM solver in ADS™. It allows you to construct the filter of any geometry or shape and it uses finite element analysis using Maxwell's equations to arrive at a solution. In other words, it determines the filters transmission response (insertion-loss and return-loss) including group delay.

The analysis will also include investigation of degenerate electromagnetic modes excited within the structures. The selected planar structure(s) will then need to be theoretically modelled and analysed to determine the salient parameters that affect the resonators transmission characteristics, and will also involve techniques of optimizing these parameters to fulfil the desired filter characteristics. The novel structure(s) will then need to be fabricated on a suitable dielectric substrate medium such as 3M Cu-clad ($\epsilon_r = 2.17$, $h = 0.794$ mm, $t = 35$ μm and $\tan\delta = 0.0009$) and its performance characterized using a Vector or Scalar Network Analyzer. The theoretical model will then be critically evaluated against its measured data, and if necessary modifications made to the model in order to improve its accuracy. The final model will then form the bases for subsequent microwave microstrip filter designs. A filter design methodology specifically for the resonant structure(s) will then

be formulated that will allow the design of filters to be implemented for any given specification. This methodology will need to be evaluated and verified by practical designs. The methodology may require further modification to improve the implementation of accurate designs.

1.3 Thesis Structure

This thesis comprises of eight chapters. A brief but concise overview of recent studies in RF/microwave planar filters is presented in chapter 2. In order to enhance the selectivity and stopband performance of the microstrip filter structure proposed in Chapter 3 employs mixed coupled (electric and magnetic) open-ring resonators whose input and output feed-lines interdigitally coupled are inductively loaded with a pair of open stub in the shape of spirals. The open stubs were spiralled to keep the structure compact in size. The open stubs are used to suppress harmonics generated by the filter across a wide bandwidth above and below the passband response. It is shown the 3-dB fractional bandwidth of the filter can be controlled by modifying the gap between the two resonators.

In Chapter 4, several novel microstrip filters are investigated. This includes a highly compact bandpass filter based on electrically coupled transmission-line that comprises 50 Ω input and output feed-lines that are electromagnetically coupled to each other with high impedance parallel transmission-lines. To realize a bandpass filter with a wideband response the filter is modified so that it is interdigitally coupled to the input and output feed-lines. The out-of-band spurious responses are suppressed by loading the resonators directly with open-circuited stubs.

In Chapter 5, a compact wideband microstrip filter is described with the desired aforementioned characteristics using stub loaded half-wavelength resonators coupled to input and output resonators. The input and output feed-lines are interdigitally coupled to reduce the passband insertion-loss and to realise a wide stopband on either side of the passband response with high rejection level. The three-finger interdigital coupling is used to reduce the need for tight which is necessary to realise wideband performance.

In chapter 6, two miniaturized microstrip UWB bandpass filters are proposed. The multimode resonator in the first UWB filter consists of multiple open stubs to create even and odd modes within the passband. The even modes can be controlled by varying width and length of the central loaded stepped impedance stub which has no effect on the odd modes. The odd modes can be shifted by simply adjusting the width of the horizontal resonator and the length of the interdigitally coupled lines, which has marginal effect on even modes. The filter investigated is compact in size, it possesses a sharp quasi-elliptic

function bandpass response with low passband insertion-loss, and ultra-wide stopband performance. The second UWB BPF is proposed in second sections created from four resonant responses and two transmission zeros. Transmission zeros are located very close to the filter's upper and lower 3-dB cut-off frequencies to create a highly sharp roll-off. Analysis shows that both even and odd frequencies can be relocated within the passband tuning different physical parameters. The measured results of UWB bandpass filter show low insertion-loss and sharp rejection.

In chapter 7, two miniature microstrip dual and triple band BPF filters are proposed. A detailed parametric study of the dual band bandpass filter is provided. The study shows even and odd resonant modes, and three transmission zeros can be tuned independently adjusted to some extent without severely degrading the passband response. Also proposed is a quasi-elliptic triple-bandpass filter, where five transmission zeros are located close to the filter's passband edge to yield a sharp roll-off response and a good out-of-band rejection. Parametric study shows, the characteristics of triple band bandpass filter can be modified by tuning specific physical parameters of the filter structure. Measured results were used to verify the filters performance.

Chapter 8 summarize the research undertaken in this thesis and suggestions are given for future work.

References

1. G.L. Matthaei, L. Young, and E.M.T. Jones, "Microwave filters, impedance matching networks, and coupling structures," *Dedham, MA: Artech House*, 1964.
2. J.G. Hong, and M.J. Lancaster, "Microstrip filters for RF/microwave applications," *New York: John Wiley & Sons*, 2001.
3. I.C. Hunter, "Theory and design of microwave filters," *Institution of Electrical Engineers*, 2001.
4. R.J. Cameron, C.M. Kudsia, and R.R. Mansour, "Microwave filters for communication systems: fundamentals, design, and applications," *Hovoken, New Jersey: John Wiley & Sons*, 2007.
5. D.M. Pozar, "Microwave engineering," *MA: Addison-Wesley*, 1990.
6. 5G Spectrum – Public Policy Position, *2016 GSM Associations*.
7. J.-S. Hong, H. Shaman, and C. Young-Hoon, "Dual-mode microstrip open-loop resonators and filters," *IEEE Transactions on Microwave Theory and Techniques*, vol. 55, pp. 1764-1770, 2007.
8. W. Chen, *The circuits and filters handbook*. *CRC Press, Inc.: Artech House*, 1995.

Overview on Microwave Filters

2.0 Microwave Filters for Radio Communications

A microwave filter is a device that is designed to operate anywhere in the frequency range between 300 MHz to 300 GHz. These devices allow the transmission of wanted signals within the filter passband but suppress signals in its stopband region [1]-[4]. Microwave filters can be classified by bandpass, lowpass, and bandstop and highpass characteristics. The focus of this research is to develop novel planar bandpass filters for new and emerging applications.

Microwave filters find applications in various terrestrial and space-borne systems including cellular, radar, satellite, remote sensing and navigation. For example, Figure 2.1 shows a simplified block diagram of a communications satellite payload where its primary function is to act as a repeater, i.e. it amplifies received microwave signals from earth before retransmitting them back to the earth ground-station [5]. In order to compensate the effect of noise and non-linearity in power amplifiers, the input signals are first divided into narrowband channels before amplification and then recombined before transmission. The division and the consequent recombination of the channels are carried out at the input and output multiplexers, which are composed of a bank of narrow bandpass filters with a fractional bandwidth of between 0.2% and 2%. These microwave bandpass filters are implemented using waveguides due to their low loss, high quality factors and high power handling capability. However, waveguide filters are heavy and bulky, which significantly increases the cost of launching the satellite. To address this issue, several advanced filter configurations have been proposed with reduced size and weight based on dual-mode and triple-mode waveguide filters [6]-[10], dielectric resonator filters [11]-[14], high-temperature superconductor filters [15][16], and a variety of coaxial, finline and microstrip filters [1]-[4].

In cellular radio communication systems, microstrip filters with stringent specifications are used extensively in base-station and mobile handset. Cellular base-station integrates the switching network and microwave repeater functions as depicted in Fig.2.2. Filters in transmitters and receivers must have strict performance characteristics such as (1) high selectivity; (2) low-loss within the passband to satisfy power amplifier linearity and efficiency demand; and (3) high rejection level at frequencies near the passband to reject the out-of-band inter-modulation and nearby channel interference. Typically, a transmit filter in base-station has insertion-loss of less than 0.8 dB and return-loss higher than 20 dB. Existing mobile handsets do not require filters with so demanding characteristics as they only handle low power (33-dBm); however, they still require filters that are low cost and highly compact.

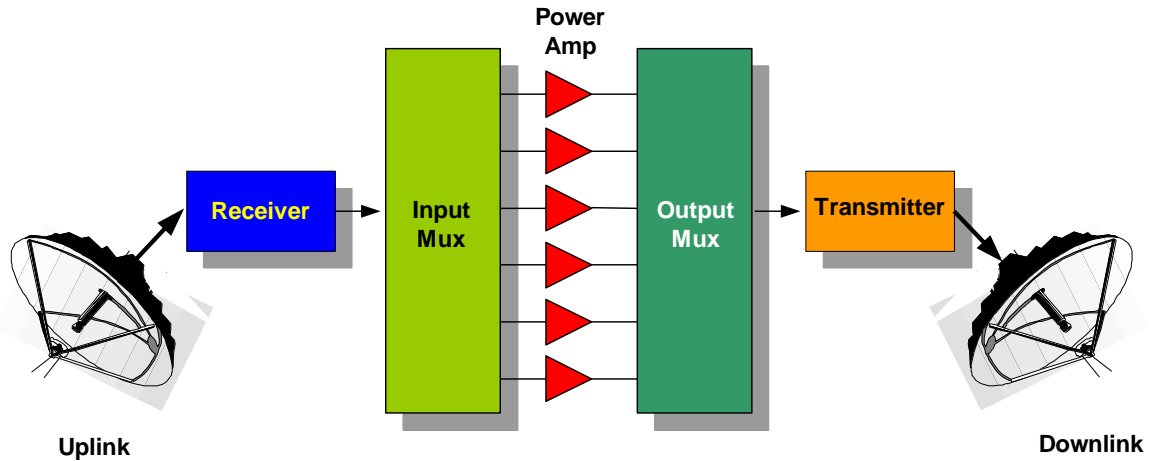


Fig. 2.1 Block diagram of a typical communications satellite.

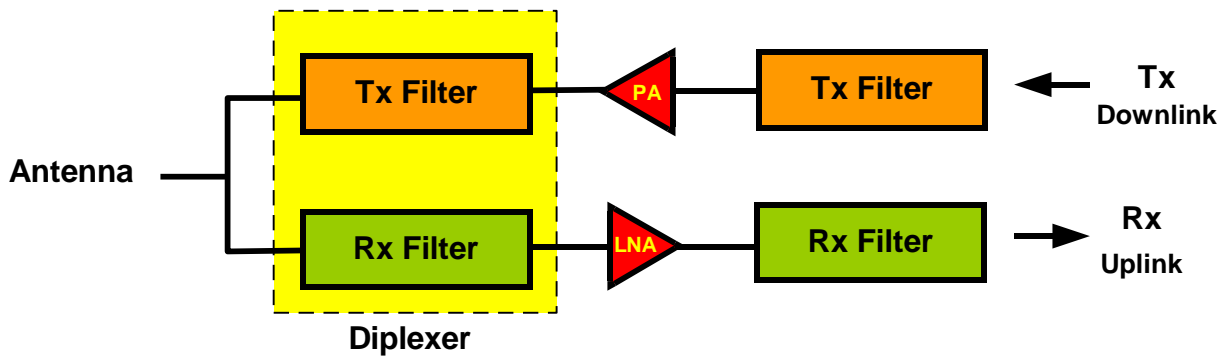


Fig. 2.2 Simplified block diagram of RF/microwave front-end of cellular base-station.

Strict requirements posed by various wireless communication systems have driven the evolution of filter design techniques. In the early stage of the development of microwave filters, most filter designs were accomplished with the image parameter method [17]. This method uses a cascaded two-port filter sections to provide the required cut-off frequency and attenuation characteristics, but not allowing a specified frequency response over the complete operating range. Therefore, even though the design procedure is relatively simple, such designs require many iterations and empirical adjustments to achieve the desired results and there is no methodical way to improve the design. Later, with the development of network synthesis techniques, a new method, termed the insertion-loss method, was developed to provide a systematic way for synthesizing the required filtering performance [17]. Filter design procedures with the insertion-loss method begin with a lowpass filter prototype that is normalized in terms of impedance and frequency. The prototype is then converted to the desired filter by using the frequency and impedance transformations. Compared to the image parameter method, the insertion-loss method

allows the design of filters with a completely specified frequency response and it has a higher degree of control over the passband and stopband characteristics. Today, with the advances in computer-aided design (CAD) technologies, synthesis techniques coupled with accurate electromagnetic simulations as well as sophisticated optimization software algorithms have allowed the design of filters to go from drawing boards almost immediately to the final product, without the need for empirical adjustments or manual tuning. This not only cuts dramatically the time required for product development, but also provides more opportunities for the implementation of more efficient communication systems.

Significant effort has been devoted to the research and development of advanced microwave structures for the implementation of microwave filters. There are mainly three categories of structures commonly used in the physical realization of filters, i.e. (i) the lumped-element LC structure; (ii) the planar microwave structure; and (iii) the cavity structure [4]. Lumped-element LC structures [1] are typically composed of chip inductors and capacitors. This type of structure is generally used in the design of filters operating at low frequencies, with a small size but relatively low Q -factor. Microstrip and stripline filters [2] are constructed of sections of transmission lines terminated in a short or open circuit with various shapes, for example, hairpin [18], ring [19] and patched [20] configuration. These planar microwave filters have the advantages of compact sizes, low cost, easy fabrication and integration with other circuits, but they are relatively lossy (Q factors between 50 and 300 at 1 GHz [4]) and have limited power capability. In contrast, cavity filters such as dielectric [21], waveguide and coaxial [22],[23] filters have quite high Q -factors (up to 30,000 [4]) and high power handling levels. However, they are heavy and bulky as well as difficult to fabricate and integrate with other circuits in comparison to their counterparts implemented with planar structures.

Major advances made recently in novel materials and technologies have further driven the rapid development of microwave filters. Several new materials and structures, such as high-temperature superconductors (HTS) [24], low-temperature cofired ceramic (LTCC) [25]-[27], photonic bandgap (PBG) [28],[29] and electromagnetic bandgap (EBG) structures [30]-[33] have been applied in the design of filters to improve the performance and reduce the size of the filter. Advanced techniques such as monolithic microwave integrated circuits (MMIC) [34],[35] and microelectromechanical systems (MEMS) [36]-[38] have provided more flexibility for the physical realization of microwave filters. Also advances in network synthesis techniques and CAD design tools have enabled the accurate design and simulation of filters, i.e. the cascaded quadruplet (CQ) filters [39][40], cascaded trisection (CT) filters [41],[42] and cross-coupled filters [43]-[46]. With the continuing advances in materials and fabrication techniques as well as synthesis

techniques and CAD techniques, it is expected that the investigation of advanced filters with higher performance, lower cost and smaller size continue to be an important research topic.

Filter structures proposed in this thesis exhibit low-loss and quasi-elliptic function response that is normally only possible with the filter designs using waveguides, high temperature superconductors and other novel materials and technologies. In fact, this research has resulted in the development of innovative and compact microstrip bandpass filters that address the issues discussed above, i.e. filters that have the following desirable characteristics: light in weight, small size, high selectivity, wide out-of-band rejection level, and low loss. The proposed designs are highly compact planar microstrip filters that provide an alternative solution to existing and next generation of wireless communications systems.

References

1. G. L. Matthaei, L. Young, and E. M. T. Jones, "Microwave filters, impedance matching networks, and coupling structures," *Dedham, MA: Artech House*, 1964.
2. J. G. Hong, and M. J. Lancaster, "Microstrip filters for RF/microwave applications," *New York: John Wiley & Sons*, 2001.
3. I. C. Hunter, "Theory and design of microwave filters," *London, Institution of Electrical Engineers*, 2001.
4. R. J. Cameron, C. M. Kudsia, and R. R. Mansour, "Microwave filters for communication systems: fundamentals, design, and applications," *Hovoken, New Jersey: John Wiley & Sons*, 2007.
5. V. E. Boria, and B. Gimeno, "Waveguide filters for satellites," *IEEE Microw. Mag.*, vol. 8, pp. 60-70, Oct. 2007.
6. G. Lastoria, G. Gerini, M. Guglielmi, and F. Emma, "CAD of triple-mode cavities in rectangular waveguide," *IEEE Microw. Guided W.*, vol. 8, pp. 339-341, Oct. 1998.
7. H. Hu, and K.-L. Wu, "A deterministic EM design technique for general waveguide dual-mode bandpass filters," *IEEE Trans. Microw. Theory Tech.*, vol. 61, pp. 800-807, Feb. 2013.
8. M. Guglielmi, P. Jarry, E. Kerherve, O. Roquebrun, and D. Schmitt, "A new family of all-inductive dual-mode filters," *IEEE Trans. Microw. Theory Tech.*, vol. 49, pp. 1764-1769, Oct. 2001.
9. K. L. Wu, "An optimal circular-waveguide dual-mode filter without tuning screws," *IEEE Trans. Microw. Theory Tech.*, vol. 47, pp. 271-276, Mar. 1999.
10. W. Steyn, and P. Meyer, "Shorted waveguide-stub coupling mechanism for narrow-band multimode coupled resonator filters," *IEEE Trans. Microw. Theory Tech.*, vol. 52, pp. 1622-1625, Jun. 2004.
11. R. Zhang, and R. R. Mansour, "Dual-band dielectric-resonator filters," *IEEE Trans. Microw. Theory Tech.*, vol. 57, pp. 1760-1766, Jul. 2009.
12. A. Panariello, M. Yu, and C. Ernst, "Ku-band high power dielectric resonator filters," *IEEE Trans. Microw. Theory Tech.*, vol. 61, pp. 382-392, Jan. 2013.
13. R. Zhang, and R. R. Mansour, "Low-cost dielectric resonator filters with improved spurious performance," *IEEE Trans. Microw. Theory Tech.*, vol. 55, pp. 2168-2175, Oct. 2007.
14. L. K. Hady, D. Kajfez, and A. A. Kishk, "Triple mode use of a single dielectric resonator," *IEEE Trans Antennas Propag.*, vol. 57, pp. 1328-1335, May 2009.
15. I. B. Vendik, V. V. Kondratiev, D. V. Kholodniak, S. A. Gal'chenko, A. N. Deleniv, M. N. Goubina, A. A. Svishchev, S. Leppavuori, J. Hagberg, and E. Jakku, "High-temperature superconductor filters: modeling and experimental investigations," *IEEE Trans. Appl. Supercon.*, vol. 9, pp. 3577-3580, Jun. 1999.
16. M. F. Sitnikova, I. B. Vendik, O. G. Vendik, D. V. Kholodnyak, P. A. Tural'chuk, I. V. Kolmakova, P. Y. Belyavskii, and A. A. Semenov, "Modeling and experimental investigation of microstrip

- resonators and filters based on High-Temperature Superconductor films," *Tech. Phys. Lett.*, vol. 36, pp. 862-864, Sep. 2010.
17. D. M. Pozar, "Microwave engineering," *Reading, MA: Addison-Wesley*, 1990.
 18. E. G. Cristal, and S. Frankel, "Hairpin-line and hybrid hairpin-line half-wave parallel-coupled-line filters," *IEEE Trans. Microw. Theory Tech.*, vol. 20, pp. 719-728, Nov. 1972.
 19. I. Wolff, "Microstrip bandpass filter using degenerate modes of a microstrip ring resonator," *Electron. Letter*, vol. 8, pp. 302-303, Jun. 1972.
 20. J. S. Hong, and S. H. Li, "Theory and experiment of dual-mode microstrip triangular patch resonators and filters," *IEEE Trans. Microw. Theory Tech.*, vol. 52, pp. 1237-1243, Apr. 2004.
 21. S. B. Cohn, "Microwave bandpass filters containing high-Q dielectric resonators," *IEEE Trans. Microw. Theory Tech.*, vol. 16, pp. 218-227, 1968.
 22. A. M. Model, "Design of waveguide and coaxial bandpass filters with directly-coupled cavities," *Telecommun. Radio Eng.*, 1967.
 23. A. E. Atia, and A. E. Williams, "Narrow-bandpass waveguide filters," *IEEE Trans. Microw. Theory Tech.*, vol. 20, pp. 258-265, Apr. 1972.
 24. S. Pal, C. J. Stevens, and D. J. Edwards, "Compact parallel coupled HTS microstrip bandpass filters for wireless communications," *IEEE Trans. Microw. Theory Tech.*, vol. 54, pp. 768-775, Feb. 2006.
 25. C. F. Chang, S. J. Chung, "Bandpass filter of serial configuration with two finite transmission zeros using LTCC technology," *IEEE Trans. Microw. Theory Tech.*, vol. 53, pp. 2383-2388, Jul. 2005.
 26. L. K. Yeung, and K. L. Wu, "A compact second-order LTCC bandpass filter with two finite transmission zeros," *IEEE Trans. Microw. Theory Tech.*, vol. 51, pp. 337-341, Feb. 2003.
 27. C. W. Tang, "Harmonic-suppression LTCC filter with the step-impedance quarter-wavelength open stub," *IEEE Trans. Microw. Theory Tech.*, vol. 52, pp. 617-624, Feb. 2004.
 28. N. C. Karmakar, and M. N. Mollah, "Investigations into nonuniform photonic-bandgap microstripline low-pass filters," *IEEE Trans. Microw. Theory Tech.*, vol. 51, pp. 564-572, Feb. 2003.
 29. T. Y. Yun, and K. Chang, "Uniplanar one-dimensional photonic-bandgap structures and resonators," *IEEE Trans. Microw. Theory Tech.*, vol. 49, pp. 549-553, Mar. 2001.
 30. Y. J. Lee, J. Yeo, R. Mittra, and W. S. Park, "Application of electromagnetic bandgap (EBG) superstrates with controllable defects for a class of patch antennas as spatial angular filters," *IEEE Trans. Antennas Propag.*, vol. 53, pp. 224-235, Jan. 2005.
 31. S. W. Wong, and L. Zhu, "EBG-embedded multiple-mode resonator for UWB bandpass filter with improved upper-stopband performance," *IEEE Microw. Wireless. Compon. Letter*, vol. 17, pp. 421-423, Jun. 2007.
 32. P. de Maagt, R. Gonzalo, Y. C. Vardaxoglou, and J. M. Baracco, "Electromagnetic bandgap antennas and components for microwave and (sub) millimeter wave applications," *IEEE Trans Antennas Propag.*, vol. 51, pp. 2667-2677, Oct. 2003.
 33. H. J. Chen, T. H. Huang, C. S. Chang, L. S. Chen, N. F. Wang, Y. H. Wang, and M. P. Houg, "A novel cross-shape DGS applied to design ultra-wide stopband low-pass filters," *IEEE Microw. Wireless. Compon. Letter*, vol. 16, pp. 252-254, May 2006.
 34. V. Aparin, and P. Katzin, "Active GAAS MMIC band-pass filters with automatic frequency tuning and insertion loss control," *IEEE J. Solid-St. Circ.*, vol. 30, pp. 1068-1073, Oct. 1995.
 35. V. Aparin, and P. Katzin, "Active GAAS MMIC band-pass filters with automatic frequency tuning and insertion loss control," *IEEE J. Solid-St. Circ.*, vol. 30, pp. 1068-1073, Oct. 1995.
 36. K. Entesari, and G. M. Rebeiz, "A 12-18-GHz three-pole RF MEMS tunable filter," *IEEE Trans. Microw. Theory Tech.*, vol. 53, pp. 2566-2571, Aug. 2005.
 37. L. Dussopt, and G. M. Rebeiz, "Intermodulation distortion and power handling in RF MEMS switches, varactors, and tunable filters," *IEEE Trans. Microw. Theory Tech.*, vol. 51, pp. 1247-1256, Apr. 2003.
 38. A. Abbaspour-Tamijani, L. Dussopt, and G. M. Rebeiz, "Miniature and tunable filters using MEMS capacitors," *IEEE Trans. Microw. Theory Tech.*, vol. 51, pp. 1878-1885, Jul. 2003.
 39. R. Levy, "Direct synthesis of cascaded quadruplet (CQ) filters," *IEEE MTT-S Int. Microwave Symp.* vol. 1-3, pp. 497-590, 1995.
 40. R. Levy, "Direct synthesis of cascaded quadruplet (CQ) filters," *IEEE Trans. Microw. Theory Tech.*, vol. 44, pp. 1517, Aug. 1996.
 41. R. Levy, and P. Petre, "Design of CT and CQ filters using approximation and optimization," *IEEE Trans. Microw. Theory Tech.*, vol. 49, pp. 2350-2356, Dec. 2001.

-
42. J.-C. Lu, C.-K. Liao, and C.-Y. Chang, "Microstrip parallel-coupled filters with cascade trisection and quadruplet responses," *IEEE Trans. Microw. Theory Tech.*, vol. 56, pp. 2101-2110, Sep. 2008.
 43. J. S. Hong, and M. J. Lancaster, "Cross-coupled microstrip hairpin-resonator filters," *IEEE Trans. Microw. Theory Tech.*, vol. 46, pp. 118-122, Jan. 1998.
 44. S. Amari, "Synthesis of cross-coupled resonator filters using an analytical gradient-based optimization technique," *IEEE Trans. Microw. Theory Tech.*, vol. 48, pp. 1559-1564, Sep. 2000.
 45. R. J. Cameron, "Advanced coupling matrix synthesis techniques for microwave filters," *IEEE Trans. Microw. Theory Tech.*, vol. 51, pp. 1-10, Jan. 2003.
 46. J. S. Hong, and M. J. Lancaster, "Couplings of microstrip square open-loop resonators for cross-coupled planar microwave filters," *IEEE Trans. Microw. Theory Tech.*, vol. 44, pp. 2099-2109, Nov. 1996.

Compact and Miniaturized Wideband Bandpass Filters

3.0 Introduction

In wireless communication and radar systems, microwave bandpass filters play an essential role to prevent interference with neighbouring channels by controlling the frequency response of the transmitter and receiver. As already mentioned in Chapter 1, the next generation of wireless communication systems requires filters of high performance specifications such as high frequency-selectivity, wide stopband rejection, low insertion-loss and high return-loss. In addition, these filters need to be compact in size and low cost to fabricate in mass production. High selectivity and wide stopband rejection are important to increase system capacity and suppress unwanted interference with other systems as the EM spectrum is highly congested. Planar filters implemented with printed circuit technology are particularly attractive as they are easy and economical to fabricate. However, conventional filter designs that are based on distributed components usually suffer from unwanted spurious responses due to their higher order resonances. The occurrence of out-of-band spurious responses can degrade the system performance.

Filters composed of half-wavelength ($\lambda_g/2$) or quarter-wavelength ($\lambda_g/4$) resonators generate harmonic responses at nf_o or $(2n+1)f_o$ (where $n = 1, 2, 3\dots$), respectively; where f_o is the fundamental frequency. Most filter structures using $\lambda_g/4$ resonators are grounded using via holes, which introduces extra complexity in design and fabrication, which can also negatively impact on fabrication reliability. Traditional way of suppressing higher order spurious is to cascade a low-pass filter with the bandpass filter. However, the use of an additional low-pass filter degrades the insertion-loss and increases the size of the filter.

The design of bandpass filters with wide stopband have been extensively investigated using numerous techniques in [1]–[5]. For example, open circuit transmission line stubs and interdigitated capacitors have been used to widen the stopband of conventional J-inverter filters [1]. In [2], “wiggly-line” structures have been used to reject multiple spurious passbands generated in parallel-coupled-line microstrip BPFs. In [3], resonators that have the same fundamental frequency as the spurious but different higher order resonant frequencies have been used to suppress spurious responses in the filter’s stopband. In [4], wide-stopband microstrip BPF is designed by using quarter-wavelength shorted coupled-lines. Stepped-impedance resonators (SIRs) have been used to shift the higher-order resonant frequencies to achieve wide stopband bandpass filters [5]. In this case the

harmonic response of SIR can be controlled by simply manipulating the impedance ratio of the resonator.

This chapter describes a technique to enhance the frequency-selectivity and stopband of a quasi-elliptic function filter implemented by coupling two open-loop ring resonator structures. This is achieved by introducing transmission zeros in the filter's frequency response by loading feed-lines with inductive stubs. Further enhancement is realized by interdigitally coupling the filter with the input/output feed-lines.

3.1 Theoretical Analysis of Stub Notch Filter

In a two-way radio communication link it is undesirable to transmit harmonic spuri as they are likely to interfere with other systems and degrade their performance. Microstrip notch filter can suppress undesired harmonics in a narrow band device such as mobile phone. A notch filter allows all frequencies pass through it except those in its stopband. High-Q notch filters eliminate a single frequency or narrow band of frequencies. The amplitude response of a notch filter is essentially flat at all frequencies except at the stopband.

The standard reference points for the roll-off on each side of the stopband are the points where the amplitude has decreased by 3-dB, to 70.7% of its original amplitude as shown in Fig. 3.1. The microstrip layout of a notch filter is shown in the Fig. 3.2. The filter consists of 50 Ω , microstrip transmission-line which is open-circuit at point S. When a signal of wavelength λ is transmitted from point A to B, the length of the open-circuit line needs to be $\lambda/4$ to eliminate it. This is because the open-circuit at S will be transformed into short-circuit at the point where the open-circuit line joins with AB and consequently the signals passing along AB will be blocked.

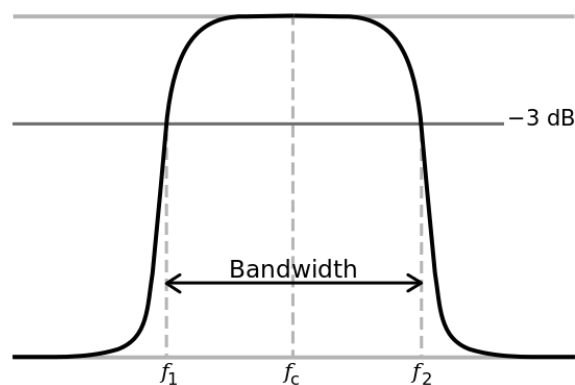


Fig. 3.1 Graph of Cut-off frequency (3-dB)

The impedance at the junction of the open-circuit stub Z_{in} , in Fig. 3.2, is given by:

$$Z_{in} = Z_S \left\{ \frac{Z_L + jZ_S \tan \beta l}{Z_S + jZ_L \tan \beta l} \right\} \quad (3.1)$$

Where β is phase constant, Z_s is stub impedance, Z_L is terminating load impedance and l is the length of the line. Since $Z_L = \infty$ we can ignore Z_s , so

$$Z_{in} = Z_S \left\{ \frac{Z_L + jZ_S \tan \beta l}{Z_S + jZ_L \tan \beta l} \right\} = -jZ_S \cot \beta l \quad (3.2)$$

However, since $l = \frac{\lambda_g}{4}$, then $\beta l = \frac{\pi}{2} \therefore \cot \beta l = 0$

so (3.2) is $Z_{in} = -jZ_S \cot \beta l = 0$ (3.3)

Hence $\Gamma_L = \frac{Z_L - Z_S}{Z_L + Z_S} = \frac{\infty}{\infty} = 1$ so $VSWR = \frac{1 + |\Gamma_L|}{1 - |\Gamma_L|} = \frac{2}{0} = \infty$

Where Γ_L is the reflection coefficient, VSWR is the voltage standing wave ratio.

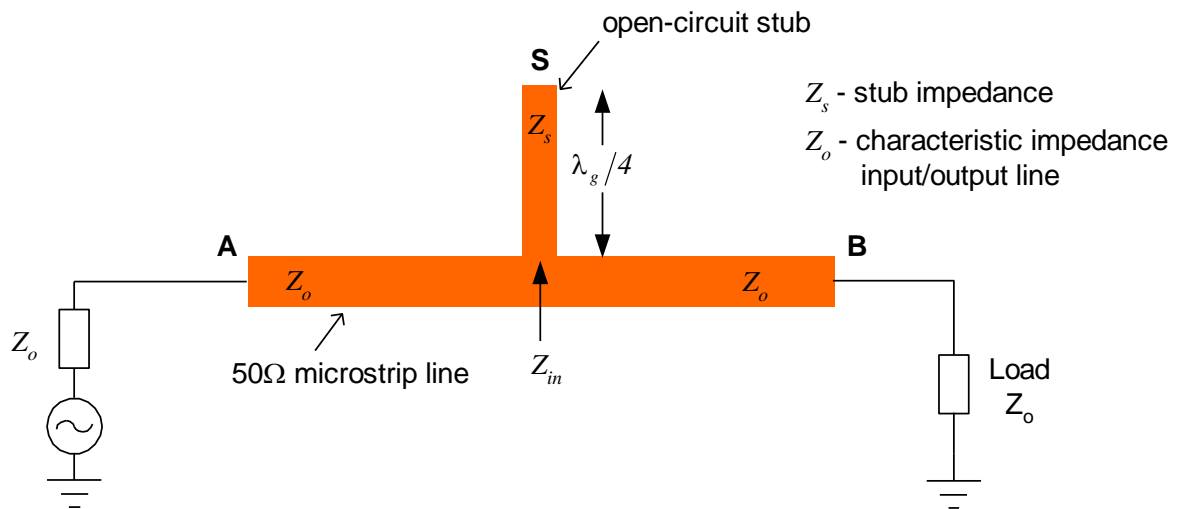


Fig. 3.2 Single stub notch filter.

These results indicate that a signal with wavelength of $\lambda_g/4$ will see very low impedance to ground at point S, which is essentially short-circuited. Hence this signal will be absorbed from the signals applied at the input A, which is manifest as high attenuation in its insertion-loss response at its frequency f_o . All other signals remain unaffected, hence low insertion-loss, except near f_o . Note, the VSWR is higher at other frequencies since the $\cot \beta l$ term is no longer zero.

An expression for the insertion-loss for the above circuit is given below.

$$IL = 10 \log \left[1 + \left(\frac{Y_s}{2} \right)^2 \right] \quad (3.4)$$

Where $Y_s = -\frac{Z_0}{Z_s} \cot \beta l$

$$IL = 10 \log \left[1 + \left(-\frac{Z_0}{2Z_s} \cot \beta l \right)^2 \right] \quad (3.5)$$

The width of the line determines its impedance, i.e. the higher the impedance the thinner the line and vice versa. When $Z_s = Z_0$, this is equivalent to width of the stub = width of input/output transmission line. So Eqn.(3.5) can be written as

$$IL = 10 \log \left[1 + \left(\frac{\cot^2 \beta l}{4} \right) \right] \quad (3.6)$$

$l = \frac{\lambda_g}{4}$, then $\beta l = \frac{\pi}{2} \quad \therefore \cot \beta l = 0$

So, $IL = 0$ dB at centre frequency. When $Z_s > Z_0$, i.e. the width of stub is less than the input/output transmission line, the $IL \rightarrow 0$ dB at centre frequency.

3.2 ABCD Matrix Model of the Notch Filter

An alternative way to theoretically model the single stub notch filter is by using ABCD matrix. ABCD parameters are known as transmission-line parameters that establish a connection between the input and output voltages and currents considering circuit elements. The ABCD matrix model of each element constituting the notch filter is shown in Fig. 3.3.

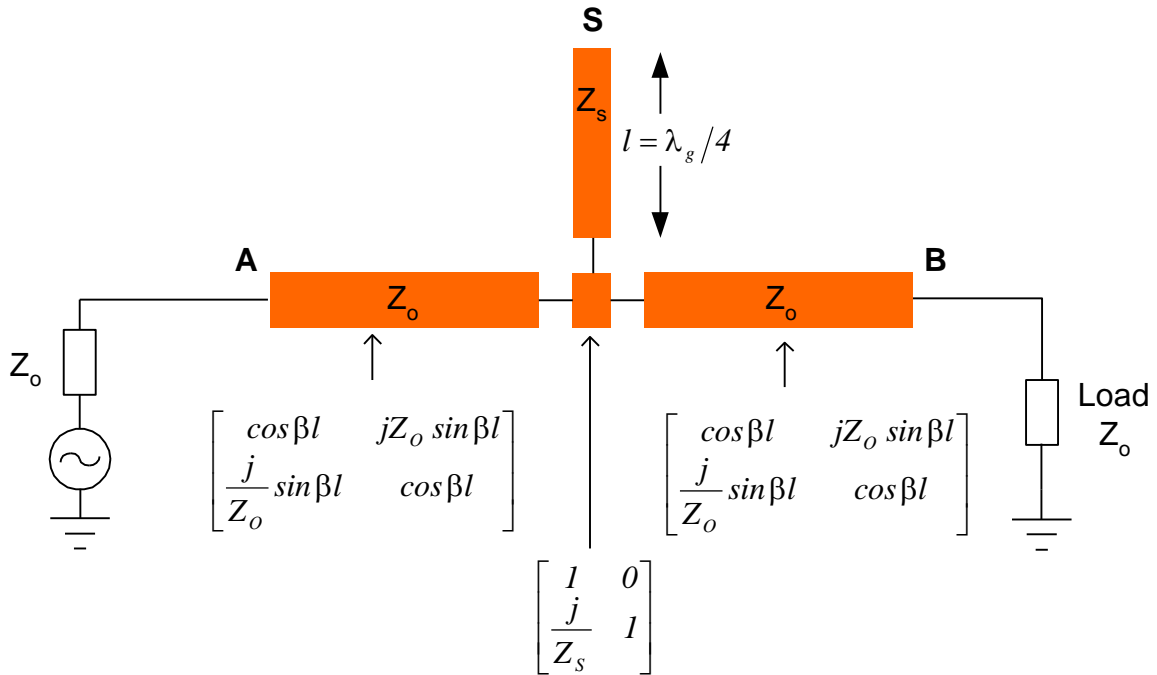


Fig. 3.3 ABCD matrix representation of the single stub notch filter

$$\text{Normalized ABCD matrix} = \begin{bmatrix} \bar{A} & \bar{B} \\ \bar{C} & \bar{D} \end{bmatrix} = \begin{bmatrix} \cos \beta l & j \sin \beta l \\ j \sin \beta l & \cos \beta l \end{bmatrix} \times \begin{bmatrix} 1 & 0 \\ \frac{j Z_0}{Z_s} & 1 \end{bmatrix} \times \begin{bmatrix} \cos \beta l & j \sin \beta l \\ j \sin \beta l & \cos \beta l \end{bmatrix}$$

$$\text{Normalized ABCD matrix} = \begin{bmatrix} \cos \beta l - \frac{Z_0}{Z_s} \sin \beta l & j \sin \beta l \\ j \sin \beta l + \frac{Z_0}{Z_s} \cos \beta l & \cos \beta l \end{bmatrix} \times \begin{bmatrix} \cos \beta l & j \sin \beta l \\ j \sin \beta l & \cos \beta l \end{bmatrix}$$

$$= \begin{bmatrix} \cos^2 \beta l - \frac{Z_0}{Z_s} \sin \beta l \cos \beta l - \sin^2 \beta l & j \sin \beta l \cos \beta l - j \frac{Z_0}{Z_s} \sin^2 \beta l + j \sin \beta l \cos \beta l \\ j \sin \beta l \cos \beta l + j \frac{Z_0}{Z_s} \cos^2 \beta l + j \sin \beta l \cos \beta l & -\sin^2 \beta l - \frac{Z_0}{Z_s} \sin \beta l \cos \beta l - \cos^2 \beta l \end{bmatrix}$$

(3.7)

$$\bar{B} = j 2 \sin \beta l \cos \beta l - j \frac{Z_0}{Z_s} \sin^2 \beta l$$

$$\bar{C} = j 2 \sin \beta l \cos \beta l + j \frac{Z_0}{Z_s} \cos^2 \beta l$$

$$\text{so } \bar{B} - \bar{C} = j \frac{Z_0}{Z_s} (\sin^2 \beta l + \cos^2 \beta l)$$

$$\bar{B} - \bar{C} = -j \frac{Z_0}{Z_s}$$

$$\frac{\bar{B} - \bar{C}}{2} = -j \frac{Z_0}{2 Z_s}$$

$$\text{Insertion-loss} = 10 \log \left| \frac{\bar{A} + \bar{B} + \bar{C} + \bar{D}}{2} \right| \quad (3.8)$$

For symmetrical, reciprocal, & dissipationless network, the following conditions apply:

$$A = D$$

A and D are real

$$AD - BC = 1$$

Where B and C are imaginary values, hence by replacing $\frac{\bar{B}-\bar{C}}{2} = -j\frac{Z_0}{2Z_S}$

$$\text{Insertion-loss} = 10\log \left[1 + \left(\frac{\bar{B} - \bar{C}}{2j} \right)^2 \right]$$

$$\text{Insertion loss} = 10\log \left[1 + \left(\frac{Z_0}{2Z_S} \right)^2 \right] \quad (3.9)$$

This indicates that when Z_S (thinner width) $> Z_0$ then $IL \rightarrow 0$

3.3 Coupled Double Open-Loop Ring Resonator Bandpass Filter

Selectivity of bandpass filters can be improved by inserting transmission zeros above and below the passband response. This can be achieved using the filter configuration shown in Fig. 3.4, where two hairpin resonators are electrically and magnetically coupled to each other with the feed-lines tapped asymmetrically [6]. The input and output feed-lines divide the resonators into two sections of l_1 and l_2 . The total length of the resonator is $l = l_1 + l_2 = \lambda_g/2$, where λ_g is the guided wavelength at fundamental resonance.

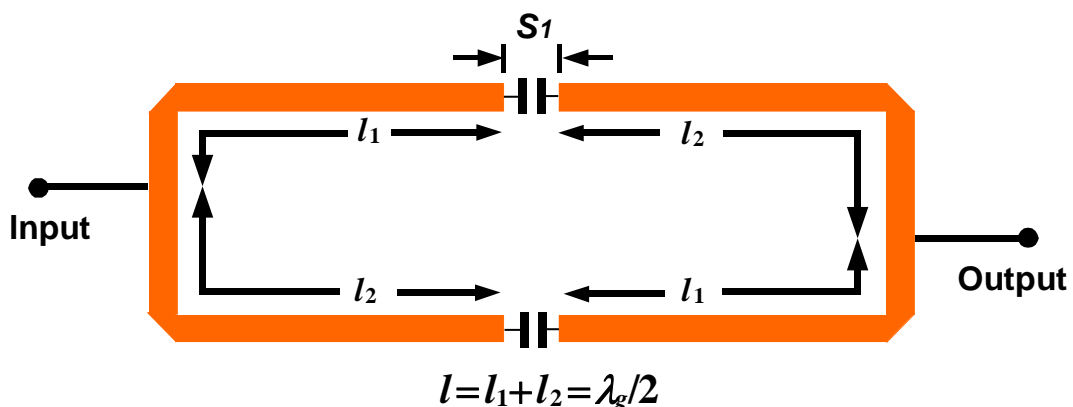


Fig. 3.4 Configuration of the filter using two hairpin resonators with asymmetric tapping feed-lines.

The coupling between the two open ends of the resonators is simply expressed by the gap capacitance [7], [8]. By inspecting the figure, the whole circuit represents a shunt circuit,

which consists of upper and lower sections. Each section is composed of l_1 , l_2 , and C_{S1} . The ABCD matrix for the upper and lower sections of the lossless shunt circuits are:

$$\begin{bmatrix} A & B \\ C & D \end{bmatrix}_{upper} = M_1 M_2 M_3 \quad (3.10a)$$

$$\begin{bmatrix} A & B \\ C & D \end{bmatrix}_{lower} = M_3 M_2 M_1 \quad (3.10b)$$

$$M_1 = \begin{bmatrix} \cos\beta l_1 & jZ_0 \sin\beta l_1 \\ jY_0 \sin\beta l_1 & \cos\beta l_1 \end{bmatrix}, \quad M_2 = \begin{bmatrix} 1 & Z_c \\ 0 & 1 \end{bmatrix}, \quad M_3 = \begin{bmatrix} \cos\beta l_2 & jZ_0 \sin\beta l_2 \\ jY_0 \sin\beta l_2 & \cos\beta l_2 \end{bmatrix}$$

Where β is the propagation constant, $Z_c = \frac{1}{j\omega C_{S1}}$ is the impedance of the gap capacitance C_{S1} , ω is the angular frequency, and $Z_0 = 1/Y_0$ is the characteristic impedance of the resonator. The Y parameters of the upper and lower sections are obtained from Eqn.(3.10) and given by:

$$\begin{bmatrix} Y_{11} & Y_{12} \\ Y_{21} & Y_{22} \end{bmatrix} = \begin{bmatrix} \frac{D_j}{B_j} & \frac{B_j C_j - A_j D_j}{B_j} \\ -1 & \frac{A_j}{B_j} \\ \frac{1}{B_j} & \frac{A_j}{B_j} \end{bmatrix} \quad (3.11)$$

Where $j =$ upper or lower section. In addition, Y parameter of the whole circuit is expressed as:

$$\begin{bmatrix} Y_{11} & Y_{12} \\ Y_{21} & Y_{22} \end{bmatrix} = \begin{bmatrix} Y_{11} & Y_{12} \\ Y_{21} & Y_{22} \end{bmatrix}_{upper} + \begin{bmatrix} Y_{11} & Y_{12} \\ Y_{21} & Y_{22} \end{bmatrix}_{lower} \quad (3.12)$$

The insertion loss (S_{21}) of the circuit can then be calculated from the total Y parameters and is expressed as:

$$S_{21} = \frac{-2Y_{21}Y_0}{(Y_{11} + Y_0)(Y_{11} + Y_0) - Y_{12}Y_{21}} \quad (3.13)$$

$$= \frac{j4 \left(Z_0 \sin\beta l - \frac{\cos\beta l_1 \cos\beta l_2}{\omega C_{S1}} \right) Y_0}{\left[2\cos\beta l + \frac{Y_0 \sin\beta l}{\omega C_{S1}} + j \left(Z_0 \sin\beta l - \frac{\cos\beta l_1 \cos\beta l_2}{\omega C_{S1}} \right) Y_0 \right]^2 - 4} \quad (3.14)$$

Eqn.(3.10)-(3.14) are more general for asymmetric feed-lines tapped at arbitrary positions on the resonators. Transmission zeros can be found by letting $S_{21} = 0$, namely

$$Z_0 \sin \beta l - \frac{\cos \beta l_1 \cos \beta l_2}{\omega C_{s1}} = 0 \quad (3.15)$$

For a small C_{s1} , the above equation can be approximated as:

$$\cos \beta l_1 \cos \beta l_2 = 0 \quad (3.16)$$

Eqn.(3.16) shows the relation between the transmission zeros and the tapping positions. By substituting $\beta = \frac{2\pi f \sqrt{\epsilon_{eff}}}{c}$ in Eqn.(3.16), the transmission zeros corresponding to the tapping positions are found to be:

$$f_1 = \frac{nc}{4l_1 \sqrt{\epsilon_{eff}}} \quad (3.17)$$

$$f_2 = \frac{nc}{4l_2 \sqrt{\epsilon_{eff}}} \quad (3.18)$$

For $n = 1, 3, 5, \dots$

Where f is frequency, f_1 is the frequency at first attenuation pole, f_2 is the frequency at second attenuation pole, ϵ_{eff} is effective dielectric constant, n is mode number and c is the speed of light in free space = 3×10^8 m/s. Therefore, at transmission zero, $S_{21} = 0$, there is maximum rejection. On the other hand, when $l_1 = l_2$, there is no transmission zero (attenuation pole).

To realize a compact filter, the arms of the two open-loop ring resonators are folded, as shown in Fig. 3.5. The filter has the same dimensions as the filter in Fig. 3.4, except for the two additional 45-degree chamfered bends and the coupling gap $g = 0.5$ mm between the two open ends of the ring.

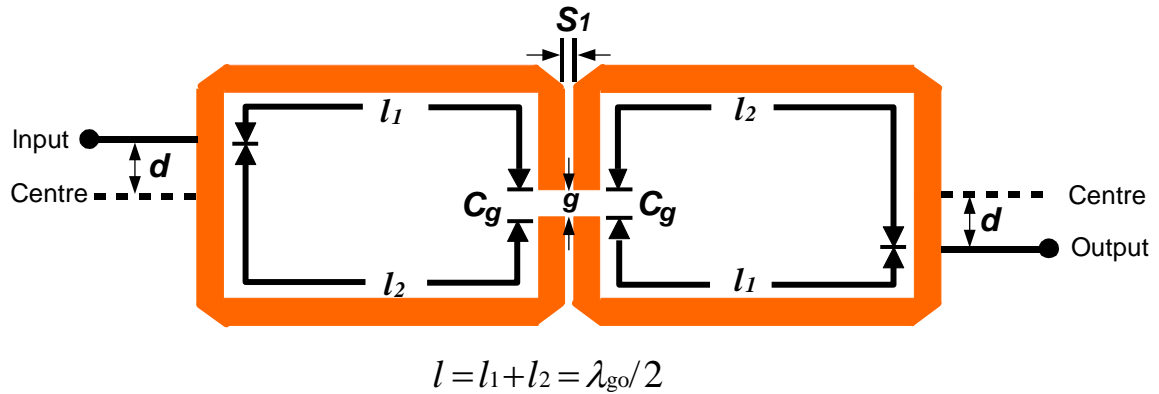


Fig. 3.5 Compact version of the filter using two open-loop ring resonators with asymmetric tapping feed-lines.

3.4 Selectivity and Stopband Performance Enhancement

To enhance the selectivity and stopband performance the filter structure in Fig. 3.6 is proposed, which consists of two mixed (electric and magnetic) coupled open-ring resonators where the input and output feed-lines are inductively loaded with a pair of open stubs in the shape of spirals. The open stubs were spiralled to keep the structure compact in size. The function of the open stubs is to suppress harmonic responses generated by the filter across a wide bandwidth above and below the passband response. The centre frequency of the passband is 3.2 GHz with a 3-dB bandwidth of 250 MHz. As the attenuation zeros are located at 2.95 GHz and 3.45 GHz, the lengths l_1 and l_2 were calculated using Eqns. (3.17) and (3.18).

The filter, shown in Fig. 3.6, was designed on Arlon CuClad217LX substrate with thickness $h = 0.794$ mm, dielectric constant $\epsilon_r = 2.17$, thickness of conductor $t = 35$ microns, and loss-tangent $\delta = 0.0009$. The feed-lines have a characteristic impedance of 50Ω with a corresponding width of 2.42 mm. The spirals on the feed-lines have an impedance of 149.8Ω with width of 0.2 mm. The spacing between the spiral gaps is 0.6 mm. To suppress the spuri the feed-lines of the filter were loaded with open stubs, as shown in Fig. 3.6(a). The locations of the stubs were determined through simulation analyses. The simulation and optimization was accomplished with the Advanced Design System (ADS™) momentum software. The optimised design parameters are: $W_1 = 0.2$ mm, $W_2 = 2.42$ mm, $l_1 = 19.1$ mm, $l_2 = 12.79$ mm, $S_1 = 0.6$ mm, $S_2 = 0.67$ mm, $L_{x1} = 13.37$ mm, $L_{x2} = 29$ mm, $L_{y1} = 21.38$ mm, $L_{y2} = 13.82$ mm, and $W_b = 0.2$ mm.

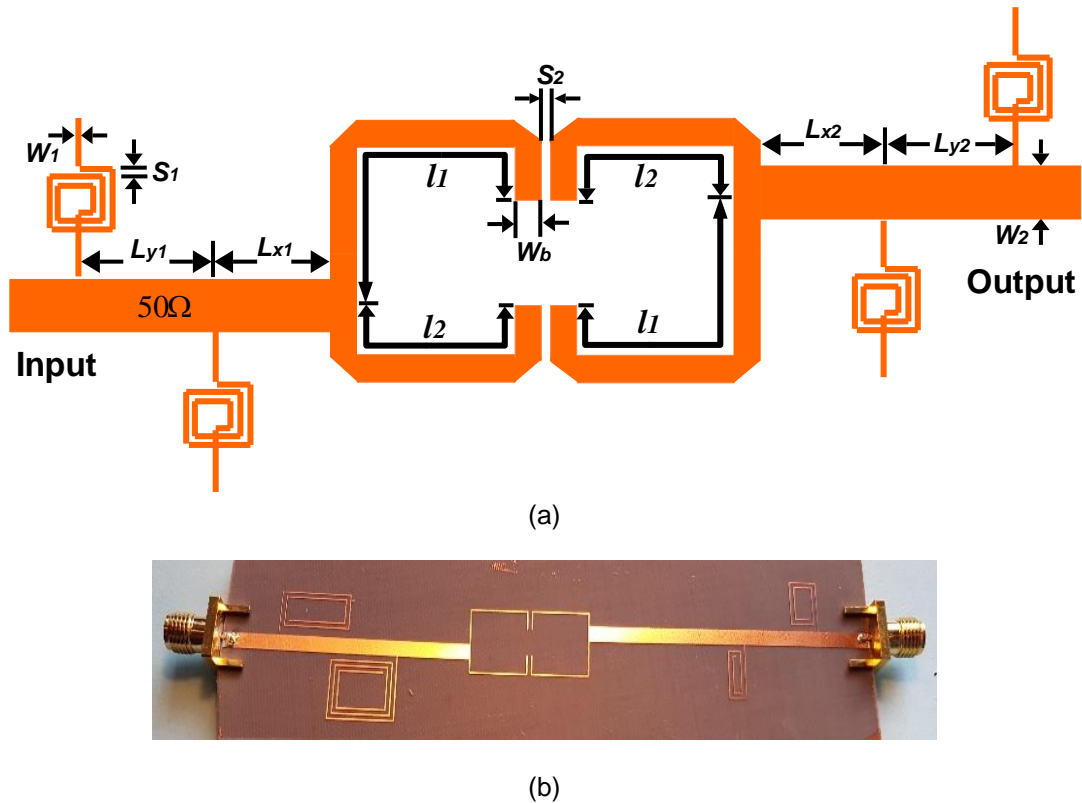


Fig. 3.6 (a) Layout, and (b) photograph of the proposed bandpass filter.

The simulated insertion and return-loss response of the proposed filter with no spiral loaded feed-line is shown in Fig. 3.7. While Fig 3.8 shows the simulated and measured performance of the proposed filter with spiral loaded feed-line. Comparison of these two responses clearly shows the filter with spiral loading generates three transmission zeros on either sides of the passband response. The transmission zeros located at 2.9 GHz and 3.5 GHz are due to resonator lengths l_1 and l_2 that determine the tapping position of the input/output feed-lines. Whereas the transmission zeros at 1.7 GHz and 2.8 GHz are due to the two spirals loaded on input feed-line, and the transmission zeros at 3.9 GHz and 4.4 GHz are due to the two spirals loaded on the output. The physical dimensions of the filter were optimized using ADS™.

The spiral loaded feed-line has improved the out-of-band performance which is greater than 20 dB; however, the filter's 3-dB bandwidth has reduced by 28.6% (from 350 MHz to 250 MHz), insertion-loss centred at 3.2 GHz is increased by 1.3-dB, which is mainly attributed to conductor losses, and its return-loss is better than 16 dB.

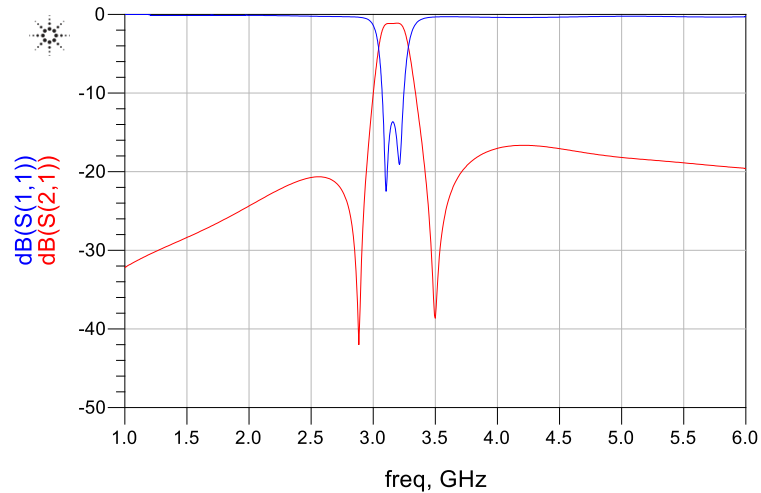


Fig. 3.7 Transmission and reflection-coefficient response of the proposed filter without spiral feed line.

The effect of coupling between the two resonators on the filter performance was assessed in terms of frequency of the two transmission zeros (f_1 and f_2), centre frequency of the filter (f_o), and insertion-loss (IL). The results are tabulated in Table 3.1 and graphically presented in Fig. 3.9. The results show the coupling coefficient has very little effect on the transmission zeros and the centre frequency however it greatly affects the filter loss. The loss shown is to be reduced by increasing the coupling gap S_2 .

Table 3.1 Effect of resonator separation on the transmission zeros, centre frequency and loss performance.

S_2 (mm)	f_{tz1} (GHz)	f_{tz2} (GHz)	f_o (GHz)	IL (dB)
0.2	2.80	3.60	3.17	3.20
0.3	2.86	3.61	3.21	2.76
0.4	2.90	3.60	3.22	2.30
0.5	2.92	3.62	3.25	1.90
0.6	2.94	3.62	3.26	1.79
0.7	2.94	3.62	3.27	1.70

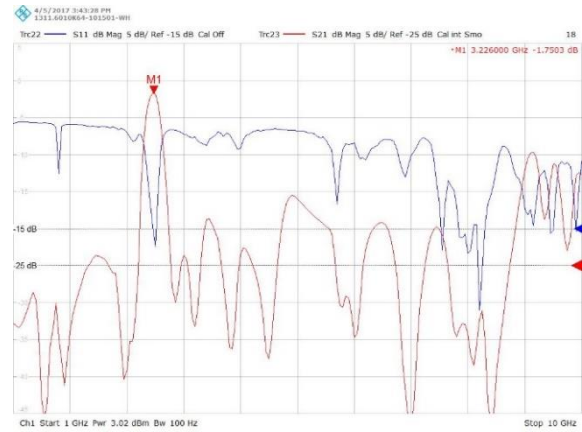
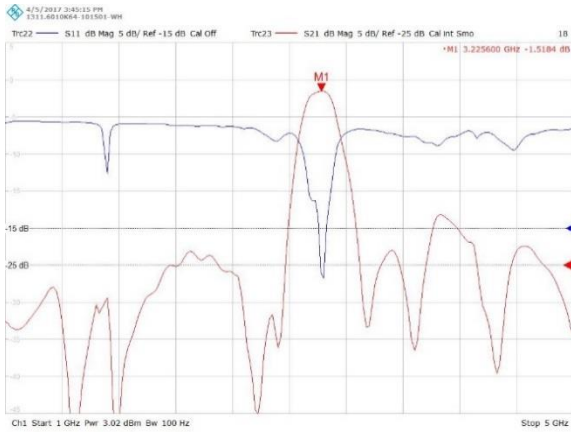
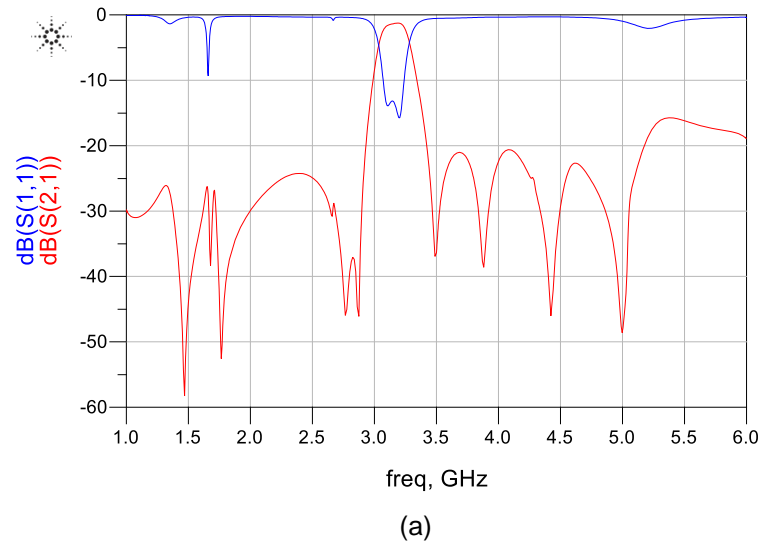


Fig. 3.8 (a) S-parameter simulation response of the proposed filter with spiral loaded feed line, (b) measured S-parameter response (narrow band view), and (c) measured S-parameter response (wideband view).

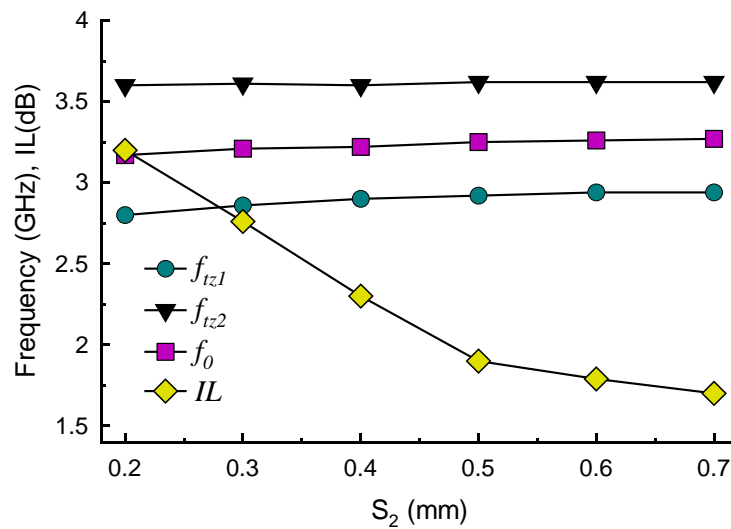


Fig. 3.9 Effect of resonator separation on the transmission zeros, centre frequency and loss performance.

Fig. 3.10 shows transmission response for different values of coupling gap (S_2). It shows when coupling gap is 0.7 mm, the passband has a reasonable sharp skirt with relatively low insertion-loss of around 1.7 dB, and the out-of-band performance is about 23-dB. As the coupling gap reduces the centre frequency of the filter moves downwards in frequency and the out-of-band rejection level deteriorates significantly. In the design an optimum separation gap used was 0.67 mm.

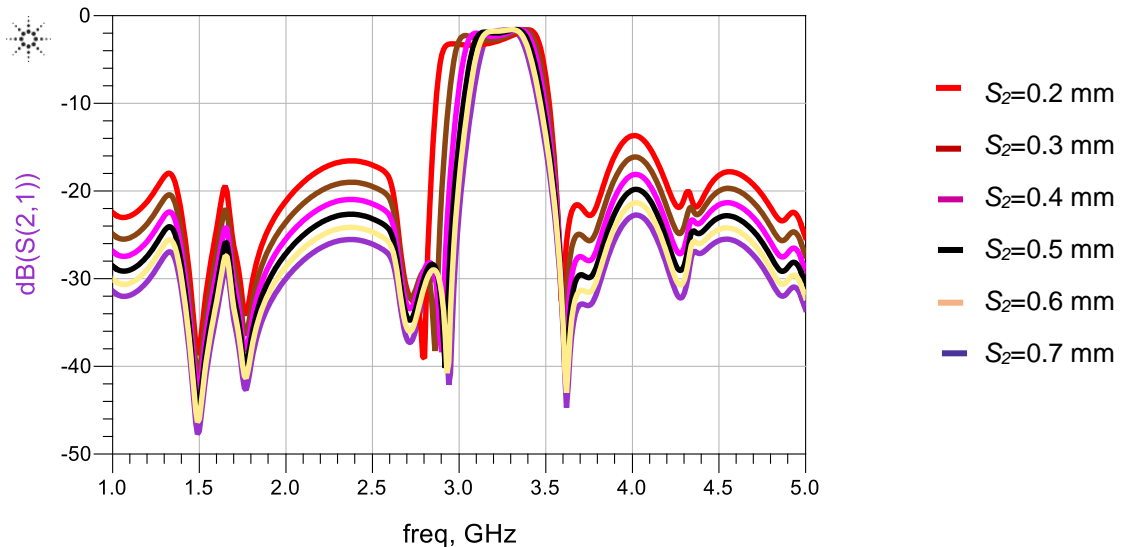


Fig. 3.10 Frequency response of the proposed filter as a function of inter-resonator coupling gap.

The effect of resonator width (W_b) on the filter's performance is tabulated in Table 3.2 and graphically presented in Fig. 3.11 and 3.12. The results show the increase in width moderately shifts the filter passband to the left however it significantly increases its insertion-loss performance. The frequency response shows the overall response and out-of-band performance are degrading with increase in width. In the design, an optimum width of 0.2 mm was used.

Table 3.2 Effect of resonator width on the transmission zeros, centre frequency and loss performance.

W_b (mm)	f_{tz1} (GHz)	f_{tz2} (GHz)	f_o (GHz)	IL (dB)
0.2	2.94	3.62	3.13	1.65
0.4	2.84	3.5	3.21	2.0
0.6	2.76	3.38	3.01	2.5
0.8	2.7	3.29	2.96	3.16
1	2.64	3.2	2.87	5.51

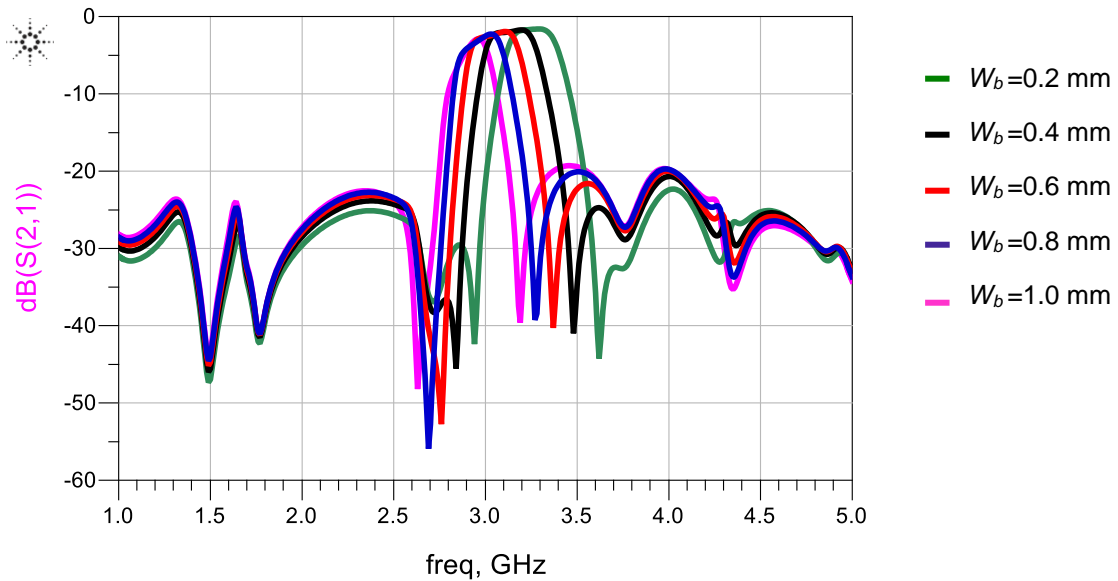


Fig. 3.11 Frequency response of the proposed filter as a function of resonator width.

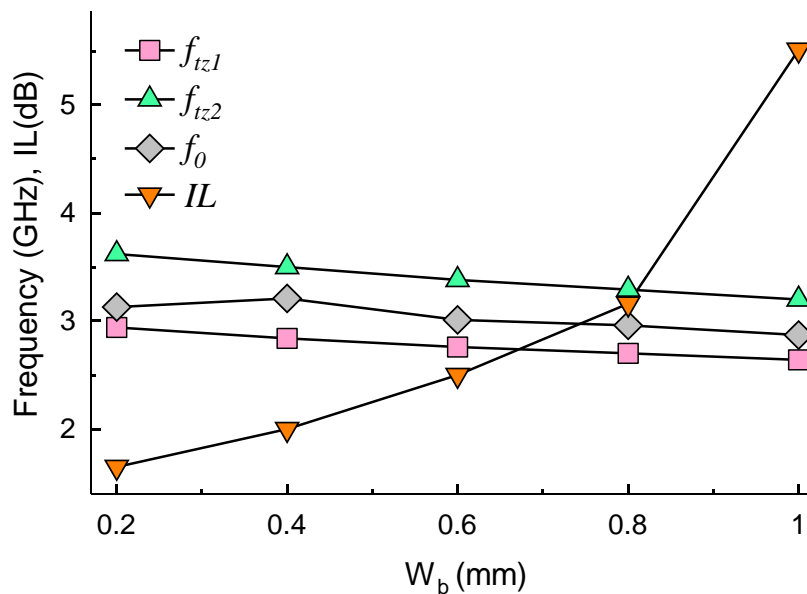


Fig. 3.12 Effect of resonator separation on the transmission zeros, centre frequency and loss performance as a function of resonator width

3.5 Ring Resonator Bandpass Filter with Interdigital Coupled Feed-line

In order to widen the stopband and improve the selectivity of the basic filter structure in Fig. 3.5, comprising coupled open-loop ring resonators, it was necessary to couple the filter with interdigital feed-lines as shown in Fig. 3.13. The dimensions of all other filter parameters remain unchanged and are defined in Section 3.4. The interdigital coupled feed-line structure was optimized using Momentum® software. The design parameters of this

structure are: $W_a = 0.2$ mm, $l_1 = 2.64$ mm, $l_2 = 19.89$ mm, $l_3 = 16.48$ mm, $L_{b1} = 1$ mm, $L_{b2} = 0.5$ mm, $L_{b3} = 16.74$ mm, $S_1 = 0.62$ mm, and $S_2 = 0.25$ mm.

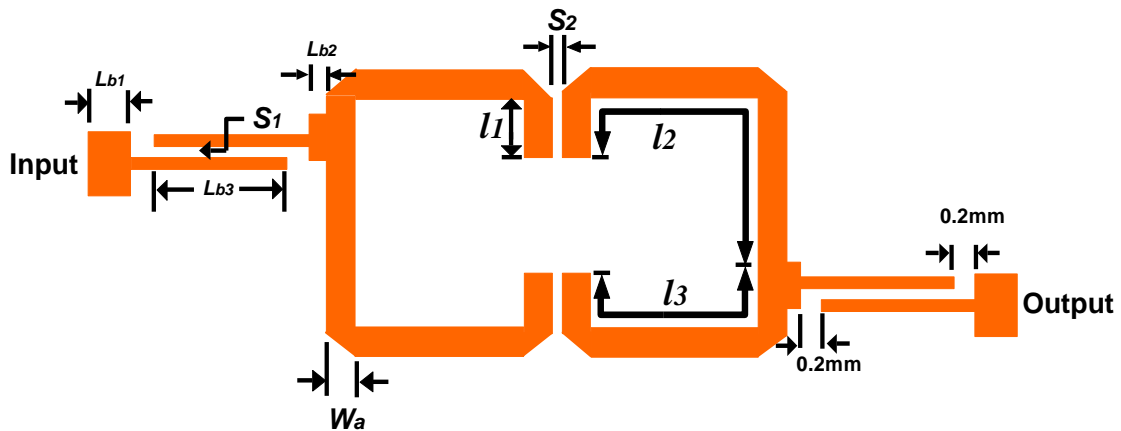


Fig. 3.13 Configuration of filter with two interdigital coupled feed-line.

The simulated response in Fig. 3.14 shows the ring resonator bandpass filter with interdigital feed-lines creates two transmission zeros outside of the passband and provides sharp out-of-band rejection with improved stopband, a wider passband as compared with the ring with the direct-connected feed lines. The filter exhibits a sharper roll-off and steep skirt selectivity. The filter has a 3-dB bandwidth of 700 MHz (3.1-3.8 GHz) centred at 3.4 GHz with insertion-loss of 1.2 dB and return-loss better than 10 dB. The filter has a 3-dB fractional bandwidth of 18.7%. The group-delay of the filter in the passband varies between 0.3-0.5 ns, as shown in Fig. 3.15. Owing to the two attenuation poles in the lower and upper cut-off frequencies, sharp selectivity is achieved with upper stopband rejection of -20 dB extending up to 9.4 GHz (i.e. $2.76f_0$), as shown in Fig. 3.16.

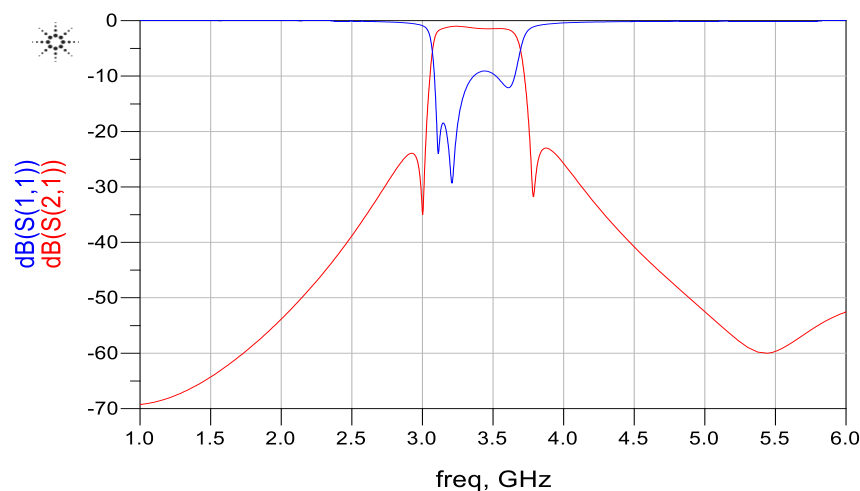


Fig. 3.14 Transmission and reflection-coefficient response of the interdigital coupled feed-line BPF.

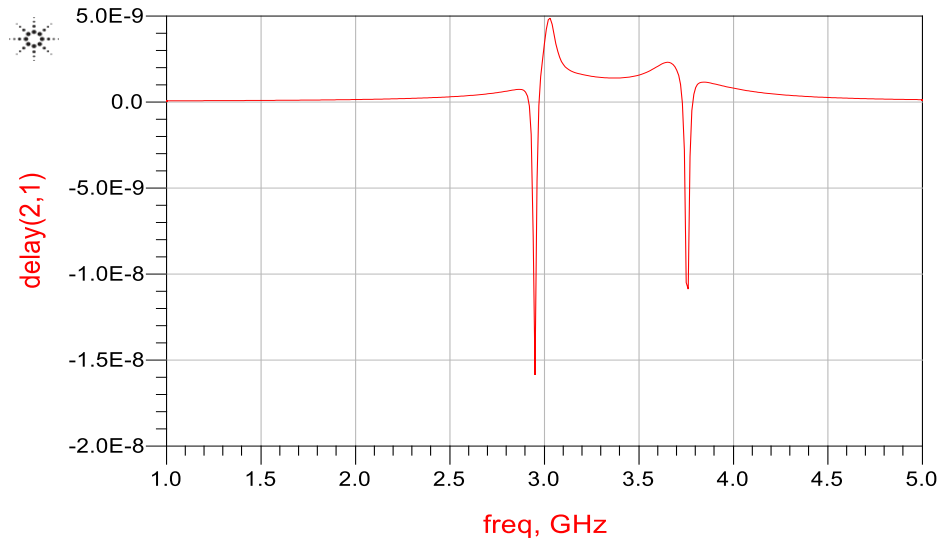


Fig. 3.15 Group delay response of the proposed bandpass filter.

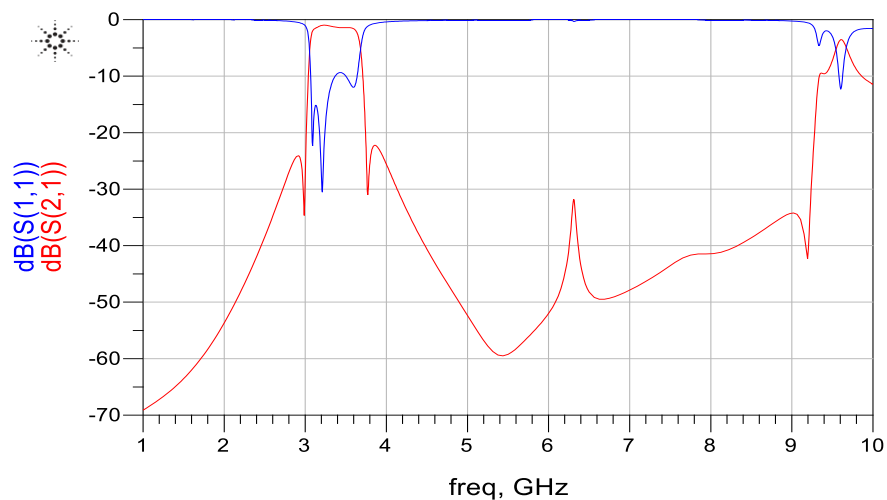


Fig. 3.16 Wide band frequency response of the proposed highly selective and very wide stopband bandpass filter.

Photograph and configuration of the filter with three finger interdigitally coupled feed-line is shown in Fig. 3.17 and simulation and measured results are depicted in Fig. 3.18 and Fig. 3.19. The interdigital feed-lines create a pair of transmission zeros above and below the filter's passband to provide a sharper roll-off and steep skirt selectivity [9]. The filter is centred at 3.34 GHz and has an insertion-loss of 1.16 dB, return-loss better than 10.46 dB, 3-dB bandwidth of 800 MHz (3-3.8 GHz). The filter has a 3-dB fractional bandwidth of 17.8% and a rejection level higher than 23-dB up to 9.3 GHz. Simulation and optimization accomplished with the ADS™ Momentum software. The design parameters of the filter are: $W_a = 0.2$ mm, $l_1 = 2.636$ mm, $l_2 = 2$ mm, $l_3 = 5.47$ mm, $l_4 = 10.69$ mm, $L_{b1} = 2$ mm, $L_{b2} = 1$ mm, $L_{b3} = 16.98$ mm, $S_1 = 0.64$ mm, $S_2 = 0.277$ mm.

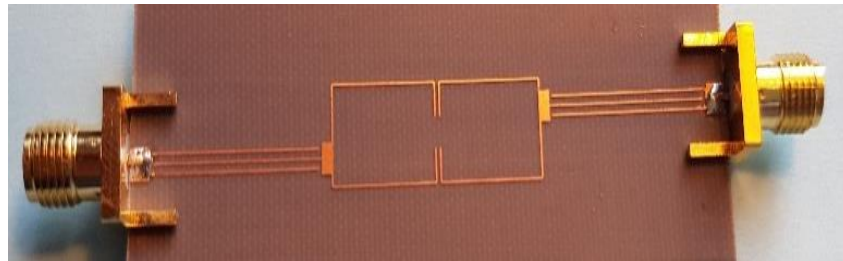
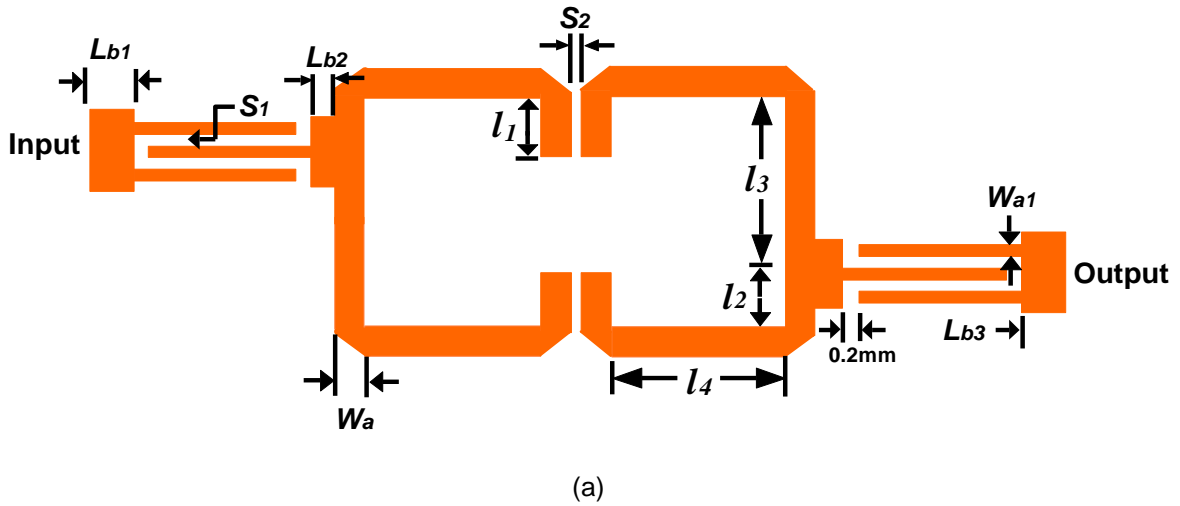


Fig. 3.17 (a) Configuration of the filter with three finger interdigital coupled feed-line, and (b) photograph of the filter.

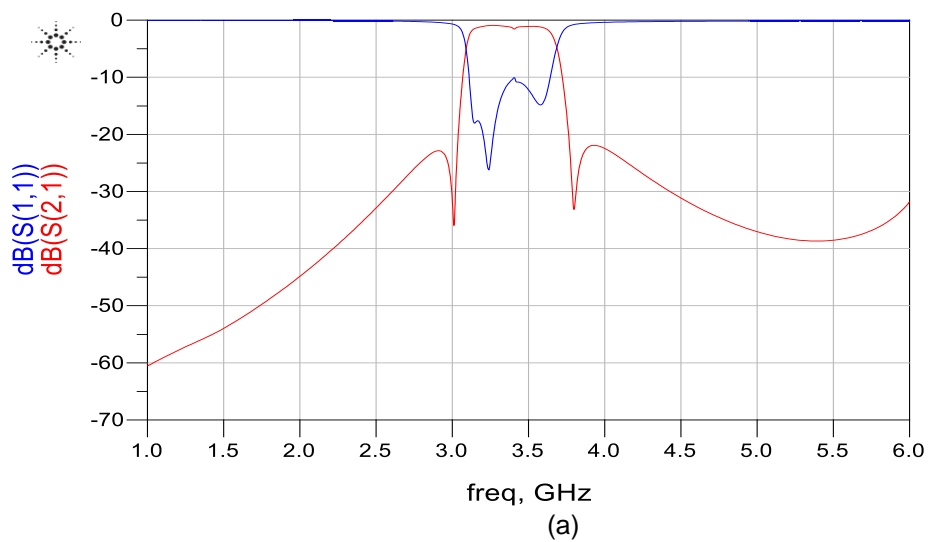
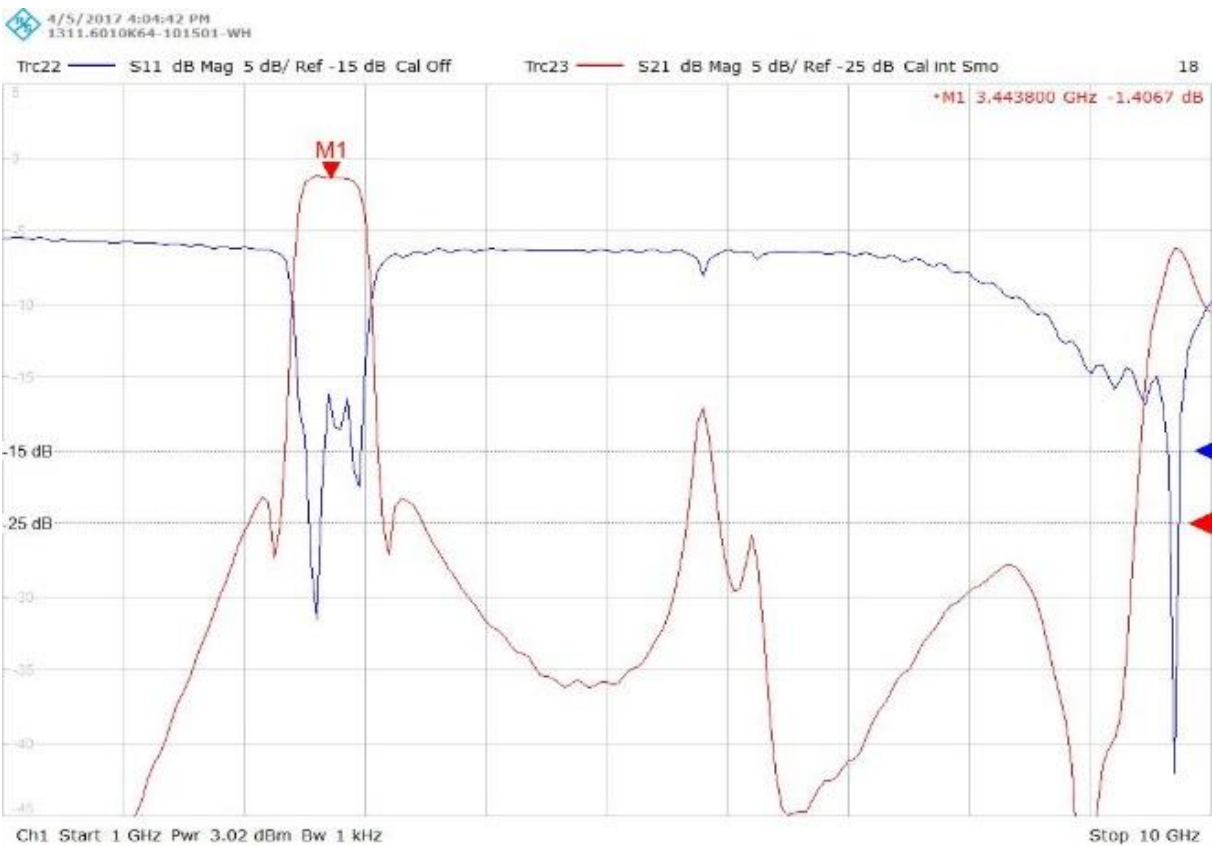


Fig. 3.18 S-parameter simulation response of the proposed filter



(a)



(b)

Fig. 3.19 Measured response (a) (narrow band view) (b) (wideband view).

Simulation analysis shows an increase in L_{b3} , degrades the return-loss, and it approaches to 7 dB as shown in Fig. 3.20. The bandwidth of the proposed filter can be reduced by increasing the separation (S_2) between the resonators as shown in above Fig. 3.10. The centre frequency of the filter can be tuned by varying the Length l_4 , as shown in Fig. 3.21. The centre frequency can be shifted by 176 MHz by changing l_4 from 11.09 mm to 10.29 mm. The upper and lower transmission zeros can be controlled by lengths l_2 and l_3 . The lower transmission zero shifts towards lower frequencies by increasing the value of l_3 . The upper transmission zero can be made to shift towards lower frequencies when l_2 is increased from its optimized value as shown in Fig. 3.22. It is also observed that length l_1 effect the filter response very much similar as the length l_4 .

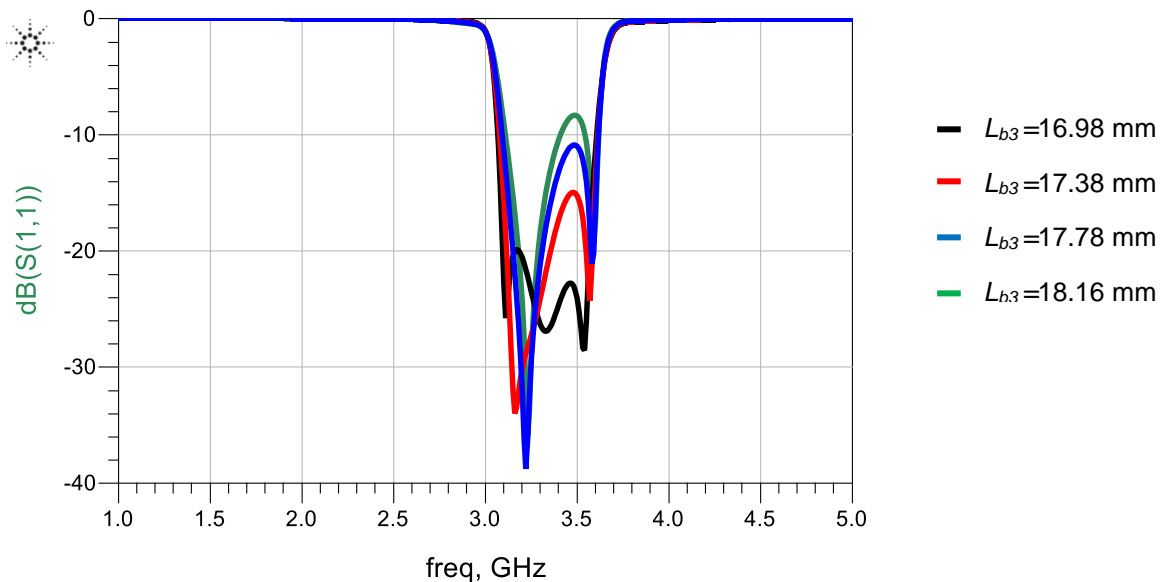


Fig. 3.20 Frequency response of the filter as a function of length L_{b3} .

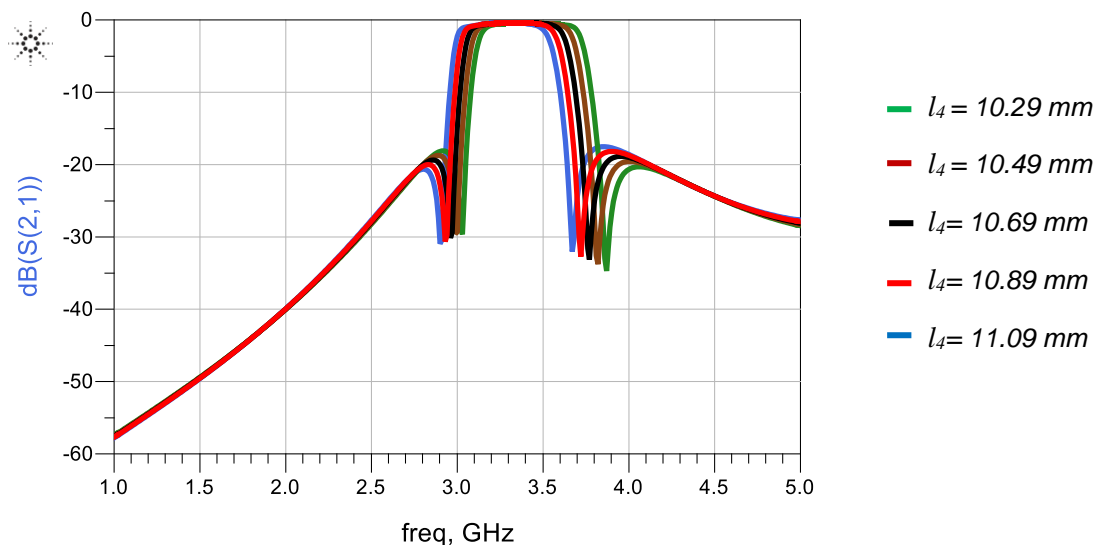


Fig. 3.21 Frequency response of the filter as a function of resonator length l_4 .

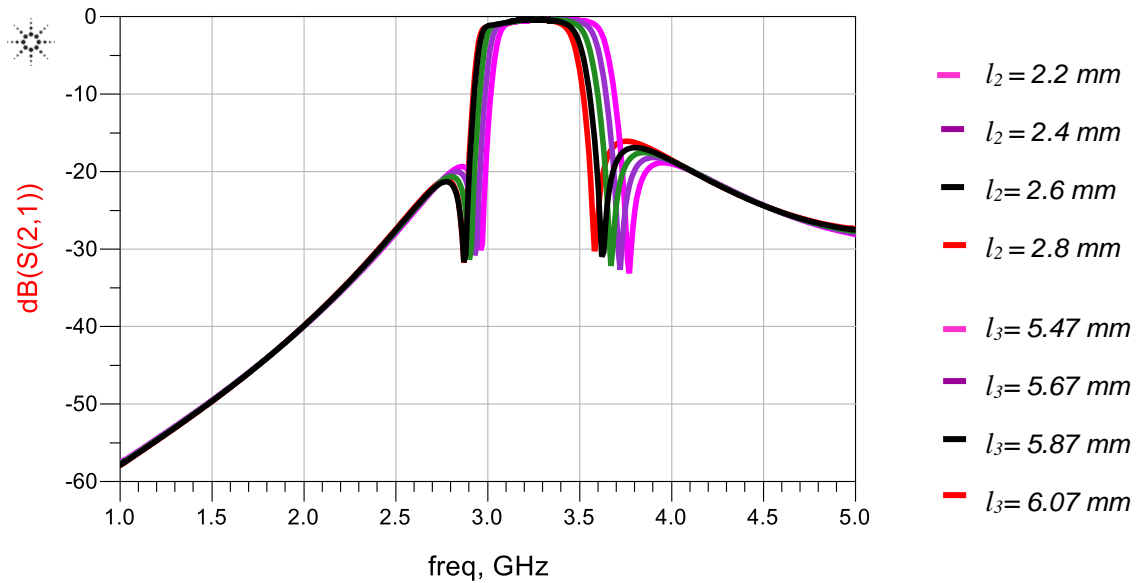


Fig. 3.22 Frequency response of the filter as a function of resonator length l_2 and l_3 , where the lower transmission zero is controlled by l_3 and the upper zero by l_2 .

The effect of the interdigital coupled feed-line length (L_{b3}) on the filter's performance is tabulated in Table 3.3 and graphically presented in Fig. 3.23. These results show the length of the interdigital coupled feed-line length has negligible effect on the filter's centre frequency and transmission zeros. However, it slightly affects the passband insertion-loss, which is 0.42 dB at $L_{b3} = 16.98$ mm. Fig. 3.24 and 3.25 show the effect of L_{b3} , on the return-loss and out-of-band rejection. Fig. 3.24 shows the return-loss improves with decrease in L_{b3} but the improvement in out-of-band rejection is marginal. Fig. 3.25 shows changes significantly with L_{b3} , which has an optimum value of 18.9 dB at 16.98 mm between 3.76 GHz to 6.03 GHz.

Table 3.3 Effect of coupled feed-line length on the characteristics of the filter.

L_{b3} (mm)	IL (dB)	RL (dB)	Out-of-band rejection (GHz)
17.78	0.84	10.88	17.7
17.38	0.46	14.99	18.4
16.98	0.45	26.64	20.8
16.58	0.46	38.72	17.76
16.18	0.52	34.72	16.87

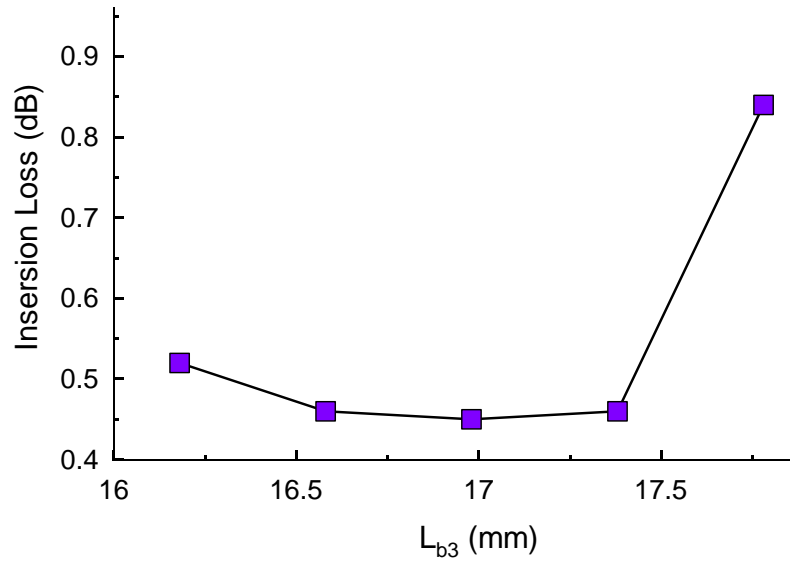


Fig. 3.23 Effect on the filter's insertion loss as a function of coupled feed-line length.

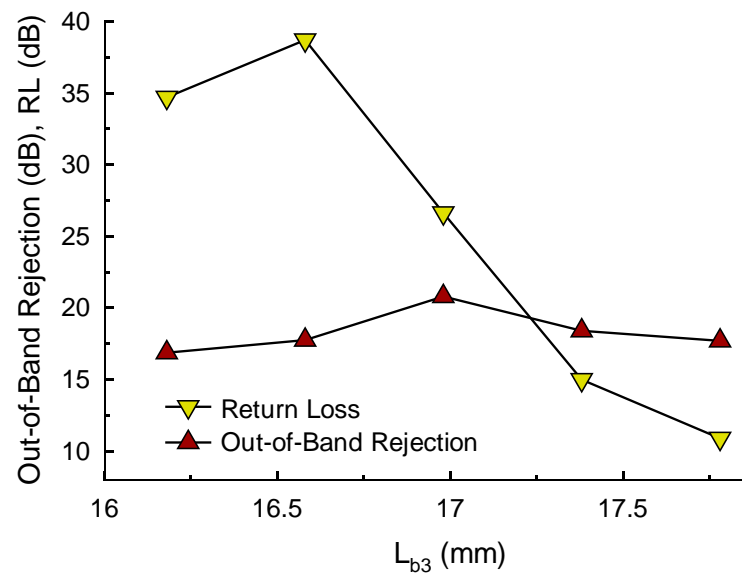


Fig. 3.24 Effect on the filter's out-of-band rejection and loss performance as a function of feed-line length L_{b3} .

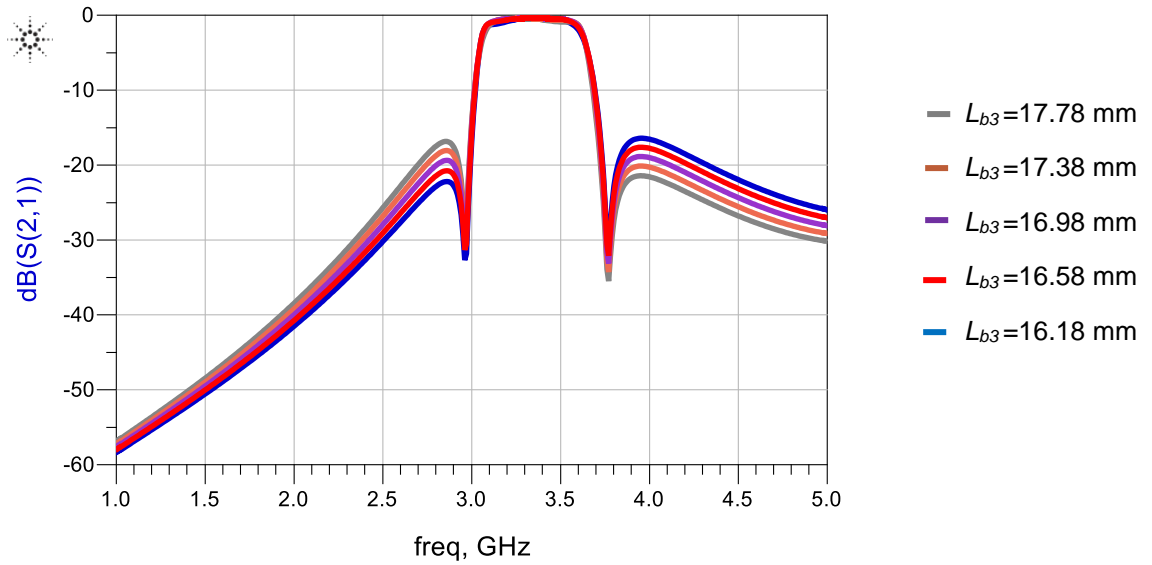


Fig. 3.25 Frequency response of the filter as a function of coupled feed-line length L_{b3} .

Table 3.4 and Figs. 3.26 to 3.28 show the effect of varying the width (W_{a1}) of the interdigital coupled lines. The results show the width affects the insertion-loss and out-of-band rejection of the filter. The insertion-loss significantly deteriorates with increase in width however the out-of-band improves moderately from 18.9 to 21.79 dB. For the optimum width of 0.2 mm the insertion-loss is 0.42 dB and out-of-band rejection is 18.9 dB between 3.76 GHz to 6.03 GHz.

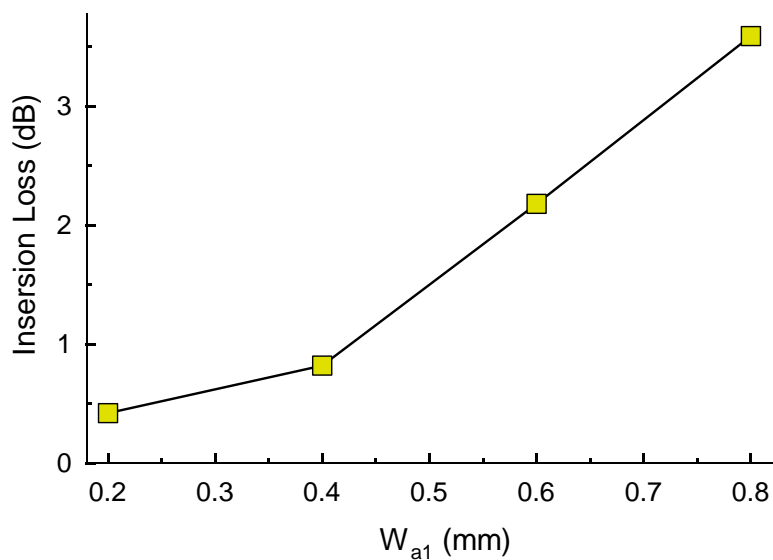


Fig. 3.26 Effect on the filter's insertion-loss as a function of coupled feed-line width.

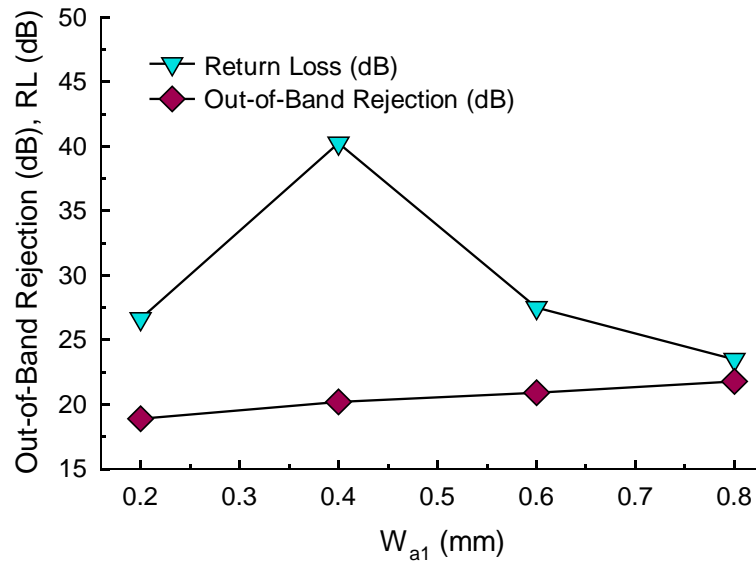


Fig. 3.27 Effect on the filter's out-of-band rejection as a function of coupled feed-line width.

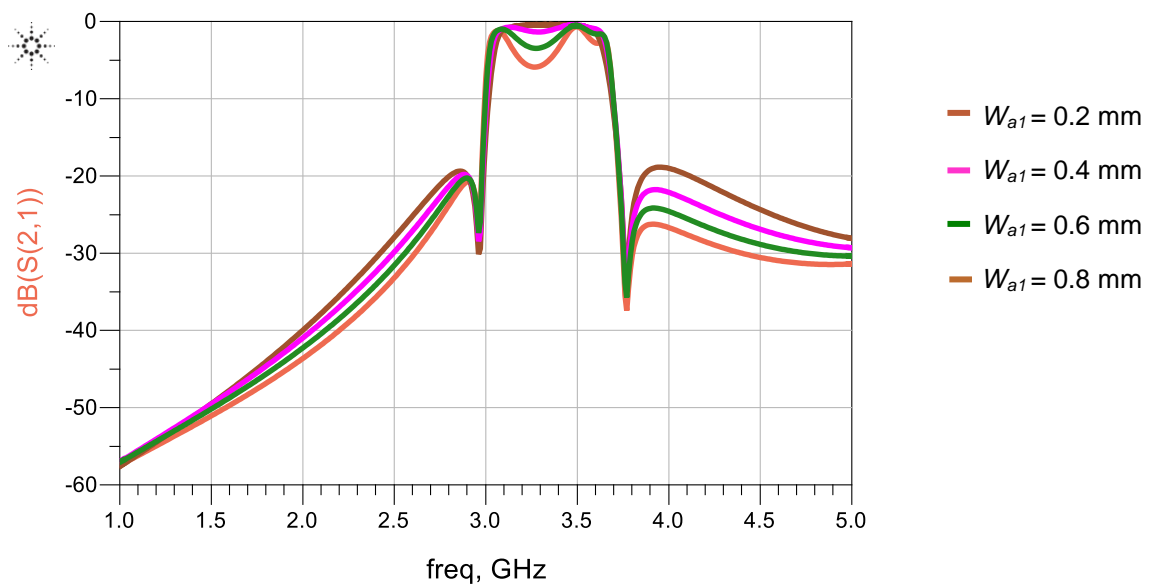


Fig. 3.28 Frequency response of filter as a function of coupled feed-line width.

Table 3.4 Effect of coupled feed-line width on the characteristics of the filter.

W_{a1} (mm)	IL (dB)	RL (dB)	Out-of-band rejection (GHz)
0.2	0.42	26.64	18.90
0.4	0.82	40.25	20.20
0.6	2.18	27.51	20.91
0.8	3.59	23.49	21.79

Simulation analysis shows the bandwidth of filter can be squeezed 38% by increasing the separation (S_2) between the two resonators as shown above in Fig. 3.10. The passband can be tuned by varying the length l_4 , in fact when the length is increased the passband shifts downwards in lower frequency. The upper and lower transmission zeros can be controlled by lengths l_2 and l_3 , as predicted by Eqs. (17) and (18). The lower transmission zero shifts downward in frequency by increasing l_3 , and the upper transmission zero shifts downward in frequencies when l_2 is increased.

The maximum 3-dB fractional bandwidth achievable is 17%, shown in Fig. 3.29. The dimensions of the structure defined in Fig. 3.17 are: $W_a = 0.2$ mm, $l_1 = 2.636$ mm, $l_2 = 2$ mm, $l_3 = 5.47$ mm, $l_4 = 10.69$, $L_{b1} = 2$ mm, $L_{b2} = 1$ mm, $L_{b3} = 15.978$ mm, $S_1 = 0.58$ mm, $S_2 = 0.277$ mm. The minimum 3-dB fractional bandwidth is about 5.52%, as shown in Fig. 3.30, and the corresponding dimensions of Fig. 3.17 are: $W_a = 0.2$ mm, $l_1 = 2.536$ mm, $l_2 = 2.736$ mm, $l_3 = 4.136$ mm, $l_4 = 10.47$ mm, $L_{b1} = 2.3$ mm, $L_{b2} = 1.74$ mm, $L_{b3} = 15.3088$ mm, $S_1 = 0.884$ mm, $S_2 = 0.89$ mm.

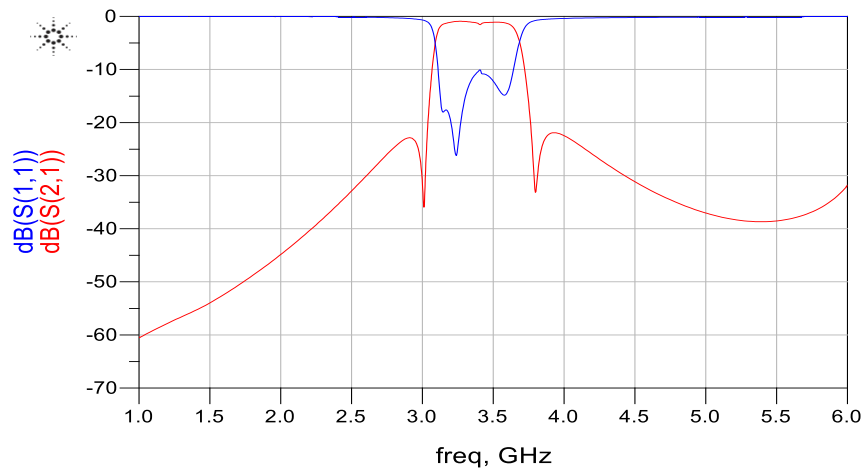


Fig. 3.29 Frequency response of the optimized filter.

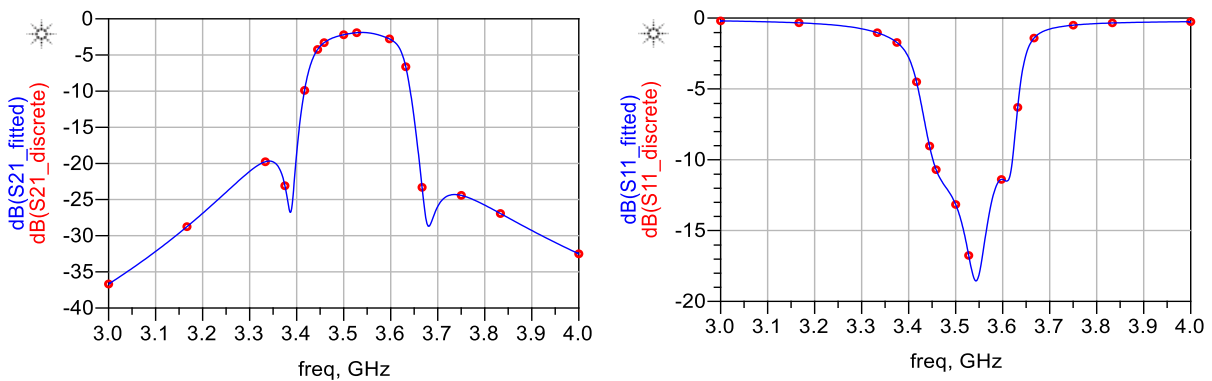


Fig. 3.30 The insertion and return-loss response for the narrowest 3-dB fractional bandwidth.

3.6 Summary

Selectivity and stopband performance of the quasi-elliptic function bandpass filter was enhanced by loading the input/output feed-lines with inductive stubs that introduce transmission zeros at specified frequencies in the filters response. Parametric study undertaken reveals the bandwidth and out-of-band rejection level can be controlled to some extent by modifying the spacing between the resonators and the width of the ring. The open-circuited inductive stubs were used to suppress harmonics generated by the filter across a wide bandwidth above and below the passband response, thereby ensuring the broad harmonic rejection characteristics without any degradation of passband characteristics.

Both theoretical analysis and simulations were done in order to validate the proposed structure. Further improvement in selectivity and stopband were achieved by interdigitally coupling the resonators to the input/output feed-lines. The interdigital feed-lines create a pair of transmission zeros above and below the filter's passband to provide a sharper roll-off and steep skirt selectivity with high rejection over a wide frequency span. This type of coupling scheme is shown to control the filter's bandwidth, and the minimum and maximum 3-dB fractional bandwidth achievable are 5.52% and 17%, respectively.

References

1. C.-W. Tang and Y.-K. Hsu, "A microstrip bandpass filter with ultrawide stopband," *IEEE Trans. Microw. Theory Tech.*, vol. 56, no. 6, pp. 1468–1472, 2008.
2. T. Lopetegi, M. A. G. Laso, F. Falcone, F. Martin, J. Bonache, J. Garcia, L. Perez-Cuevas, M. Sorolla, and M. Guglielmi, "Microstrip 'wiggly-line' bandpass filters with multispurious rejection," *IEEE Microw. Wireless Compon. Letter*, vol. 14, no. 11, pp. 531–533, Nov. 2004.
3. C.-F. Chen, T.-Y. Huang, and R.-B. Wu, "Design of microstrip bandpass filters with multiorder spurious-mode suppression," *IEEE Trans. Microw. Theory Tech.*, vol. 53, no. 12, pp. 3788–3793, Dec. 2005.
4. X. Luo, H. Qian, J.-G. Ma, and K. S. Yeo, "A compact wide stopband microstrip bandpass filter using quarter-wavelength shorted coupled lines," *Proc. Asia-Pacific Microw. Conf.*, 2010, pp. 1142–1145.
5. C.H. Kim and K. Chang, "Wide-stopband bandpass filters using asymmetric stepped-impedance resonators," *IEEE Microw. Wireless Compon. Letter*, vol. 23, no. 2, pp. 69–71, Feb. 2013.
6. L.-H. Hsieh and K. Chang, "Tunable microstrip bandpass filters with two transmission zeros," *IEEE Trans. Microw. Theory Tech.*, vol. 51, no. 2, pp. 520–525, Feb. 2003.
7. S.-Y. Lee and C.-M. Tsai, "New cross-coupled filter design using improved hairpin resonators," *IEEE Trans. Microwave Theory Tech.*, vol. 48, pp. 2482–2490, Dec. 2000.
8. K.C. Gupta, R. Garg, I. Bahl, and P. Bhartia, *Microstrip Lines and Slotlines*, 2nd ed. Boston, MA: Artech House, ch. 3.
9. S. Sun and L. Zhu, "Wideband microstrip ring resonator bandpass filters under multiple resonances," *IEEE Trans. Microw. Theory Tech.*, vol. 55, no. 10, pp. 2176–2182, Oct. 2007.

Compact Microstrip Bandpass Filter with Wideband Spurious Suppression

4.0 Introduction

Network synthesis techniques allow the efficient design of a bandpass filter for a given specifications. The resulting electrical network typically consists of ideal lumped element resonators, which are not practical at RF and microwave frequencies because of the short wavelength. Therefore, an additional step in the development of microwave bandpass filters is the realization of ideal resonators in distributed transmission-line media. Distributed resonators however do not behave as their ideal lumped element counterparts since they suffer from limited unloaded Q-factor and spurious harmonic resonances [1]. Although microwave filters are designed around the fundamental resonance frequency of the resonators, spurious passbands are almost always present at integer multiples of the first passband. While a multitude of bandpass filtering functions may be realised by various coupling schemes [2], the particular frequency behaviour of the resonator may also be exploited to realize enhanced filters such as those with wider stopbands or multiple passbands. This is especially applicable to distributed resonators since there is usually some degree of control over their frequency behaviour. The frequency response of planar resonators can be readily altered by introducing various structural changes for example to shift spurious harmonics outwards [3], introduce additional transmission zeros in the stopband [4],[5].

In this chapter a novel and highly compact microwave filter structure is proposed that is based on distributed transmission-lines. A simple technique to mitigate/reduce out-of-band spuri over a wideband. Finally, a filter structure is investigated that enables control of its 3-dB bandwidth by modifying its physical parameters.

4.1 Transmission-line Coupling Schemes

There are essentially three coupling configurations possible in cross-coupled microstrip filters, as shown in Fig. 4.1, where the coupling configuration results from various orientations of a pair of identical square open-loop resonators. It is evident that the coupling is from the proximity of the resonators through fringe electromagnetic fields associated with the microstrip lines constituting the resonators. In fact the nature and the extent of the fringe fields determine the nature and the strength of the coupling. At resonance, each of the resonators has a maximum

electric-field density at the side with an open gap, and the maximum magnetic-field density at the opposite side [2]. Because the fringe field exhibits an exponentially decaying character outside the region, the electric fringe field is stronger near the side having the maximum electric-field distribution, while the magnetic fringe field is stronger near the side having the maximum magnetic-field distribution. Electric coupling can be achieved when the open sides of coupled resonators are proximately placed as shown in Fig. 4.1(a).

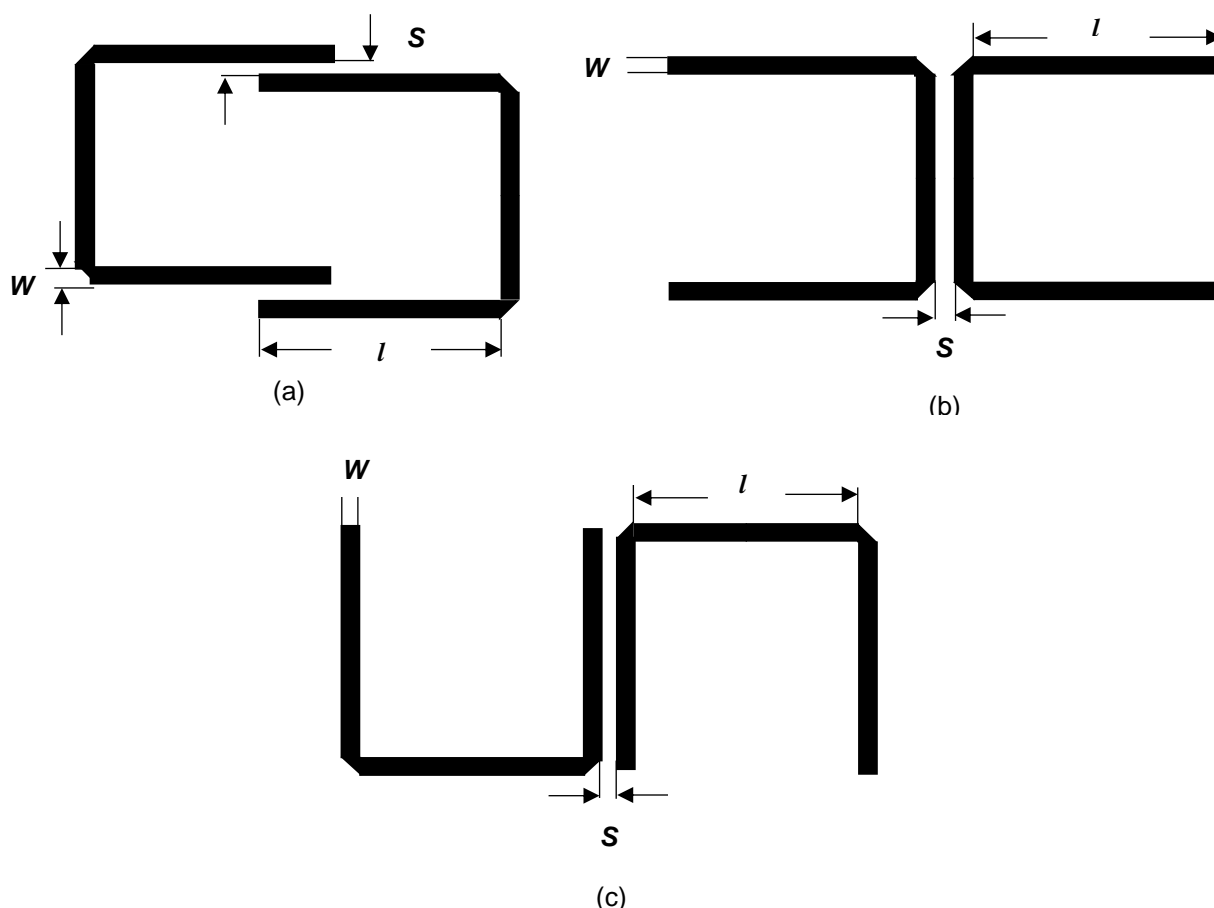


Fig.4.1 Transmission-line coupling configuration schemes, (a) electric coupling, (b) magnetic coupling, and (c) mixed coupling.

4.1.1 Electric Coupling

The equivalent lumped-element circuit model for the coupling structure in Fig. 4.1(a) at the fundamental mode near its resonance is shown in Fig. 4.2(a), where L and C are the self-inductance and self-capacitance so that \sqrt{LC} equals the angular resonant frequency of uncoupled resonators, and C_m represents the mutual capacitance. In this case the coupled structure considered is inherently distributed element so that the lumped-element circuit equivalence is valid over narrowband, near its resonance.

An alternative form of the equivalent circuit in Fig. 4.2(a) can be obtained from network theory [7], which is represented by the circuit in Fig. 4.2(b). When the symmetry plane T-T' in Fig. 4.2(b) is replaced by an electric wall (or a short-circuit), the resulting circuit has a resonant frequency:

$$f_e = 1/2\pi\sqrt{L(C + C_m)} \quad (4.1)$$

This resonant frequency is lower than that of uncoupled single resonator because the coupling effect enhances storage of charge of the single resonator when the electric wall is inserted in the symmetrical plane of the coupled structure. Similarly, replacing the symmetry plane in Fig. 4.2(b) by a magnetic wall (or an open-circuit) results in a single resonant circuit having a resonant frequency:

$$f_m = 1/2\pi\sqrt{L(C - C_m)} \quad (4.2)$$

In this case the resonant frequency is increased because the coupling effect reduces the capability of storing charge. Eqn. (4.1) and (4.2) can be used to determine the electric coupling coefficient k_E

$$k_E = \frac{f_m^2 - f_e^2}{f_m^2 + f_e^2} = \frac{C_m}{C} \quad (4.3)$$

This coupling coefficient is identical with the definition of ratio of the coupled electric energy to the stored energy of uncoupled single resonator.

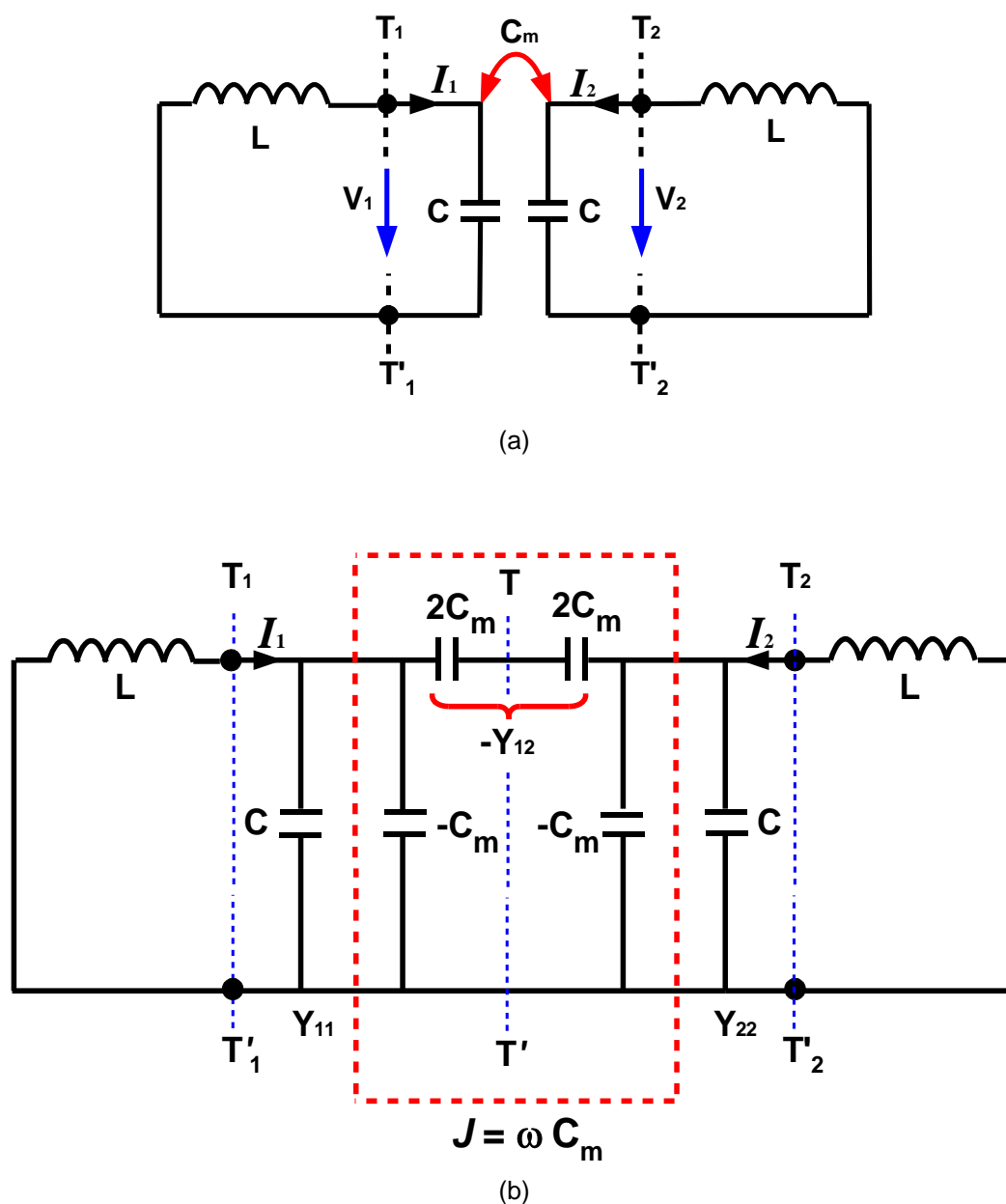


Fig. 4.2 (a) Equivalent lumped element model of electrical coupling, and (b) simplified equivalent circuit.

4.1.2 Magnetic Coupling

For the magnetically coupled resonator structure in Fig. 4.1 (b), the equivalent lumped element model is shown in Fig. 4.2(a), where L_m represents the mutual inductance. When the symmetry plane T-T' in Fig. 4.3(b) is replaced by an electric wall (or a short-circuit), the resultant circuit has a resonant frequency given by:

$$f_e = 1/2\pi\sqrt{(L - L_m)C} \quad (4.4)$$

The resonant frequency is increased due to the coupling effect reducing the stored flux in the single resonator when the electric wall is inserted in the symmetric plane. If a magnetic wall (or an open-circuit) replaces the symmetric plane in Fig. 4.3(b), the resultant single resonant circuit has a resonant frequency given by:

$$f_m = 1/2\pi\sqrt{(L + L_m)C} \quad (4.5)$$

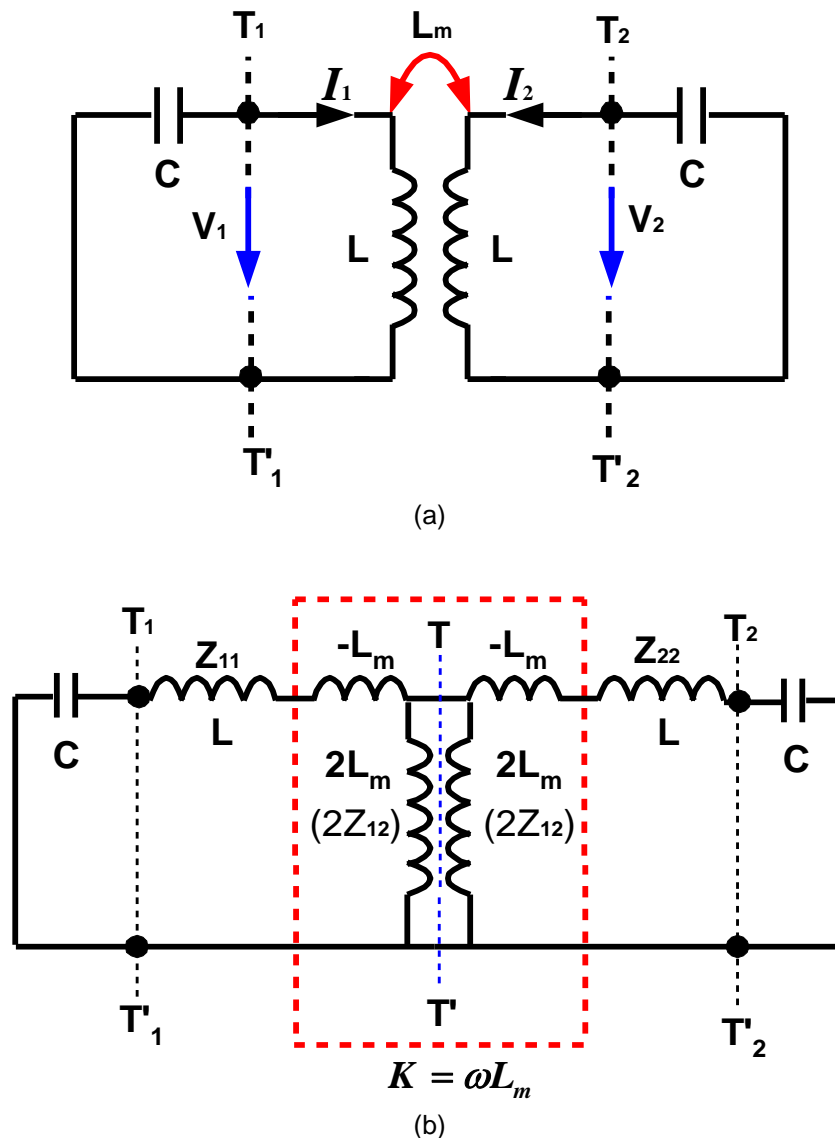


Fig. 4.3 (a) Equivalent lumped element model of magnetic coupling, and (b) simplified equivalent circuit.

The coupling has an effect of increasing the stored flux, so that the resonant frequency is shifted downward. Eqn. (4.4) and (4.5) can be used to find the magnetic coupling coefficient k_M

$$k_M = \frac{f_e^2 - f_m^2}{f_e^2 + f_m^2} = \frac{L_m}{L} \quad (4.6)$$

The magnetic coupling defined in Eqn.(4.6) corresponds to the definition of ratio of the coupled magnetic energy to the stored energy of uncoupled single resonator.

4.1.3 Mixed Coupling

The coupled resonator structure in Fig. 4.1(c) employs both the electric and magnetic coupling. This coupled structure can be representation by the network shown in Fig. 4.4(a), where C , L , C'_m and L'_m are the self-capacitance, the self-inductance, the mutual capacitance, and the mutual inductance of the associated equivalent lumped element circuit in Fig. 4.4(b).

By inserting an electric wall and a magnetic wall into the plane of the symmetry in Fig. 4.4(b) we obtain the following electric and magnetic resonant frequencies:

$$f_e = \frac{1}{2\pi\sqrt{(L - L'_m)(C - C'_m)}} \quad (4.7)$$

$$f_m = \frac{1}{2\pi\sqrt{(L + L'_m)(C + C'_m)}} \quad (4.8)$$

These two equations show both the magnetic and electric couplings have the same effect on the resonant frequency shift. From Eqn. (4.7) and (4.8), the mixed coupling coefficient k_X

$$k_X = \frac{f_e^2 - f_m^2}{f_e^2 + f_m^2} = \frac{CL'_m + LC'_m}{LC + L'_mC'_m} \quad (4.9)$$

This indicates that the mixed coupling results from the superposition of the magnetic and electric couplings.

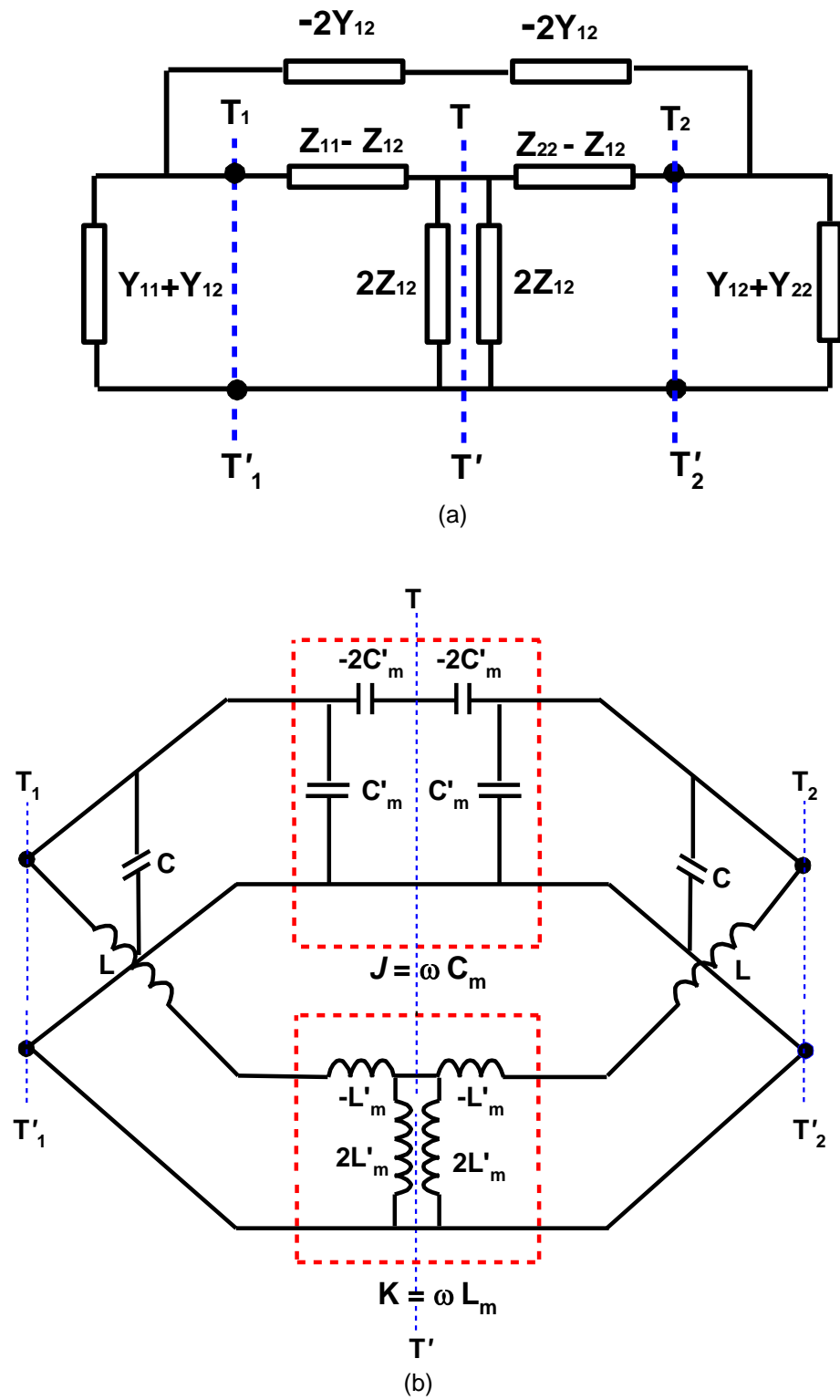
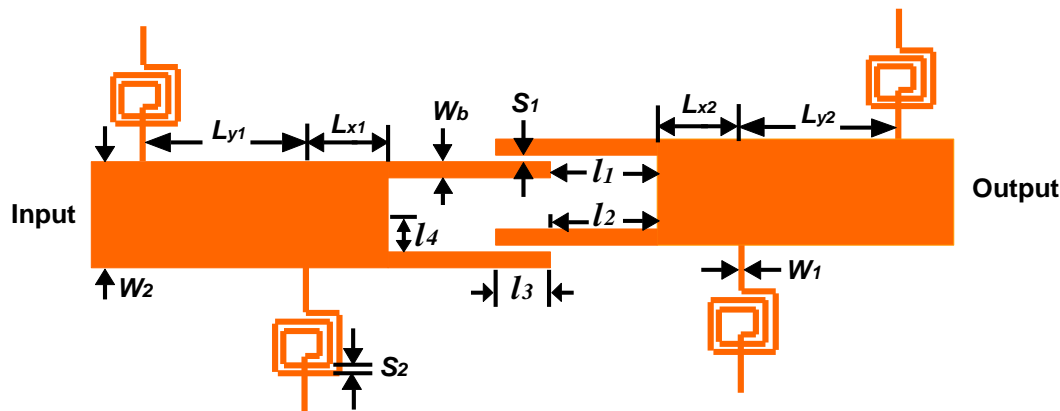


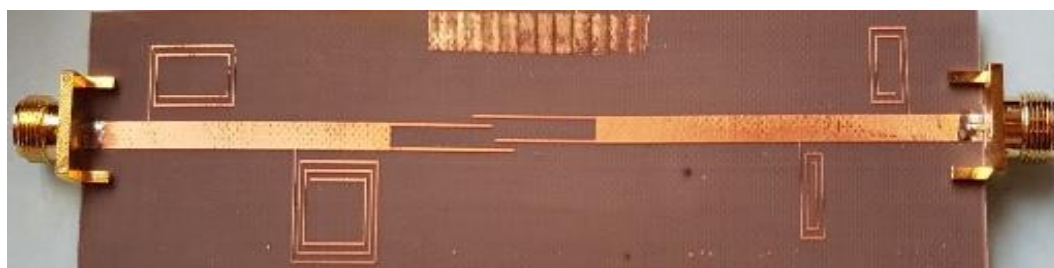
Fig. 4.4 (a) Network representation of coupled resonator with mixed coupling, and (b) simplified equivalent circuit.

4.2 Electrically Coupled Bandpass Filter Structure

A highly compact bandpass filter structure based on electrically coupled transmission-line is proposed in Fig. 4.5, which comprises 50Ω input and output feed-lines that are electromagnetically coupled to each other with high impedance parallel transmission-lines. The filter's out-of-band rejection was initially only -15 dB. The out-of-band spurious responses are suppressed by loading the input and output feed-lines with a pair of spiral shaped inductive lines of width 0.2 mm and gap spacing of 0.6 mm, as shown in Fig. 4.5. The inductive lines are spiralled to reduce the width of structure. The filter was constructed on dielectric substrate Arlon CuClad217LX with thickness (h) of 0.794 mm, dielectric constant (ϵ_r) of 2.17 mm, copper conductor thickness (t) of $35\ \mu\text{m}$, and loss-tangent ($\tan\delta$) of 0.0009. The width of the 50Ω feed-lines is 2.42 mm. Fig. 4.6 shows the simulated response of the filter with no spiral loading on the feed-lines. The filter has a passband centred at 3.35 GHz with transmission zeros located above and below the passband at 3.08 GHz and 3.71 GHz, respectively. The parameters of the filter were optimized using ADSTM software, which are: $W_1 = 0.2\ \text{mm}$, $W_2 = 2.42\ \text{mm}$, $l_1 = 15.26\ \text{mm}$, $l_2 = 11.89\ \text{mm}$, $l_3 = 2.84\ \text{mm}$, $l_4 = 0.9\ \text{mm}$, $S_1 = 0.7\ \text{mm}$, $S_2 = 0.6\ \text{mm}$, $L_{x1} = 13.37\ \text{mm}$, $L_{x2} = 29\ \text{mm}$, $L_{y1} = 21.38\ \text{mm}$, $L_{y2} = 14.78\ \text{mm}$, and $W_b = 0.2\ \text{mm}$.



(a)



(b)

Fig. 4.5 (a) Layout of proposed bandpass filter with loaded inductive lines, and (b) Photograph of the implemented filter.

The simulated frequency response of the filter with and without spirals on feed-line, shown in Fig. 4.6, is centred at 3.4 GHz and has an insertion-loss of better than 1.71 dB, which is mainly attributed to losses in the conductor and dielectric substrate. The filter has a return-loss higher than 23-dB and stopband rejection level of better than 20 dB between 1-3 GHz and 3.7-5.0 GHz. The filter has a 3-dB bandwidth and fractional bandwidth of 0.24 GHz and 7.4%, respectively. The transmission zeros at 3.03 GHz and 3.72 GHz are due to the tapping positions of the feed-lines with resonators, which were calculated using Eqns. 3.17 and 3.18. Fig. 4.6 (a) shows transmission zeros at 1.8 GHz and 2.8 GHz, which are due to the two spirals loaded on left-hand side feed-line, while transmission zeros at 3.9 GHz and 4.4 GHz are due to the two spirals loaded on the right-hand side feed-line.

The effect of the inter-resonator coupling gap (S_1) on the filter's centre frequency (f_0), insertion-loss (IL) and out-of-band rejection level performance is tabulated in Table 4.1 and graphically depicted in Fig. 4.8 and 4.9. The coupling gap has a slight effect on the centre frequency ($\pm 2.4\%$), however the insert-loss drops significantly from 3-dB to 1.71 dB with increase in gap size from 0.3 mm to 0.7 mm. Hence, in the design the gap size was made to be 0.7 mm. Fig. 4.9 and Fig. 4.10 show the out-of-band rejection level increases with increase in coupling gap. The out-of-band rejection increases by 6.4 dB for change in coupling gap from 0.3 mm to 0.7 mm. The 3-dB fractional bandwidth changes from 16.72% to 8.98% for coupling gap increase from 0.3 mm to 0.7 mm. Fig. 4.10 shows the filter exhibits a very sharp 3-dB roll-off or skirt. As explained in [19], this kind of filter structure with parallel coupled resonators provides comparatively large coupling for a given space and has a wider bandwidth as compared to conventional end-coupled microstrip filter structures.

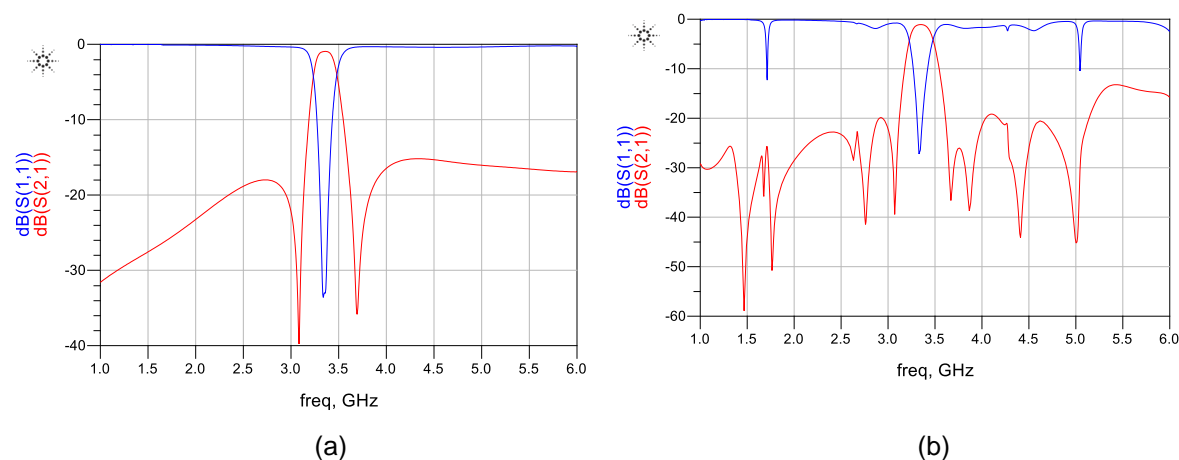
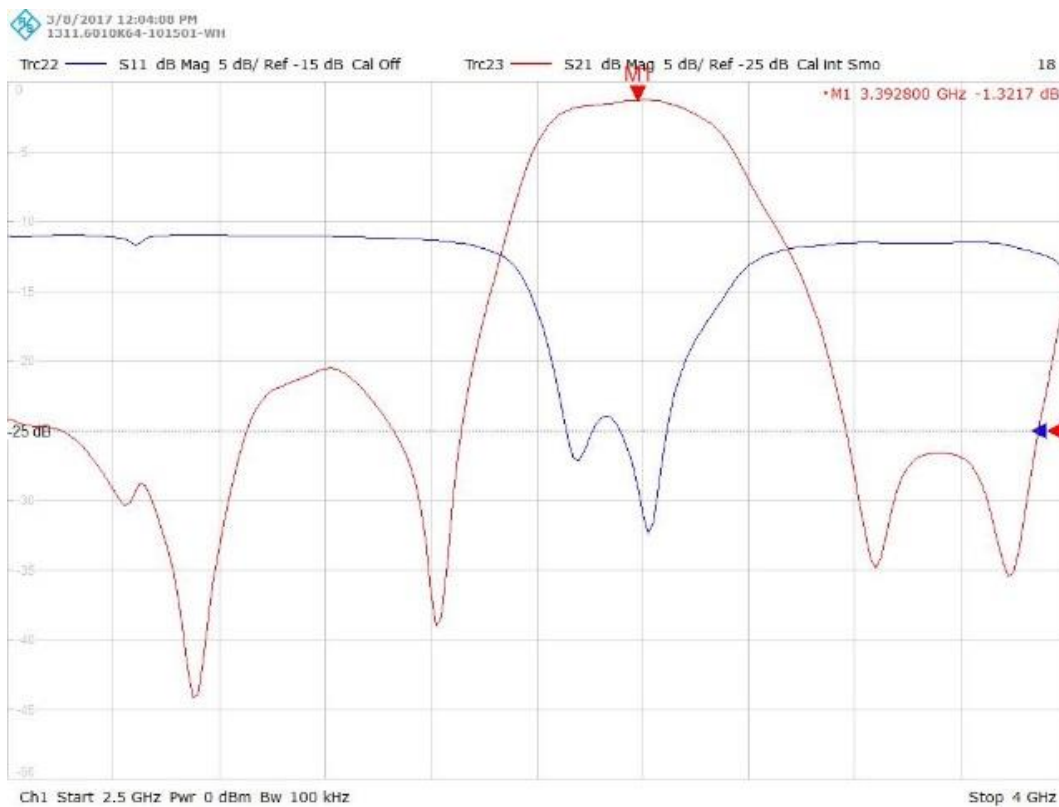
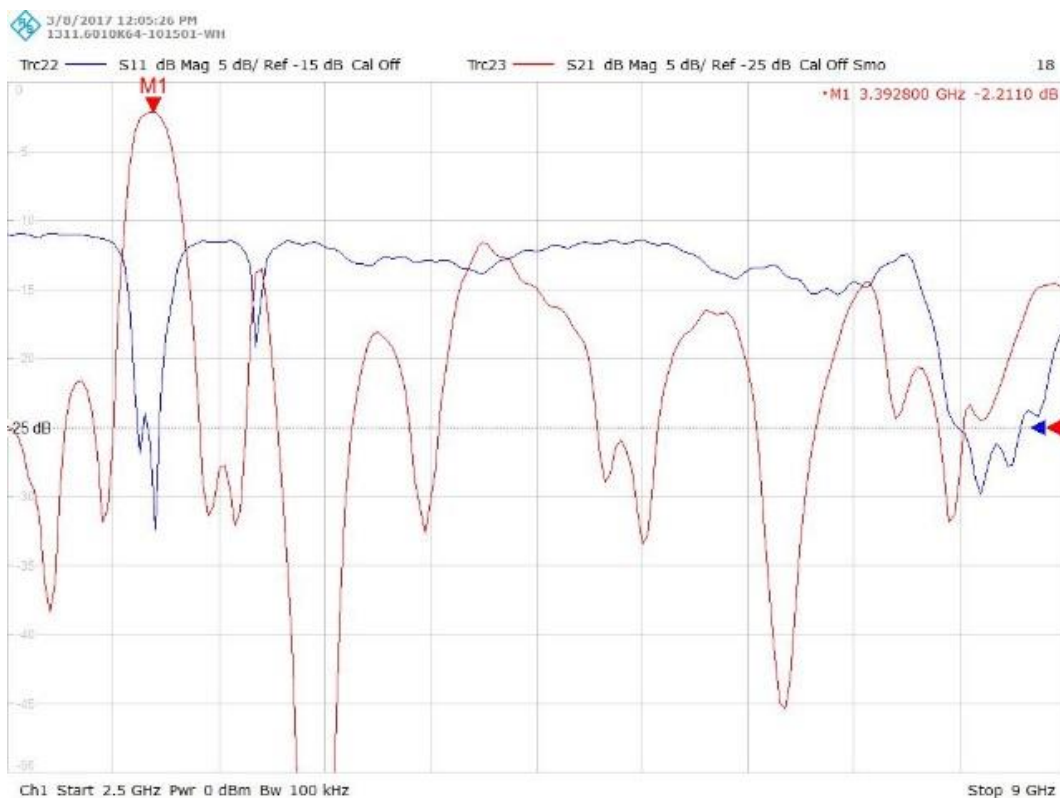


Fig. 4.6 Simulated S-parameter response of the proposed bandpass filter (a) without spirals (b) with spirals



(a)



(b)

Fig. 4.7 Measured performance (a) (narrowband view) (b) (wideband view)

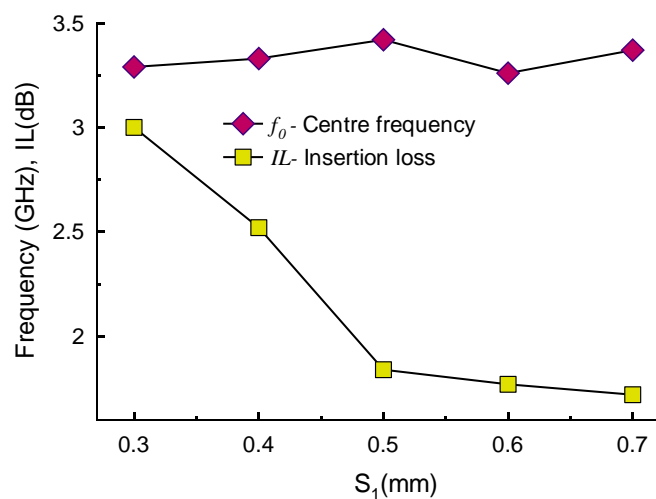


Fig. 4.8 Effect of inter-resonator coupling gap on the centre frequency and loss performance of the filter.

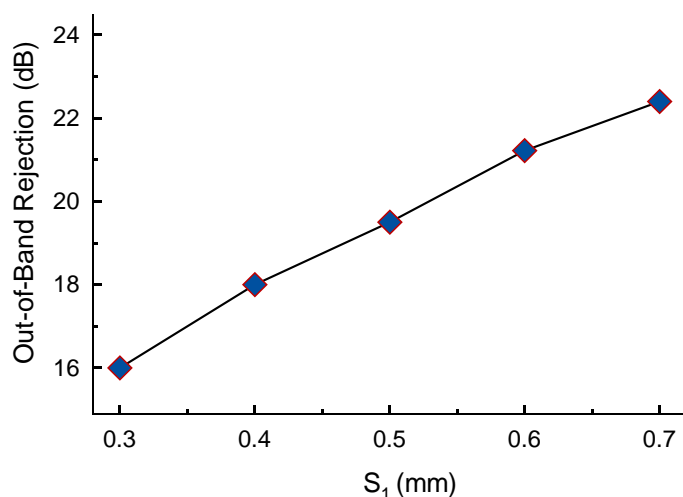


Fig. 4.9 Effect of inter-resonator coupling gap on the out-of-band rejection level of the filter.

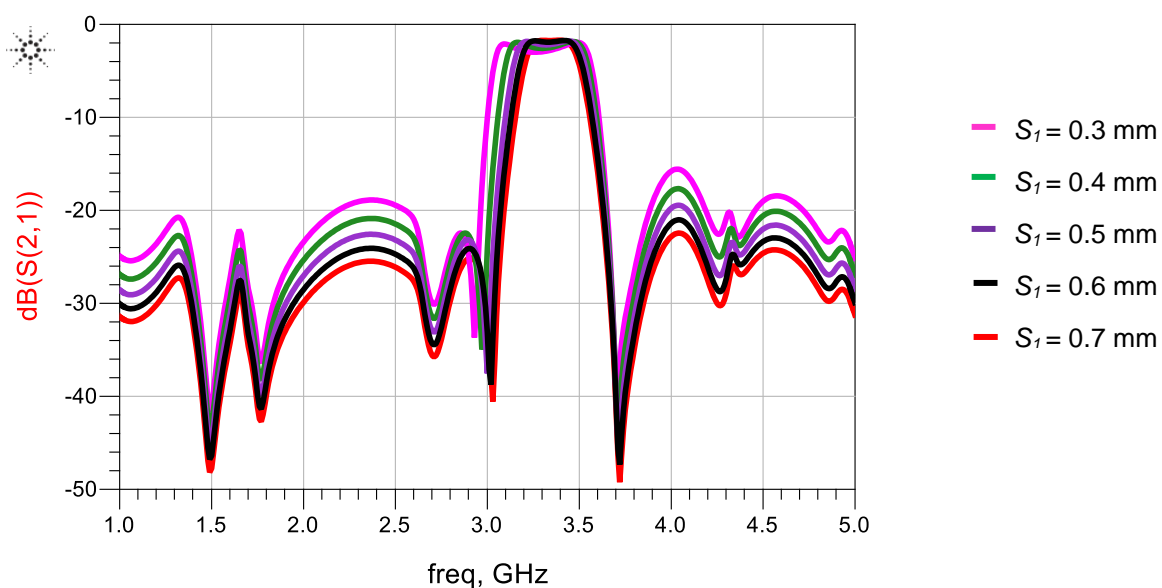


Fig. 4.10 Frequency response of the proposed filter as a function of inter-resonator coupling gap.

Table 4.1. Effect of inter-resonator coupling on the filter's centre frequency, insertion-loss, out-of-band rejection level, 3-dB bandwidth and fractional bandwidth performance.

S_1 (mm)	f_o (GHz)	IL (dB)	Out-of-band rejection (dB)	3dB Bandwidth (GHz)	3dB Fractional bandwidth (%)
0.3	3.29	3.00	16.0	0.55	16.72
0.4	3.33	2.52	18.0	0.44	13.17
0.5	3.40	1.84	19.5	0.38	11.38
0.6	3.26	1.77	21.2	0.35	10.48
0.7	3.37	1.71	22.4	0.30	8.98

A comparison study of coupling length (l_3) on the proposed filter's passband transmission zero frequencies (f_{tz4} and f_{tz5}), centre frequency (f_o), insertion-loss and out-of-band rejection level is tabulated in Table 4.2 and graphically depicted in Fig.4.11 and 4.12. It is evident from Fig. 4.11 the passband response shifts linearly downwards in frequency with increase in coupling length. However, the insertion-loss abruptly increased to a maximum of 3.9 dB at a coupling length of 4.84 mm. Low-loss is obtained for shorter coupling lengths of about 3 mm. The out-of-band rejection also increased as coupling length was reduced to about 3 mm, as shown in Fig. 4.12.

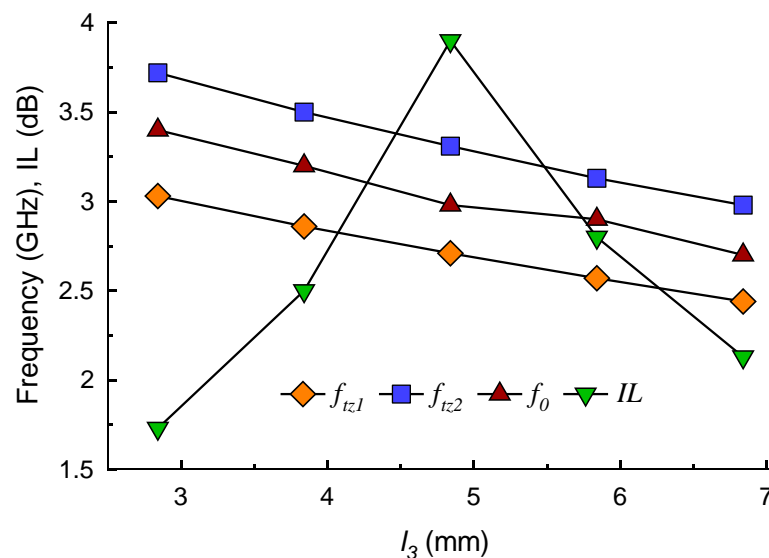


Fig. 4.11 Effect of coupling length on the filter's passband transmission zeros, centre frequency, and insertion-loss.

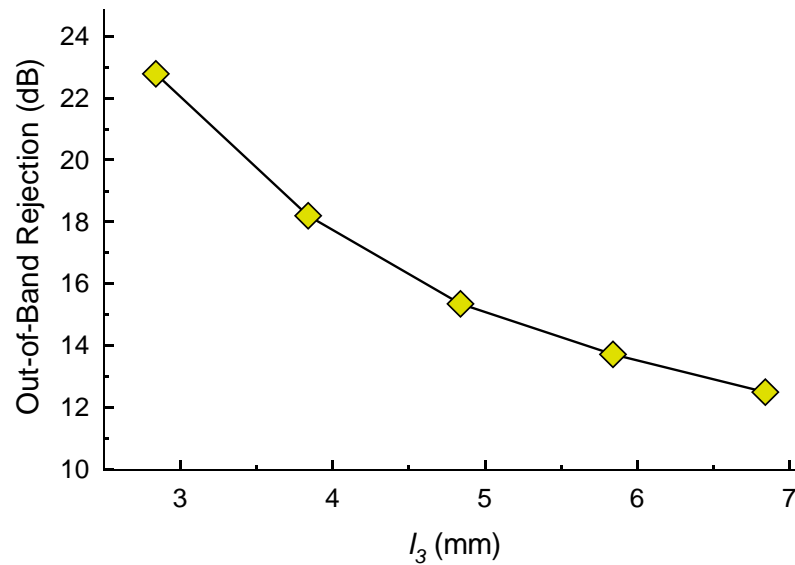


Fig. 4.12 Effect of coupling length on the out-of-band rejection level.

The filter's response is affected by the coupling length (l_3) as shown in Fig. 4.13. When the coupling length is increased, the centre frequency of the filter, and the lower and upper transmission zeros, shift downward in frequency. The consequence of this is severe deterioration in its passband and out-of-band response. These results show that the coupling length is very critical in determining the overall transmission response of the filter and out-of-band rejection. The optimized value of the coupling length was determined to be 2.84 mm for which the passband was centred at 3.34 GHz with insertion-loss of about 1.33-dB and the out-of-band rejection level was about 23-dB between 1 to 3 GHz and 3.7 to 5 GHz. The filter had a sharp passband skirt.

Table 4.2. Effect of coupling length on the filter's passband transmission zeros, centre frequency, insertion-loss and out-of-band rejection level performance.

l_3 (mm)	f_{tz4} (GHz)	f_{tz5} (GHz)	f_o (GHz)	IL (dB)	Out-of-band rejection (dB)
4.04	2.83	3.46	3.12	2.65	17.27
3.74	2.88	3.52	3.17	2.36	18.25
3.44	2.93	3.58	3.21	2.12	19.40
3.14	2.98	3.65	3.29	1.88	20.77
2.84	3.03	3.72	3.40	1.71	22.48

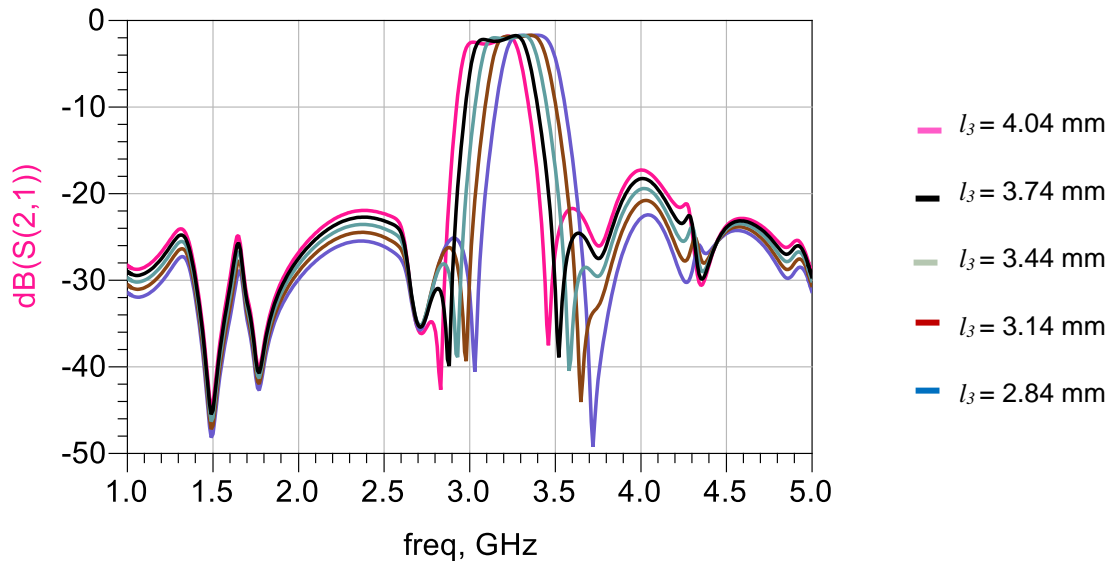


Fig. 4.13 Frequency response of the proposed filter as a function of coupled resonator length.

The effect of the position of the spiral load (L_{x2}) on the filter's characteristics is tabulated in Table 4.3 and graphically presented in Fig. 4.14 to 4.16. The location of the spiral load has no effect on the transmission zeros and centre frequency, however it increases the insertion-loss by 31% and reduces the out-of-band rejection by 30% when the location is reduced from 29 mm to 13 mm. The position of spiral load (L_{x1}) behaves similarly.

Table 4.3. The effect of the spiral load location on the filter's passband transmission zeros, centre frequency, insertion-loss and out-of-band rejection performance.

L_{x2} (mm)	f_{tz4} (GHz)	f_{tz5} (GHz)	f_o (GHz)	IL (dB)	Out-of-band rejection (dB)
29	3.03	3.72	3.4	1.71	22.4
25	3.03	3.72	3.4	1.80	13.2
21	3.03	3.72	3.4	1.92	12.4
17	3.03	3.72	3.4	2.13	12.3
13	3.03	3.72	3.4	2.26	15.7

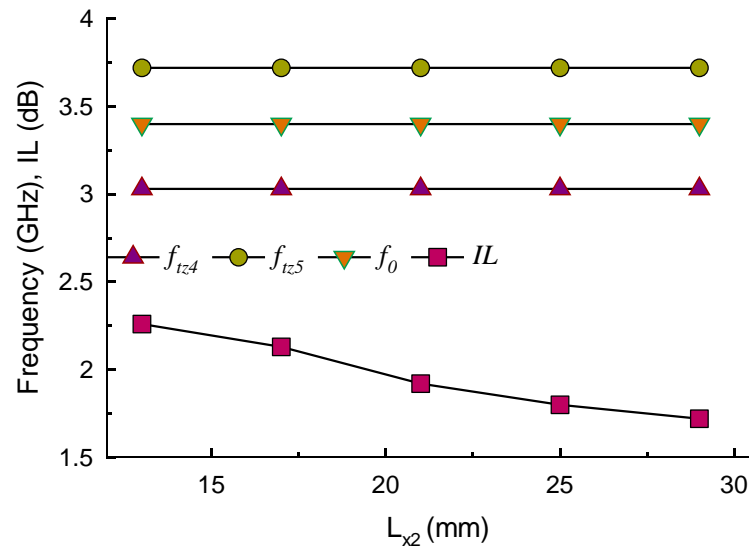


Fig. 4.14 Effect of spiral stub location (L_{x2}) on the filter's passband transmission zeros, centre frequency and insertion-loss performance.

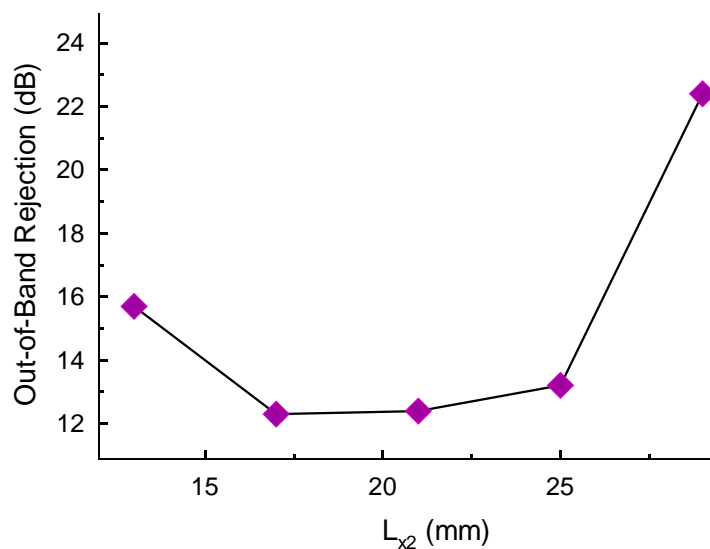


Fig. 4.15 Effect of spiral stub location (L_{x2}) on the filter's out-of-band rejection.

The impact on the filter's characteristics by the distance between the two spiral loading (L_{y2}) was also investigated. The results of this investigation are tabulated in Table 4.4 and presented in Fig. 4.17 to 4.19. The inter-spiral load gap has no effect on the filter's centre frequency and the passband transmission zeros; however, it causes the filter loss to increase by 15.6% and reduces the out-of-band by 31.7% when it's reduced from 14.78 mm to 6.78 mm. The inter-spiral load gap (L_{y1}) behaves similarly.

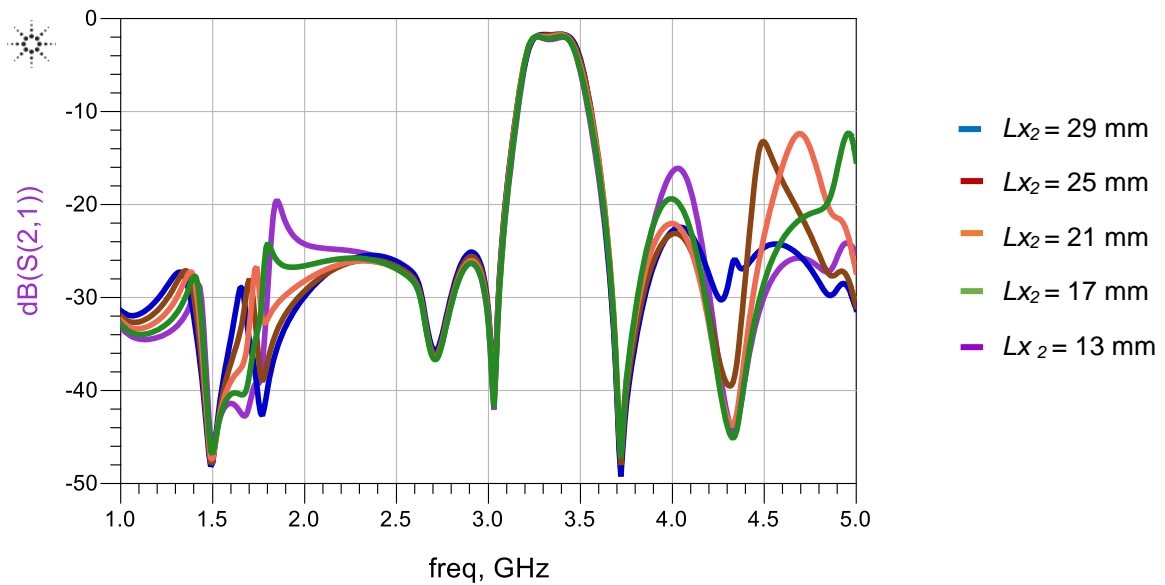


Fig. 4.16 Frequency response of the proposed filter as a function of spiral stub location (L_{x2}).

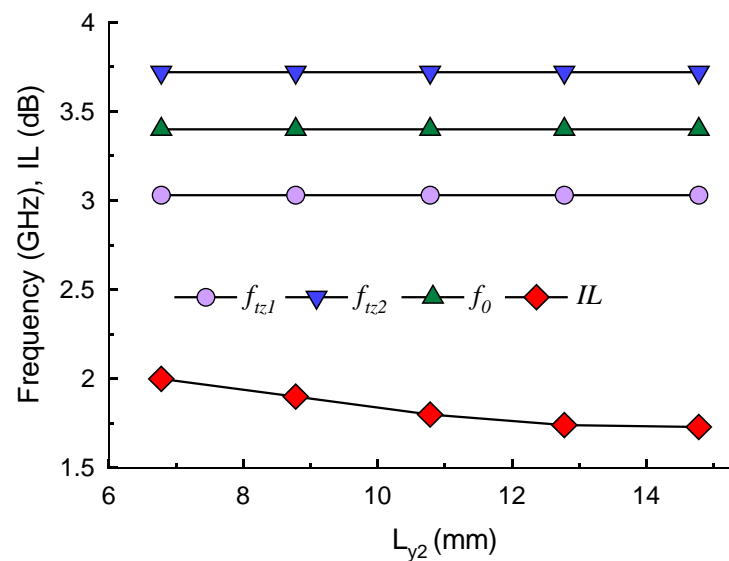


Fig. 4.17 Effect of the inter-spiral loading gap (L_{y2}) on the passband transmission zeros, centre frequency and loss performance.

Table 4.4 Effect of the inter-spiral loading gap (L_{y2}) on the filter's passband transmission zeros, centre frequency, insertion-loss and out-of-band rejection level performance.

L_{y2} (mm)	f_{1z4} (GHz)	f_{1z5} (GHz)	f_0 (GHz)	IL (dB)	Out-of-band rejection (dB)
14.78	3.03	3.72	3.4	1.71	22.4
12.78	3.03	3.72	3.4	1.74	21.6
10.78	3.03	3.72	3.4	1.80	18.0
8.78	3.03	3.72	3.4	1.90	16.0
6.78	3.03	3.72	3.4	2.00	15.3

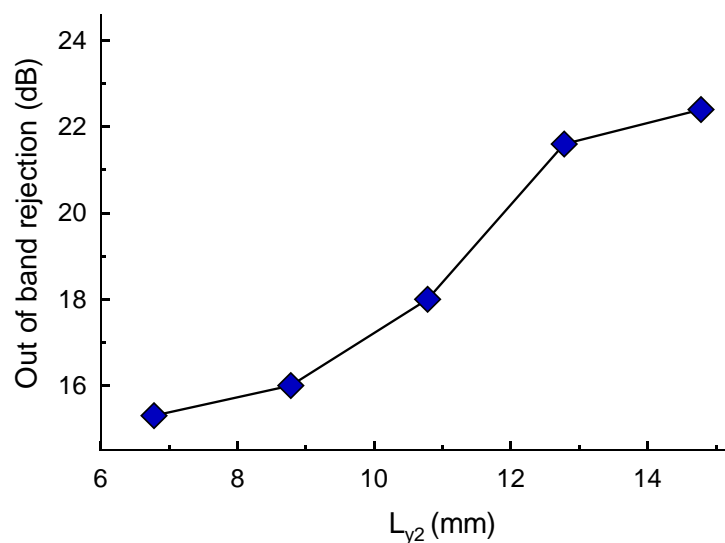


Fig. 4.18 Effect of feed-line length on band rejection level as a function of L_{y2} .

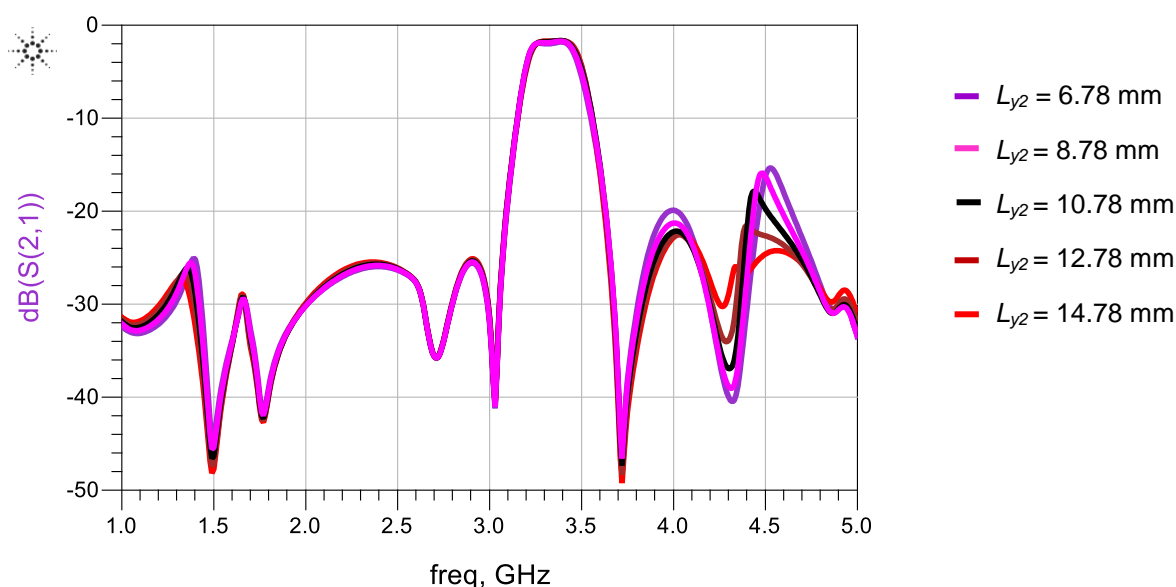


Fig. 4.19 Frequency response of the proposed filter as a function of inter-spiral gap (L_{y2}).

Width of the coupled resonators (W_b) on the filter's characteristics was also investigated. The results are given in Table 4.5 and graphically presented in Fig. 4.20 and 4.21. With increase in width from 0.20 mm to 1.40 mm the centre frequency and passband transmission zeros of the filter drops down in frequency almost linearly by 16.5%, however the loss increases severely by 1.57 dB from 1.71 dB to 3.30 dB, and its 3-dB bandwidth deteriorates for widths less than 0.8 mm as is evident in Fig. 4.21. The results show the width (W_b) can be used to control the centre frequency of the passband by 225 MHz with negligible impairment in loss and out-of-band rejection level.

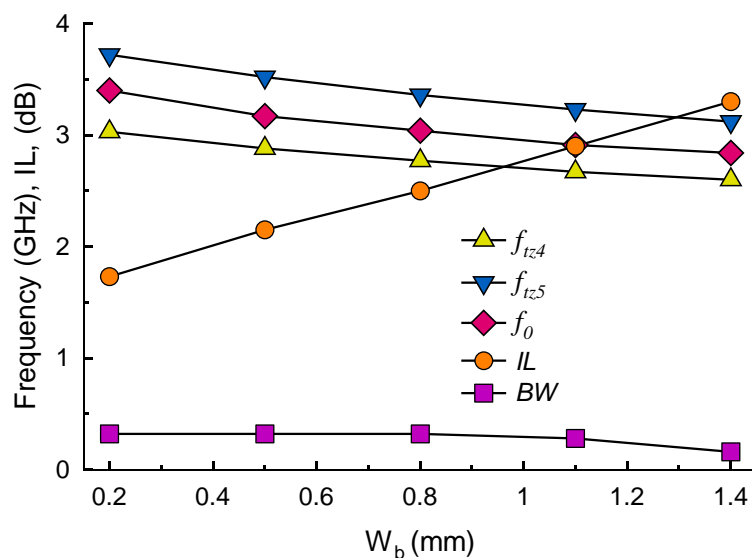


Fig. 4.20 Effect of coupled resonator width on filter's passband transmission zeros, centre frequency, and loss performance.

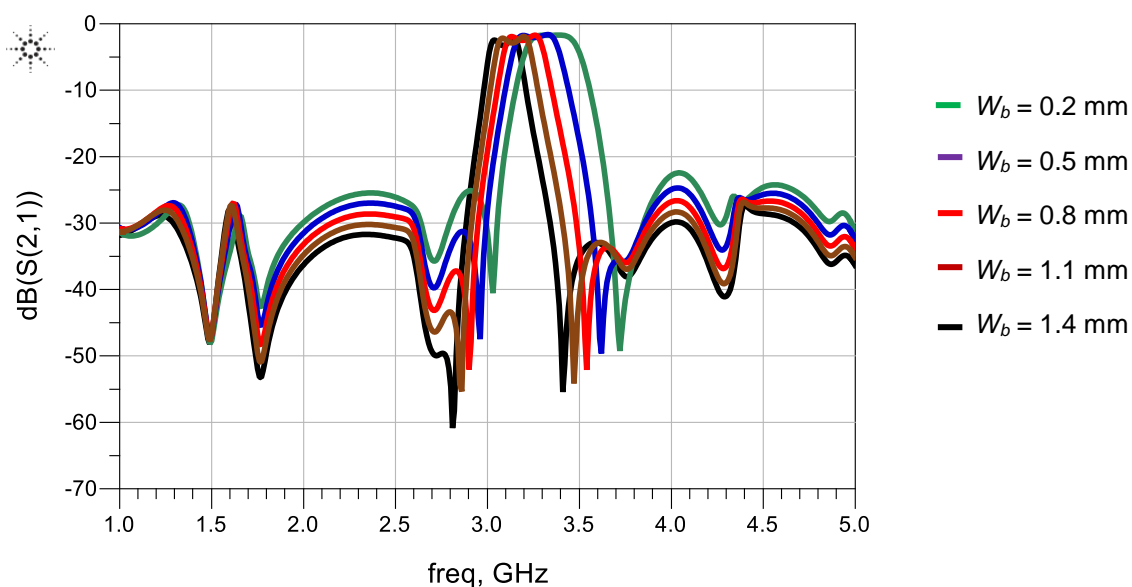


Fig. 4.21 Frequency response of the proposed filter as a function of coupled resonator width (W_b).

Table 4.5 Effect of coupled resonators width on the filter's transmission zeros, bandpass rejection level, centre frequency and insertion-loss performance.

W_b (mm)	f_{tz4} (GHz)	f_{tz5} (GHz)	f_0 (GHz)	IL (dB)	3dB Bandwidth (GHz)
0.2	3.03	3.72	3.40	1.71	0.32
0.5	2.88	3.52	3.17	2.15	0.32
0.8	2.77	3.36	3.04	2.50	0.32
1.1	2.67	3.23	2.91	2.90	0.28
1.4	2.60	3.12	2.84	3.30	0.16

The space between the spiral lines (S_2) has a significant effect on the filter's passband response as shown in Figs. 4.22 and 4.23. Salient results are tabulated in Table 4.6. Variation in this space controls the transmission zeros ($f_{tz1}, f_{tz2}, f_{tz3}, f_{tz6}$ and f_{tz7}). When this space is reduced from 0.6 mm to 0.2 mm, transmission zero f_{tz1} changes from 1.5 GHz to 1.7 GHz and f_{tz2} changes from 2.2 to 2.4 GHz, constituting a shift in frequency by 13%. Similarly, transmission zeros f_{tz3} changes from 2.75 GHz to 2.55 GHz; f_{tz6} changes from 4.4 GHz to 4.05 GHz; and f_{tz7} from 5.0 GHz to 4.65 GHz, which constitute a shift of 6%. However, the passband response is greatly distorted while other characteristics of the filter maintain their optimized value.

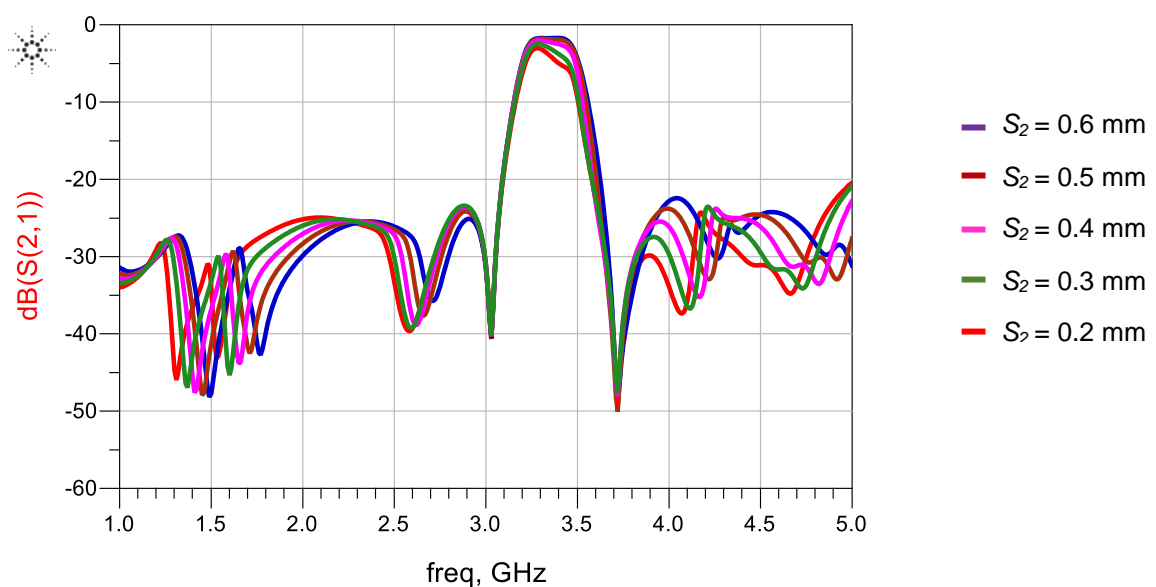


Fig. 4.22 Frequency response of the proposed filter as a function of coupling space between spirals shaped inductive lines (S_2).

Table 4.6. Effect of coupling space between spiral shaped inductive lines on transmission zeros.

S_2 (mm)	f_{tz1} (GHz)	f_{tz2} (GHz)	f_{tz3} (GHz)	f_{tz6} (GHz)	f_{tz7} (GHz)
0.6	1.5	1.77	2.71	4.27	4.86
0.5	1.45	1.71	2.66	4.22	4.76
0.4	1.41	1.65	2.62	4.17	4.67
0.3	1.37	1.60	2.59	4.12	4.57
0.2	1.31	1.53	2.58	4.07	4.46

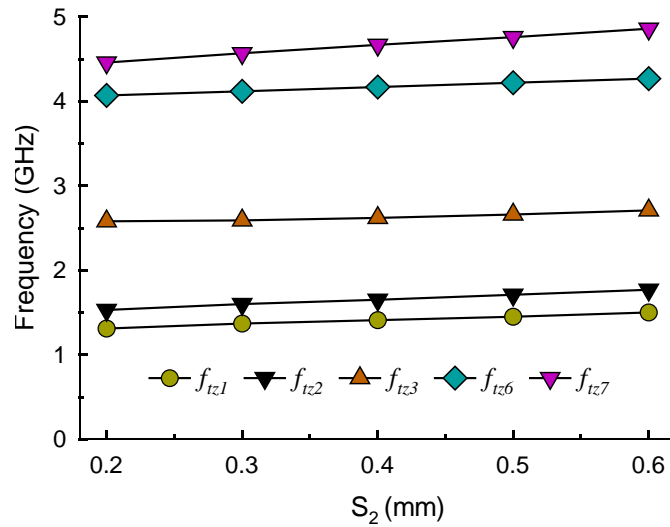


Fig. 4.23 Effect of the space between spiral lines on filter's passband transmission zeros.

The resonator length (l_4) on the filter's performance is shown in Fig.4.24 and Fig.4.25. The results are also tabulated in Table 4.7. The study shows when the length is varied from 0.9 mm to 0.1 mm, the filter's passband shifts moderately downward in frequency, whereas the centre frequency increases from 3.40 GHz to 3.51 GHz, transmission zero f_{1z4} shifts from 3.0 GHz to 3.15 GHz, and transmission zero f_{1z5} shifts from 3.7 GHz to 3.9 GHz. The overall shape of the response remains the same with a slight change in the insertion-loss as the length is reduced from 0.9 mm to 0.1 mm. The effect on the out-of-band rejection performance is negligible.

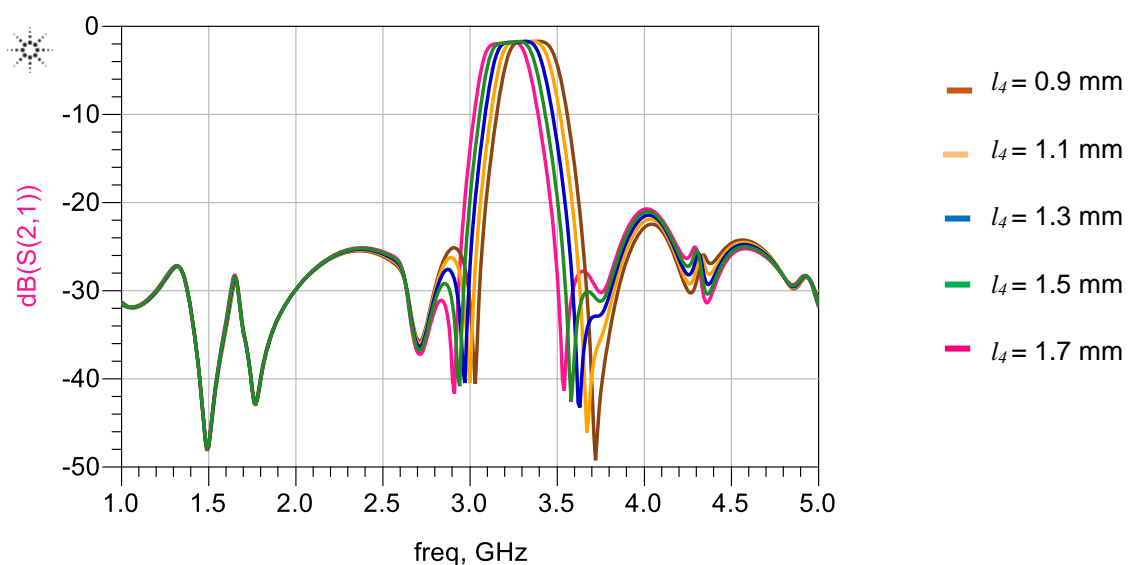


Fig. 4.24 Effect of resonator length (l_4) on passband transmission zeros.

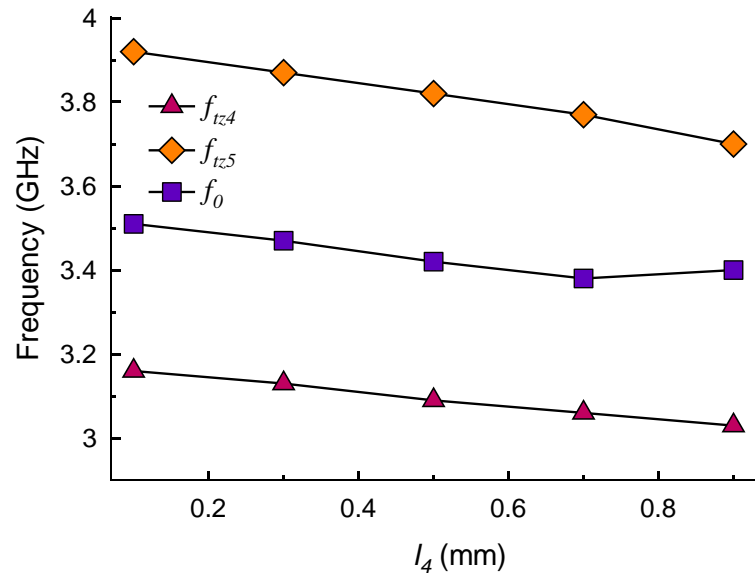


Fig. 4.25 Effect of coupled resonator length on filter's passband transmission zeros and centre frequency.

Table 4.7. Effect of resonator length (l_4) on the filter's passband transmission zeros and centre frequency.

l_4 (mm)	f_{tz4} (GHz)	f_{tz5} (GHz)	f_0 (GHz)
0.9	3.03	3.72	3.40
1.1	3.00	3.67	3.31
1.3	2.97	3.63	3.26
1.5	2.94	3.58	3.21
1.7	2.91	3.54	3.19

Fig. 4.26 shows the frequency response for variation in the resonator length (l_1), which is graphically presented in Fig.4.27. It is observed as the length is reduced from its optimized value the transmission zero f_{tz4} shifts upward in frequency from 3.03 GHz to 3.16 GHz, and a dip is created in the centre of the passband. The out-of-band performance on lower side of the passband deteriorates with variation in the length from 15.26 mm to 13.66 mm. Length (l_1) gives us freedom to control the transmission zero f_{tz4} by about (5%) to some extent without significantly effecting the other transmission zero and filter characteristics.

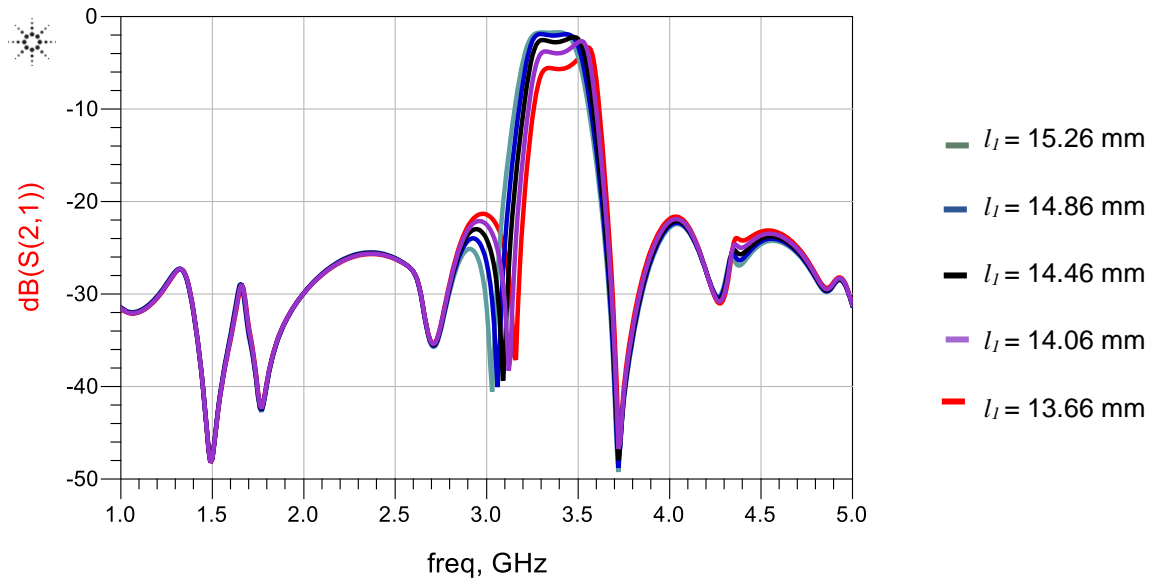


Fig. 4.26 Effect of resonator length (l_1) on passband transmission zeros and centre frequency.

Table 4.8. Effect of resonator length (l_1) on the filter's passband transmission zero.

l_1 (mm)	f_{tz4} (GHz)
15.26	3.03
14.86	3.06
14.46	3.09
14.06	3.12
13.66	3.15

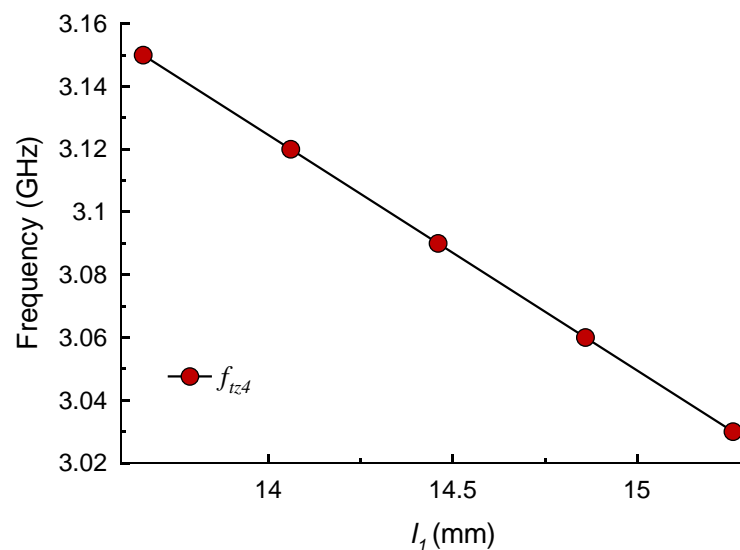


Fig. 4.27 Effect of coupled resonator length (l_1) on passband transmission zero (f_{tz4}).

The frequency response in Fig. 4.28 shows the impact on the filter's characteristics as the resonator length (l_2) when it's changed from optimized value 11.89 mm to 9.89 mm. The transmission zero f_{tz5} shifts linearly upward in frequency from 3.72 GHz to 3.97 GHz with minor deterioration in filter passband. However, the out-of-band performance on upper side of the passband deteriorated severely but it remains unchanged on lower side of the passband. It is observed that with variation in the length (l_2) the transmission zero f_{tz5} can be tuned independently by about ($\pm 7\%$) without effecting the filter characteristics as shown in Fig. 4.29.

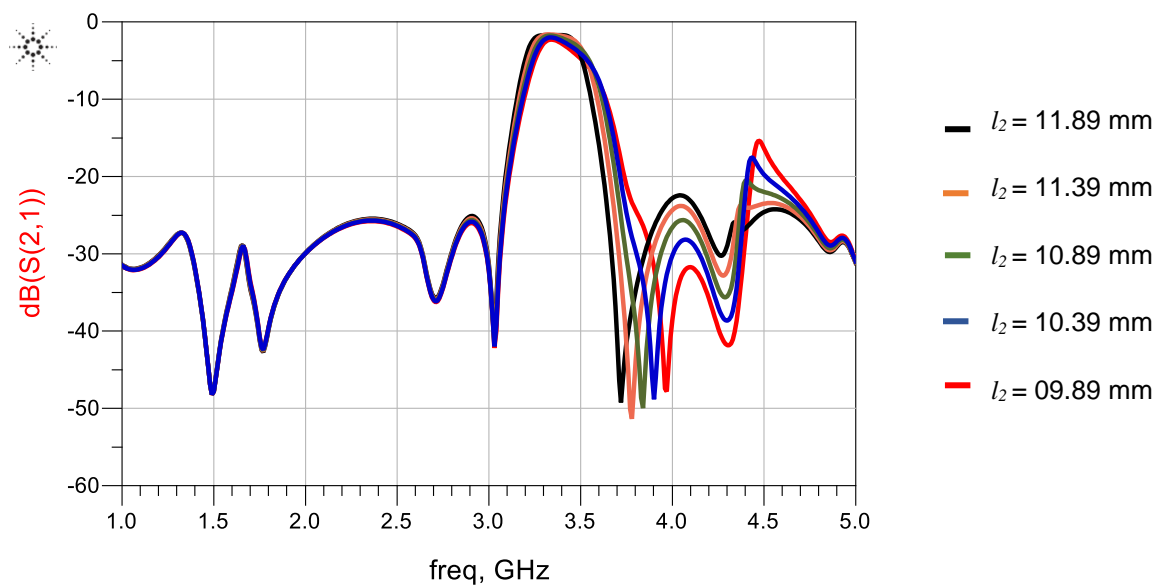


Fig. 4.28 Effect of resonator length (l_2) on the filter's passband transmission zero (f_{tz5}).

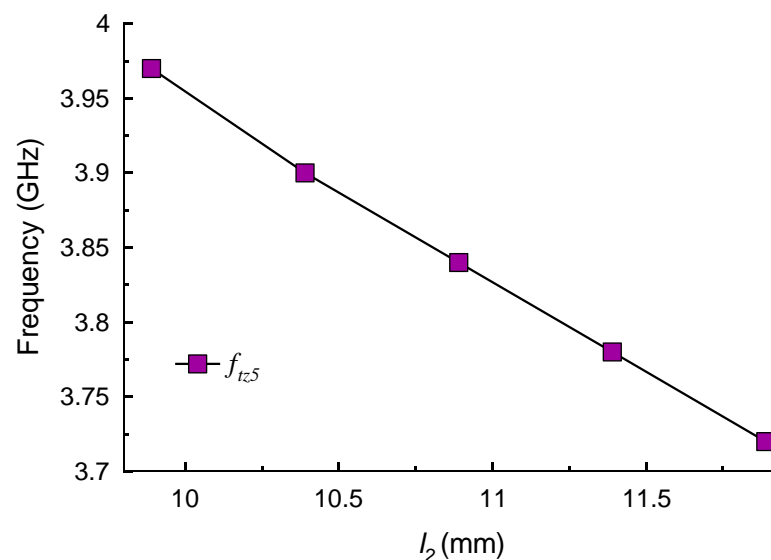


Fig. 4.29 Effect of coupled resonator length (l_2) on passband transmission zero (f_{tz5}).

Table 4.9. Effect of resonator length (l_2) on the passband transmission zero.

l_2 (mm)	f_{tz5} (GHz)
11.89	3.72
11.39	3.78
10.89	3.84
10.39	3.90
9.89	3.97

4.3 Wideband Bandpass Filter with Coupled Feed-line Sections

Theoretical analysis in [12] shows a three-line coupled microstrip structure can support three quasi-TEM or dominant modes, where each mode has its own modal phase constant, eigen voltage vector, and characteristic impedance. Compared with the traditional coupled-line design, the three-line section has two important advantages. One is that the tight line spacing for designing wideband bandpass filters can be greatly relaxed, and the other is that the stopband characteristics of the filter can be improved. Hence, in the following section a novel wideband bandpass filter structure is designed with two and three coupled lines feed-line sections.

To realize a wideband bandpass filter response the proposed filter in Fig. 4.5 was modified so that it is interdigitally coupled to the input and output feed-lines, as shown in Fig. 4.30. The out-of-band spurious responses are suppressed by loading the resonators directly with open-circuited stubs. The filter is constructed on dielectric substrate Arlon CuClad217LX with $h = 0.794$ mm, $\epsilon_r = 2.17$ mm, $t = 35$ μ m, and $\tan\delta = 0.0009$. The parameters of the filter were optimized using ADSTM software, which are: $W_a = 0.2$ mm, $W_c = 0.2$ mm, $W_{a1} = 0.2$ mm, $l_a = 0.79$ mm, $L_{b1} = 2$ mm, $L_{b2} = 1$ mm, $L_1 = 16.436$, $L_2 = 0.9$ mm, $L_3 = 11.89$ mm, $L_4 = 2.84$ mm, $L_5 = 7.46$ mm, $L_6 = 7.4$ mm, $S_1 = 0.56$ mm, and $S_2 = 0.314$ mm. The frequency response of the filter in Fig. 4.31 shows it is centred at 3.3 GHz with insertion-loss of 1.3-dB, return-loss better than 16 dB, and 3-dB fractional bandwidth of 18.3%. The compact filter exhibits a sharp 3-dB skirt with a wide stopband with rejection greater than 20 dB between 1 to 2.9 GHz and 3.7 to 5 GHz.

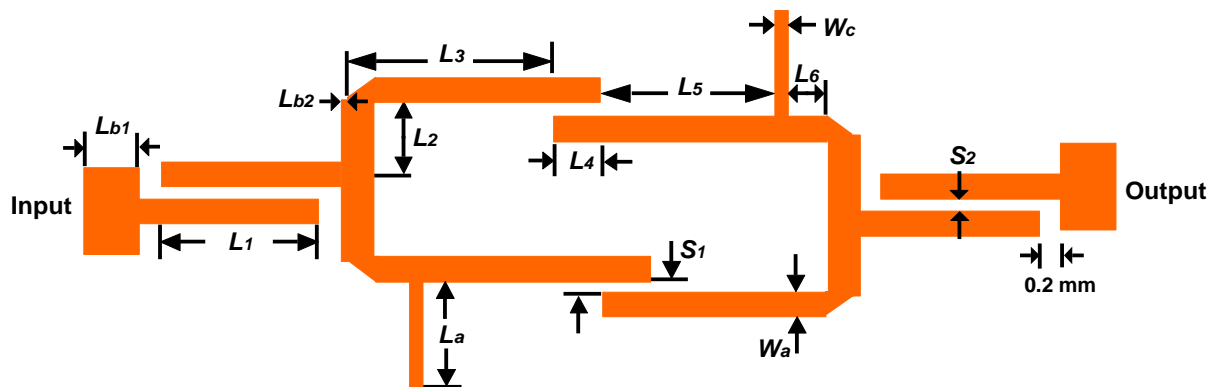


Fig. 4.30 Configuration of the interdigital coupled feed-line microwave bandpass filter.

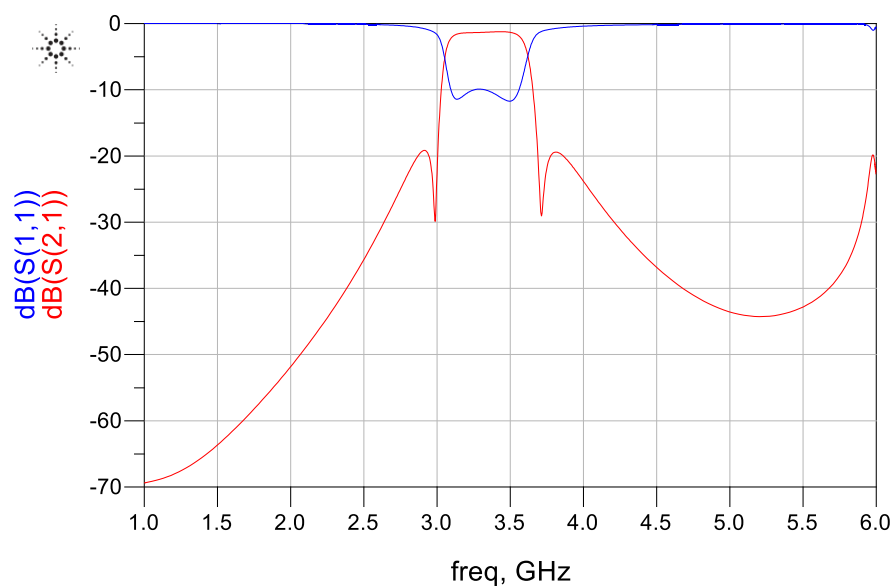


Fig. 4.31 Transmission and reflection-coefficient response of the proposed filter.

The two finger interdigital coupled feed-line was replaced with three finger interdigital coupled feed-line, as shown in Fig. 4.32(a). All other physical dimensions were unaltered as in Fig. 4.30. The frequency response of the filter in Fig. 4.33 shows the filter has a centre frequency of 3.33 GHz, insertion-loss of 1.2 dB, and significantly improved return-loss of -10 dB. It has a 3-dB fractional bandwidth of 16.8%. The filter has a sharp 3-dB roll-off and a wideband out-of-band rejection level of 20 dB from 1 to 3 GHz and 3.2 to 5.8 GHz.

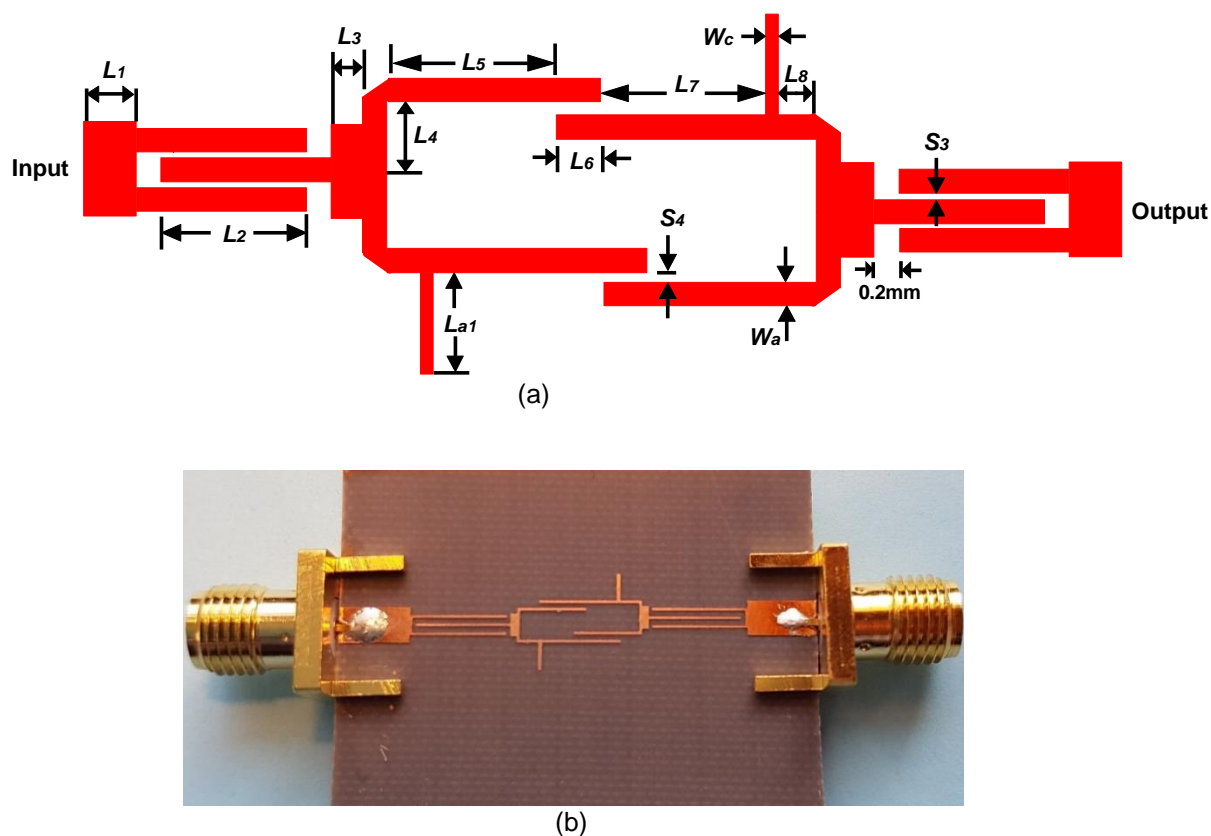
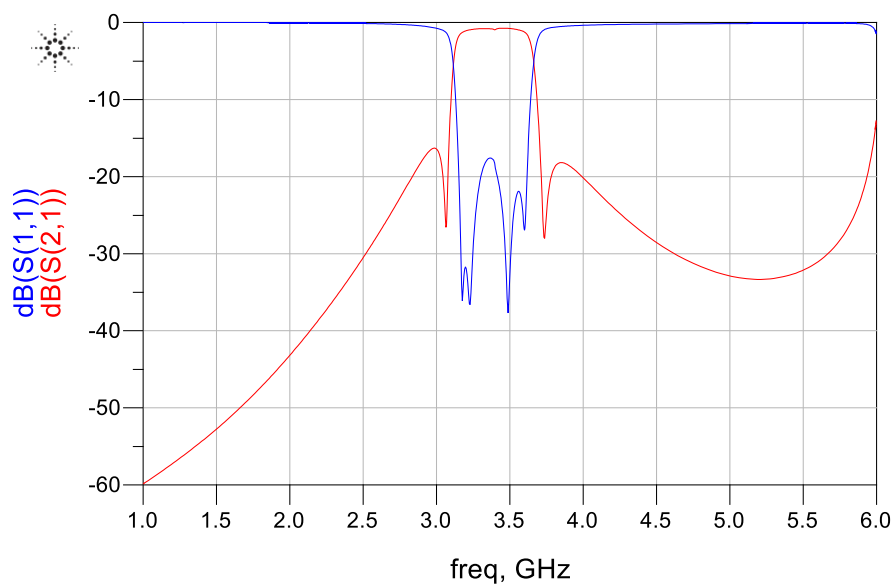


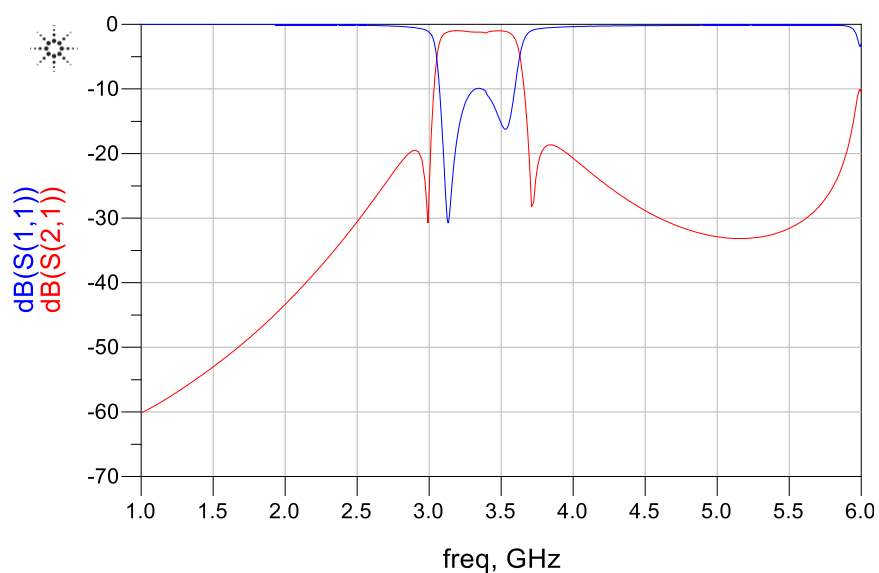
Fig. 4.32 (a) Layout of the three finger interdigital coupled feed-line bandpass filter, and (b) photograph of the implemented filter.

The filter's out-of-band rejection without the loaded resonators was -15 dB, as shown in Fig. 4.33(a). The out-of-band spurious are suppressed by loading the resonators directly with open-circuited stubs, and the out-of-band rejection on lower side of the passband increases to -20 dB, and on the upper side to about -19 dB, as shown in Fig. 4.33 (b). Fig. 4.34 shows the measured results. The filter has a passband insertion-loss of only 1.09 dB with return-loss better than 15 dB. The optimized physical dimensions of the filter are: $W_a = 0.2$ mm, $W_c = 0.2$ mm, $l_{a1} = 0.654$ mm, $L_1 = 2$ mm, $L_2 = 15.98$ mm, $L_3 = 1$ mm, $L_4 = 0.9$ mm, $L_5 = 11.79$ mm, $L_6 = 2.84$ mm, $L_7 = 7.36$ mm, $L_8 = 7.4$ mm, $S_3 = 0.58$ mm, and $S_4 = 0.31$ mm.

Effect of open stub length on the filter's characteristics is given in Table 4.10 and shown in Fig. 4.35 and Fig. 4.36. As the stub length is increased the filter's centre frequency and lower transmission zero drop down 8.7% and 14.9%, respectively; however the upper transmission zero remains virtually constant. As the stub length is increased from 0.69 to 4.69 mm the insertion-loss increases exponentially from 0.55 to 3.9 dB, and the filter response distorts even though the out-of-band rejection improves. At the optimum value of the stub length of 0.69 mm, the filter's centre frequency is 3.32 GHz. The open stub length can be used to tune the passband with increase in out-of-band rejection from -15 dB to -20 dB, as evident in Fig. 4.33 (a), however with a penalty in increased insertion-loss.

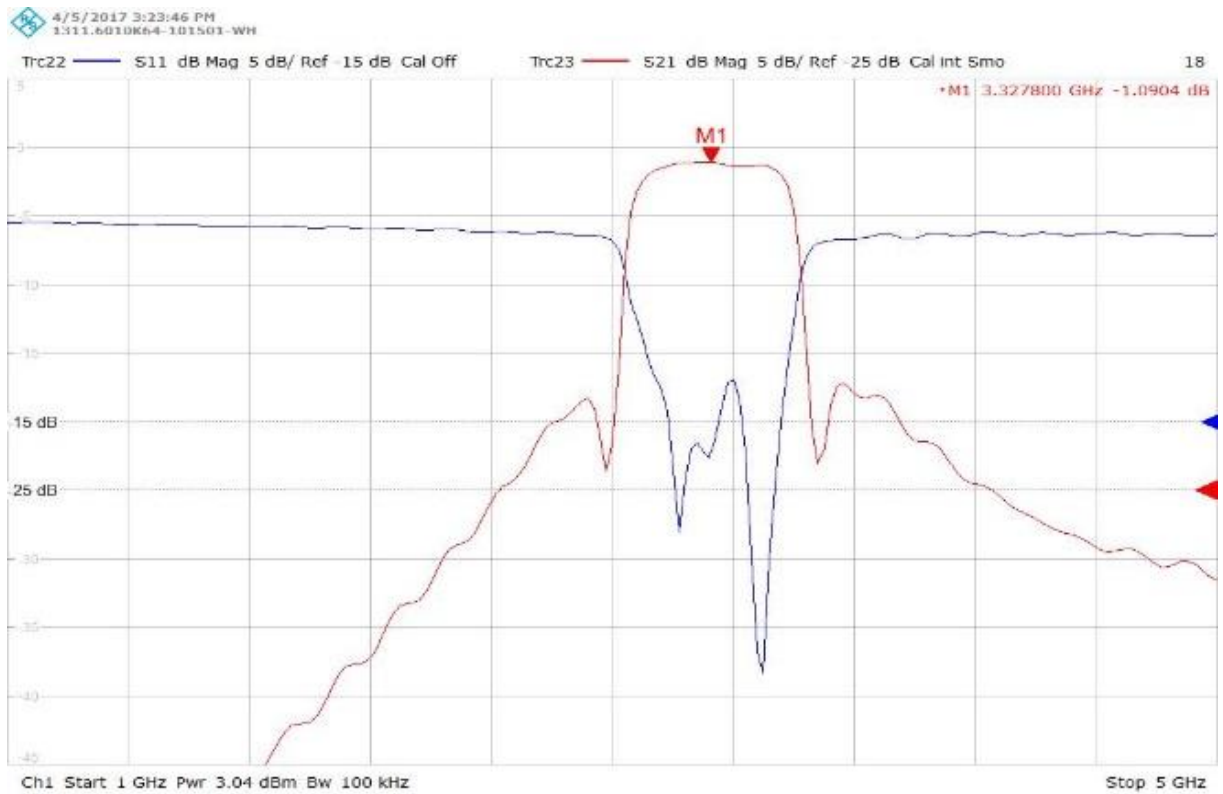


(a)

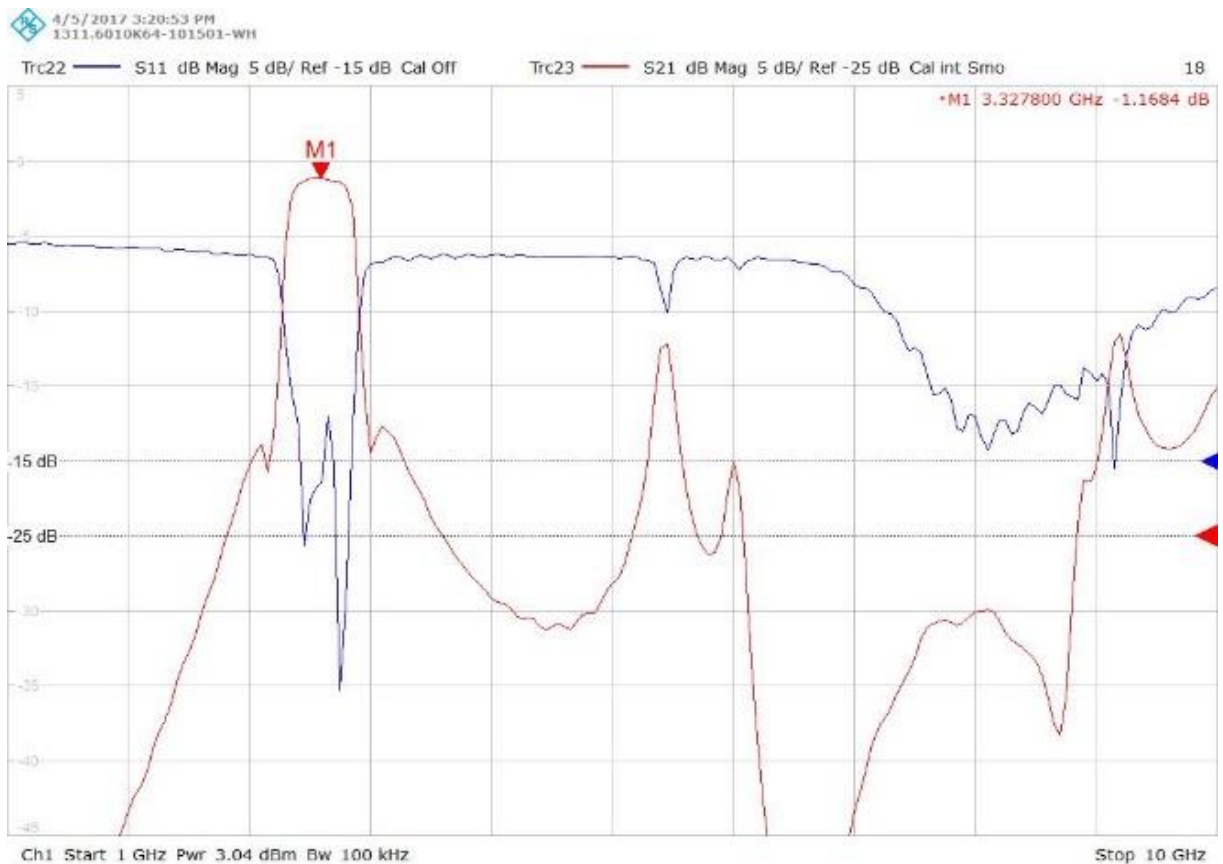


(b)

Fig. 4.33 (a) Simulated S-parameter response of the proposed filter without stub loaded resonators, (b) simulated S-parameter response with stub loaded resonators,



(a)



(b)

Fig. 4.34 (a) measured S-parameter response (narrowband view), and (b) measured S-parameter response (wideband performance).

Table 4.10 Effect of open stub length on the filter's transmission zeros, centre frequency and insertion-loss performance.

L_{a1} (mm)	f_{tz1} (GHz)	f_{tz2} (GHz)	f_o (GHz)	IL (dB)
0.69	2.96	3.71	3.32	0.55
1.69	2.86	3.69	3.25	0.56
2.69	2.75	3.67	3.10	0.76
3.69	2.64	3.65	3.01	1.88
4.69	2.52	3.64	3.03	3.90

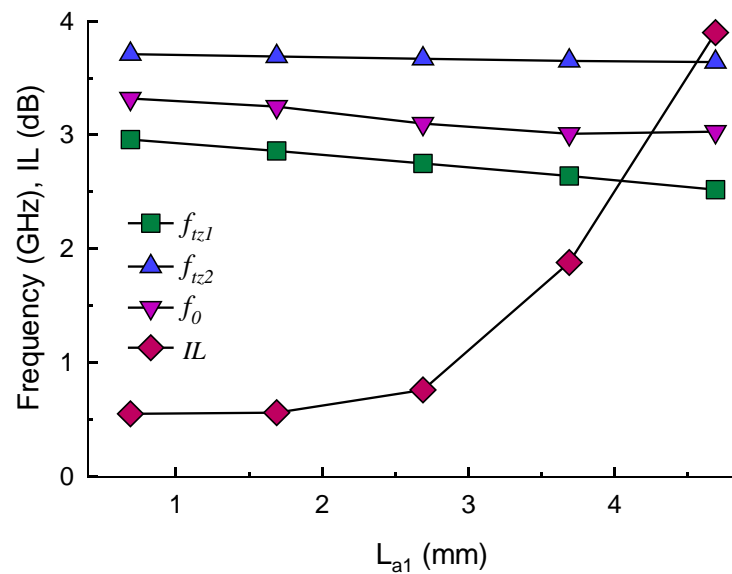


Fig. 4.35 Effect of open stub length on the filter's transmission zeros, centre frequency, and insertion-loss performance.

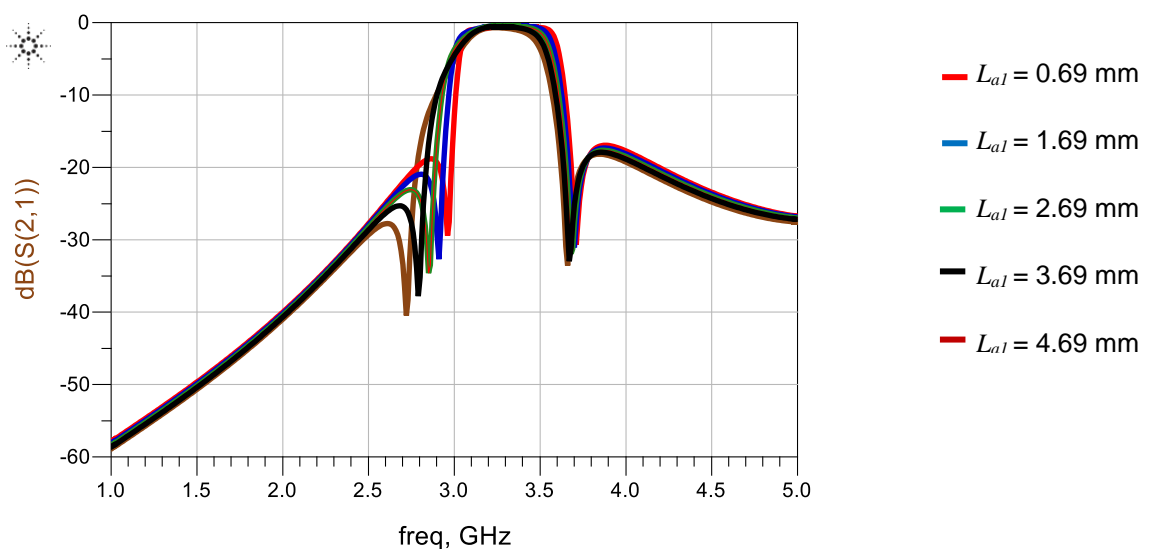


Fig. 4.36 Frequency response of the filter in Fig. 4.31 as a function of open stub length.

The effect of the interdigital feed-line coupling gap (S_3) is tabulated in Table 4.11 and shown in Fig. 4.37 to Fig. 4.39. The results show the coupling gap has no effect on the filter's centre frequency however with a smaller gap the insertion-loss can be greatly improved but this causes the out-of-band rejection level to decline in linear fashion. The position of resonators length (L_7) and (L_8) behaves almost similarly.

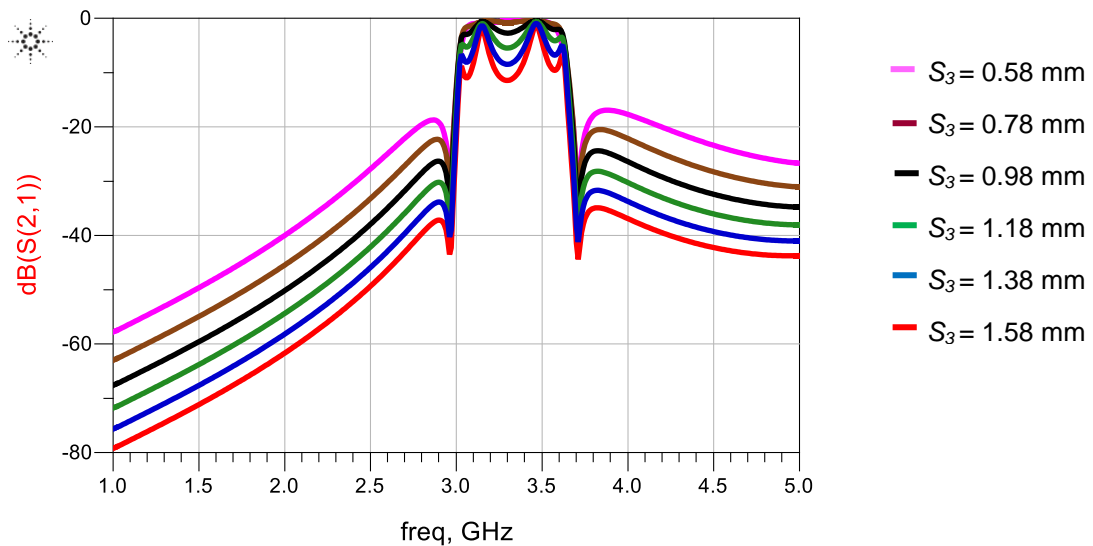


Fig. 4.37 Frequency response of the filter in Fig. 4.32 as a function of interdigital feed-line coupling gap.

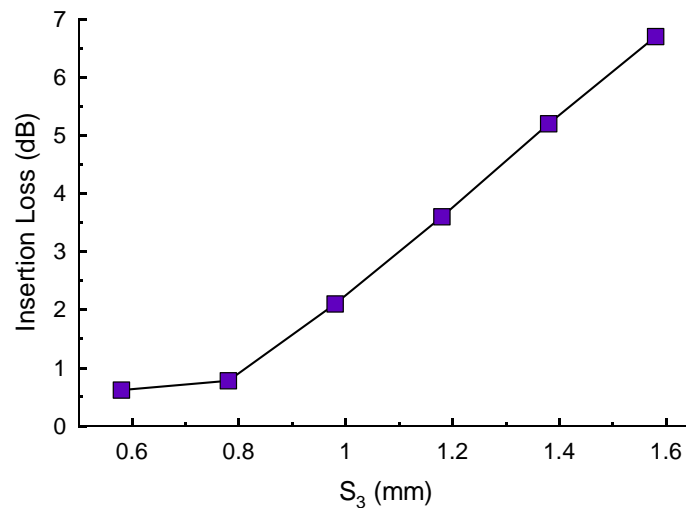


Fig. 4.38 Effect on centre frequency and loss by interdigital feed-line coupling gap.

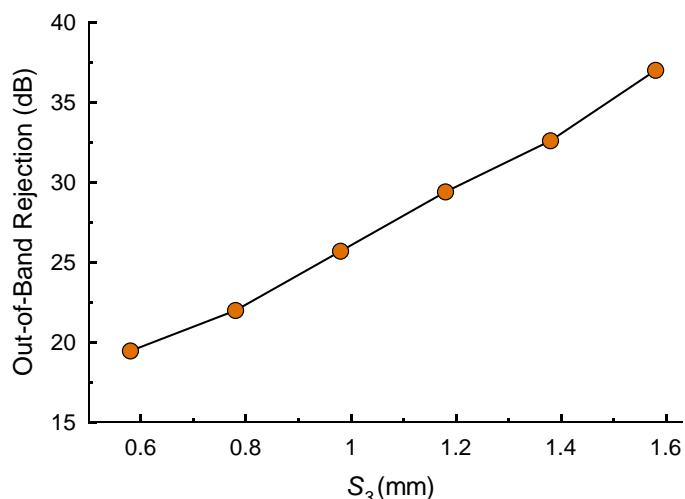


Fig. 4.39 Effect on out-of-band rejection level as a function of interdigital feed-line coupling gap.

Table 4.11 Effect of coupling space between coupled feed lines on the filter's centre frequency, bandpass rejection level and insertion-loss performance.

S_3 (mm)	f_o (GHz)	IL (dB)	Out-of-band rejection (dB)
1.58	3.3	6.70	37.0
1.38	3.3	5.20	32.6
1.18	3.3	3.60	29.4
0.98	3.3	2.10	25.7
0.78	3.3	0.78	22.0
0.58	3.3	0.62	19.5

The filter's passband can be squeezed by decreasing the coupling space between the two resonators (S_4), and the consequence of this is improvement in the filter's out-of-band rejection level, as shown in the Fig. 4.40. The bandwidth of the filter can be squeezed by 103 MHz or 3.2% by decreasing the coupling space from 0.34 mm to 0.22 mm. In order to improve the passband response, the lower transmission zero can be controlled by length L_{a1} . By reducing the length L_{a1} the location of lower transmission zero moves towards higher frequencies, but it reduces the out-of-band rejection level at higher frequencies as shown in Fig.4.40.

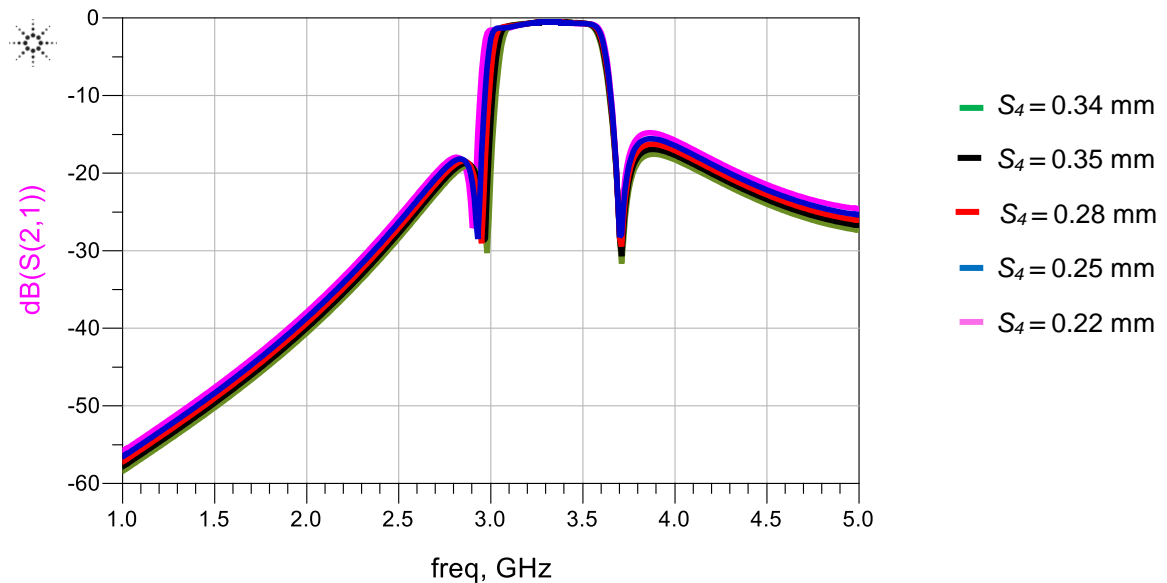


Fig. 4.40 Frequency response of the filter as a function of resonator coupling gap (S_4).

By decreasing length L_2 from its optimum value of 16.98 mm, the passband response remains unaffected but the out-of-band rejection level deteriorates, as shown in the Fig. 4.41. As shown in Fig. 4.37 the interdigital feed-line coupling gap (S_3) can be increased to improve the out-of-band rejection level and to further flatten the passband response. Fig. 4.42 shows the response of the widest 3-dB fractional bandwidth obtainable by the filter, which is 16.8%. The narrowest 3-dB fractional bandwidth obtainable by the filter is 9.8%, shown in Fig. 4.43.

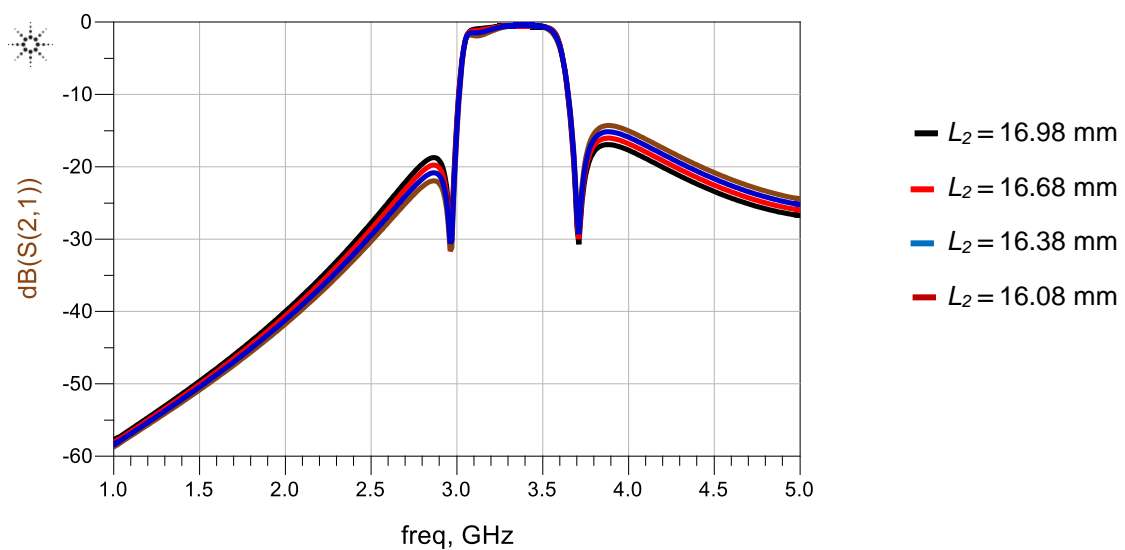


Fig. 4.41 Frequency response of the filter as a function of interdigital feed-line coupling length.

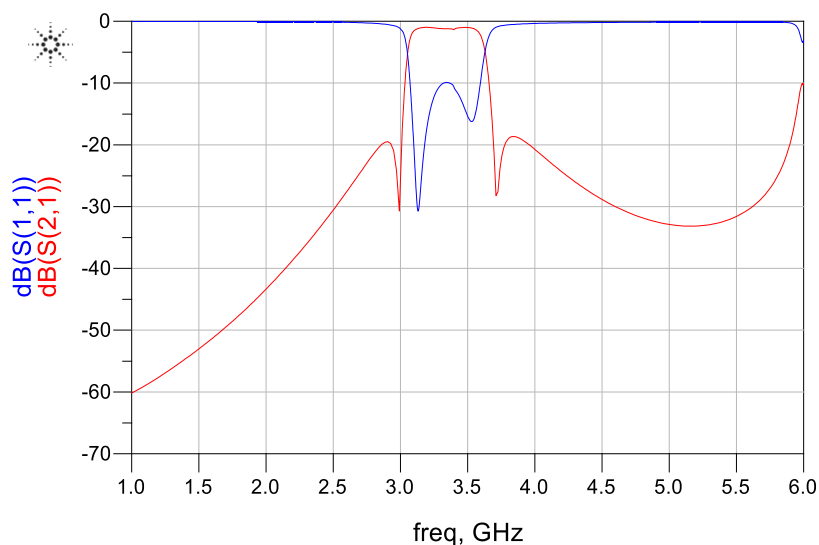


Fig. 4.42 Transmission and reflection-coefficient response of the optimized filter.

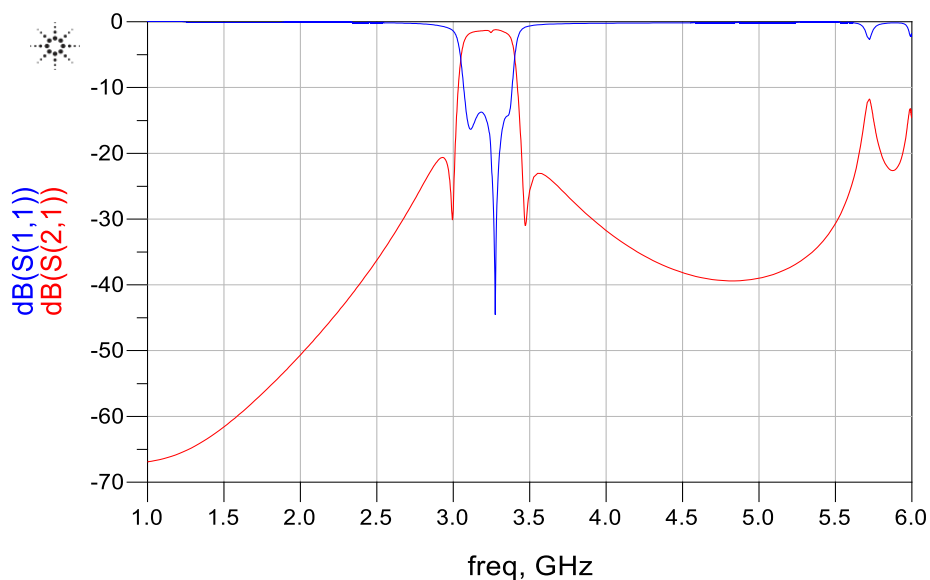


Fig. 4.43 Transmission and reflection-coefficient response of the narrowest 3-dB fractional bandwidth.

Simulation analysis in Fig 4.44 shows the influence of varying the resonator length (l_6) on filter's performance. The position of the passband shifts downward in frequency by ($\pm 8\%$) as the length is increased from 2.84 mm to 3.64 mm; however the out-of-band performance on the upper side of the passband deteriorates, while it remain unchanged on the lower side. It is also noticed as the length approaches to 3.44 mm, a dip appears at the top left corner of the passband. Fig. 4.45 shows how the passband transmission zeros are affected by varying the resonator length. This data is also given in Table 4.12. Investigation shows the resonator length (l_4) behaves similarly.

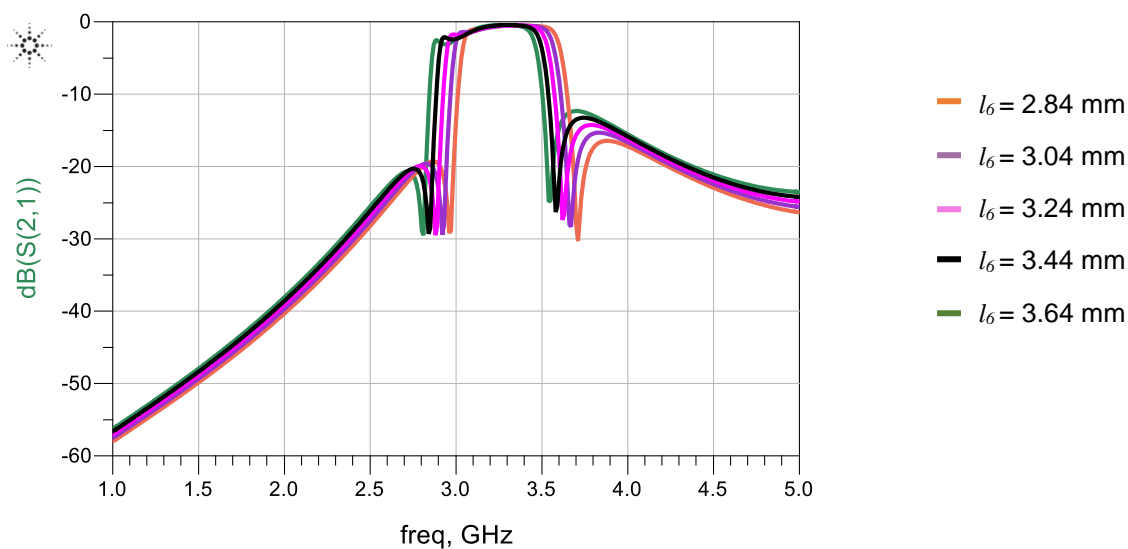


Fig. 4.44 Frequency response of the filter as a function of resonator length (l_6).

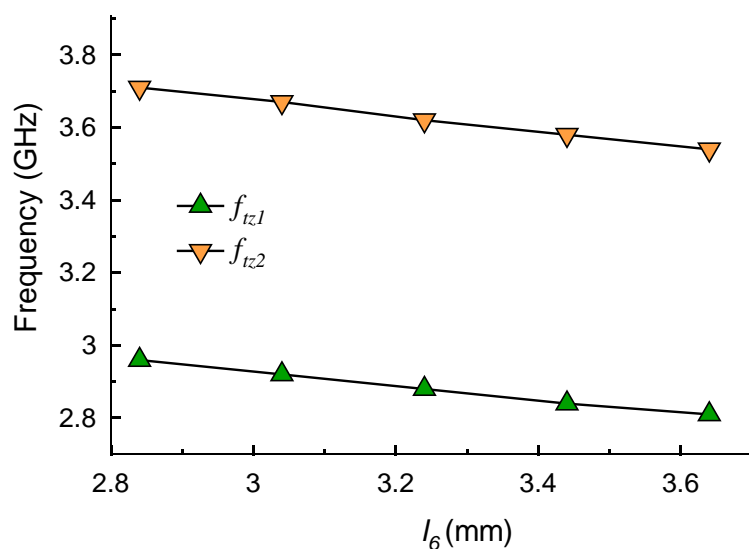


Fig. 4.45 Effect on transmission zeros as a function of resonator length (l_6).

Table 4.12. Effect of resonator length (l_6) on the filter's passband transmission zero.

l_6 (mm)	f_{tz1} (GHz)	f_{tz2} (GHz)
2.84	2.96	3.71
3.04	2.92	3.67
3.24	2.88	3.62
3.44	2.84	3.58
3.64	2.81	3.54

The frequency response in Fig. 4.46 shows how the filter's response is affected by the resonator length (l_5) when it's changed from the optimized value of 11.59 mm to 10.59 mm. The transmission zero f_{tz2} shifts upward in frequency (from 3.7 GHz to 4.0 GHz), as shown in

Fig. 4.47, without any deterioration in filter passband. This results in a wider passband whose 3-dB fractional bandwidth is increased from 16.6% to 24%. The out-of-band performance on upper side of the passband improves moderately by about 28%, whereas it remains unchanged on lower side of the passband. With variation in the resonator length the transmission zero f_{tz2} can be controlled independently, resulting in significant improvement in 3-dB fractional bandwidth without effecting the overall filter performance.

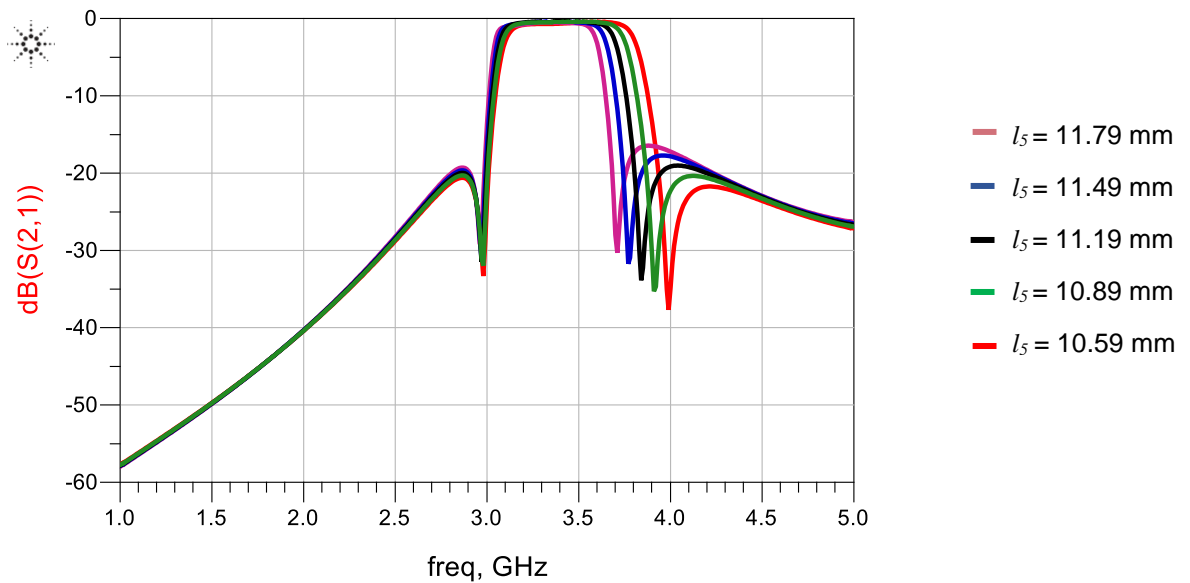


Fig. 4.46 Frequency response of the filter as a function of resonator length (l_5).

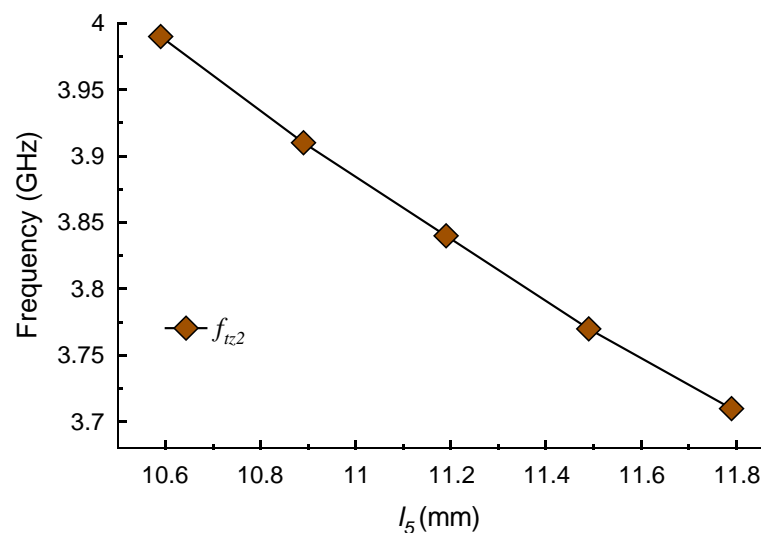


Fig. 4.47 Effect on transmission zeros as a function of resonator length (l_5).

4.4 Summary

Various coupling schemes were theoretically analysed. A highly compact microwave filter design was proposed where the input/output feed-lines are parallel coupled to the resonant structure using high impedance lines. Spurious harmonics generated by the filter are suppressed by loading the feed-lines with inductive stubs. The inductive lines are spiraled to reduce the width of the structure. The filter structure was analyzed to gain insight of how the geometric parameters of the structure effect the filter's response. The filter was optimized to minimize out-of-band spuri over a wide frequency bandwidth. To realize a bandpass filter with a wide passband it was necessary to investigate another design which is composed of coupled open-loop resonators where each resonator is directly loaded with an open-circuited inductive stub, and the feed-lines are interdigitally coupled to the resonators. It is shown the 3-dB fractional bandwidth of the filter can be controlled by manipulating its geometric parameters. The proposed filter design has the capability to vary its 3-dB fractional bandwidth from 9.8% to 16.8%. Both filters designs investigated are (i) compact in size when fabricated on a low dielectric constant substrate; (ii) possess a sharp quasi-elliptic function bandpass response with low passband insertion-loss; and exhibits a wide stopband performance.

References

1. L. Athukorala, D. Budimir, "Design of compact dual mode microstrip filters," *IEEE Transactions on Microwave Theory and Techniques*, vol.58, no. 11, Nov 2010.
2. J.-S Hong and M. J. Lancaster, *Microstrip filters for RF/microwave applications*, New York: John Wiley & Sons, 2001.
3. J.-S. Hong and M.J. Lancaster, "Theory and experiment of novel microstrip slow-wave open-loop resonator filters," *IEEE Transactions on Microwave Theory and Techniques*, vol. 45, no. 12, pp. 2358-2365, Dec. 1997.
4. P. Hoi-Kai, H. Ka-Meng, T. Kam-Weng, and R. P. Martins, "A compact microstrip g/4-SIR interdigital bandpass filter with extended stopband," *IEEE MTT-S, Int. Microwave Symp. Dig.*, pp. 1621- 1624, Jun. 2004.
5. A. Griol, J. Marti, and L. Sempere, "Microstrip multistage coupled ring bandpass filters," vol. 37, no. 9, pp. 572-573, 2001.
6. B.I. Bleaney and B. Bleaney, *Electricity and Magnetism*, 3rd ed. Oxford: Oxford Univ. Press, 1976, vol. 1, ch. 7.
7. C.G. Montgomery, R.H. Dicke, and E.M. Purcell, *Principles of Microwave Circuits*. New York: McGraw-Hill, 1948, ch. 4.
8. J.-S. Hong, M. J. Lancaster, "Couplings of microstrip square open-loop resonators for cross coupled planar microwave filters," *IEEE Transactions on Microwave Theory and Techniques*, vol. 44, no. 12, December 1996
9. X.Y. Zhang and Q. Xue, "Novel centrally loaded resonators and their applications to bandpass filters," *IEEE Trans. on Microwave Theory and Techniques*, vol. 56, no. 4, April 2008, pp 913 - 921
10. X.Y. Zhang, J.-X. Chen, Q. Xue, and S.-M Li, "Dual-band filters using stub-loaded resonators," *IEEE Microw. Wireless Compon. Letter.*, vol. 17, no. 8, Aug. 2007, pp. 583–585.
11. K. Chang, L.-H. Hsieh, "Microwave Ring Circuits and Related Structures", June 2004, Wiley.
12. J.-T. Kuo and E. Shih, "Wideband bandpass filter design with three-line microstrip structures," *IEE Proc. Microw. Antennas Propagation*, vol. 149, no. 516, Oct/Dec. 2002, pp. 243 - 247.
13. R. Schwindt, and C. Nguyen, "Spectral domain analysis of three symmetric coupled lines and application to a new bandpass filter," *IEEE Trans. Microw. Theory Tech.*, 1994, vol. 42, no. 7, pp. 1183-1189.

14. J.-T. Kuo "Accurate quasi-TEM spectral domain analysis of single and multiple coupled microstrip lines of arbitrary metallization thickness," *IEEE Trans. Micro. Theory Tech.*, 1995, vol. 43, no.8, pp. 1881-1888.
15. C.R. Paul, *Analysis of Multiconductor Transmission Lines*, *John Wiley & Sons*, New York, 1994.
16. J.-T. Kuo, and E. Shih, "Wideband bandpass filter design with three-line microstrip structures," *IEEE MTT-S Int. Microw. Symp. Dig.*, 2001, pp. 1593-1596.
17. F.-L. Lin, C.-W. Chiu, and R.-B. Wu, "Coplanar waveguide bandpass filter-a ribbon-of-brick-wall design," *IEEE Trans. Microw. Theory Tech.*, 1995, vol. 43, no. 7, pp. 1589-1596.
18. D.M. Pozar, *Microwave Engineering*, *John Wiley & Sons*, New York, 1998, 2nd edition.
19. J.-S. Hong and M.J. Lancaster, *Microstrip filters for RF/Microwave applications*, page 127, *John Wiley & sons*, New York.

Compact Wide Stopband Bandpass Filter Using Stub Loaded Half-Wavelength Resonators

5.0 Introduction

Design of narrowband microwave bandpass filters using parallel coupled or end-coupled microstrip-lines is well established. However, modern wireless communications systems demand compact wideband filters with sharp skirts, low insertion-loss and high return-loss characteristics, as well as a wide stopband with high rejection level. Filters with highly sharp skirts are necessary to efficiently utilise the finite EM spectrum, and a wide stopband is necessary to suppress/eliminate undesired harmonic and spurious responses that could seriously degrade the performance of system and/or detrimentally interfere with other wireless systems. Unfortunately, filters based on half-wavelength resonators generate spurious passbands at multiples of the fundamental frequency. Moreover filters constructed using quarter-wavelength resonators produce spurious passbands at odd multiples of the fundamental frequency. These traditional types of filter exhibit poor out-of-band performance.

In this chapter a novel and compact wideband microstrip filter design is described possessing the aforementioned desired characteristics using stub loaded half-wavelength resonators that are coupled to input and output feed-lines. The input and output feed-lines are interdigitally coupled to reduce the passband insertion-loss and realise a wide stopband on either side of the passband response with high rejection level. Wideband performance requires tight coupling of the feed-lines with the resonator structure however this can be prohibitive using conventional manufacturing techniques. This issue was alleviated here using three finger interdigital coupling.

5.1 Even and Odd Mode Analysis of Stub Loaded Resonator

5.1.1 Even Mode Analysis

The stub loaded resonator (SLR) consisted of a conventional microstrip half-wavelength resonator and an open stub, as shown in Fig. 5.1(a), where Z_1 , θ_1 and Z_2 , θ_2 denote the characteristic impedance and lengths of the microstrip-line and open stub, respectively. The open stub is shunted at the midpoint of the microstrip-line, as depicted in Fig. 5.1(a). Since

the SLR is a symmetrical structure, odd- and even-mode analysis can be applied to characterize its behaviour.

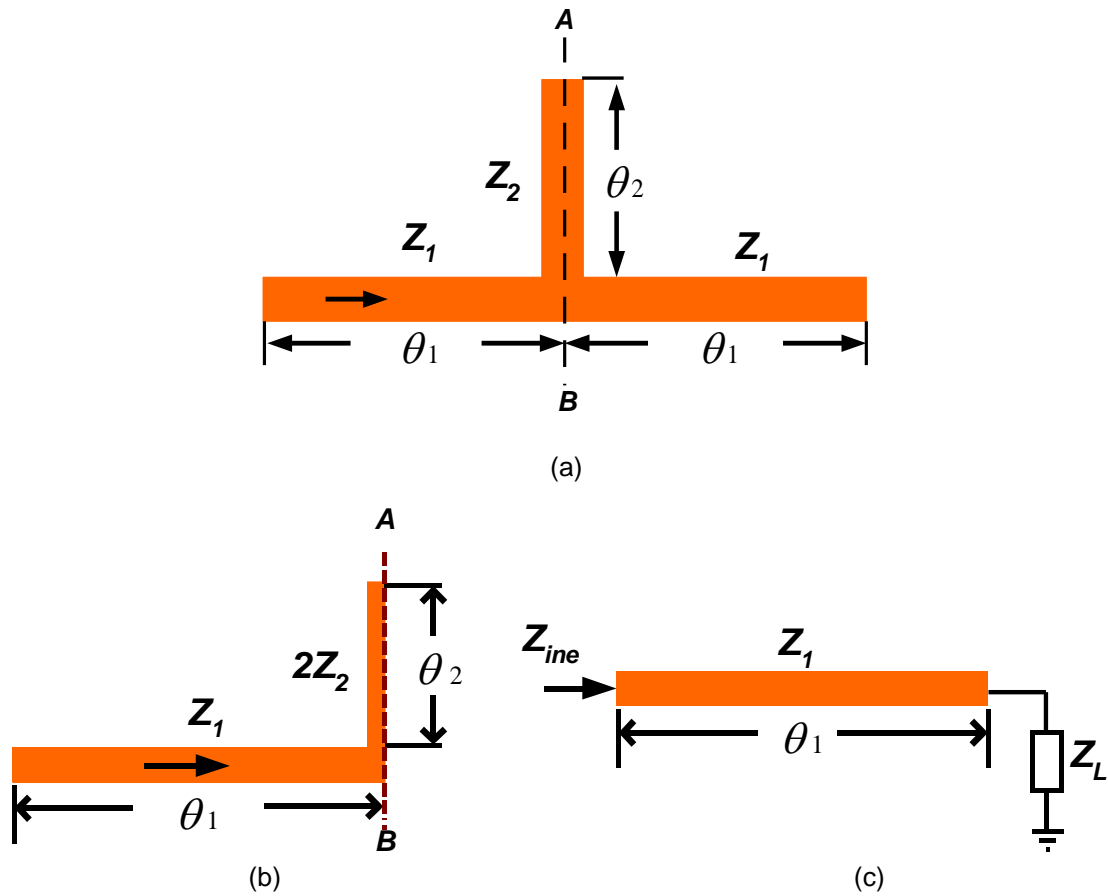


Fig. 5.1 (a) Structure of the stub-loaded resonator, (b) even-mode representation, and (c) simplified even-mode resonator.

For even-mode excitation, there is a voltage null along the middle of the SLR. This leads to the equivalent circuit representation in Fig. 5.1(b), which is simplified in Fig. 5.1(c).

$$Z_L = j2Z_2 \cot \theta_2 \quad (5.1)$$

where $\theta_2 = \beta l_2$ is the electric length of the stub, and $\theta_1 = \beta l_1$ is the electric length of the microstrip-line.

$$Z_{ino} = Z_0 \left(\frac{Z_L + jZ_0 \tan \beta l}{Z_0 + jZ_L \tan \beta l} \right) = jZ_1 \left(\frac{2Z_2 \tan \theta_2 + Z_1 \tan \theta_1}{Z_1 - 2Z_2 \tan \theta_1 \tan \theta_2} \right) \quad (5.2)$$

$$\text{Condition for resonance: } \frac{1}{Z_{ino}} = 0 \quad \text{or} \quad Y_{ino} = 0$$

$$Y_{ino} = -jY_1 \left(\frac{Z_1 - 2Z_2 \tan \theta_1 \tan \theta_2}{2Z_2 \tan \theta_2 + Z_1 \tan \theta_1} \right) = 0 \quad (5.3)$$

$$\text{i.e. } \tan\theta_1 \tan\theta_2 = \frac{Z_1}{2Z_2} = k \quad (5.4)$$

Resonance condition is determined by θ_1 , θ_2 and impedance ratio k .

The total resonator length and the normalized resonator length are given by

$$\theta_T = \theta_1 + \theta_2 \quad (5.5)$$

$$\theta_T = \theta_1 + \tan^{-1}\left(\frac{k}{\tan\theta_1}\right) \quad (5.6)$$

Normalized resonator length L_n with respect to the electrical length of a corresponding $\pi/2$ (180°) resonator is:

$$L_n = \frac{\theta_T}{\pi/2} = \frac{2\theta_T}{\pi}$$

$$\text{or } L_n = \frac{2}{180^\circ} \left[\theta_1 + \tan^{-1}\left(\frac{k}{\tan\theta_1}\right) \right] \quad (5.7)$$

Fig. 5.2 shows the relationship between θ_1 and L_n as a function of k . The graph shows that L_n attains maximum value when $k \geq 1$ and a minimum value when $k < 1$.

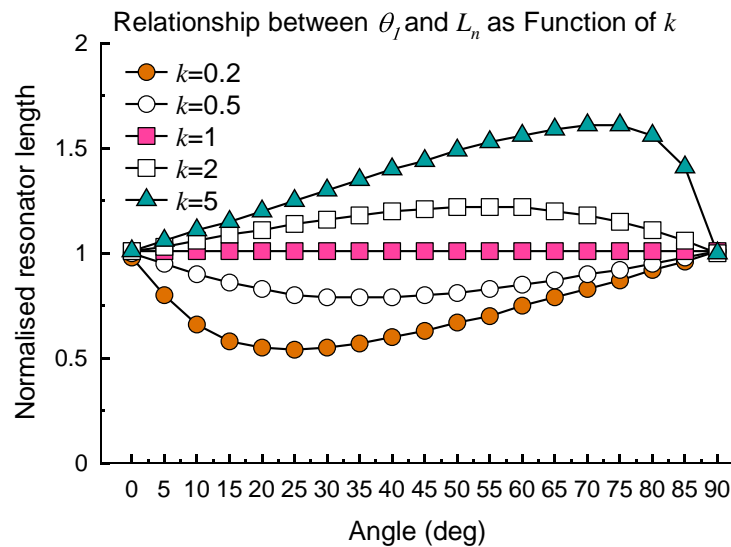


Fig. 5.2 Normalized resonator length against microstrip-line length (in degrees) as a function of impedance ratio.

Condition for Maximum and Minimum θ_T

The maximum and minimum length θ_T can be deduced from Eqn.(5.4), i.e.

$$\tan\theta_1 \tan\theta_2 = k$$

But from Eqn.(5.5) $\theta_T = \theta_1 + \theta_2$ or $\theta_2 = \theta_T - \theta_1$

so $\tan\theta_1 \tan(\theta_T - \theta_1) = k$

When $0 < k < 1$ and $0 < \theta_T < \pi/2$

$$\tan\theta_T = \frac{\sqrt{k}}{(1-k)} \left(\frac{\tan\theta_1}{\sqrt{k}} + \frac{\sqrt{k}}{\tan\theta_1} \right) \geq \frac{2\sqrt{k}}{1-k} \quad (5.8)$$

This expression is equated when

$$\frac{\tan\theta_1}{\sqrt{k}} = \frac{\sqrt{k}}{\tan\theta_1} \quad (5.9)$$

This is equivalent to $\tan^2\theta_1 = k$

Thus, when $\theta_1 = \theta_2 = \tan^{-1}\sqrt{k}$ θ_T attains a minimum value of

$$\theta_{T_{min}} = \tan^{-1} \left(\frac{2\sqrt{k}}{1-k} \right) \quad (5.10)$$

Similarly if $k > 1$ and $\pi/2 < \theta_T < \pi$, we obtain the following equation

$$\tan\theta_T = -\frac{\sqrt{k}}{1-k} \left(\frac{\tan\theta_1}{\sqrt{k}} + \frac{\sqrt{k}}{\tan\theta_1} \right) \quad (5.11)$$

As $0 < \theta_1 < \pi/2$, θ_T attains a maximum value of

$$\theta_{T_{max}} = \tan^{-1} \left(\frac{2\sqrt{k}}{1-k} \right) \quad (5.12)$$

When $\theta_1 = \theta_2 = \tan^{-1}\sqrt{k}$

This analysis reveals that $\theta_1 = \theta_2$ yields a resonator with maximum and minimum length.

When $\theta_1 = \theta_2 = \theta_0$, the normalized resonator length is:

$$L_{n_0} = \frac{2\theta_T}{\pi} = \frac{2}{\pi} \tan^{-1}\sqrt{k} \quad (5.13)$$

This graph in Fig. 5.3 illustrates the fact that resonator length can be shortened by applying a smaller k value, while a maximum resonator length is limited to twice that of the corresponding resonator.

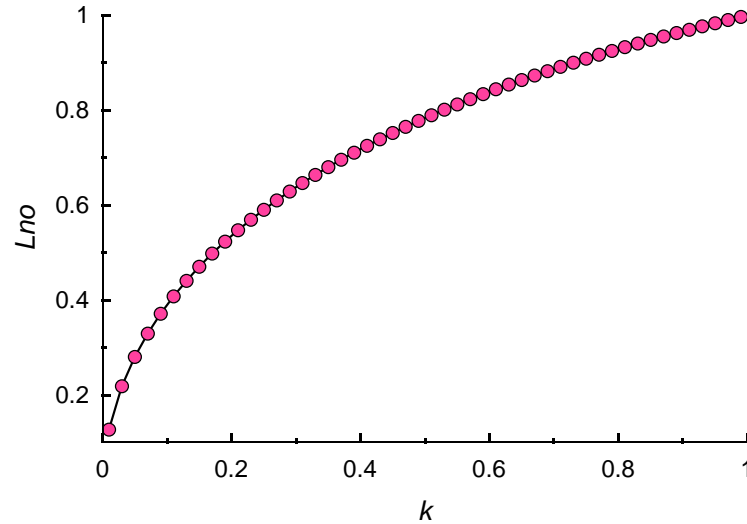


Fig. 5.3 Normalized length as a function of impedance ratio.

Spurious Resonance Frequencies

Fundamental resonance frequency is represented by f_o , whilst the lowest spurious frequencies of $\lambda_g/4$, $\lambda_g/2$ and λ_g are represented by f_{SA} , f_{SB} and f_{SC} , respectively. By assuming $\theta_1 = \theta_2 = \theta_o$ in the analysis, the resonator electrical lengths corresponding to spurious frequencies f_{SA} , f_{SB} and f_{SC} can be represented as θ_{SA} , θ_{SB} , and θ_{SC} , respectively. From Eqn.(5.4), i.e. $\tan\theta_1 \tan\theta_2 = k$. As $\theta_1 = \theta_2 = \theta_o$ so $\tan^2\theta_o = k$. $\therefore \theta_o = \tan^{-1}\sqrt{k}$ for f_{SA} . The resonance conditions for $\lambda_g/2$ and λ_g resonators can be derived from the expression:

$$(k \tan\theta_1 + \tan\theta_2)(k - \tan\theta_1 \tan\theta_2) = 0$$

$$\text{or } (k \tan\theta_o + \tan\theta_o)(k - \tan^2\theta_o) = 0$$

$$\tan\theta_o(k + 1)(k - \tan^2\theta_o) = 0$$

Solutions of this equation are:

$$\theta_o = \tan^{-1}\sqrt{k} \quad (5.14)$$

$$\text{As } \theta_{SB} = \theta_{SC} = \frac{\pi}{2}$$

$$\therefore \frac{f_{SA}}{f_o} = \frac{\theta_{SA}}{\theta_o} = \frac{\pi - \theta_o}{\theta_o} = \frac{\pi}{\theta_o} - 1 = \frac{\pi}{\tan^{-1}\sqrt{k}} - 1 \quad (5.15)$$

$$\frac{f_{SB}}{f_o} = \frac{f_{SC}}{f_o} = \frac{\theta_{SB}}{\theta_o} = \frac{\pi}{2\tan^{-1}\sqrt{k}} \quad (5.16)$$

The fundamental and spurious frequencies should be as far as possible. The graph in Fig. 5.4 suggests that a $\lambda_g/4$ resonator with a small k value should be chosen for optimal design, which simultaneously minimizes resonator length. In particular, the frequency ratio between its second and first resonant modes can be made greater than 2 for smaller magnitudes of k .

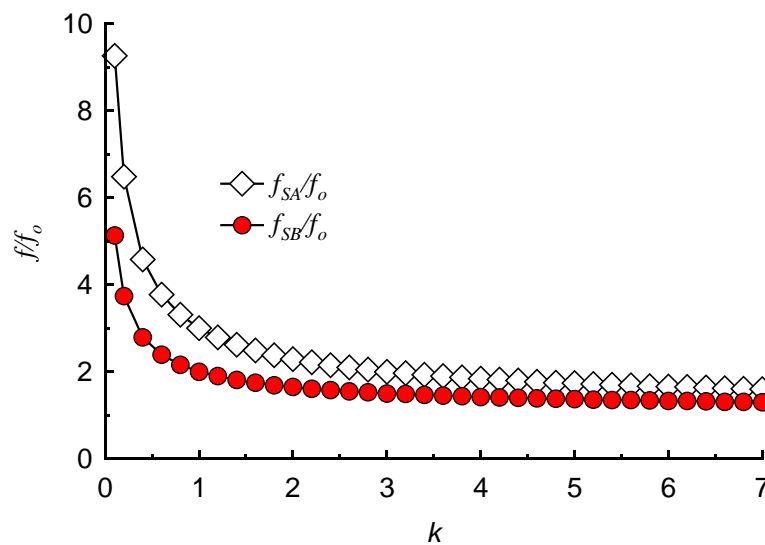


Fig. 5.4 Ratio of lowest spurious frequencies f_{SA} ($\lambda_g/4$) and f_{SB} ($\lambda_g/2$) to fundamental frequency (f_o).

5.1.2 Odd Mode Analysis

In odd mode asymmetric excitation is assumed at the input and output ports. The consequence of this is virtual short circuit in the symmetry plane A-B of the resonator. The short-circuited stub, with characteristic impedance $2Z$, is bypassed by the virtual short circuit as it appears in parallel to it. Therefore, the odd mode equivalent resonator circuit configuration takes the form of that in Fig. 5.5.

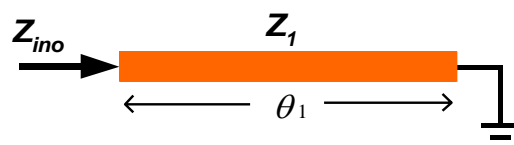


Fig. 5.5 Odd-mode equivalent circuit model.

$$\therefore Z_{ino} = jZ_1 \tan \theta_1 \quad (5.17)$$

5.2 Wideband Filter Structure

The layout structure of the wideband filter is shown in Fig. 5.6. The high impedance three finger input/output feed-lines are coupled in a parallel to realize strong EM coupling. The middle finger of the three finger feed-line is connected to a low impedance microstrip section whose possible side comprises two high impedance lines each of which are coupled to a stub-loaded half-wavelength resonator. The stub-loaded resonators are arranged on opposite sides to each other to form a parallel resonant doublet, which results in the filter exhibiting a significantly widened passband.

The filter was constructed on dielectric substrate Arlon CuClad217LX with thickness (h) of 0.794 mm, dielectric constant (ϵ_r) of 2.17 mm, copper conductor thickness (t) of 35 μm , and loss-tangent ($\tan\delta$) of 0.0009. The filter was analysed using a full wave electromagnetic simulator (ADS™) and Momentum software. The optimized geometric parameters are: $W_a = 0.2$ mm, $W_{a1} = 0.82$ mm, $W_{a2} = 0.2$ mm, $W_d = 1.23$ mm, $L_a = 6.78$ mm, $L_{a1} = 4.85$ mm, $L_{b1} = 4$ mm, $L_{b2} = 3.63$ mm, $L_{b3} = 11.486$ mm, $L_1 = 4.97$ mm, $L_2 = 3.3$ mm, $L_3 = 1.57$ mm, $L_4 = 1.72$ mm, $L_5 = 5.15$ mm, $L_6 = 1.09$ mm, $S_3 = 0.52$ mm, and $S_4 = 0.2$ mm. The measured frequency response of the filter in Fig. 5.8 shows it possesses a very sharp roll-off centred around 5.05 GHz with insertion-loss of 0.73-dB and return-loss better than 10 dB. The loss is attributed to conductor and dielectric losses. The two transmission zeros near the lower and upper cut off frequencies at 4.42 GHz and 5.74 GHz, respectively, result in the sharp selectivity of the filter. The 3-dB fractional bandwidth of the filter is 23%. Fig. 5.9 shows the filter has out-of-band rejection is better than 20 dB over a very wideband between 2 to 4.42 GHz and 5.74 to 11.6 GHz. The group-delay of the filter is approximately flat in the passband (< 0.4 ns), as shown in Fig. 5.10.

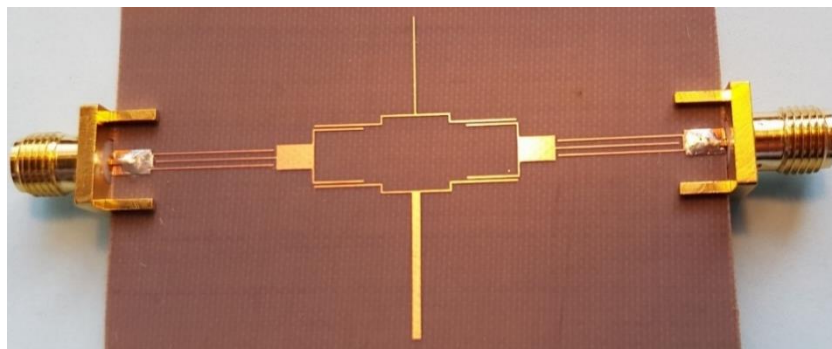
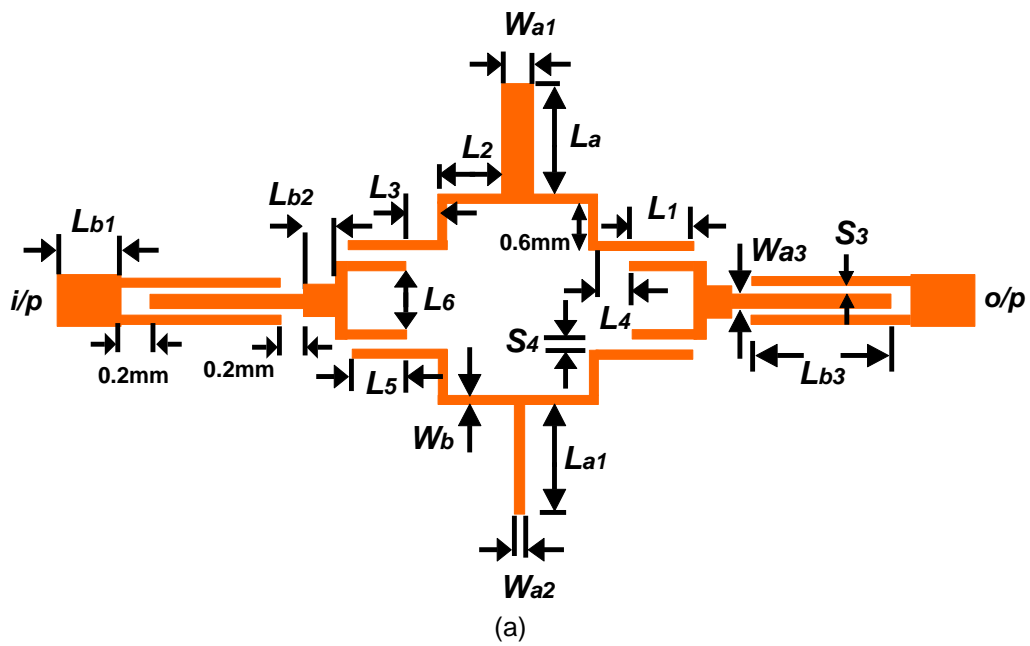


Fig. 5.6 (a) Configuration of the three finger interdigital coupled feed-line bandpass filter using stub loading resonator, and (b) photograph of the filter.

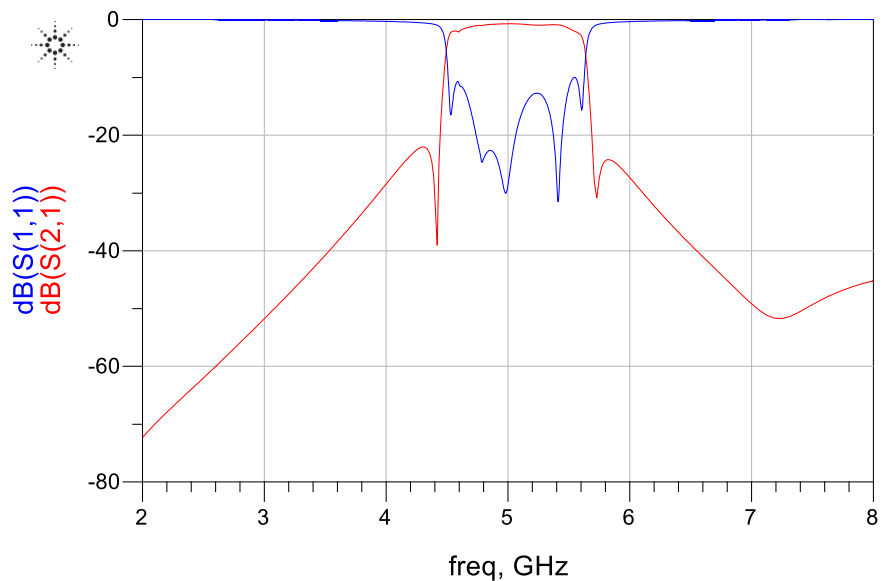


Fig. 5.7 Simulated frequency response of the stub loaded resonator filter

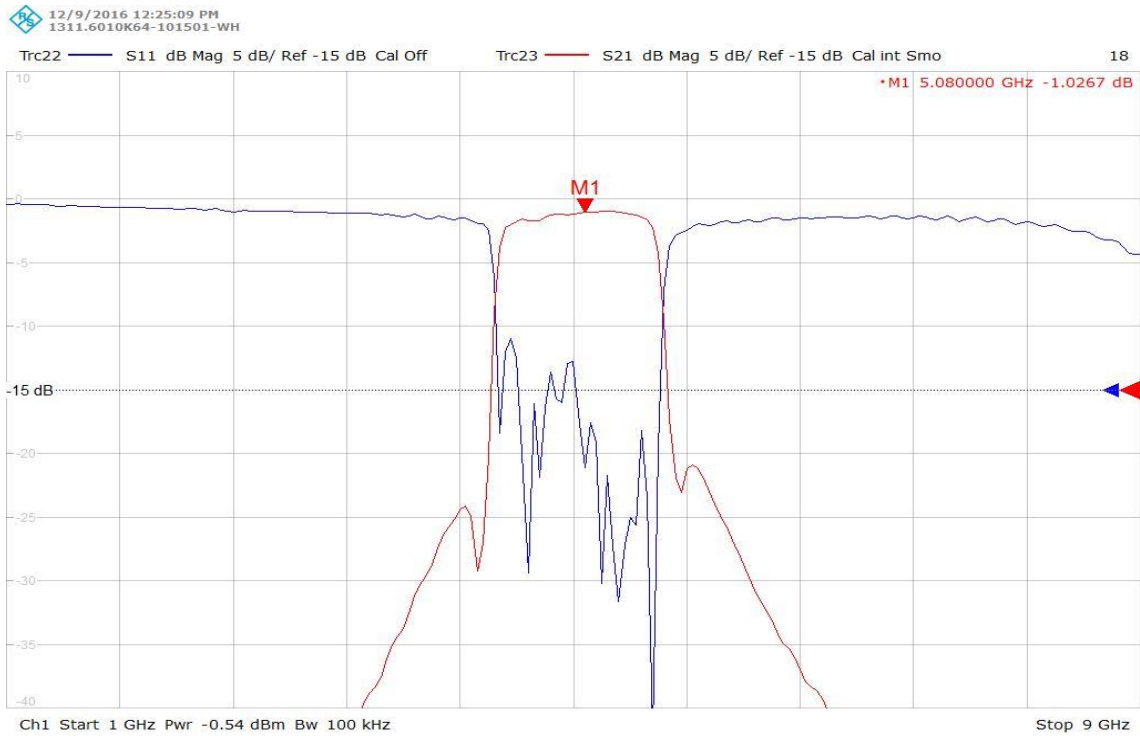


Fig. 5.8 Measured response of stub loaded resonator filter.

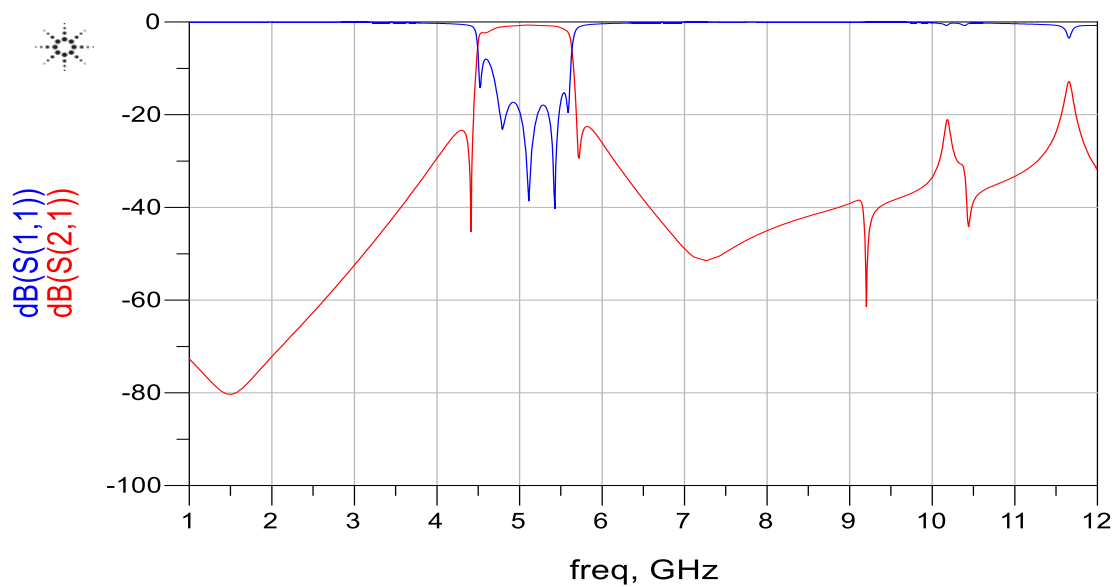


Fig. 5.9 Wide stopband performance of the stub loaded resonator filter with -20 dB attenuation.

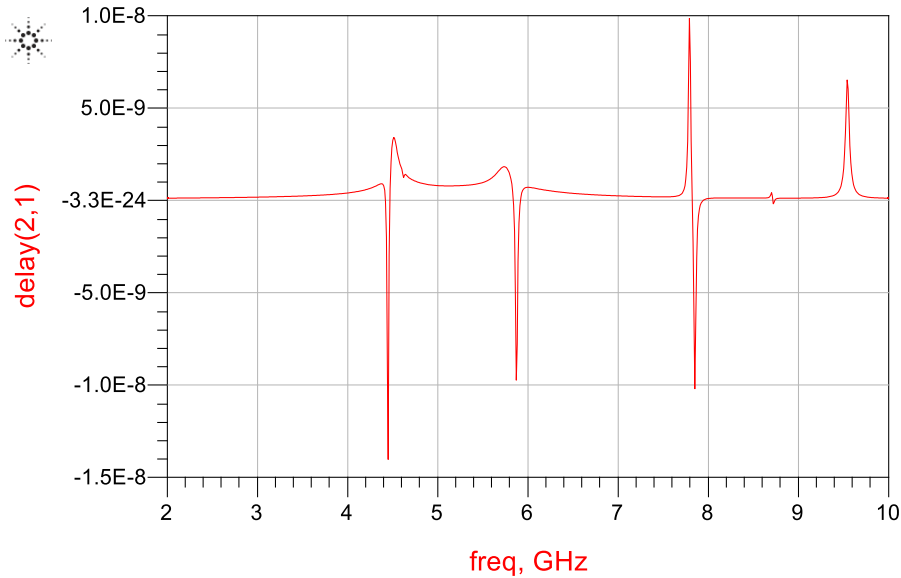


Fig. 5.10 Group-delay response of the stub loaded resonator filter.

The length of the low impedance section (L_{b2}) on the filter's response was investigated. The results of this study are shown in Figs. 5.11 to Fig. 5.13 and given in Table 5.1. As the length is reduced the out-of-band rejection on the right-hand side of the filter's passband deteriorates significantly. With a length of 1.83 mm the rejection is around 10 dB. Although the length has no effect on the filter's centre frequency however the insertion-loss increases slightly from 0.43-dB to 0.65 dB with reduction in L_{b2} from 4.83 mm to 1.83 mm.

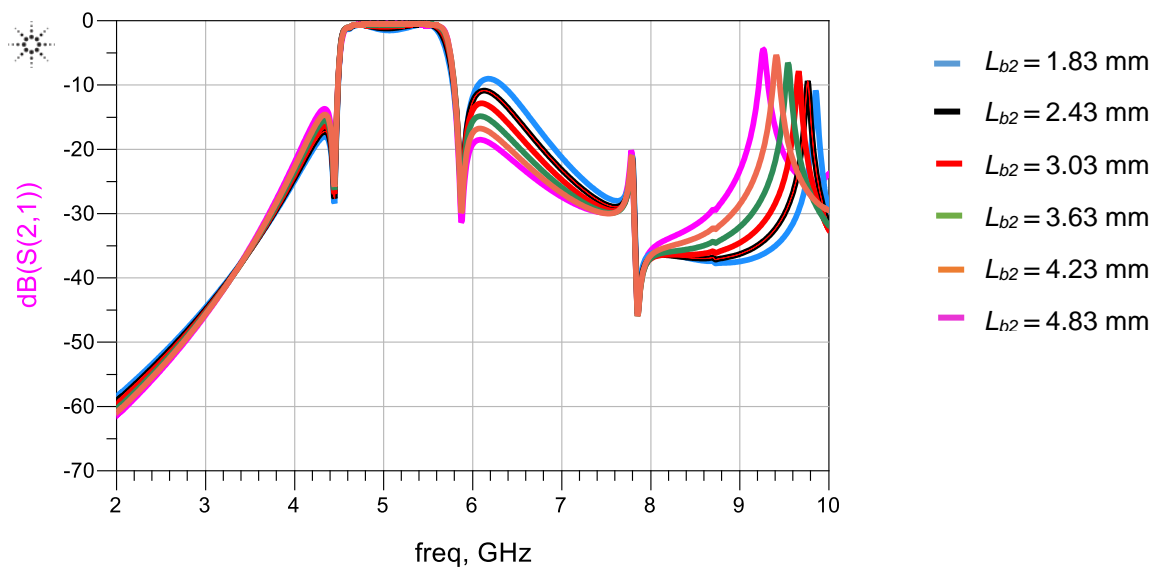


Fig. 5.11 Frequency response of the filter as a function of low impedance section length L_{b2} .

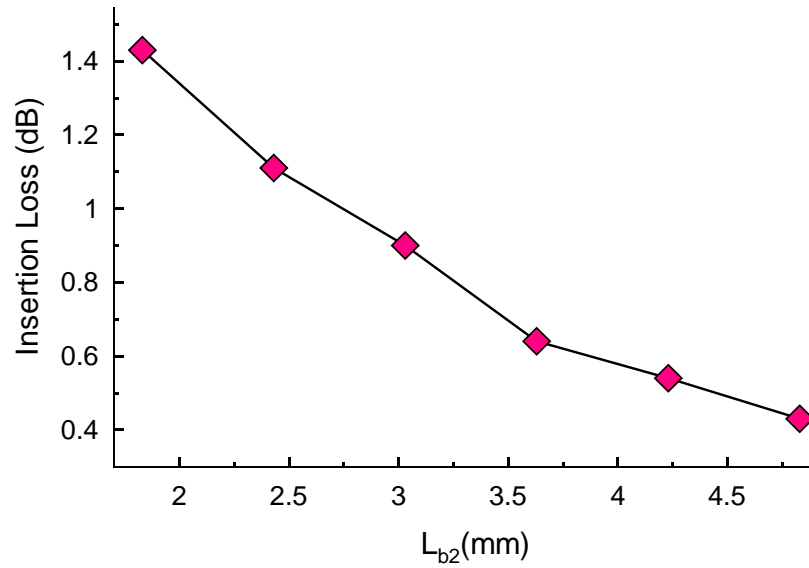


Fig. 5.12. Effect of low impedance section length L_{b2} on insertion-loss performance.

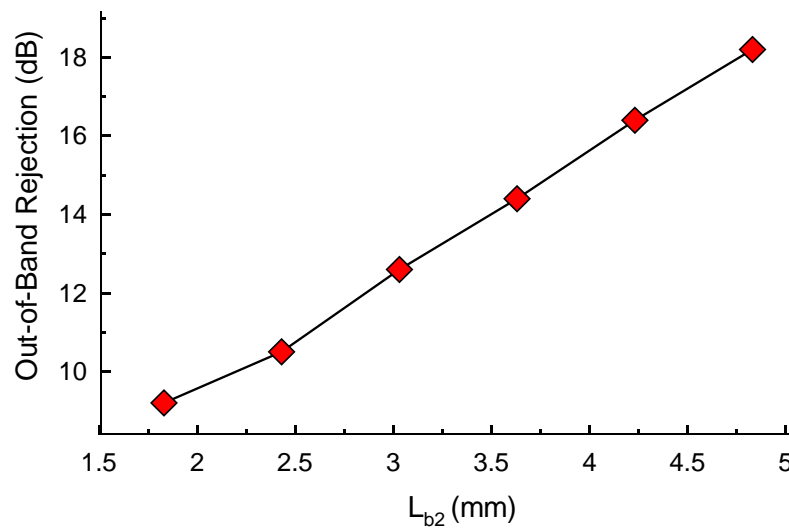


Fig. 5.13. Effect of low impedance section length L_{b2} on out-of-band rejection level.

Table 5.1 Effect of low impedance section length L_{b2} on the filter's centre frequency, loss performance and band rejection level.

L_{b2} (mm)	IL (dB)	Out-of-band rejection (GHz)
1.83	1.43	9.2
2.43	1.11	10.5
3.03	0.90	12.6
3.63	0.64	14.4
4.23	0.54	16.4
4.83	0.43	18.2

As the coupling gap (S_4) between the feed-line resonators and the stub loaded half-wavelength resonator is increased from its optimized value of 0.2 mm, the passband response becomes distorted as shown in Fig. 5.14.

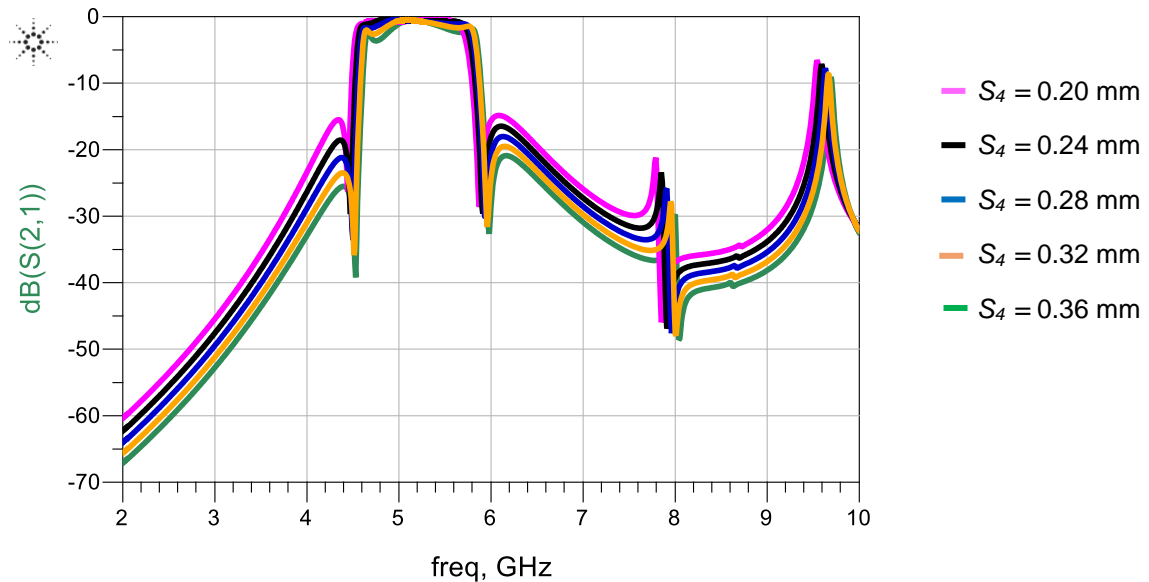


Fig. 5.14 Frequency response of the proposed filter as a function of inter-resonator coupling gap.

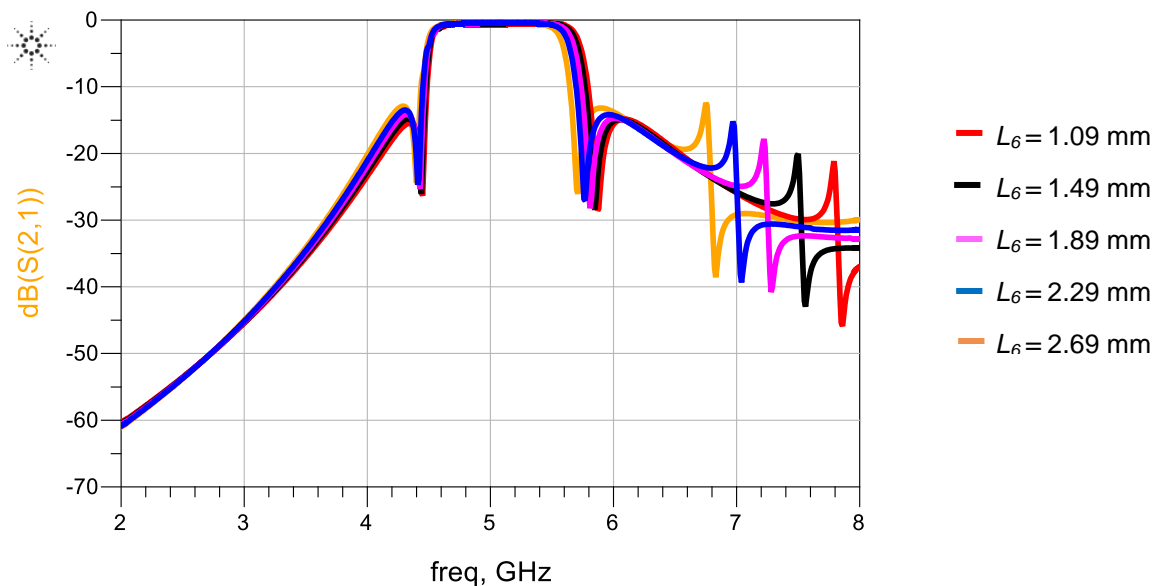


Fig 5.15 Frequency response of the filter as a function of resonator separation (L_6).

The effect of the input and output resonator separation (L_6) is shown in Figs. 5.15 and 5.16, and tabulated in Table 5.2. When the resonator length is reduced from 2.69 mm to 1.09 mm the bandwidth of the filter reduces from 1.33 GHz to 1.19 GHz and the insertion-loss increases from 0.39 dB to 0.64 dB. There is negligible effect on its centre frequency

and the lower transmission zero. However, the out-of-band transmission zeros moves down in frequency from 7.89 GHz to 6.89 GHz, thus reducing the upper stopband range.

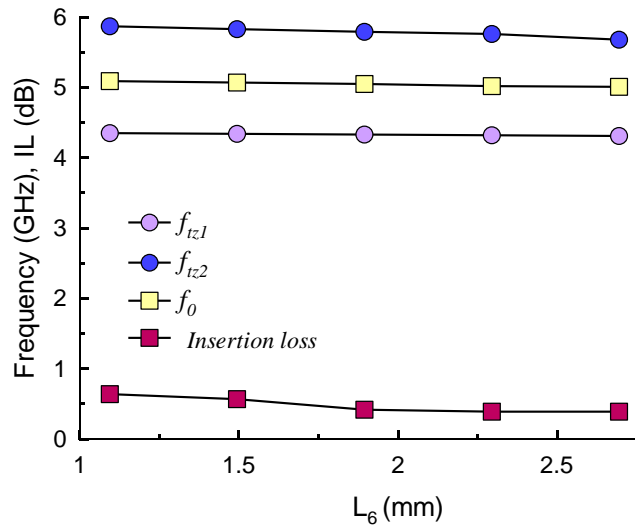


Fig. 5.16 Effect of resonator separation (L_6) on the centre frequency, loss performance and transmission zeros.

Table 5.2. Effect of resonator separation length (L_6) on the transmission zeros, centre frequency and loss performance.

L_6 (mm)	f_{z1} (GHz)	f_{z2} (GHz)	f_0 (GHz)	IL (dB)
1.094	4.35	5.87	5.09	0.64
1.494	4.34	5.83	5.07	0.57
1.894	4.33	5.79	5.05	0.42
2.294	4.32	5.76	5.02	0.39
2.694	4.31	5.68	5.01	0.39

The resonator coupling length (L_5) has insignificant effect on the filter's passband response as is evident from the results in Figs. 5.17 and 5.18, and Table 5.3. The transmission zero at 7.89 GHz shifts down in frequency to 7.61 GHz when the length is reduced from 5.55 mm to 4.75 mm. However, the out-of-band rejection is maintained around -20 dB.

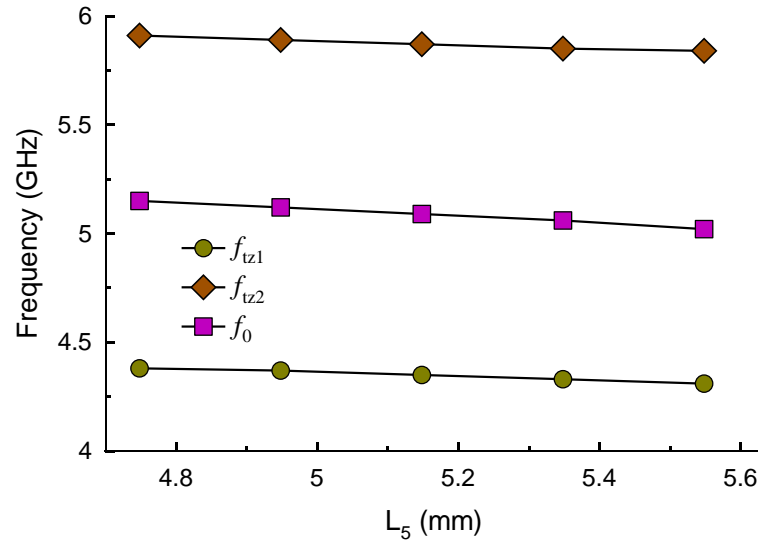


Fig. 5.17 Effect of resonator coupling length (L_5) on centre frequency and transmission zeros.

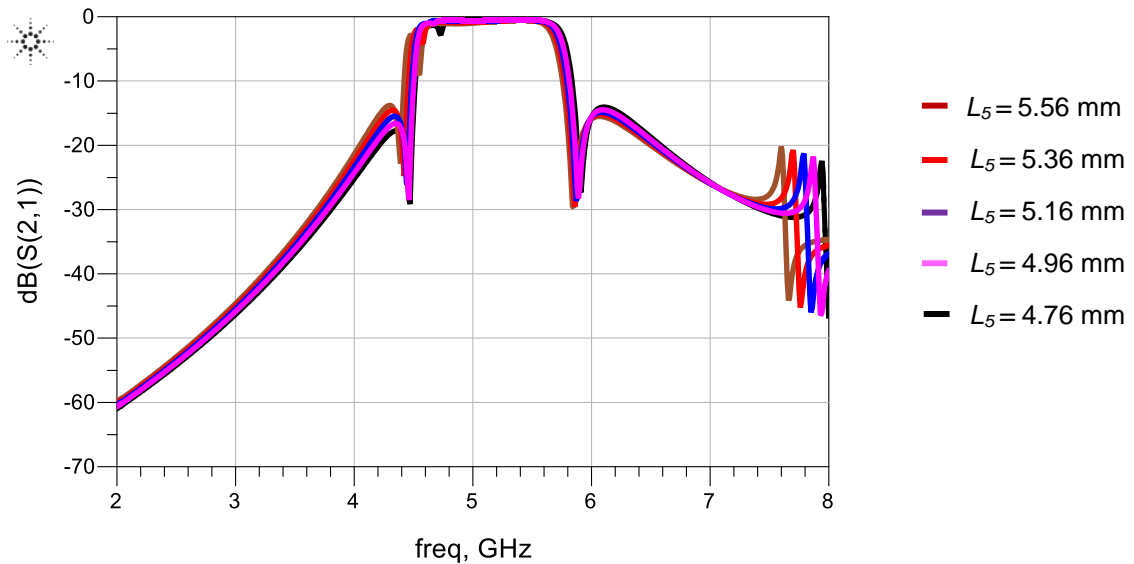


Fig. 5.18 Frequency response of the proposed filter as a function of resonator coupling length (L_5).

Table 5.3. Effect of resonator coupling length (L_5) on the transmission zeros and centre frequency.

L_5 (mm)	f_{z1} (GHz)	f_{z2} (GHz)	f_0 (GHz)
5.548	4.31	5.84	5.02
5.348	4.33	5.85	5.06
5.148	4.35	5.87	5.09
4.948	4.37	5.89	5.12
4.748	4.38	5.91	5.15

Fig. 5.19 shows the frequency response for different values of feed-line coupling gap (S_3). As the coupling gap is increased the out-of-band rejection improves however this is at the expense of creating larger passband ripples. The optimum value of coupling gap is 0.72 mm to realize a flat passband and wide stopband with around 20 dB of rejection.

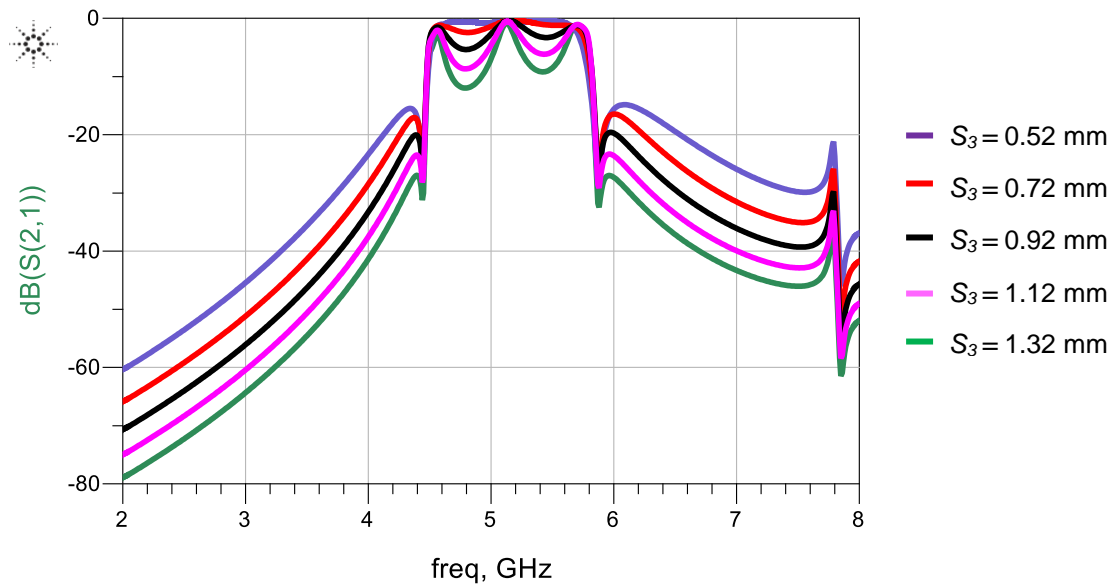


Fig. 5.19 Frequency response of the proposed filter as a function of feed-line coupling gap (S_3).

The effect of open stub length (L_a) is assessed by varying its value from 7.78 mm to 6.78 mm as shown in Figs. 5.20 and Fig. 21, and in Table 5.4. It is observed as the length L_a increased from its optimized value (i) the lower transmission zero shifts downward in frequency; (ii) a dip is created at the top left corner of the passband; and (iii) the out-of-band rejection level on lower frequency side of the passband improves greatly from -15.8 dB to -32.80 dB. The change has only minor effect on upper band rejection level, while centre frequency, insertion-loss and upper transmission zero remain unchanged. These result show the length L_a gives us freedom to control the lower transmission zero to some extent without significantly effecting the upper transmission zero and other filter characteristics.

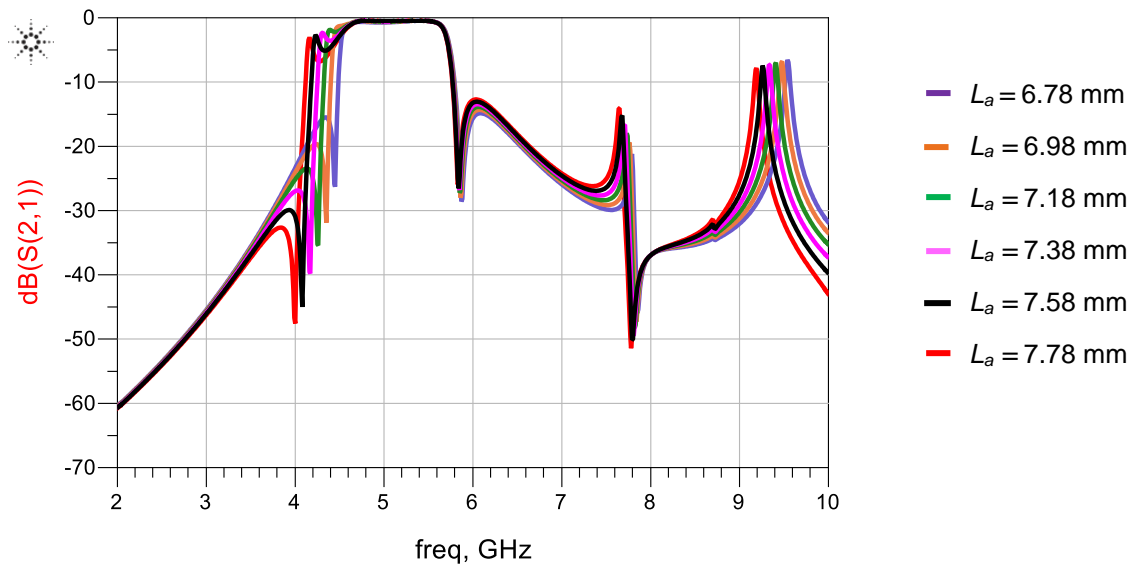


Fig. 5.20 Frequency response of the proposed filter as a function of open stub length (L_a).

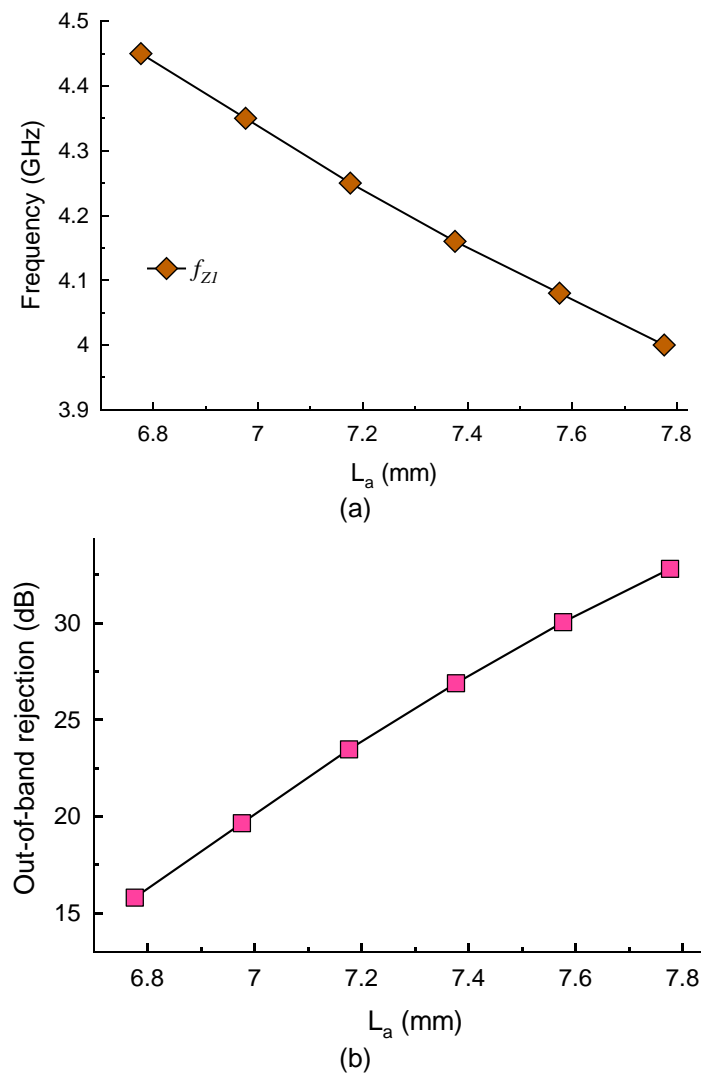


Fig. 5.21 Effect of open stub length (L_a) on (a) lower transmission zero, and (b) lower out-of-band rejection level.

Table 5.4 Effect of open stub length on lower transmission zero and lower out of band rejection level.

L_a (mm)	f_{z1} (GHz)	Out-of-band rejection (GHz)
6.78	4.45	15.80
6.98	4.35	19.65
7.18	4.25	23.47
7.38	4.16	26.89
7.58	4.08	30.04
7.78	4.00	32.80

In Fig.5.22 shows when the length L_{a1} is changed from 4.83 to 4.03 mm, the upper transmission zero moves upward in frequency, a dip appears at the top right corner of the passband, and the out-of-band rejection level improves significantly on the high frequency side of passband. However, the lower transmission zero, insertion-loss, out-of-band rejection level on lower frequency side of passband and the centre frequency remain virtually fixed. The results are also tabulated in Table 5.5. The length L_{a1} also give us freedom to control the upper transmission zero to some extent without affecting the other filter characteristics. It is also observed the width W_{a2} of the open stub can be used to control the upper transmission zero with little degradation in filter response but not as effectively as with length L_{a1} .

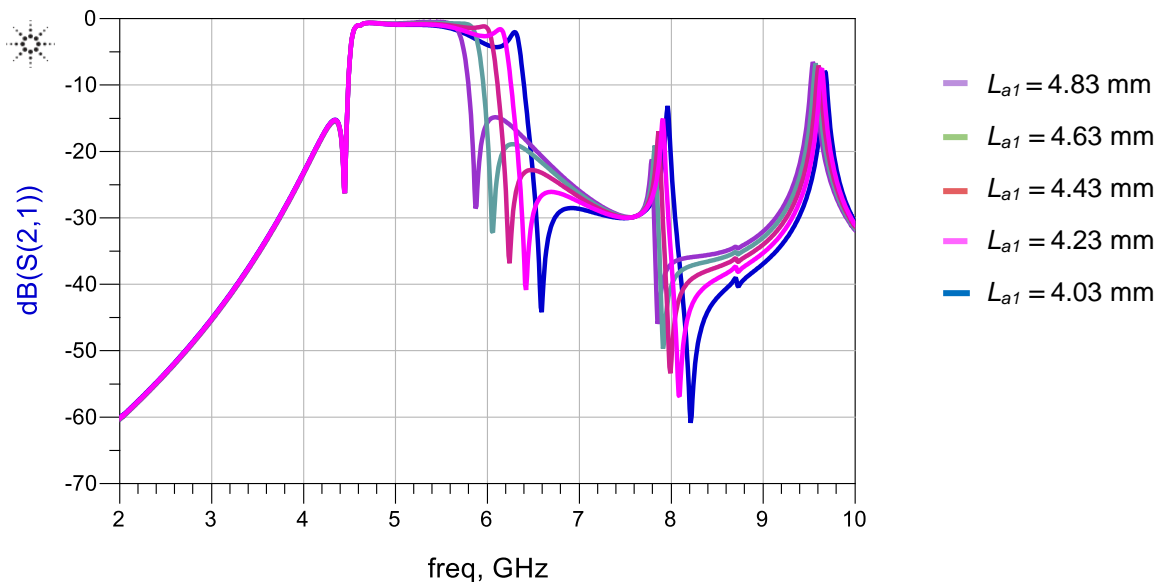
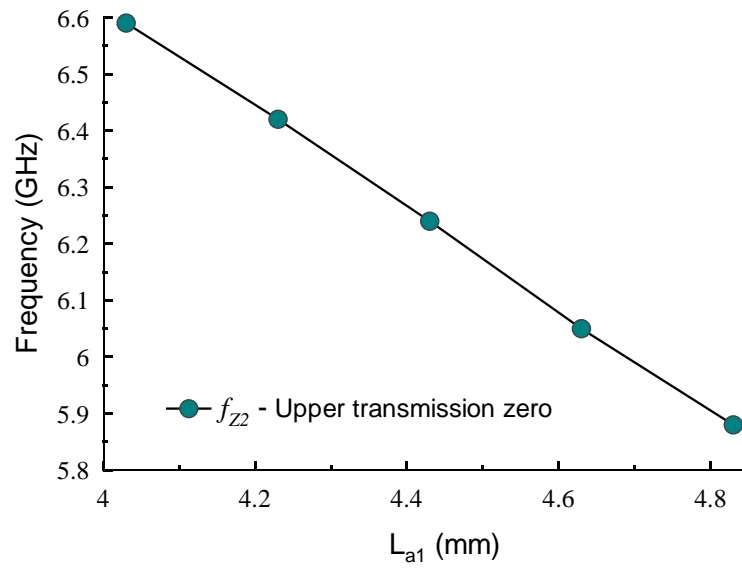
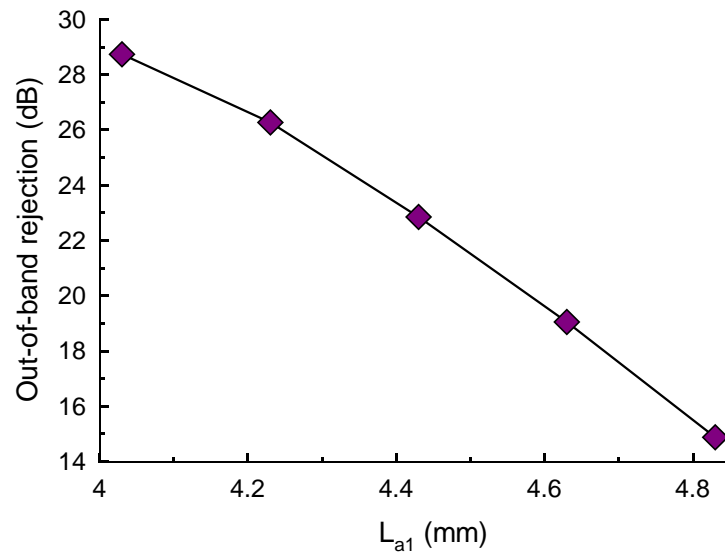


Fig. 5.22 Frequency response of the proposed filter as a function of open stub length (L_{a1}).



(a)



(b)

Fig. 5.23 Effect of open stub length (L_{a1}) on (a) upper transmission zero, and (b) upper out-of-band rejection level.

Table 5.5 Effect of open stub length on upper transmission zero and upper out of band rejection level.

L_{a1} (mm)	f_{z2} (GHz)	Out-of-band rejection (GHz)
4.83	5.88	14.88
4.63	6.05	19.05
4.43	6.24	22.85
4.23	6.42	26.27
4.03	6.59	28.74

The effect of the interdigital coupled feed length (L_{b3}) on the filter's characteristics was also investigated. The results are presented graphically in Fig. 5.24 and 5.25, and given in Table 5.6. The out-of-band rejection level on either side of passband decreased significantly with decrease in L_{b3} from 11.49 mm to 9.89 mm. The change in L_{b3} causes a deep dip at the centre of the passband, but this has no effect on other characteristics of the filter.

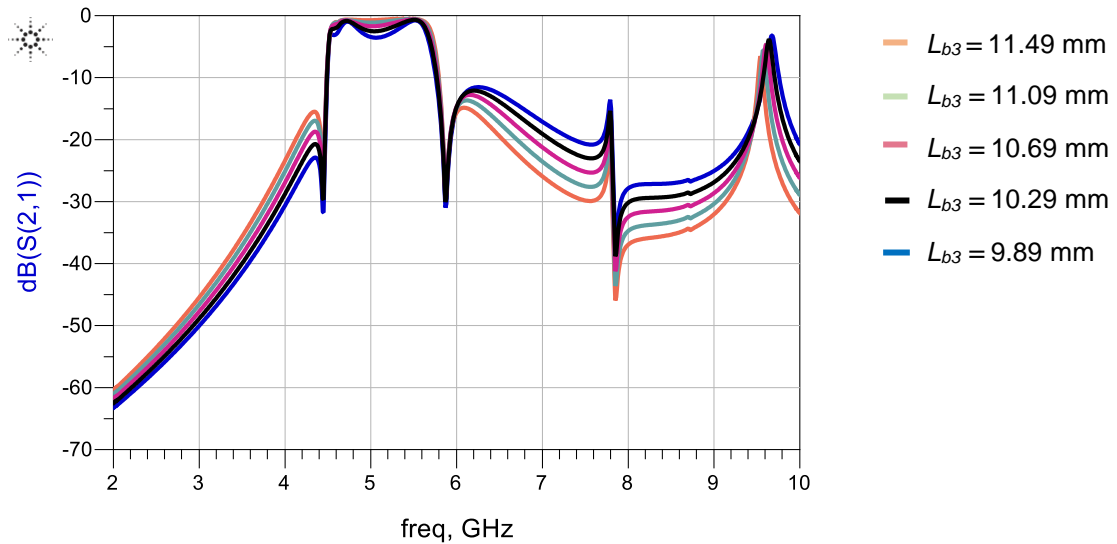


Fig. 5.24 Frequency response of the proposed filter as a function of length (L_{b3}).

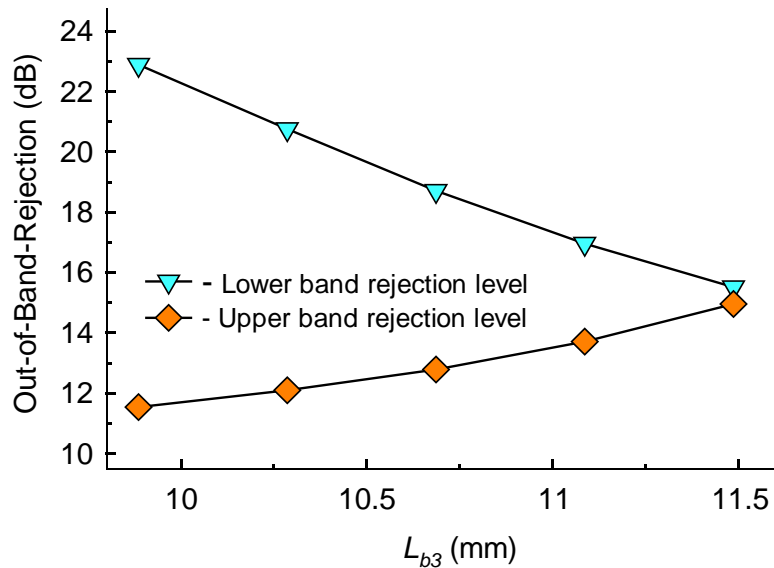
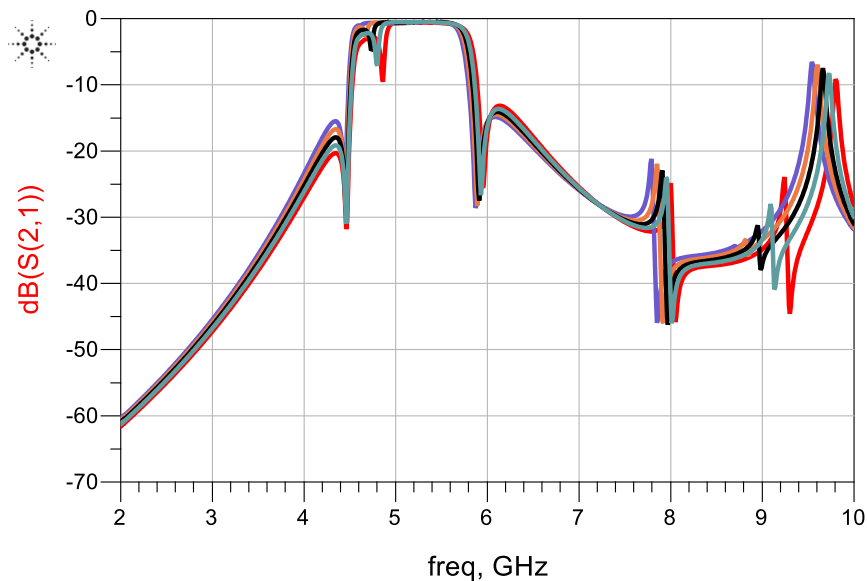


Fig. 5.25 Effect of length (L_{b3}) on out of band rejection levels.

Table 5.6 Effect of coupled feed-lines length on bandpass rejection levels.

L_{b3} (mm)	Lower rejection level (GHz)	Upper rejection level (GHz)
11.49	15.52	14.96
11.09	16.96	13.71
10.69	18.71	12.79
10.29	20.76	12.10
9.89	22.89	11.54

It is observed the length (L_i) creates a notch which appears next to the lower edge of the passband, which moves slightly towards the centre of the passband as the length is varied from 4.97 mm to 4.17 mm. It also improves the lower out-of-band rejection level but only marginally improves the upper out-of-band rejection level. The other filter characteristics remain unchanged, as shown in Fig. 5.26. Lengths (L_4) and (L_3) have almost a similar effect on filter response.

Fig. 5.26 Frequency response of the proposed filter as a function of coupled length (L_i).

Increase in width W_{a1} of the open stub from 0.22 mm to its optimized value 0.82 mm improves the out-of-band rejection level on both sides of the passband but there is a slight increase in the insertion-loss; however other filter characteristics remain unchanged, as shown in Fig. 5.27.

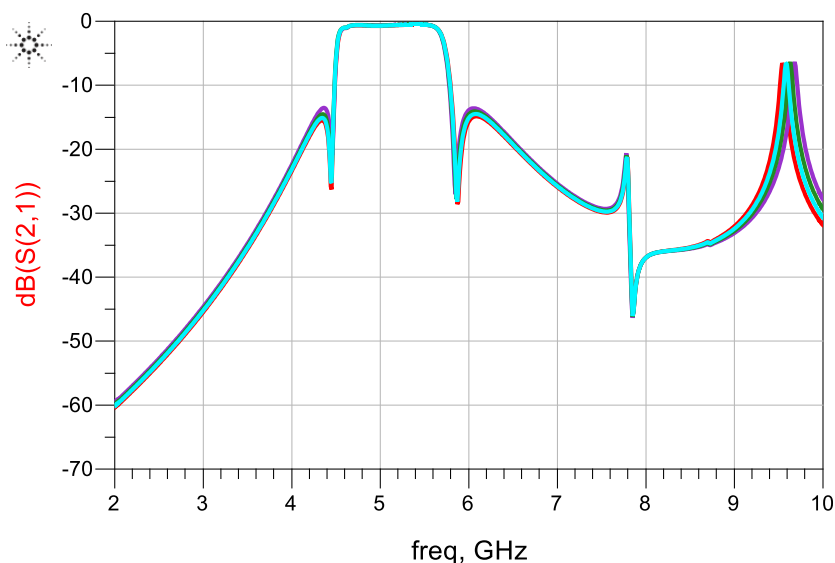


Fig. 5.27 Frequency response of the proposed filter as a function of width (W_{a1}).

5.3 Summary

Stub loaded resonator (SLR) was analyzed in terms of odd-mode and even-mode. The result of this analysis reveals that the length of SLR can be reduced by increasing the impedance of the stub in relation to the resonator, i.e. reducing the impedance ratio k . Also the spacing between the fundamental and spurious responses generated by the SLR can be increased by reducing the impedance ratio k . A novel wideband bandpass filter structure was proposed that exhibits a sharp roll-off with high out-of-band rejection. The quasi-elliptic function filter comprises open-loop resonators that are coupled to each other using a SLR. The input/output feed-lines are interdigitally coupled to the filter structure. The proposed filter can achieve a 3-dB fractional bandwidth of 23%.

References

1. R. Lerdwanittip, A. Namsang, "Bandpass filters using stepped impedance resonators and stub loads for wide harmonics suppression," *Electrical Engineering/Electronics, Computer, Telecommunications and Information Technology (ECTI-CON)*, May 2014, pp.1-4
2. X.Y. Zhang, Q. Xue, "Novel centrally loaded resonators and their applications to bandpass filters," *IEEE Transactions on Microwave Theory and Techniques*, vol. 56, no. 4, April 2008, pp.913-921
3. X.Y. Zhang, J.-X. Chen, Q. Xue, and S.-M Li, "Dual-band filters using stub-loaded resonators," *IEEE Microw. Wireless Compon. Letter.*, vol. 17, no. 8, Aug. 2007, pp. 583–585.
4. W.-Y. Chen, M.-H. Weng, "A new tri-band bandpass filter based on stub-loaded step-impedance resonator," *IEEE Microwave and Wireless Components Letters*, vol. 22, no. 4, April 2012, pp.179-181.

Design of Miniaturised UWB Bandpass Filters for Sharp Rejection Skirts and Very Wide Stopband Performance

6.0 Introduction

Being a vital component of UWB wireless communication systems, ultra-wideband bandpass filters are receiving great attention by researchers in industry and academia ever since Federal Communications Commission (FCC) in 2002 permitted the commercial use of the frequency band between 3.1 to 10.6 GHz [1]. This is because design and realization of an UWB filter possessing characteristics of small size, high selectivity, low insertion-loss, high return-loss, flat group delay and wide stopband are presenting a great challenge.

The accepted definition of an UWB bandpass filter is one that allows a signal through it with minimum bandwidth of 500 MHz or has a minimum fractional bandwidth of 20%. This definition is mathematically expressed as [1]:

$$\text{Fractional bandwidth} = 2 \left(\frac{f_1 - f_0}{f_1 + f_0} \right) \quad (1)$$

Where f_0 and f_1 are lower and upper cut off frequencies, respectively. In the recent years there has been a tremendous increase in the development of various UWB filter structures using various techniques. These devices have been employed in diverse military and commercial applications, requiring high data rate and immune to multi-path fading such as wireless communication systems, localization and ground penetration radar, and medical imaging [2]. Although traditional filter designs based on microstrip technology possess desirable features of low insertion-loss, high return-loss and light weight, however these filters do not meet the stringent requirements of modern systems including sharp roll-off, high rejection stopband and flat passband group delay [2].

Makimoto in [3] first proposed the use of stepped impedance resonators (SIR) in the design of bandpass filters to address issues that degrade filter performance in terms of parasitic bands and narrow stopband between the first spurious response and the fundamental mode. These issues cannot be eradicated using traditional filters based on quarter or half wavelength parallel coupled resonators. The impedance ratio of SIR can be used to control the parasitic band and spurious responses without enlarging the overall circuit size. In [4], the authors report an UWB bandpass filter using SIR that is implemented on a superconducting material. The filter exhibits sharp rejection skirts and is highly

compact in size. Here multiple-modes are excited by loading a stepped-impedance open-end stub in shunt to a modified SIR. The SIR generates three resonant modes within the 3.1–10.6 GHz band, and the stepped impedance open-end stub creates two transmission zeros and two additional resonant modes, shown in Fig. 6.1. The input and output feed-lines are through interdigital coupled lines to realize a passband insertion-loss of 0.58 dB, return-loss better than 10.6 dB, and the group delay variation of 1.76 ns.

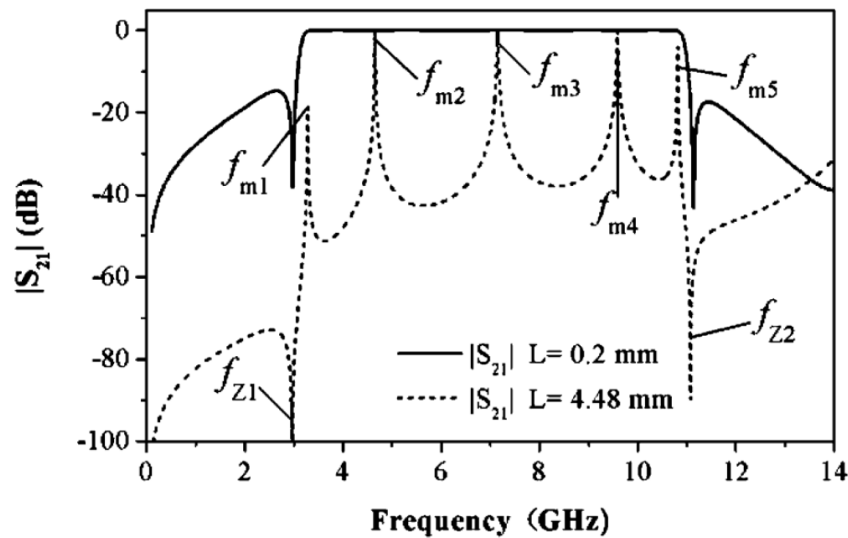


Fig. 6.1. Simulated insertion-loss response of the UWB filter proposed in reference [4].

Fig. 6.2 shows the S-parameter response of an UWB BPF proposed in [5]. It comprises of multi stub loaded ring resonator that acts as a multimode structure. In this filter, the length of stubs can be used to tune the resonant modes of the resonator. Four resonant frequencies are contained within the passband and two transmission zeros are generated. The measured S_{21} response in Fig. 6.2 shows the passband rejection skirts, especially the lower, are not sharp or steep and upper stopband is limited to about 1 GHz.

In [6], an ultra-wideband bandpass filter is designed using multi-mode resonators that generate four modes, i.e. two odd and two even, which are located within the passband, as shown in Fig. 6.3. The multi-mode resonators comprise three pairs of coupled line sections and two pairs of open circuited stubs. With this filter structure, there are two transmission zeros near the lower and upper cut off frequencies of passband, however the roll off frequency-selectivity, especially the lower, is considered wide and the upper stopband performance is 6 GHz, from 12 GHz to 18 GHz.

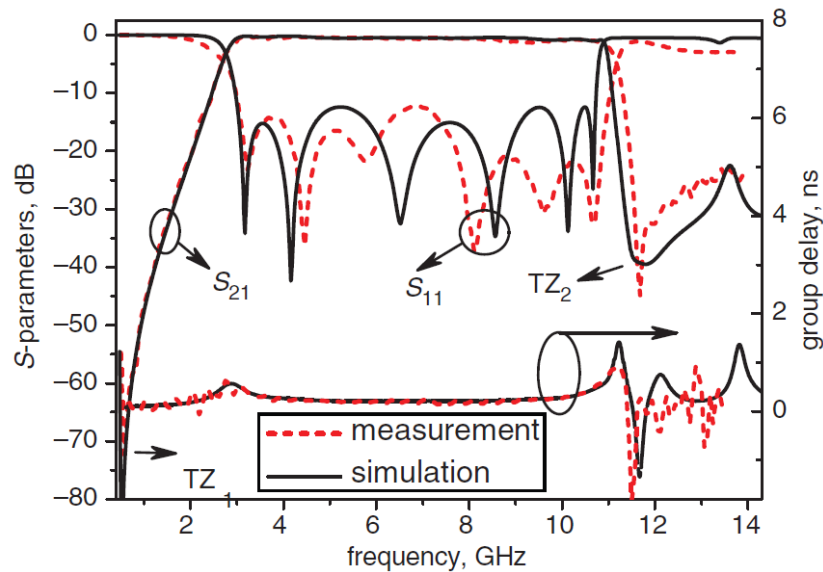


Fig. 6.2. Measured and simulated S-parameter and group delay response of UWB filter proposed in reference [5].

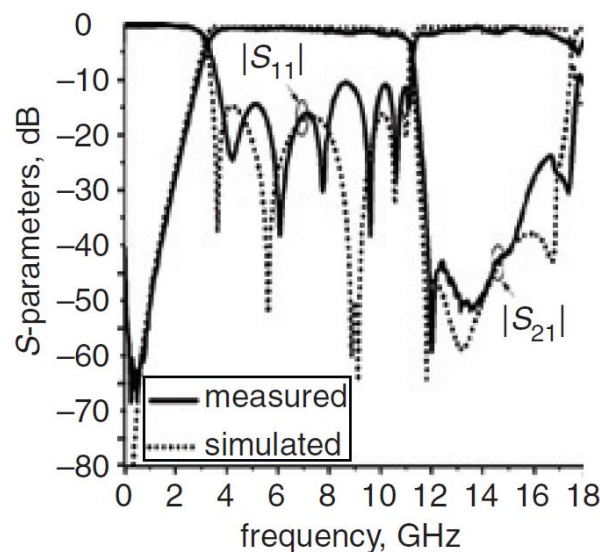


Fig. 6.3. Simulated and measured frequency responses of proposed UWB bandpass filter [6].

Researchers have used different techniques and structures to realize ultra-wideband bandpass filters. In [7], lowpass and highpass combining technique are utilized to develop the UWB BPF, but the resulting structure is too big for modern systems.

An UWB bandpass filter using quintuple mode stub loaded resonator is presented in this chapter, which possess steep selectivity skirts and wide upper stopband performance. The UWB bandpass response is realized by combining the first five resonant modes created by the multimode resonator structure, shown in Fig. 6.4(a). This structure gives greater degree of freedom to control its resonant modes so that the resonant frequencies can be

relocated to realize the required UWB response. In the final filter structure multiple stubs and parallel coupled lines are used to generate transmission zeros that suppress the higher order modes. The two transmission zeros near the lower and upper cut off frequencies of passband provide sharp frequency-selectivity.

6.1.0 Proposed Multiple Mode Resonator Design

The MMR constituting the proposed UWB filter is essentially a stepped impedance transmission-line resonator loaded with a centrally located stepped impedance open-circuited stub, which is folded to minimize the overall space occupied by the filter, as shown in Fig. 6.4. Wide out-of-band rejection is implemented by loading the basic MMR structure with two sets of parallel connected high impedance open-circuit stubs that are inwardly folded. The two-parallel open-circuit stubs have admittance and length defined by Y_{01} and θ_s , in Fig. 6.5. These two stubs create finite transmission zeros determined by its length. The MMR structure is electromagnetically coupled to the input and output through interdigital capacitance. The characteristic admittance and length of the horizontal stepped impedance transmission-line resonator are Y_1, θ_1 , and Y_2, θ_2 , respectively; and the characteristic admittance and length of the central stepped impedance stub are Y_3, θ_3 , and Y_4, θ_4 , respectively, as depicted in Fig. 6.5. Since the MMR is symmetrical about B-B' plane it can be analyzed using odd and even-mode analysis. Fig. 6.6(a) and 6.6(b) show the even- and odd-mode circuits. Under odd-mode excitation there is a voltage null in the middle of the MMR structure. This leads to the equivalent circuit of Fig. 6.6(b).

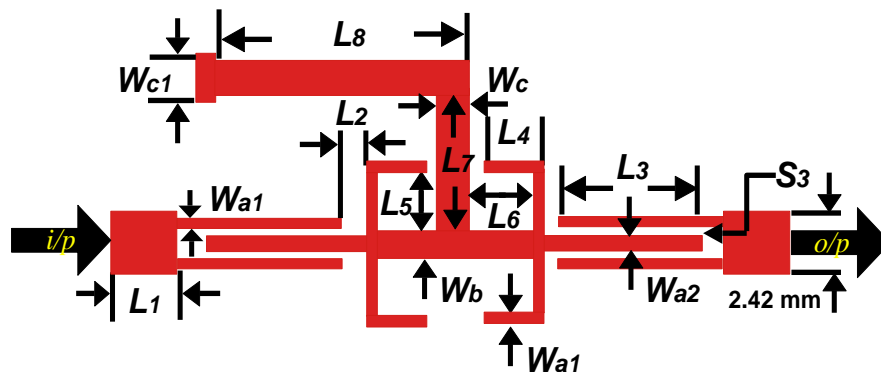


Fig. 6.4. Structure of the proposed UWB quasi-elliptical bandpass filter.

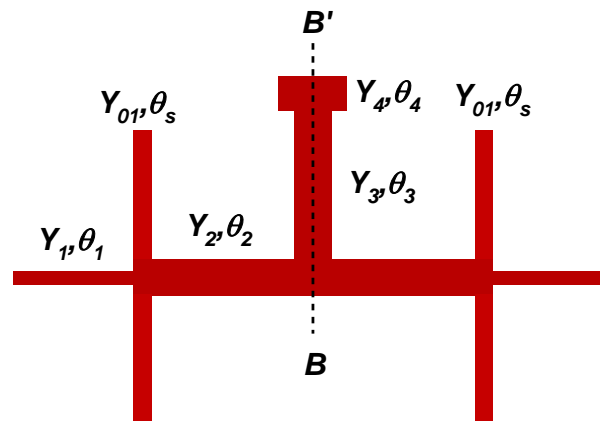


Fig. 6.5. Configuration of basic MMR structure. Parallel open-circuit stubs are indicated in dotted lines.

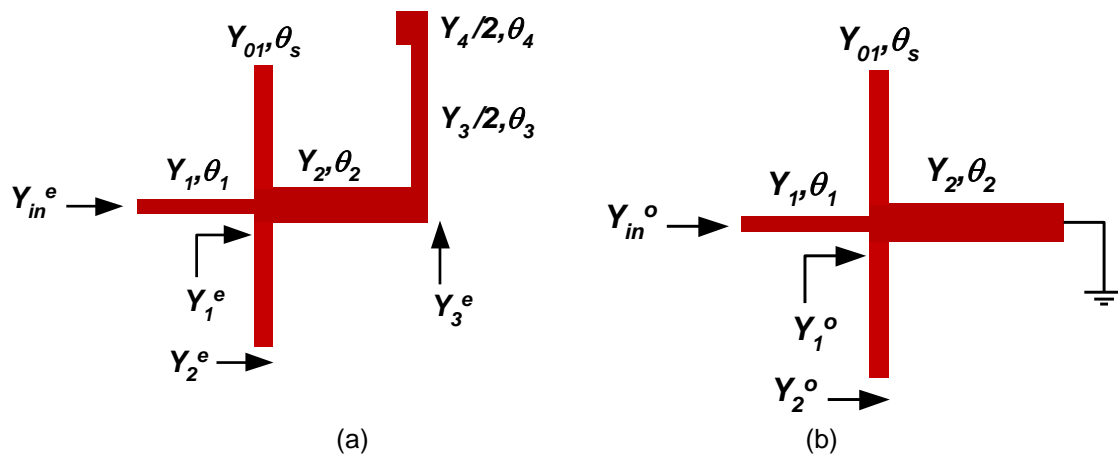


Fig. 6.6. Equivalent circuit model of the MMR structure, (a) even-mode circuit, and (b) odd-mode circuit model.

The admittances in the even-mode structure are represented by

$$Y_{in}^e = Y_1 \left[\frac{Y_1^e + jY_1 \tan \theta_1}{Y_1 + jY_1^e \tan \theta_1} \right] \quad (6.2)$$

$$Y_1^e = Y_{01} \left[\frac{Y_2^e + jY_{01} \tan \theta_s}{Y_{01} + jY_2^e \tan \theta_s} \right] \quad (6.3)$$

$$Y_2^e = Y_2 \left[\frac{Y_3^e + jY_2 \tan \theta_2}{Y_2 + jY_3^e \tan \theta_2} \right] \quad (6.4)$$

$$Y_3^e = j \frac{Y_3}{2} \left[\frac{jY_3 \tan \theta_3 + Y_4 \tan \theta_4}{Y_3 - jY_4 \tan \theta_3 \tan \theta_4} \right] \quad (6.5)$$

Admittances in the odd-mode structure are represented by

$$Y_{in}^o = Y_1 \left[\frac{Y_1^o + jY_1 \tan \theta_1}{Y_1 + jY_1^o \tan \theta_1} \right] \quad (6.6)$$

$$Y_1^o = Y_{01} \left[\frac{Y_2^o + jY_{01} \tan \theta_s}{Y_{01} + jY_2^o \tan \theta_s} \right] \quad (6.7)$$

$$Y_2^o = -jY_2 \cot \theta_2 \quad (6.8)$$

At resonance $Y_{in}^e = 0$ and $Y_{in}^o = 0$, so Eqn.(6.2) simplifies to $Y_1^e = -jY_1 \tan \theta_1$. Eqn.(6.3) is then given by

$$Y_{01} \left[\frac{Y_2^e + jY_{01} \tan \theta_s}{Y_{01} + jY_2^e \tan \theta_s} \right] = jY_1 \tan \theta_1$$

$$\therefore Y_2^e = -Y_{01} \left[\frac{Y_1 \tan \theta_1 + Y_{01} \tan \theta_s}{Y_{01} + Y_1 \tan \theta_1 \tan \theta_s} \right] = Y_2 \left[\frac{Y_3^e + jY_2 \tan \theta_2}{Y_2 + jY_3^e \tan \theta_2} \right]$$

$$\text{or } Y_{01}(Y_1 \tan \theta_1 + Y_{01} \tan \theta_s)(Y_2 + jY_3^e \tan \theta_2) = Y_2(Y_3^e + jY_2 \tan \theta_2)(Y_{01} + Y_1 \tan \theta_1 \tan \theta_s) \quad (6.9)$$

Resonance frequency of the even-mode can then be determined from Eqn.(6.9), i.e. when $\tan \theta_1 \tan \theta_s = 1/k_1$, where $k_1 = Y_1/Y_{01}$. When $\theta_1 = \theta_2 = \theta$ then $\theta(f_1) = \tan^{-1} \sqrt{1/k_1}$ and $\theta(f_3) = \pi - \tan^{-1} \sqrt{1/k_1}$. Similarly from Eqn. (6.9), $k_1 \tan \theta_1 + \tan \theta_s = 0$. Electrical length of the resonator is sum of θ_1 and θ_s . When $\theta_1 = \theta_s = \theta$ then $\theta(f_2) = \pi/2$ and $\theta(f_4) = \pi$. Also from Eqn. (6.9), $\tan \theta_3 \tan \theta_4 - k_3 = 0$, where $k_3 = Y_3/Y_4$. When $\theta_3 = \theta_4 = \theta$ then $\theta(f_5) = \tan^{-1} \sqrt{k_3}$ and $\theta(f_6) = \pi - \tan^{-1} \sqrt{k_3}$. The odd-mode structure results in identical expressions at resonance frequency.

The fundamental and higher order resonant frequencies can be adjusted over a wide frequency range by modifying the admittance ratio (k) and the length ratio α defined as

$$\alpha = \theta_i / (\theta_i + \theta_i + 2) \quad \text{where } i = 1, 2, 3 \dots$$

Depending on the choice of α and k , it is feasible to couple different resonant modes to obtain a wide passband. Assuming that the microstrip lines are non-dispersive and line sections have equal phase velocity as $\alpha \propto f$, we obtain

$$f_1/f_2 = (2/\pi) \tan^{-1} \sqrt{1/k_1} \quad (6.10)$$

$$f_3/f_2 = (2/\pi) (\pi - \tan^{-1} \sqrt{1/k_1}) \quad (6.11)$$

$$f_4/f_2 = 2 \quad (6.12)$$

$$f_5/f_2 = (2/\pi) \tan^{-1} \sqrt{k_3} \quad (6.13)$$

$$f_6/f_2 = (2/\pi) (\pi - \tan^{-1} \sqrt{k_3}) \quad (6.14)$$

The normalized separation is

$$\Delta f_{13} = \frac{f_3 - f_1}{f_2} = (2/\pi) (\pi - 2 \tan^{-1} \sqrt{1/k_1}) \quad (6.15)$$

$$\Delta f_{56} = \frac{f_5 - f_6}{f_2} = (2/\pi)(\pi - 2\tan^{-1}\sqrt{k_3}) \quad (6.16)$$

$$\Delta f_{15} = \frac{f_1 - f_5}{f_2} = (2/\pi)(\tan^{-1}\sqrt{1/k_1} - \tan^{-1}\sqrt{k_3}) \quad (6.17)$$

$$\Delta f_{36} = \frac{f_3 - f_6}{f_2} = (2/\pi)(\tan^{-1}\sqrt{k_3} - \sqrt{1/k_1}) \quad (6.18)$$

From the above analysis, it can be seen that the five resonance frequencies can be used to create the passband of the filter with f_2 being the mid band frequency and separation equations determining the bandwidth. It can be seen that f_4 is always twice the mid band frequency and is responsible for forming a higher spurious passband. Fig. 6.7 shows the variation of various frequency parameters with changing value of the impedance ratio. The graph shows when the impedance ratio (k) decreased, the normalized frequency of f_1 / f_2 increases and f_3 / f_2 decreases. Thus, their trajectories move towards convergence. However, when k is increased f_5 / f_2 tends to increase and f_6 / f_2 tends to decrease so that their response as a function of increase in k tend towards convergence. This analysis shows by appropriately choosing k filters of wide or narrow passbands can be realized. The Fig. 6.8 shows the separation between the resonant mode frequency for mode 1 and 3, and 3 and 6 increases and the contrary is true for modes 1 and 5, and 5 and 6. The transmission zeros can be determined when $Y_{in}^e = Y_{in}^o$.

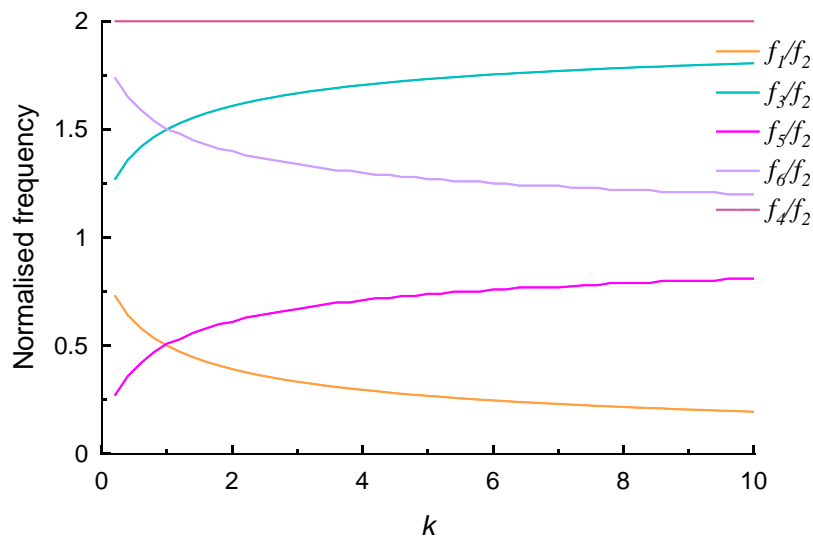


Fig.6.7. Normalized frequency of resonance modes as a function of impedance ratio.

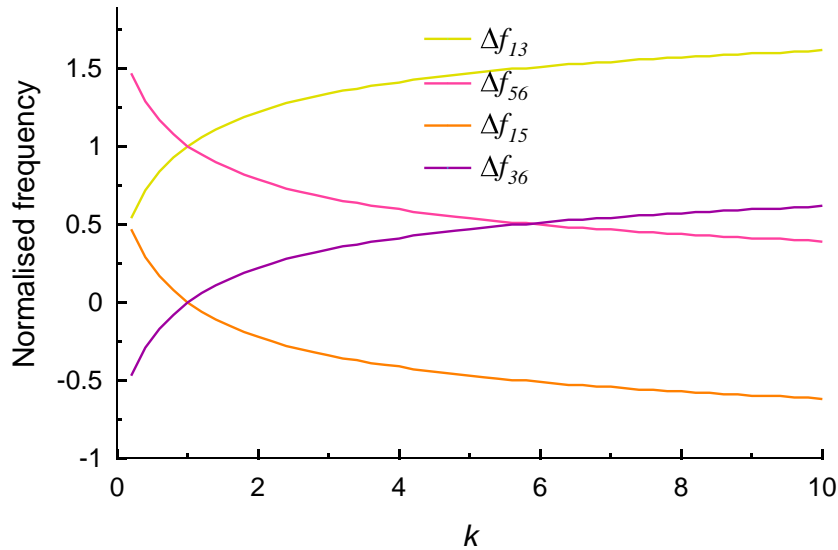


Fig.6.8. Separation of the resonance mode frequencies as a function of impedance ratio.

6.1.1 Parameter Analysis and Measured Results

An ultra-wideband bandpass filter was synthesized using the proposed MMR structure shown in Fig. 6.4. The filter is excited through three finger interdigital capacitor to realize strong EM coupling. The filter was constructed on dielectric substrate Arlon CuClad217LX with thickness (h) of 0.794 mm, dielectric constant (ϵ_r) of 2.17 mm, copper conductor thickness (t) of 35 μm , and loss-tangent ($\tan\delta$) of 0.0009. To maintain good in-band performance, the physical dimensions were optimized by using Momentum in Advanced Design System (ADSTM). Optimised parameters are: $W_b = 0.98$ mm, $W_a = 0.19$ mm, $W_c = 1.41$ mm, $W_{c1} = 1.96$ mm, $W_{a1} = 0.18$ mm, $W_{a2} = 0.18$ mm, $L_1 = 3$ mm, $L_5 = 1.51$ mm, $L_6 = 2.92$ mm, $L_4 = 0.39$ mm, $L_7 = 3.2$ mm, $L_8 = 6.91$ mm, $L_3 = 5.92$ mm, $L_2 = 0.2$ mm, and $S_3 = 0.17$ mm.

The fabricated MMR UWB bandpass filter is shown in Fig. 6.9. Simulated and measured performance of the proposed UWB bandpass filter is shown in Fig. 6.10. The filter exhibits quasi-elliptical characteristics with an excellent in-band insertion-loss of 0.4 dB centred at 8.25 GHz with return-loss better than 10 dB. The two transmission zeros near the upper and lower cut-off frequencies of 4.14 GHz and 12.1 GHz, respectively, result in a filter with high selectivity. The out-of-band rejection is better than 20 dB over a very wideband between 2 to 3.59 GHz and 12.2 to 20.74 GHz. Fig. 6.11 the group delay of the filter is approximately flat and is less than 0.1 ns in the passband.

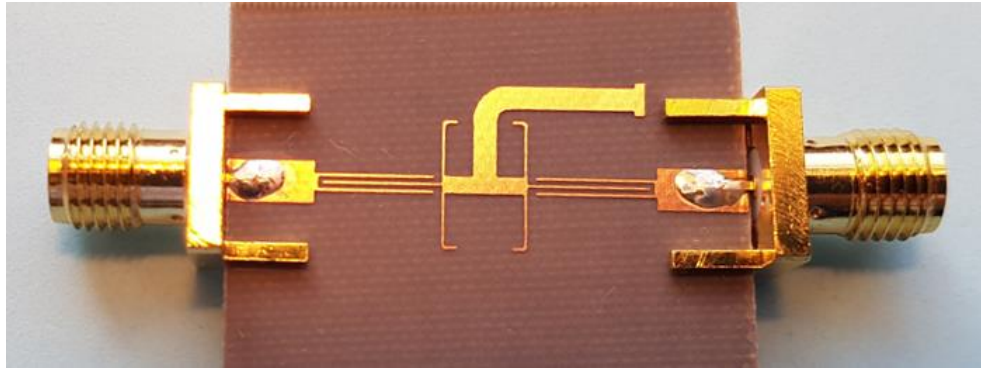


Fig. 6.9. Photograph of the proposed fabricated UWB BPF.

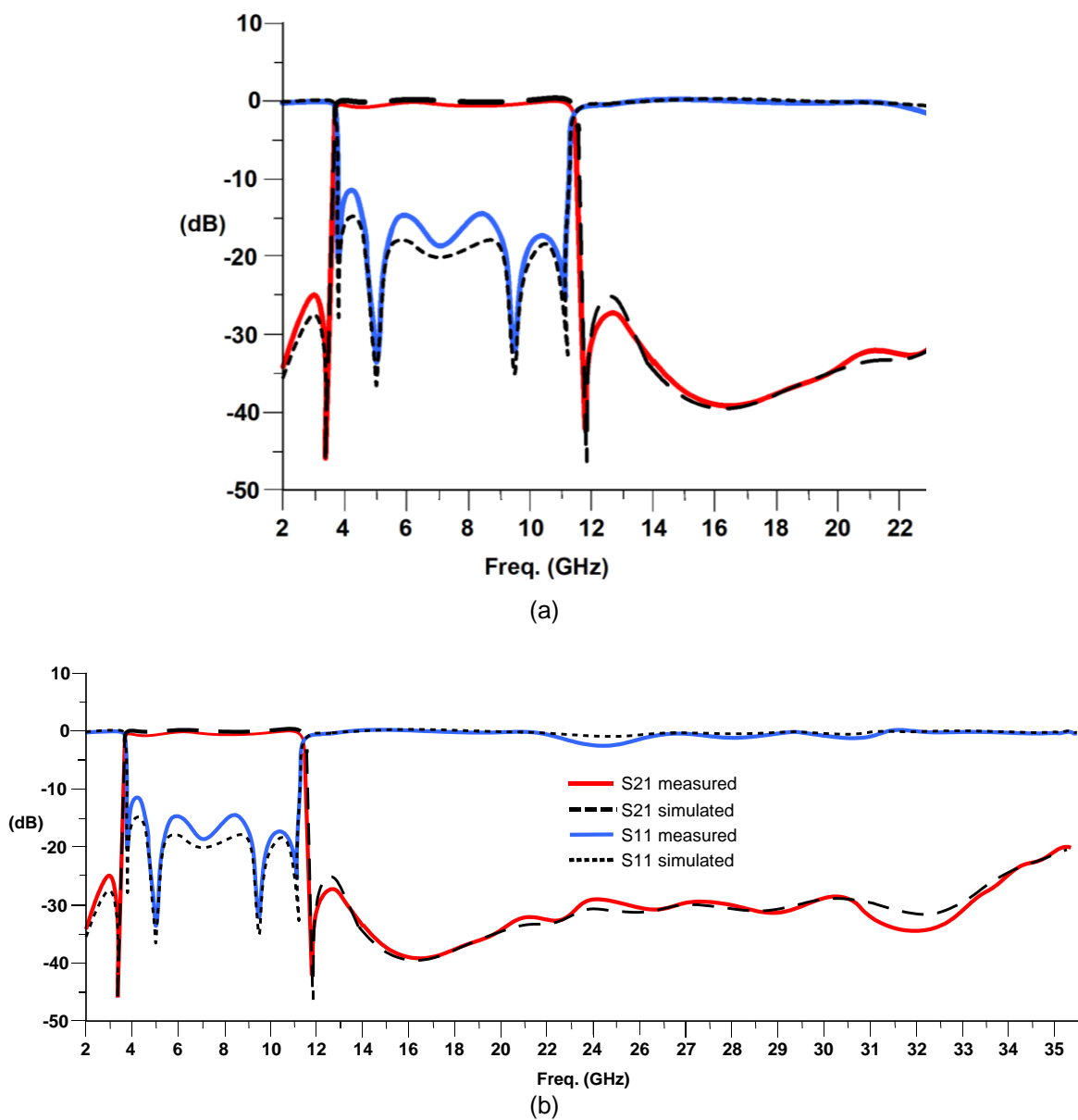


Fig. 6.10. Simulated and measured insertion-loss and return-loss response of the UWB BPF, (a) close-up view, and (b) wideband view.

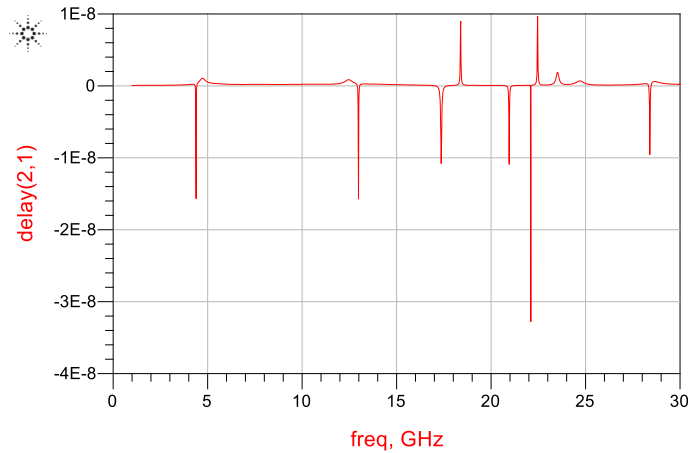


Fig. 6.11. Group-delay response of UWB BPF.

6.1.2 Simulation Results and Discussion

In this section the effect of resonator width (W_b) on filter performance is examined in terms of upper transmission zero f_{z2} (GHz) and resonant frequency f_{odd1} (GHz). Fig. 6.12 show the passband consists of five resonant peaks ($f_{even1}, f_{odd1}, f_{even2}, f_{odd2}, f_{even3}$) located between 5 GHz and 13 GHz, and two transmission zeros (f_{tz1}, f_{tz2}), at the lower and upper cut off frequencies. Results of this study are shown in Figs. 6.12 and 6.13, and tabulated in Table 6.1. This investigation reveals that the resonator width (W_b) mainly controls the resonant mode f_{odd1} and the upper transmission zero f_{tz2} as it increases from optimized value 0.2 mm to 1.0 mm. The upper transmission zero f_{tz2} shows about 5% shift downward in frequency and resonant mode f_{odd1} shift by about 12% upward in frequency. It is also noticed that W_b has a negligible impact on resonant mode f_{odd2} , and other resonant modes and transmission zero remain unchanged.

Table 6.1. Effect of resonator width on upper transmission zero and resonant frequency.

W_b (mm)	f_{odd1} (GHz)	f_{tz2} (GHz)
1.0	6.47	12.97
0.8	6.35	13.11
0.6	6.18	13.24
0.4	5.99	13.36
0.2	5.72	13.53

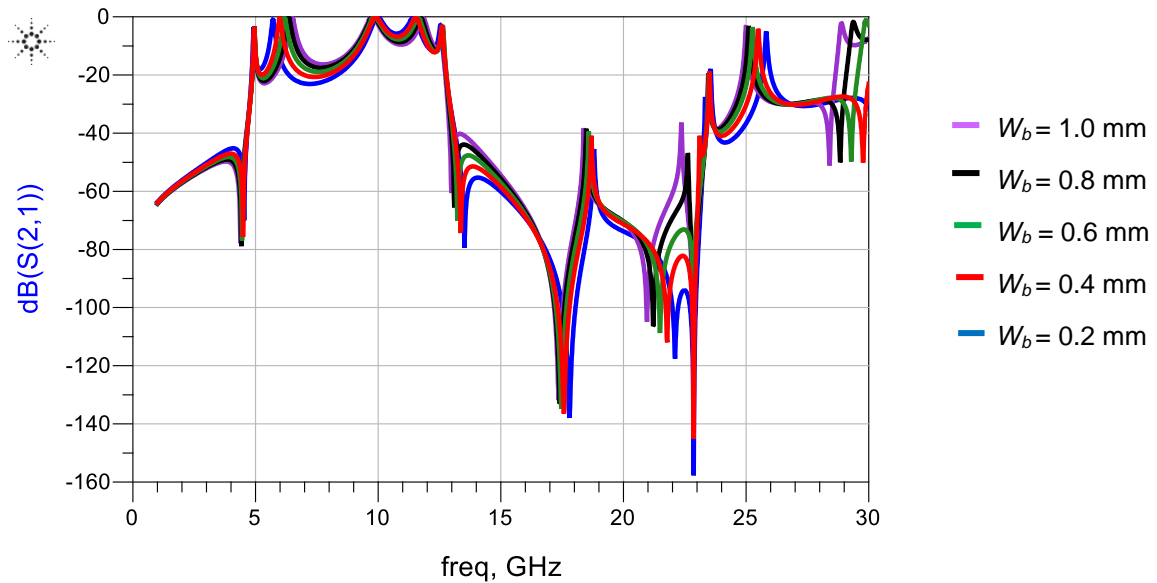


Fig. 6.12. Frequency response of the filter as a function of resonator width.

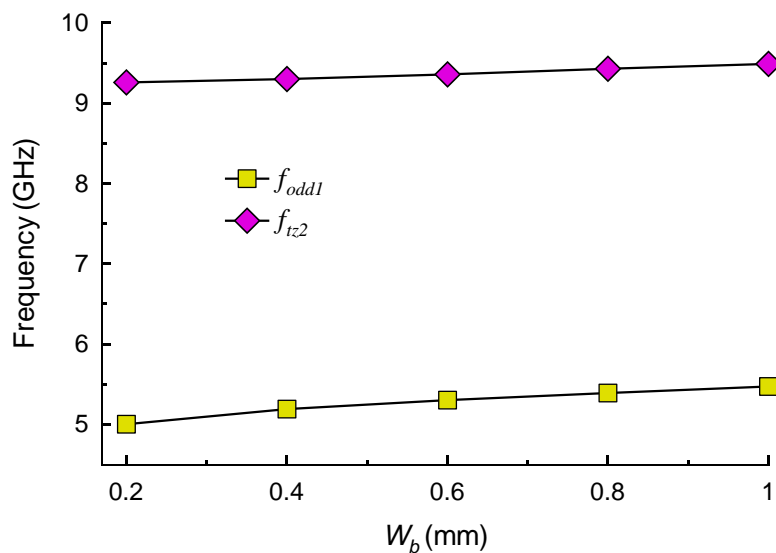


Fig. 6.13. Effect on the filter's upper transmission zero, first odd resonant frequency as a function of resonator width.

The filter's performance with variation in open stub width (W_c) is shown in Figs. 6.14 and 6.15, and tabulated in Table 6.2. When W_c is changed from 0.8 mm to 1.4 mm, the resonant frequency f_{even3} is displaced by about $\pm 11\%$ (12.56 GHz-13.84 GHz), the upper transmission zero f_{iz2} by about 9% (12.98 GHz-14.16 GHz) and lower transmission zero f_{iz1} by about 8% (4.38 GHz-4.75 GHz). W_c helps to create wideband with sharp selectivity. A minor change is also observed in resonant frequencies f_{odd1}, f_{odd2} but other resonant modes remain unchanged as the open stub width (W_c) is reduced from 1.4 mm to 0.5 mm.

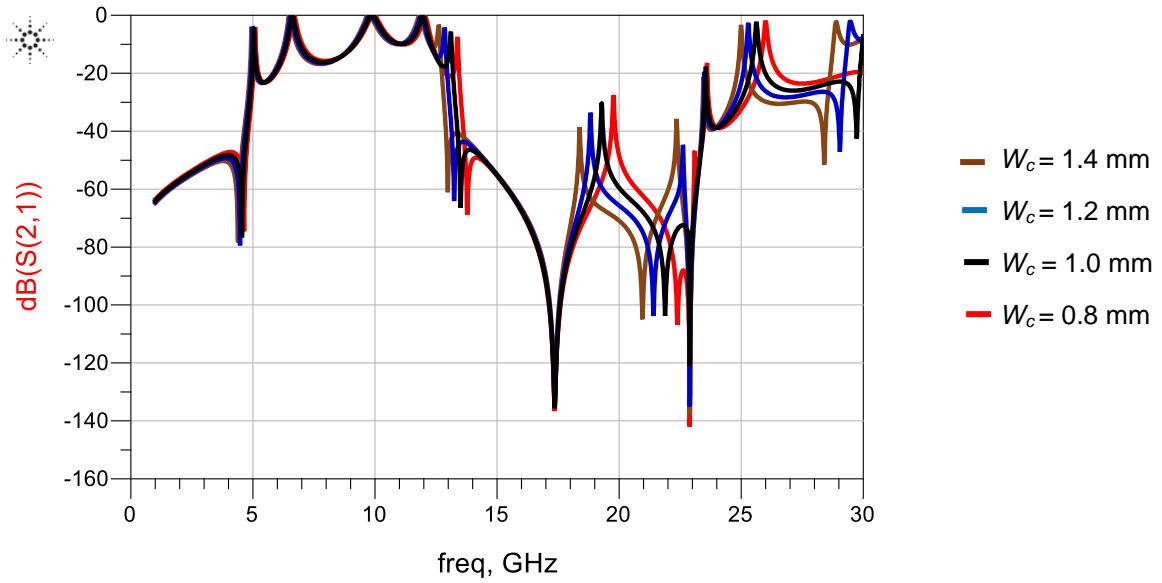


Fig. 6.14. Frequency response of the filter as a function of open stub width.

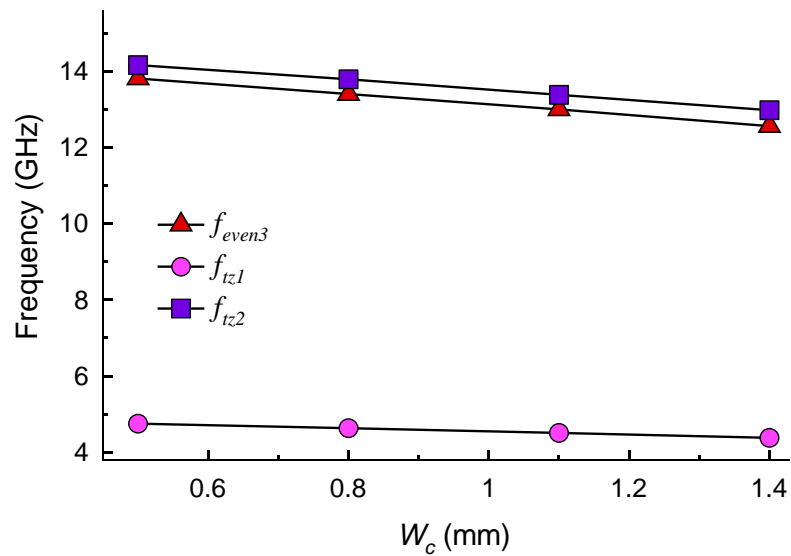


Fig. 6.15. Effect on the filter's lower and upper transmission zeros and third even resonant frequency as a function of open stub width.

Table 6.2. Effect of open stub width on the lower and upper transmission zeros and third even resonant frequency.

W_c (mm)	f_{even3} (GHz)	f_{z1} (GHz)	f_{z2} (GHz)
1.4	12.56	4.38	12.98
1.1	13.00	4.51	13.38
0.8	13.40	4.63	13.79
0.5	13.81	4.75	14.16

The impact on the filter's characteristics by the open stub length (L_B) was investigated. The results of this study are shown in Fig. 6.16 and Fig. 6.17, and in Table 6.3. Open stub length (L_B) mainly influences the first and third resonant frequencies, f_{even1} and f_{even3} , and the lower and upper transmission zeros. It is observed as the length is reduced from 6.96 mm to 5.34 mm, the lower and upper transmission zero shift down in frequency from 12.98 GHz to 14.72 GHz, however, the resonant frequency f_{even1} shows a slight shift from 4.96 GHz to 5.45 GHz. It is also noticed that the length has a negligible effect on resonant frequency f_{even2} and on other resonant frequencies.

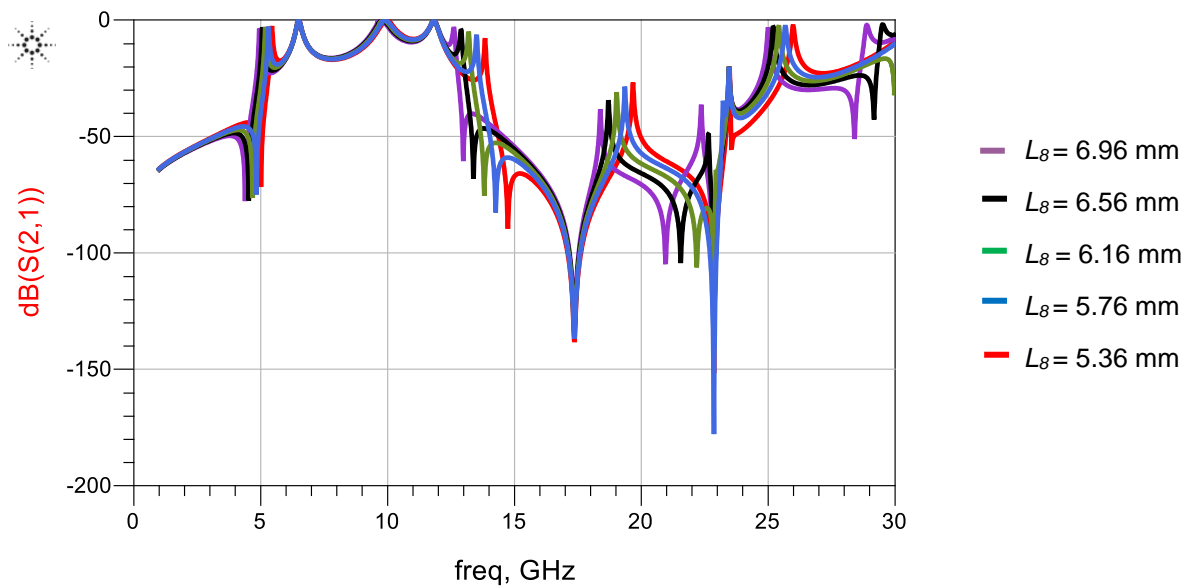


Fig. 6.16. Frequency response of the filter as a function of stub resonator length.

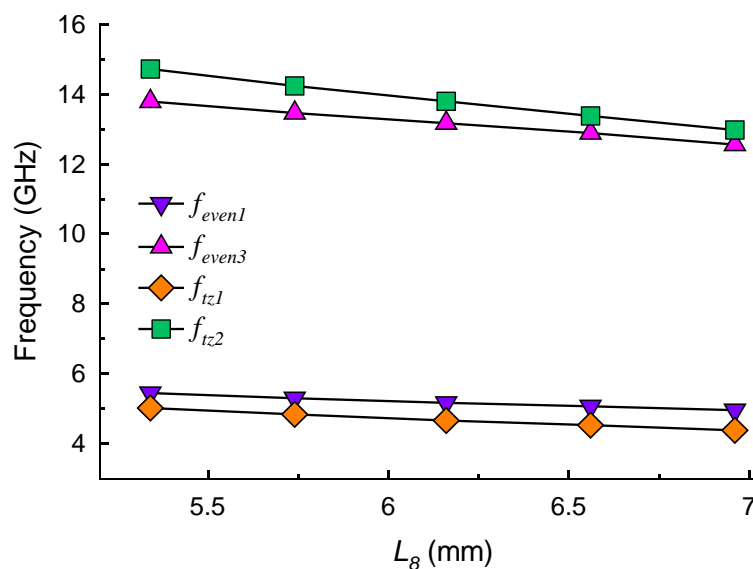


Fig. 6.17. Effect on the filter's lower and upper transmission zeros, and first and third resonant frequencies as a function of stub resonator length.

Table 6.3. Effect of stub resonator length on lower and upper transmission zeros, and first third even resonant frequencies.

L_8 (mm)	f_{even1} (GHz)	f_{even3} (GHz)	f_{tz1} (GHz)	f_{tz2} (GHz)
6.96	4.96	12.56	4.38	12.98
6.56	5.07	12.89	4.53	13.38
6.16	5.17	13.17	4.66	13.80
5.74	5.3	13.46	4.84	14.24
5.34	5.45	13.79	5.02	14.72

Fig. 6.18 shows the simulated S_{21} frequency response as a function of horizontal resonator length (L_6). The results are graphically shown in Fig. 6.19, and tabulated in Table 6.4. These results show the horizontal resonator length mainly affects the resonant frequencies f_{odd2} and f_{even3} , and has virtually no impact on resonant frequencies f_{even2} , f_{odd1} and f_{even1} . As the horizontal resonator length (L_6) is reduced from 3.72 mm to 2.92 mm, the resonant frequencies f_{odd2} and f_{even3} shift upward in frequency by about 13% and 5%, respectively, while the lower and upper transmission zeros remain fixed.

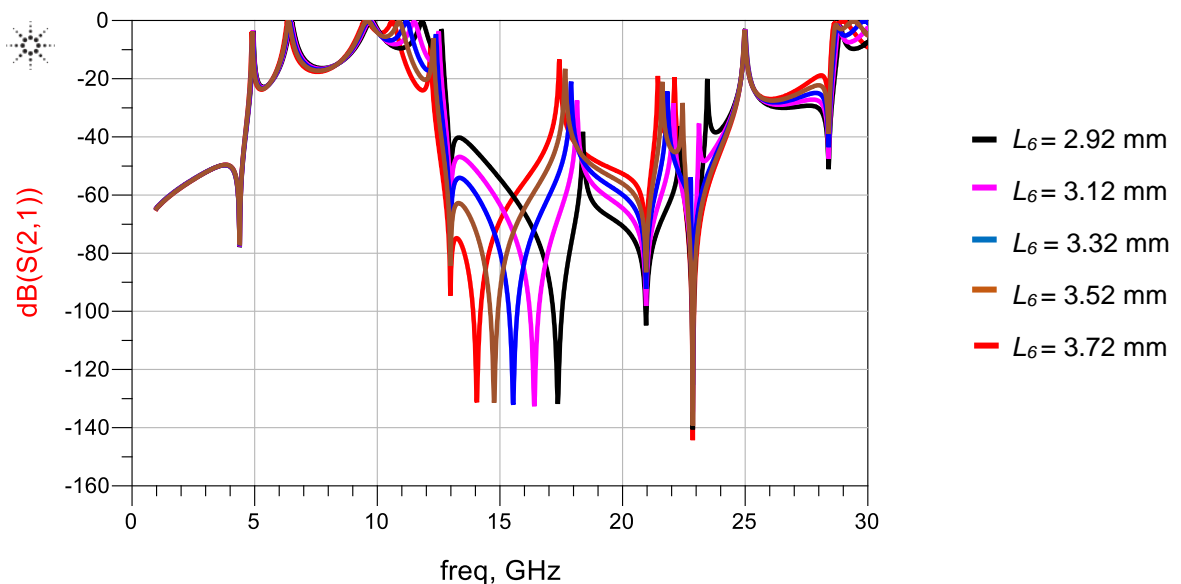


Fig. 6.18. Frequency response of the filter as a function of horizontal resonator length.

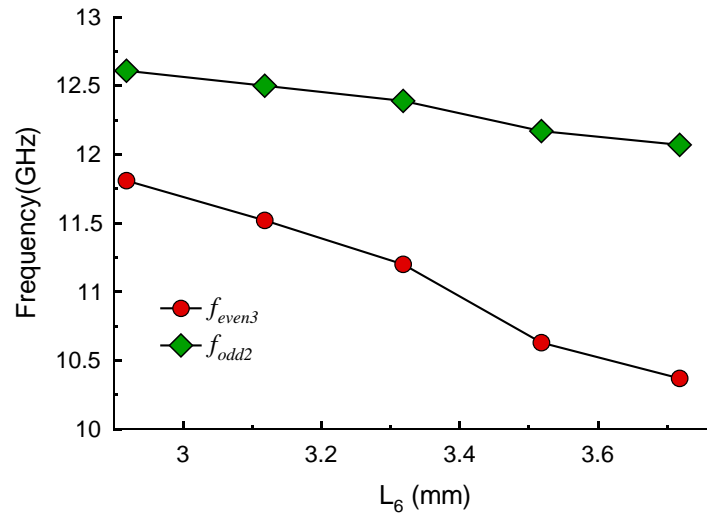


Fig. 6.19. Effect on the filter's second odd and third even resonant frequencies as a function of resonator length.

Table 6.4. Effect of horizontal resonator length on second odd and third even resonant frequencies.

L_6 (mm)	f_{odd2} (GHz)	f_{even3} (GHz)
2.918	11.81	12.61
3.118	11.52	12.50
3.318	11.20	12.39
3.518	10.63	12.17
3.718	10.37	12.07

The effect of varying the interdigital coupled feed-line length (L_3) on the filter's characteristics was also investigated. The results are shown in Fig. 6.20 and Fig. 6.21, and tabulated in Table 6.5. The study reveals the resonant frequencies f_{odd1} , f_{even2} and f_{odd2} shift significantly upward in frequency by about 15%, 14% and 11%, respectively, when the length (L_3) is increased from 4.34 mm to 5.94 mm. Transmission zeros and other resonant modes remain fixed. It is also noticed that resonator length (L_5) effects the in a similar way except that the upper rejection does not vary as much.

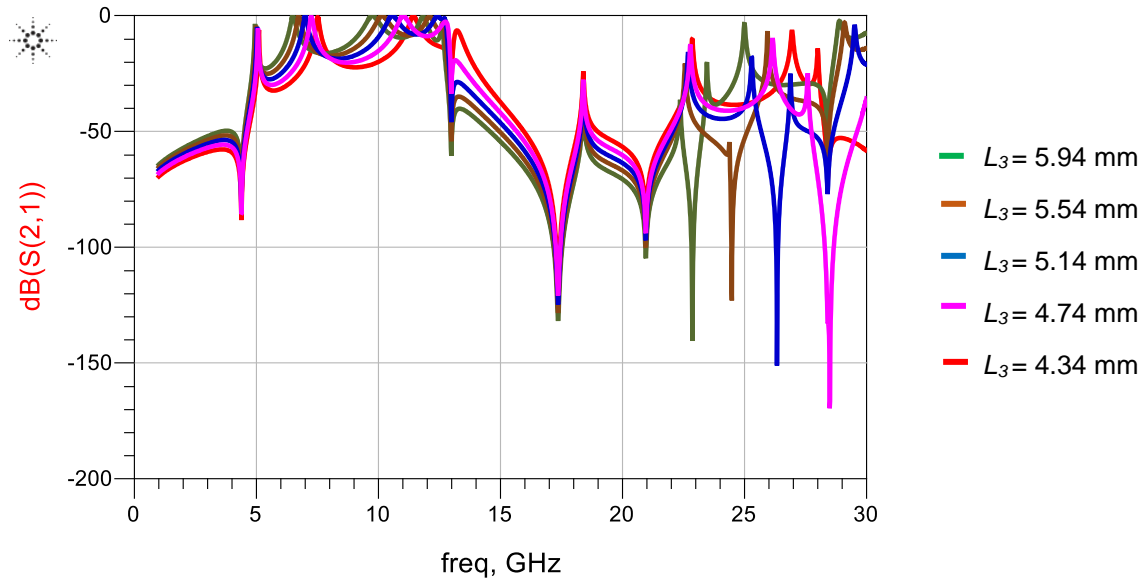


Fig. 6.20. Frequency response of the filter as a function of interdigital feed-line coupling length.

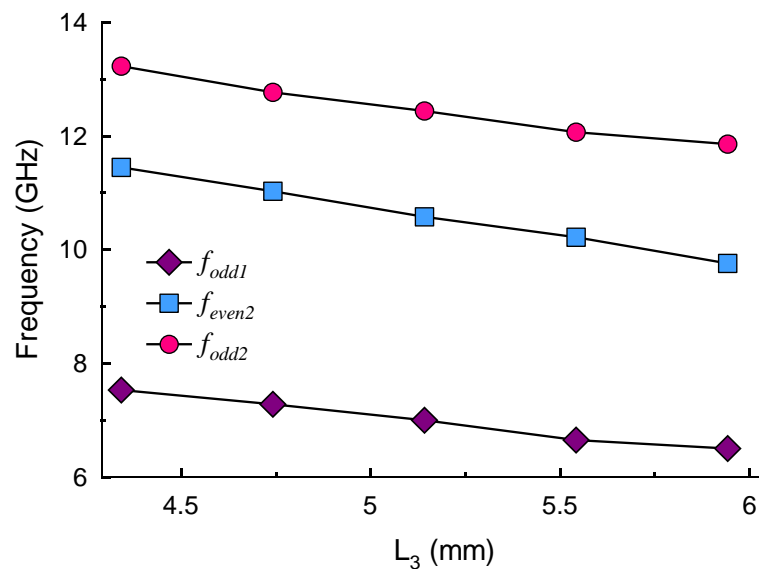


Fig. 6.21. Effect on the filter's first and second odd and second even resonant frequencies as a function of interdigital feed-line coupling length.

Table 6.5. Effect of interdigital feed-line coupling length on odd and even resonant frequencies.

L_3 (mm)	f_{odd1} (GHz)	f_{even2} (GHz)	f_{odd2} (GHz)
5.942	6.50	9.76	11.86
5.542	6.65	10.22	12.07
5.142	7.00	10.58	12.44
4.742	7.28	11.03	12.77
4.342	7.53	11.45	13.23

Fig. 6.22 and Fig. 6.23 show how the resonator length (L_4) control the resonant mode f_{odd2} . The results are also given in Table 6.6. As the resonator length (L_4) is varied from its optimized value of 0.30 mm to 1 mm, the resonant mode f_{odd2} varies from 11.80 GHz to 11.09 GHz. The upper rejection level reduces from about 65 dB to 45 dB, and it has a very minor effect on the resonant mode f_{even2} .

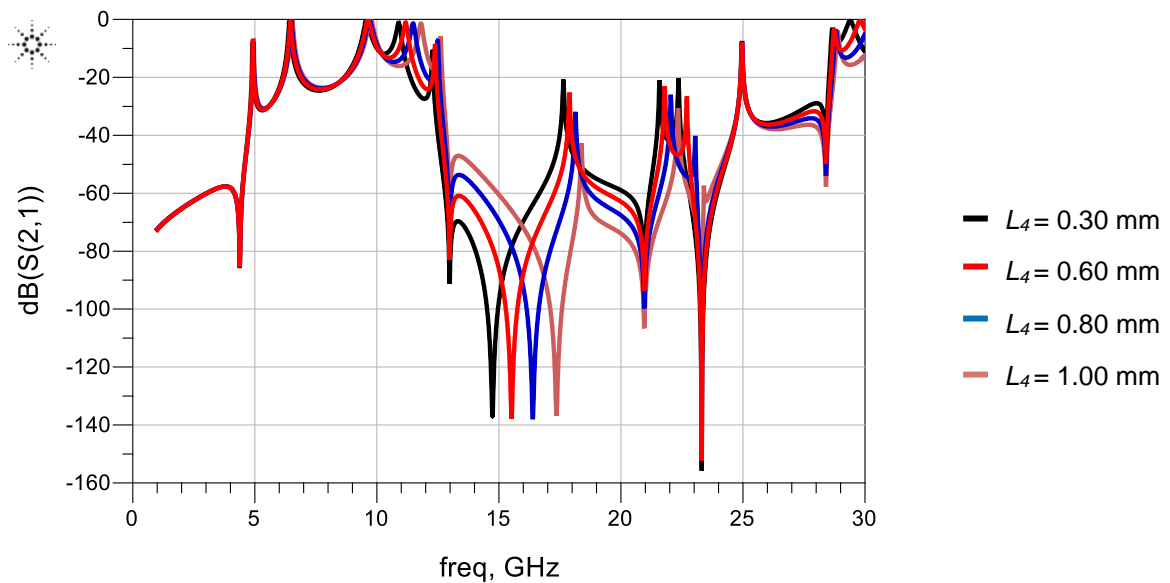


Fig. 6.22. Frequency response of the filter as a function of resonator length (L_4)

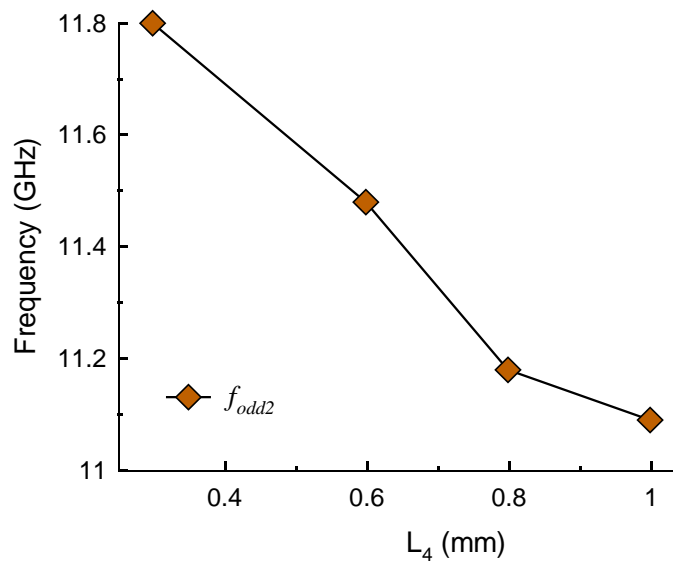


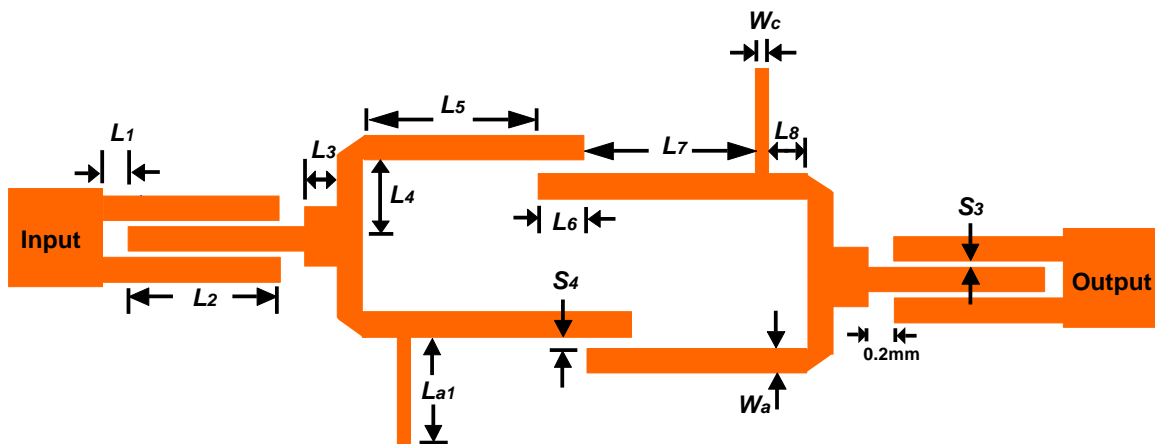
Fig. 6.23. Effect on the resonant frequency f_{odd2} as a function of resonator length (L_4).

Table 6.6. Effect of resonator length (L_4) on resonant mode

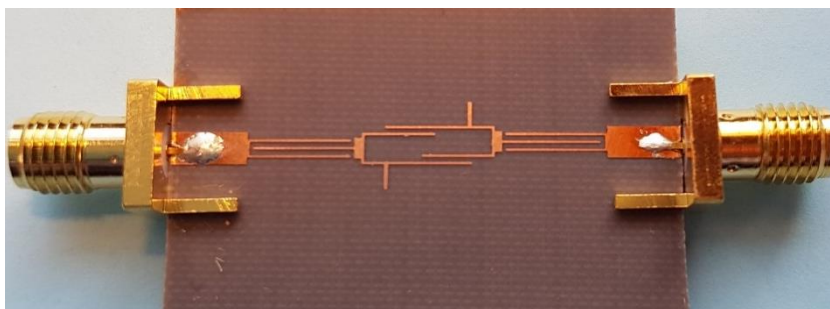
L_4 (mm)	f_{odd2} (GHz)
0.30	11.80
0.60	11.48
0.80	11.18
1.00	11.09

6.2.0 Wideband BPF Design

In this section, a novel miniature wideband BPF is proposed where the filter is realized by loading the resonators directly with open-circuited stubs. The configuration of the proposed bandpass filter is same as shown in Fig. 4.32 in Chapter 4, except that some of the physical dimensions of the mentioned filter have been modified to realize wideband BPF shown in Fig. 6.24. The filter exhibits four resonant modes and two transmission zeros close to passband edges to create a sharp roll off as shown in Fig. 6.25. The filter was optimized using Agilent ADS™ Momentum software. The optimized dimensions of the filter are: $W_a = 0.2$ mm, $W_c = 0.3$ mm, $L_1 = 2$ mm, $L_2 = 6.08$ mm, $L_3 = 0.5$ mm, $L_4 = 0.9$ mm, $L_5 = 1.51$ mm, $L_6 = 3.02$ mm, $L_7 = 2.45$ mm, $L_8 = 1.38$ mm, $S_3 = 0.42$ mm, and $S_4 = 0.35$ mm.



(a)



(b)

Fig. 6.24 (a) Configuration of the three finger interdigital coupled feed-line wideband bandpass filter, and (b) photograph of the fabricated filter.

Fig. 6.25 shows the simulated frequency response of the wideband BPF, which has a centre frequency of 8.3 GHz and 3-dB passband that covers 6.7 GHz – 9.9 GHz. The filter's insertion-loss is about 0.87 dB, the return-loss is about 10 dB, and the out-of-band rejection on lower and upper side of the passband is about 19 dB. The frequency response shows the 3-dB fractional bandwidth is 40% and upper stopband of -20 dB level extends up to 13 GHz. Fig. 6.26 shows the frequency response under weak coupling when S_3 is 1 mm, which has four resonant peaks ($f_{even1}, f_{odd1}, f_{even2}, f_{odd2}$) that are located in the passband range from 6.7 GHz to 10.3 GHz, and two transmission zeros (f_{tz1}, f_{tz2}) at the lower and upper cut off frequencies to provide a steep skirt selectivity. Fig. 6.27 shows the worst case group delay of the filter in the passband is 2 ns.

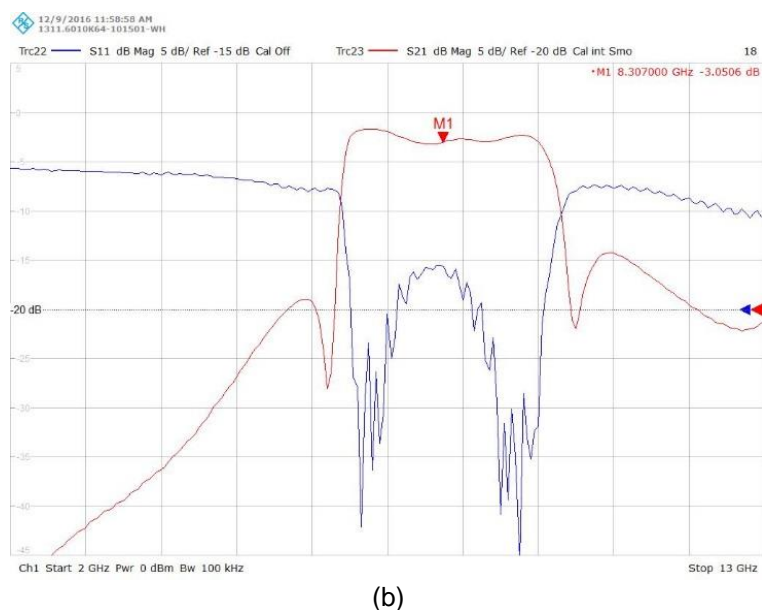
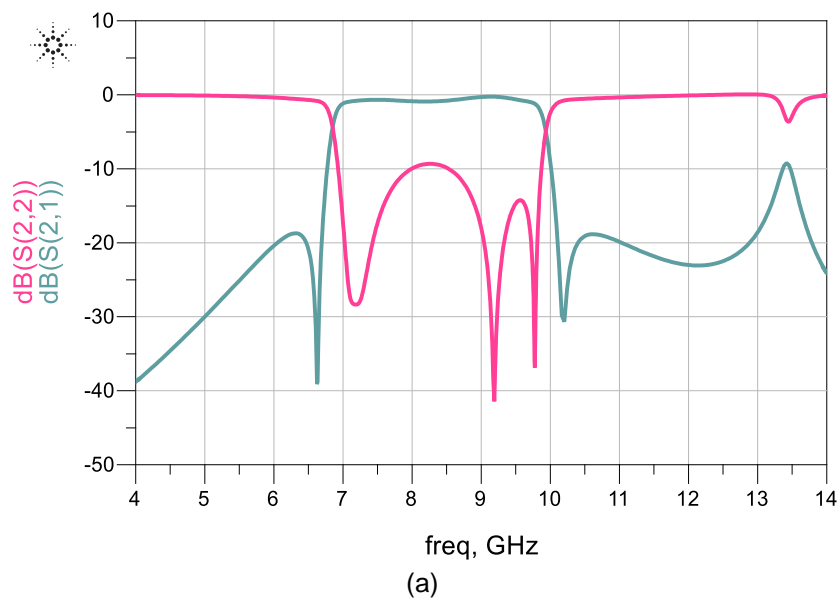


Fig. 6.25. (a) Simulated (b) measured results of the wideband bandpass filter.

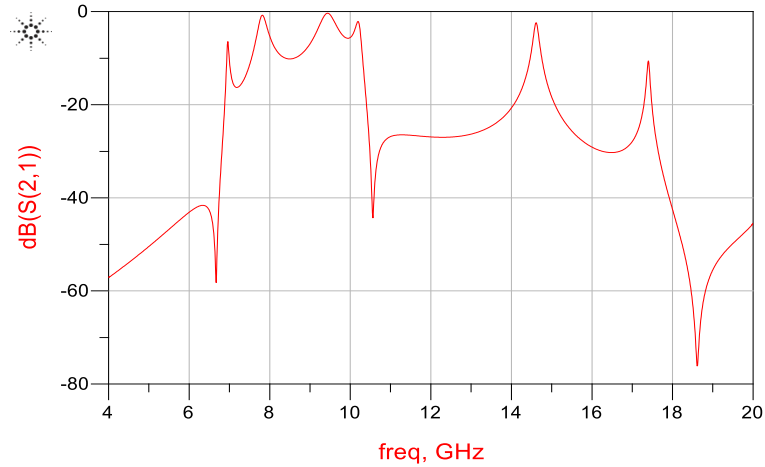


Fig. 6.26. Frequency response of the wideband bandpass filter under weak coupling.

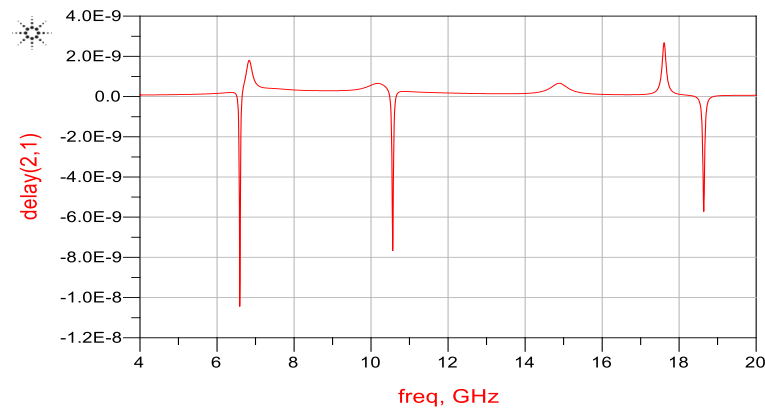


Fig. 6.27. Group delay response of the wideband bandpass filter.

6.2.1 Simulation Results and Discussion

Fig. 6.28 shows the frequency response of the filter with variation in resonator length (L_7). As the length is reduced from 2.45 mm to 0.85 mm the transmission zeros, f_{tz1} shift from 6.65 GHz to 7.68 GHz, and f_{tz2} from 10.55 GHz to 11.11 GHz; and the resonant frequencies f_{even1} shift from 6.96 GHz to 7.78 GHz, and f_{odd2} from 10.20 GHz to 11.02 GHz. With change in the resonator length the out-of-band rejection level on lower side of the bandpass deteriorates from 40 dB to 28 dB; however, the upper rejection level and resonant frequency f_{even2} remain unchanged. The results are graphically presented in Fig. 6.29, and tabulated in Table 6.6. The resonator length (L_8) affected the filter response in exactly the same way as resonator length (L_7), when it is varied from its optimized value.

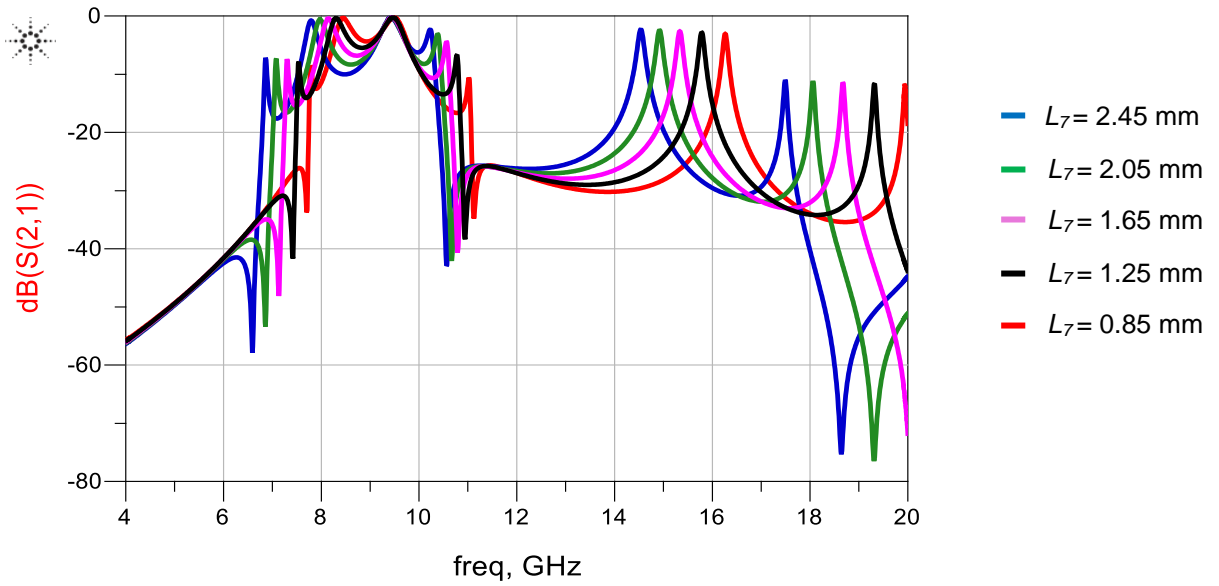


Fig. 6.28. Frequency response of the filter as a function of resonator length L_7 .

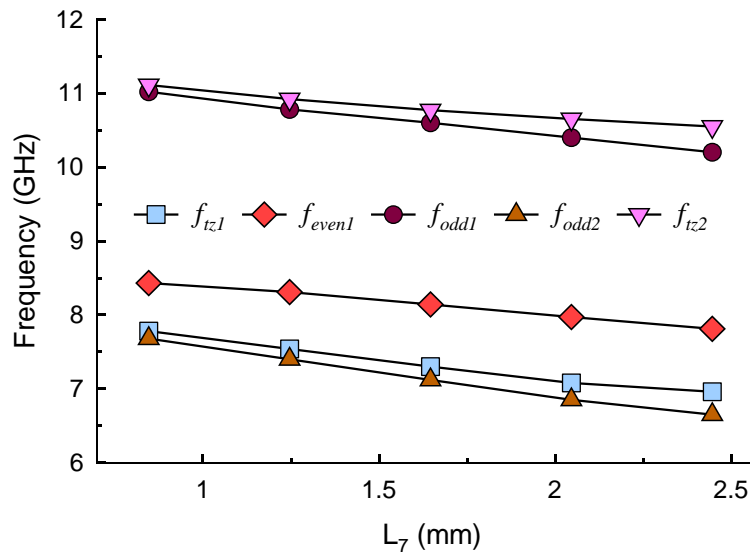


Fig. 6.29. Effect on the filter's transmission zeros and resonant frequencies as a function of resonator length (L_7).

Table 6.7. Effect of resonator length (L_7) on transmission zeros and resonant frequencies.

L_7 (mm)	f_{even1} (GHz)	f_{odd1} (GHz)	f_{odd2} (GHz)	f_{tz1} (GHz)	f_{tz2} (GHz)
2.446	6.96	7.81	10.20	6.65	10.55
2.046	7.08	7.97	10.40	6.85	10.65
1.646	7.30	8.14	10.60	7.12	10.77
1.246	7.54	8.31	10.78	7.40	10.92
0.846	7.78	8.43	11.02	7.68	11.11

The effect on the filter's performance with variation in the interdigital coupled feed-line length (L_2) is shown in Fig. 6.30 and Fig. 6.31, and in Table 6.8. It is noticed as the length varied from 6.08 mm to 4.88 mm, the resonant frequency f_{odd1} tend to shift upward almost linearly by 9%, and f_{even2} by 11%. Although the rejection performance improves on lower side of the passband with change in L_2 , however it deteriorates on higher side. Moreover, it does not show any effect on the first resonant mode and the transmission zeros. This results show we can control the resonant frequencies f_{odd1} and f_{even2} independently by varying the coupled length at the expense of deterioration in rejection level on upper side of the passband.

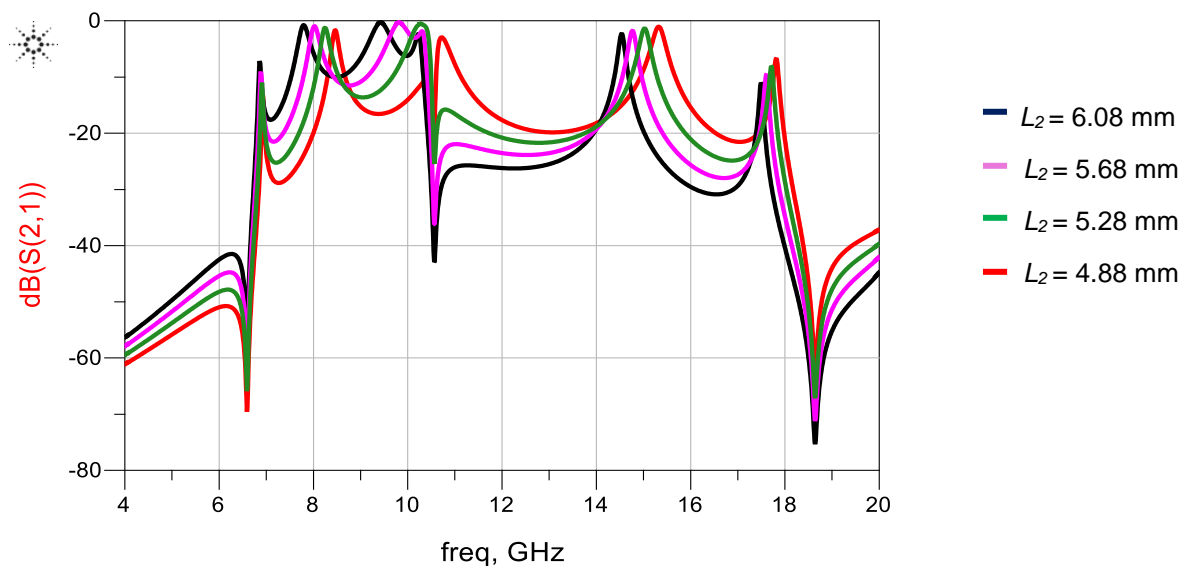


Fig. 6.30. Frequency response of the filter as a function of interdigital feed-line coupling length (L_2).

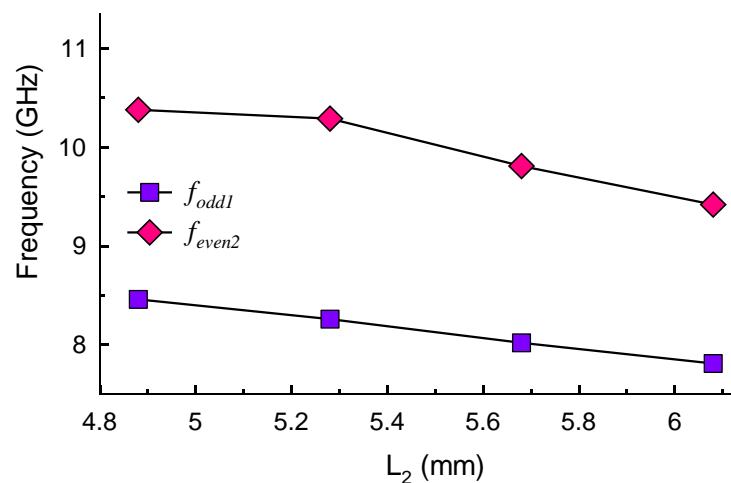
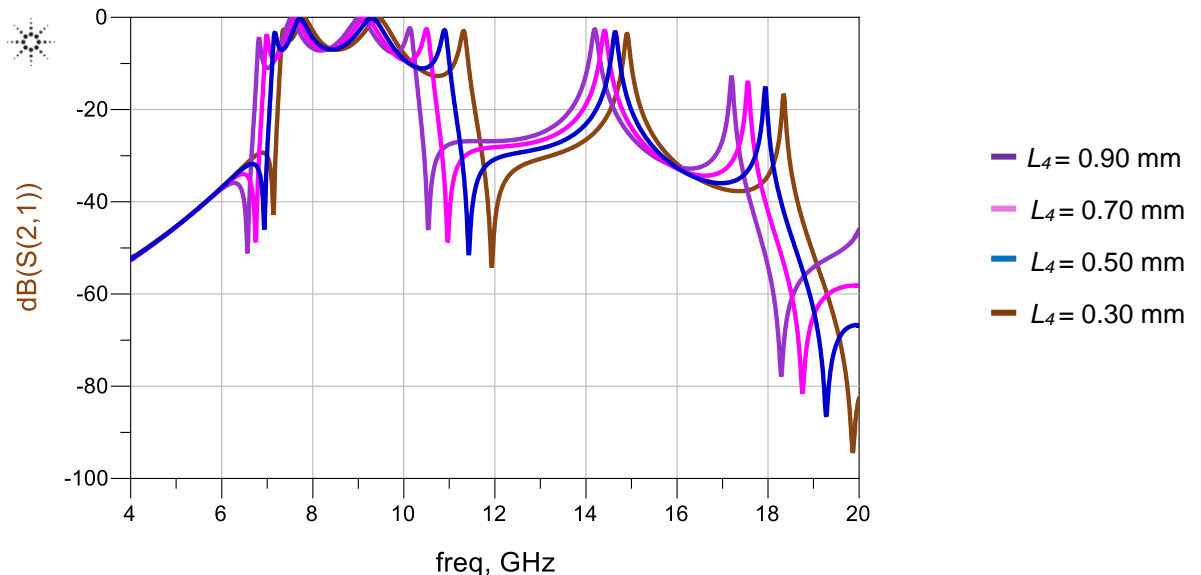


Fig. 6.31. Effect on the filter's resonant frequencies as a function of interdigital feed-line coupling length.

Table 6.8. Effect of interdigital feed-line coupling length (L_2) on resonant frequencies.

L_2 (mm)	f_{odd1} (GHz)	f_{even2} (GHz)
6.08	7.81	9.42
5.68	8.02	9.81
5.28	8.26	10.29
4.88	8.46	10.38

To analyse the effect of resonator separation length (L_4) on the filter performance, it was varied from 0.90 mm to 0.30 mm. The results of the analysis are shown in Fig. 6.32 and 6.33, and tabulated in Table 6.9. A significant change of about 8% and 13% is observed in the position of the lower and upper transmission zeros, respectively, however, a moderate shift is noticed in the resonant frequencies, f_{even1} shifted from 6.96 GHz to 7.40 GHz, f_{odd1} from 7.81 GHz to 8.11 GHz, f_{even2} from 7.81 GHz to 8.11 GHz, and f_{odd2} changed by 14%. By varying the resonator separation length, we can control both transmission zeros as well all resonant modes to some extent without significantly degrading the filter's passband.

Fig 6.32. Frequency response of the filter as a function of resonator separation (L_4).

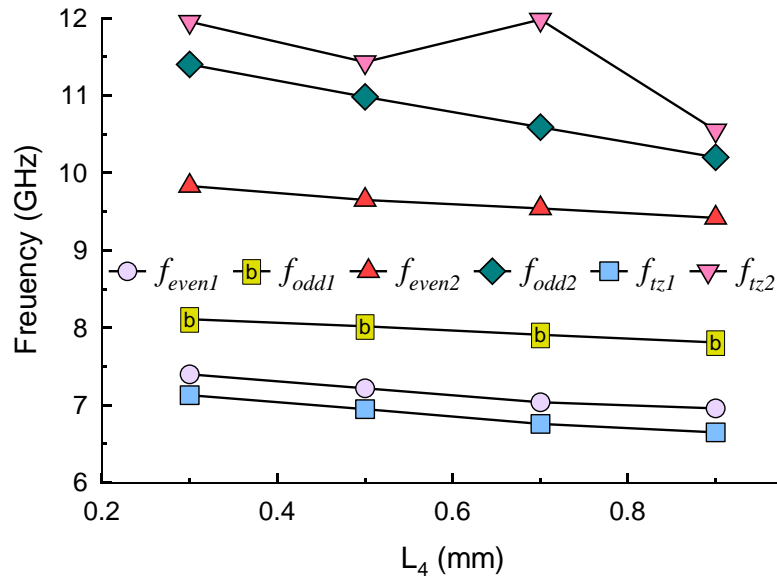


Fig. 6.33. Effect of resonator separation (L_4) on resonant frequencies and transmission zeros.

Table 6.9. Effect of resonator separation length (L_4) on the transmission zeros and resonant frequencies.

L_4 (mm)	f_{even1} (GHz)	f_{odd1} (GHz)	f_{even2} (GHz)	f_{odd2} (GHz)	f_{tz1} (GHz)	f_{tz2} (GHz)
0.90	6.96	7.81	9.42	10.20	6.65	10.55
0.7	7.04	7.91	9.54	10.59	6.76	11.98
0.5	7.22	8.02	9.65	10.98	6.95	11.43
0.3	7.40	8.11	9.83	11.40	7.13	11.95

Fig. 6.34 shows the frequency response of the filter as the resonator coupled length (L_6) is varied from 3.02 mm to 1.82 mm. The salient features are presented in Fig. 6.35 and tabulated in Table 6.10. The variation in the length L_6 from its optimized value of 3.02 mm to 1.82 mm mainly influences the resonant modes. In fact f_{odd1} and f_{even2} tend to shift moderately upwards in frequency and resonant modes f_{even1} and f_{odd2} move significantly upward in frequency. The transmission zeros too tend to move significantly higher in frequency. It is also observed that L_6 can significantly affect the filter's upper rejection level. The variation in resonators coupled length can be used to relocate both transmission zeros as well as the resonant modes to achieve a wide passband bandpass filter with sharp frequency-selectivity.

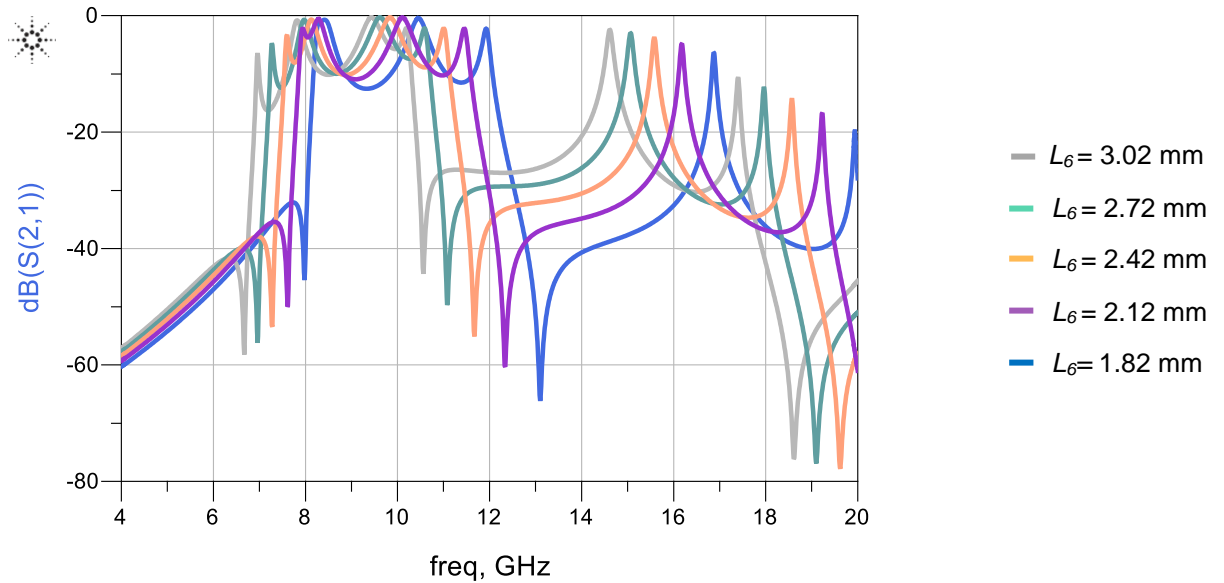


Fig. 6.34. Frequency response of the proposed filter as a function of coupled length (L_6)

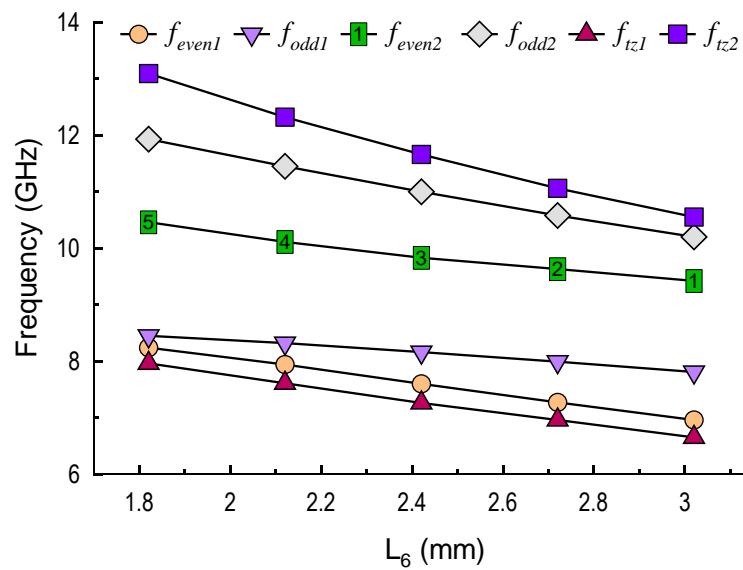


Fig. 6.35. Effect of coupled length (L_6) on resonant frequencies and transmission zeros.

Table 6.10. Effect of resonator coupled length (L_6) on the transmission zeros and resonant frequencies.

L_6 (mm)	f_{even1} (GHz)	f_{odd1} (GHz)	f_{even2} (GHz)	f_{odd2} (GHz)	f_{tz1} (GHz)	f_{tz2} (GHz)
3.02	6.96	7.81	9.42	10.20	6.65	10.55
2.72	7.27	7.99	9.63	10.58	6.96	11.06
2.42	7.60	8.16	9.83	11.00	7.26	11.66
2.12	7.94	8.32	10.11	11.45	7.61	12.32
1.82	8.24	8.45	10.46	11.93	7.96	13.09

The effect of resonator length (L_5) when it's varied 1.51 to 0.30 mm on the filter's transmission zeros and resonant modes is shown in Fig. 6.36 and Fig. 6.37, and the results are also tabulated in Table 6.11. This study shows a minor change in the position of resonant mode f_{even1} and a significant shift in resonant mode f_{even2} that moves upward in frequency as the length is reduced from its optimized value. The position of resonant mode f_{odd2} changes by 9% and f_{even2} by 14%, and transmission zero f_{tz2} moves upward in frequency by 20%, while resonant mode f_{odd1} and transmission zero f_{tz1} remain fixed. The resonator length (L_5), can control resonant modes f_{odd2} , f_{even2} , and transmission zero f_{tz2} , independently without a major effect on other characteristics of the filter passband. Fig. 6.38 shows the passband is unaffected by open stub length (L_a).

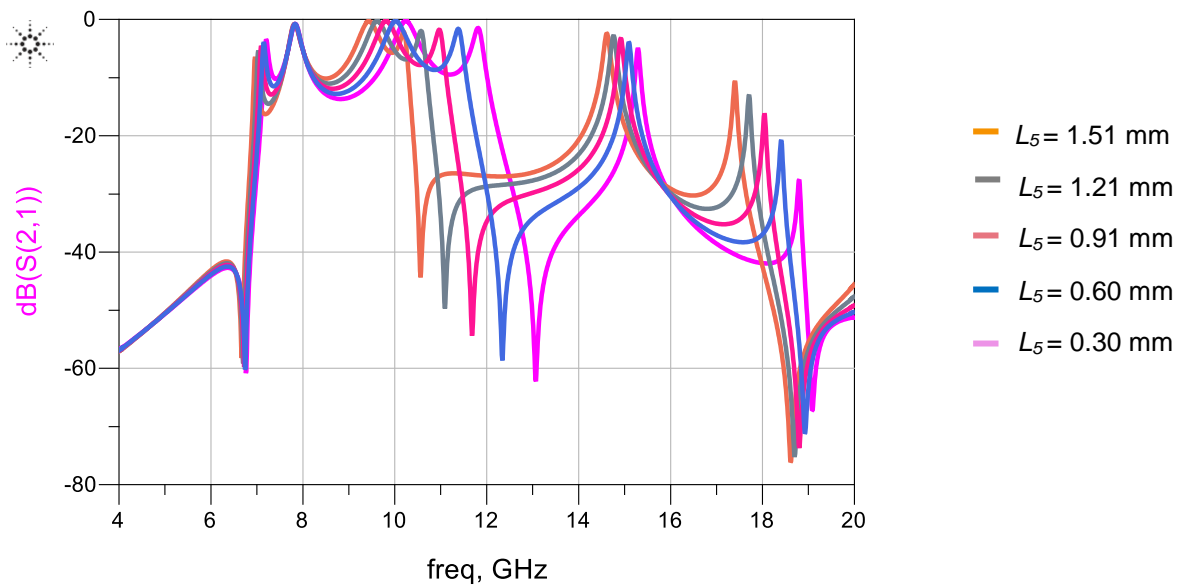


Fig. 6.36. Frequency response of the proposed filter as a function of length (L_5).

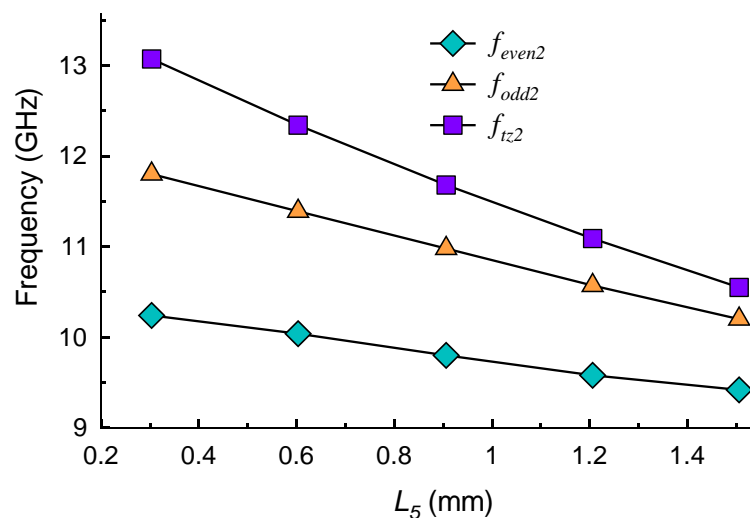
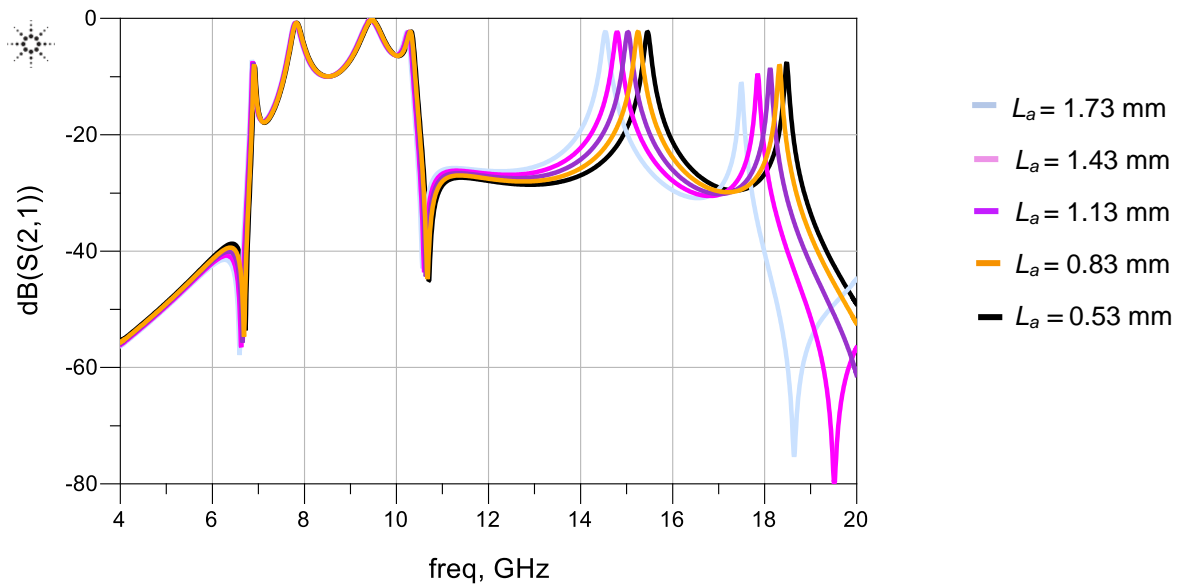


Fig. 6.37. Effect of length (L_5) on the filter's resonant frequencies and transmission zero.

Table 6.11. Effect of resonator length (L_5) on the filter's transmission zero and resonant modes.

L_5 (mm)	f_{even2} (GHz)	f_{odd2} (GHz)	f_{z2} (GHz)
1.506	9.42	10.20	10.55
1.206	9.58	10.57	11.09
0.906	9.8	10.98	11.68
0.603	10.04	11.39	12.34
0.303	10.24	11.80	13.07

Fig. 6.38. Frequency response of the proposed filter as a function of open stub length (L_a).

6.3 Summary

This chapter presented a miniature microstrip UWB and wideband BPF designs. The UWB BPF was implemented using a multimode resonator structure that employed multiple open stubs to create even and odd modes within the passband. Analysis showed that even modes are mainly controlled by varying width and length of the central loaded stepped impedance stub but has no effect on the odd modes. The odd modes can be relocated by adjusting the width of the horizontal resonator and the length of the interdigitally coupled lines, which has very minor effect on even modes. The filter investigated is compact in size when fabricated on a low dielectric constant substrate, possesses a sharp quasi-elliptic function bandpass response with low passband insertion-loss, and ultra-wide stopband performance. The measured results validated the theoretical analysis and simulations results. A miniature wideband microstrip BPF design was also proposed and analyzed. The wideband passband was created by exciting four resonant modes, and two transmission

zeros at the cut off frequencies enabled the realisation of a sharp roll off skirt. Analysis shows that both even and odd modes can be relocated within the passband by tuning different physical parameters of the wideband filter structure. Correlation between the simulated and measured results is excellent.

References

1. "FCC, Revision of Part 15 of the Commission's Rules Regarding Ultra-Wideband Transmission Systems," Washington, DC, *Tech. Rep*, ET-Docket 98-153, FCC02-48, Feb. 2002.
2. Sohail Khalid, Wong Peng Wen, "Analysis of ultra-wide bandpass filter," IEEE Asia-Pacific Conference on Applied Electromagnetics (APACE), 2012, pp 199 – 204.
3. Ye Yuan, Su Song Yang, Ran Liu, "A compact ultra-wideband bandpass filter design based on open stub loaded SIR structure," *15th International Conference on Electronic Packaging Technology (ICEPT)*, pp. 1341 – 1343, 2014
4. Zhaojiang Shang, Xubo Guo, "Design of a superconducting ultra-wideband (UWB) bandpass filter with sharp rejection skirts and miniaturized size," *IEEE Microwave And Wireless Components Letters*, Vol. 23, no. 2, Feb. 2013.
5. Lei Lin, Shuai Yang, Shou-Jia Sun, Bian Wu and Chang-Hong Liang, "Ultra-wideband bandpass filter using multi stub-loaded ring resonator," *Electronics Letters*, Vol. 50 No. 17 pp. 1218–1220, 14th August 2014.
6. Ting Zhang, Fei Xiao, Jingfu Bao and Xiaohong Tang, "Compact ultra-wideband bandpass filter with good selectivity," *Electronics Letters*, Vol. 52 No. 3 pp. 210–212, 4th February 2016.
7. Ching-Luh, H., Fu-Chieh, H., and Jen-Tsai, K., "Microstrip bandpass filters for ultra-wideband (UWB) wireless communications," *IEEE MTT-S Int. Microwave Symp. Dig.*, June 2005, pp. 4.
8. Xiao-Hu Wu, Qing-Xin Chu, and X.-K. Tian, "Quintuple-mode UWB bandpass filter with sharp roll-off and super-wide upper stopband," *IEEE Microw. Wireless Compon. Letter*, Vol. 21, no. 12, Dec. 2011.

Design of Novel Dual and Triple Band Filters Based on Stub Loaded Resonators

7.0 Introduction

Filters play an irreplaceable role in virtually any type of RF/Microwave system today. With the recent rapid development and widespread use of various wireless communication systems, even more stringent requirements are posed on RF/microwave filters, in particular, smaller size, higher performance and multi operation are considered necessary to solve the challenges of insufficient capacity of the various wireless systems. To that end, high performance and compact microwave filters that operate at two or more none harmonically related frequencies are in demand, and various approaches to their design are being investigated today [1].

Development of several wireless communication standards and devices impose the requirement for filters to simultaneously operate at two or more frequencies that corresponds to the standards such as IEEE 806.16, IEEE 806.11, GSM, CDMA, etc. Dual-band bandpass filters are the first multiband circuits to answer this requirement. Compared to dual-band filters, the design of bandpass filters with three or more bands represents a greater challenge when it comes to performance and compactness, because good characteristics have to achieve in three or more closely positioned passbands. Closely positioned passbands can cause undesired signal crosstalk, therefore the design of these filters is a demanding task since it requires a transfer function steep slopes. What is more, almost all bands that are commercially used are closely positioned, for instant Wi-Fi, WiMAX, and GSM systems that operate at 0.9/1.8GHz, 2.4/2.45 GHz, 3.5 GHz and 5.2/5.25 GHz [1].

With the rapid development of dual-band operation in modern and next generation wireless communication systems, planar microstrip dual bandpass filters with a small physical size, low insertion-loss, and good passband frequency-selectivity are highly sought components. In recent years with the development of multi-mode technology, which is capable of reducing the number of resonators required for a prescribed order of filter makes it possible to achieve a small filter size and compact design. Particularly, dual mode resonator can be utilized as a doubly tuned resonant circuit and hence the number of required filter order is reduced by half [2]. As a result, dual bandpass filters have received extensive attention recently which has resulted in several design approaches being

reported in the literature. In [3], multiple stub loaded ring resonators (MSLRR) is proposed to design directly coupled multi-band bandpass filters with mixed electric and magnetic coupling (MEMC). The proposed MSLRR exhibits multiple-mode resonant behaviour. The increased number of loaded stubs excites many more useful resonant modes, but these resonant modes can still be independently controlled. In [3], a dual-band BPF, a tri-band BPF, a quad-band BPF, and a quint-band BPF are designed and fabricated using different types of MSLRRs. The passband frequencies and return-loss of these multi-band BPFs can be independently controlled. Multiple transmission zeros, due to the cancelling effect of MEMC and virtual grounds in the MSLRR, can be observed around the passbands resulting in sharp passband selectivity and high band-to-band isolation but with poor out-of-band rejection and a poor roll-off skirt on one side of the passband, as shown in Fig 7.1.

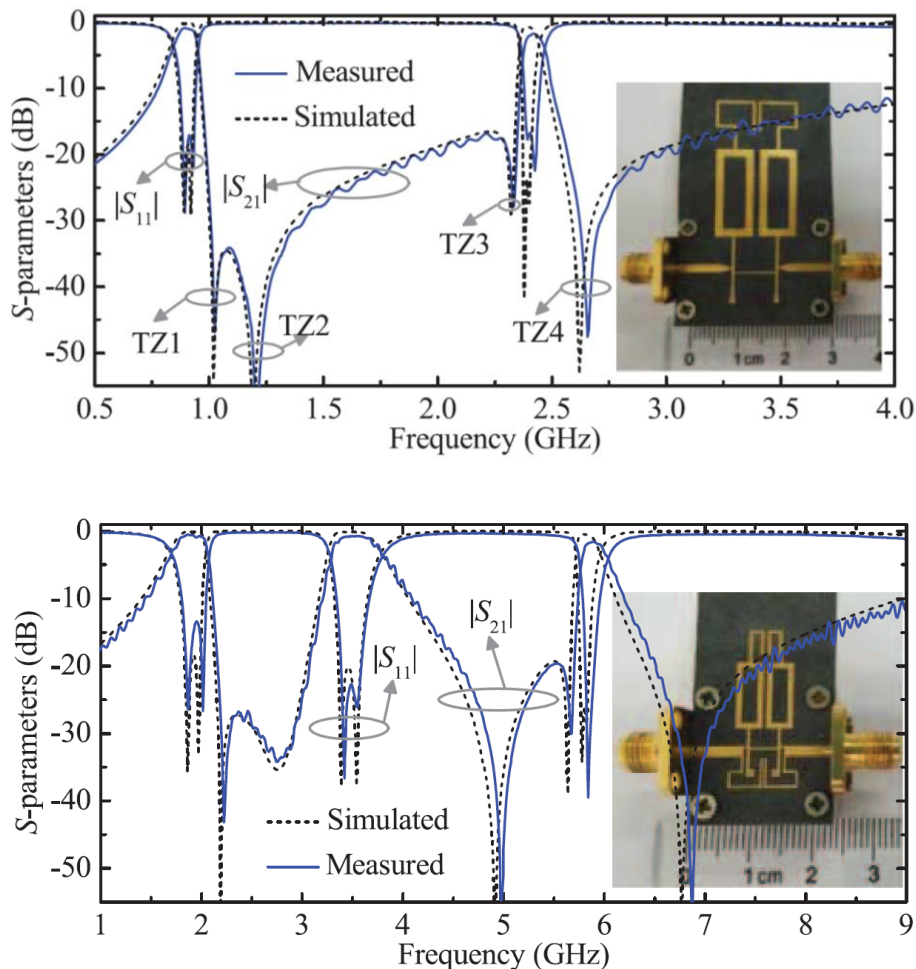


Fig. 7.1. Simulated and measured results of a dual and tri-band BPF. The inset is the photographs of fabricated dual and tri-band BPF [3].

Two types of modified open- or short-circuited stub loaded $\lambda/4$ resonator and their applications to second-order dual-band bandpass filters are proposed in [4]. Resonance

characteristic analysis shows that the first two resonant frequencies of the two resonators can be independently controlled and furthermore, different frequency ratios can be achieved by loading different stubs. By adopting the configuration of coupling loaded stubs, the bandwidths and frequencies of both passbands can be tuned to desirable values in a certain range. The results in Fig. 7.2 show the filter's passbands have a low insertion-loss, good return-loss, good mutual band isolation, but its roll-off rejection skirts are not so good.

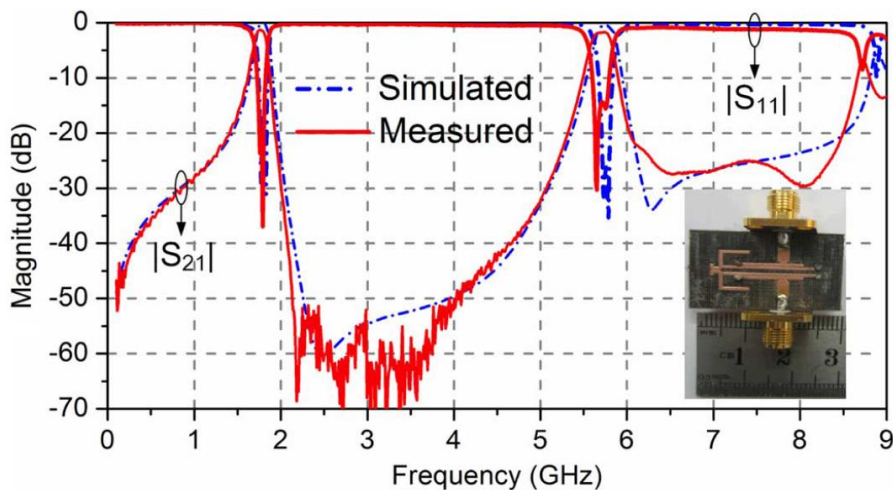


Fig. 7.2. Simulated and measured results of Filter [4].

A dual-wideband BPF proposed in [5] allows its two passbands to be controlled using shorted SIRs, but the disadvantage of this filter is that it suffers from poor passband selectivity and low band-to-band isolation. In [6] a dual-band BPF design is described with a single modified SIR, which is miniature and has a good out-of-band rejection. However, the filter configuration design is complex and its resonant frequency is difficult to adjust.

In this chapter, a compact dual-band BPF is presented with desired characteristics using stub loaded half-wavelength resonators coupled to input and output resonators. The input and output feed-lines are interdigitally coupled to reduce the passband insertion-loss and to realise a wide stopband on either side of the dual-band response with high rejection level. The three finger interdigital coupling is used to reduce the need for tight, which is necessary to realise wideband performance.

7.1 Analysis of Stub Loaded Resonator

Configuration of the dual wideband filter, shown in Fig. 7.3(a), can be considered essentially consisting of a pair of resonators that are shunt loaded with a half-wavelength open-

circuited stub, as shown in Fig. 7.3(b). These resonators are coupled electromagnetically to SIR structure, where the SIRs are inter-digitally coupled to the input/output feed lines. Characteristic impedance and electrical length of the resonator and the shunt open-circuit stub in Fig. 7.3(b) have different impedances and electrical lengths. The first transmission line has an impedance of Z_1 and an electrical length of θ_1 . The vertically loaded stub has an impedance of Z_3 and an electrical length of θ_3 . The horizontal open-ended stub has an impedance of Z_2 and an electrical length of θ_2 . By bending the open-circuit stubs by 90° the lateral size of the structure, shown in Fig. 7.3(a), is reduced.

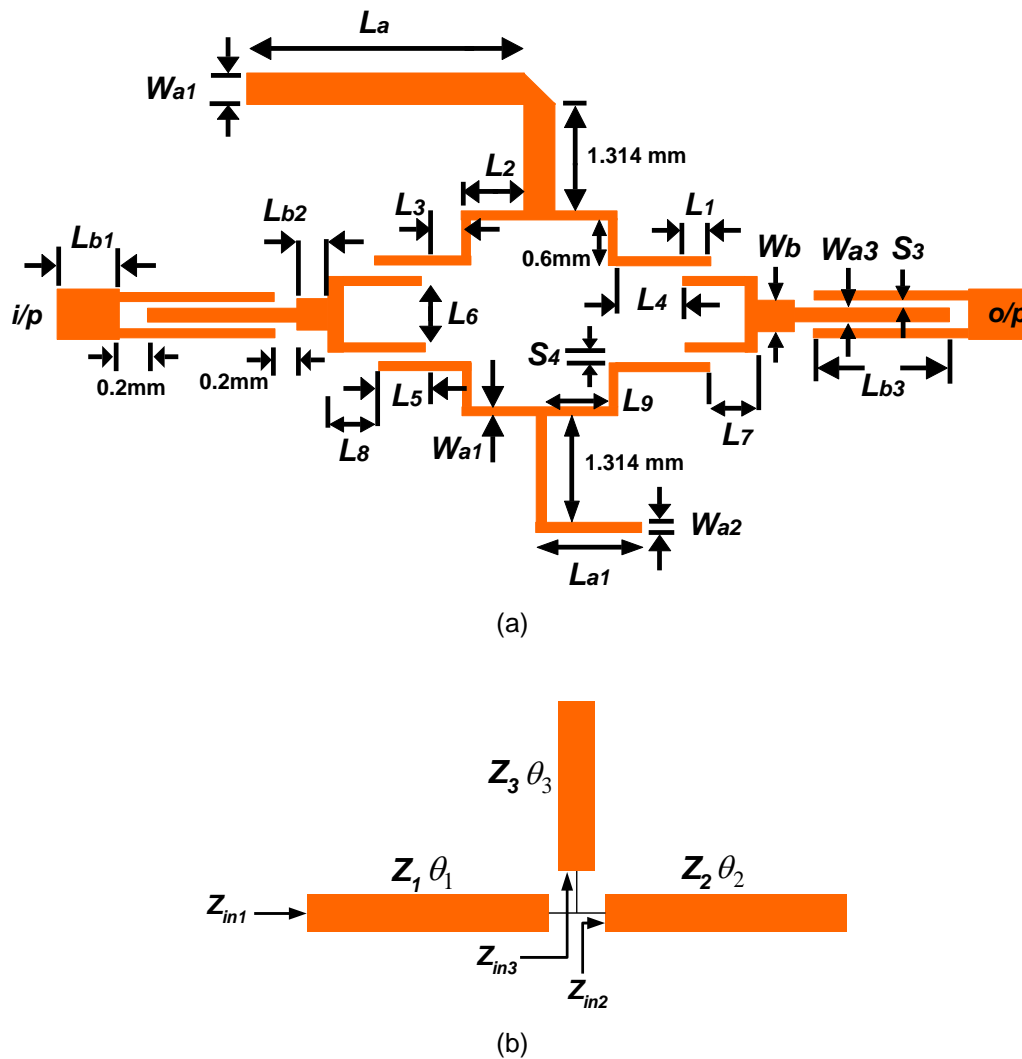


Fig. 7.3. (a) Configuration of the dual-band bandpass filter using stub loaded resonator, and (b) structure of the stub-loaded resonator.

Using impedance transformation, the input impedances looking into the horizontal stub and the vertically loaded stub, as labeled in Fig. 7.3(b), are:

$$Z_{in2} = -jZ_2 \cot \theta_2 \quad (7.1)$$

$$Z_{in3} = -jZ_3 \cot \theta_3 \quad (7.2)$$

By combining (7.1) and (7.2) in parallel, we obtain:

$$Z_L = \frac{-jZ_2C_2Z_3C_3}{(Z_2C_2 + Z_3C_3)} \quad (7.3)$$

Where $C_2 = \cot\theta_2$ and $C_3 = \cot\theta_3$. Then application of impedance transformation, the input impedance of the overall resonator is:

$$Z_{in1} = \frac{-jZ_1Z_2C_2Z_3C_3 - jZ_1^2t_1Z_2C_2 - jZ_1^2t_1Z_3C_3}{Z_1Z_2C_2 - Z_1Z_3C_3 - Z_2C_2Z_3C_3t_1} \quad (7.4)$$

When $Z_{in1} = \infty$ (resonant condition) occurs when:

$$Z_1Z_2C_2 + Z_1Z_3C_3 + Z_2Z_3C_2C_3t_1 = 0 \quad (7.5)$$

Where $t_i = \tan\theta_i$ and $C_i = \cot\theta_i$, $i = 1, 2, 3 \dots$

When $Z_2 = Z_3 = Z$ and $\theta_2 = \theta_3 = \theta$ (6) simplifies to

$$\tan(n\theta_2) + \tan(n\theta_3) + k\tan(n\theta_1) = 0 \quad (7.6)$$

Where n is the ratio of resonance frequency f_r to the fundamental resonance f_i ; and impedance ratio $k = Z/Z_1$. A pre-set stub length of θ_1 and θ_2 requires determination of θ_3 to realize the fundamental resonance condition, which can be obtained by solving (7.6) by putting $n = 1$. Assuming $\theta_2 = \theta_3 = \theta$, (7.6) simplifies to:

$$\tan(n\theta) + \frac{k}{2}\tan(n\theta_1) = 0 \quad (7.7)$$

Resonance frequency ratio of higher order modes relative to the fundamental mode of the stub-loaded structure is plotted in Fig. 7.4(a) as a function of θ_1 and k for a stub length of 120° . This plot suggests that the mode positions are controllable by changing θ_1 and k . Fig. 7.4(b) shows how the stub length (in degrees) affects the frequency ratio for a fixed value of k . This result reveals that dual-band filter functionality at two frequencies is realizable by using this stub-loaded structure.

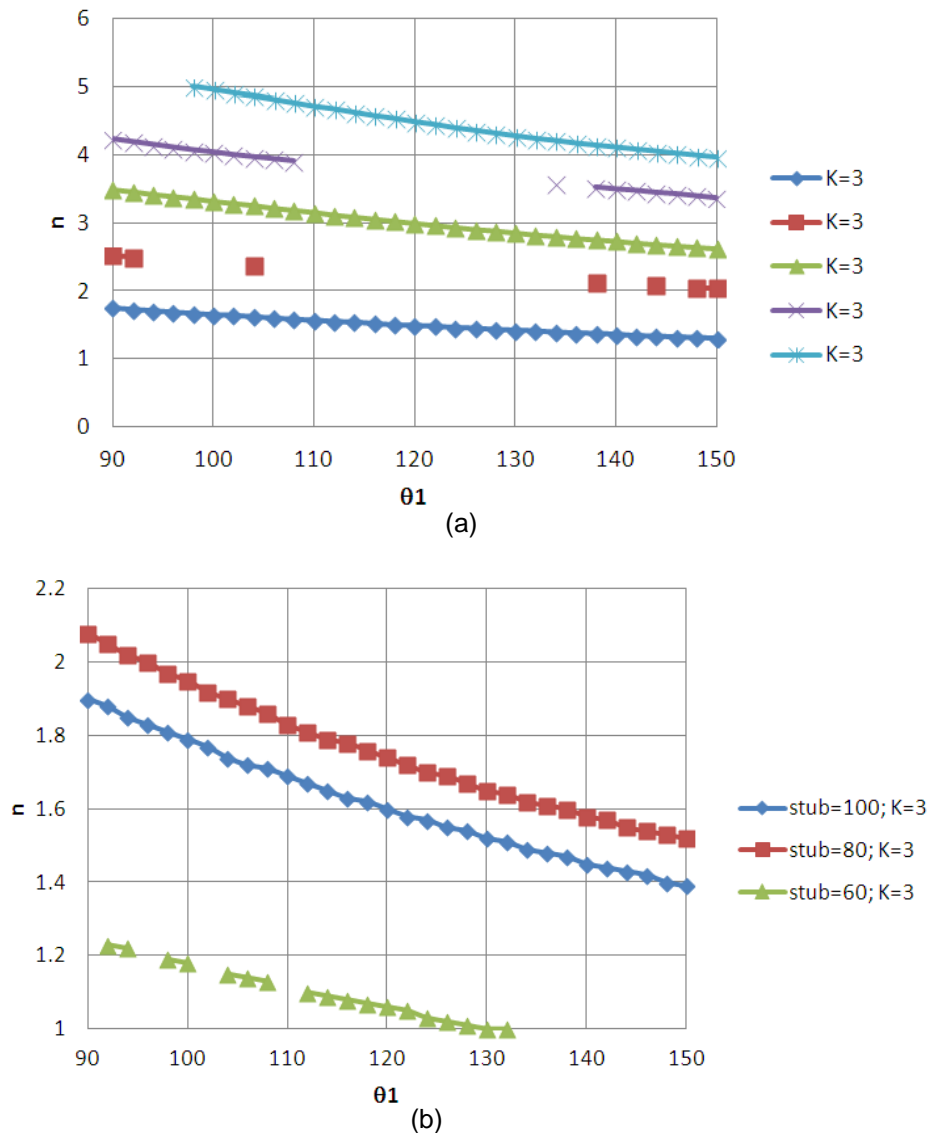


Fig. 7.4. (a) Solution of resonance frequency ratio of higher order modes relative to the fundamental frequency as a function of θ_1 and k for a stub length of 120° , and (b) resonance frequency ratio as a function of θ_1 for different stub lengths.

7.1.1 Dual-Band Bandpass Filter Design

The layout structure of the dual-band BPF shown in Fig. 7.3(a) is a modification of filter structure shown in Fig. 5.6(a) in chapter 5, where the dimensions of the structure have been changed to create a notch in the middle of filter's passband. To demonstrate the validity of proposed wideband duplexer it was constructed on dielectric substrate Arlon CuClad217LX with thickness (h) of 0.794 mm, dielectric constant (ϵ_r) of 2.17 mm, copper conductor thickness (t) of 35 μm , and loss-tangent ($\tan\delta$) of 0.0009. The structure was analysed using ADSTM Momentum and the simulated results of the filter are shown in Fig. 7.5.

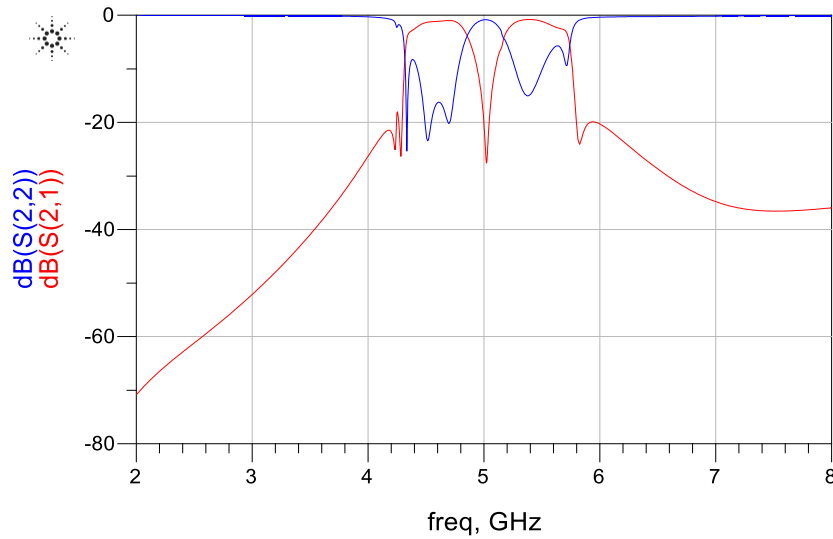


Fig. 7.5. Transmission and reflection-coefficient response of the proposed dual-band bandpass filter.

To reduce the structure size, two open stubs are bent in a L-shape, as shown in Fig. 7.6. Simulation analysis was carried out by using full wave electromagnetic simulator ADSTM Momentum software. The optimized values of geometric parameters are: $W_a = 1.2$ mm, $W_{a1} = 0.2$ mm, $W_{a2} = 0.87$ mm, $W_b = 2.42$ mm, $W_d = 1.66$ mm, $L_a = 10.36$ mm, $L_{a1} = 8.24$ mm, $L_{b1} = 3$ mm, $L_{b2} = 0.2$ mm, $L_{b3} = 10$ mm, $L_1 = 5.36$ mm, $L_2 = 3.3$ mm, $L_3 = 1.76$ mm, $L_4 = 1.71$ mm, $L_5 = 5.44$ mm, $L_6 = 0.89$ mm, $L_7 = 4.37$ mm, $L_8 = 4.17$ mm, $L_9 = 3.29$ mm, $S_3 = 0.4$ mm, and $S_4 = 0.24$ mm. Fig. 7.7 shows the simulated results of the S-parameters. The centre frequencies (f_1, f_2) of the two passbands are at 4.66 GHz and 5.5 GHz, and their corresponding 3-dB fractional bandwidth are 13% and 12%, respectively. Minimum insertion-loss at their respective centre frequencies are 1.02 and 0.8 dB, and the return-loss are better than 13 and 21 dB, respectively. The three transmission zeros ($f_{tz1}, f_{tz2}, f_{tz3}$) are located at 4.2 GHz, 5.0 GHz and 5.9 GHz, respectively, which results in the dual-band filter exhibiting an excellent sharp frequency-selectivity.

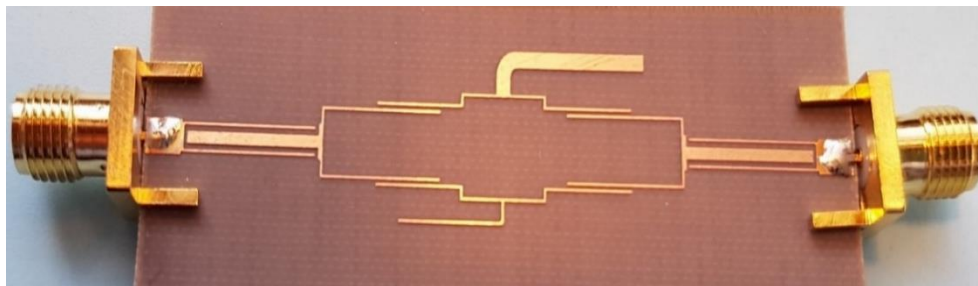


Fig. 7.6. Photograph of the three-finger interdigital coupled feed-line dual-band bandpass filter.

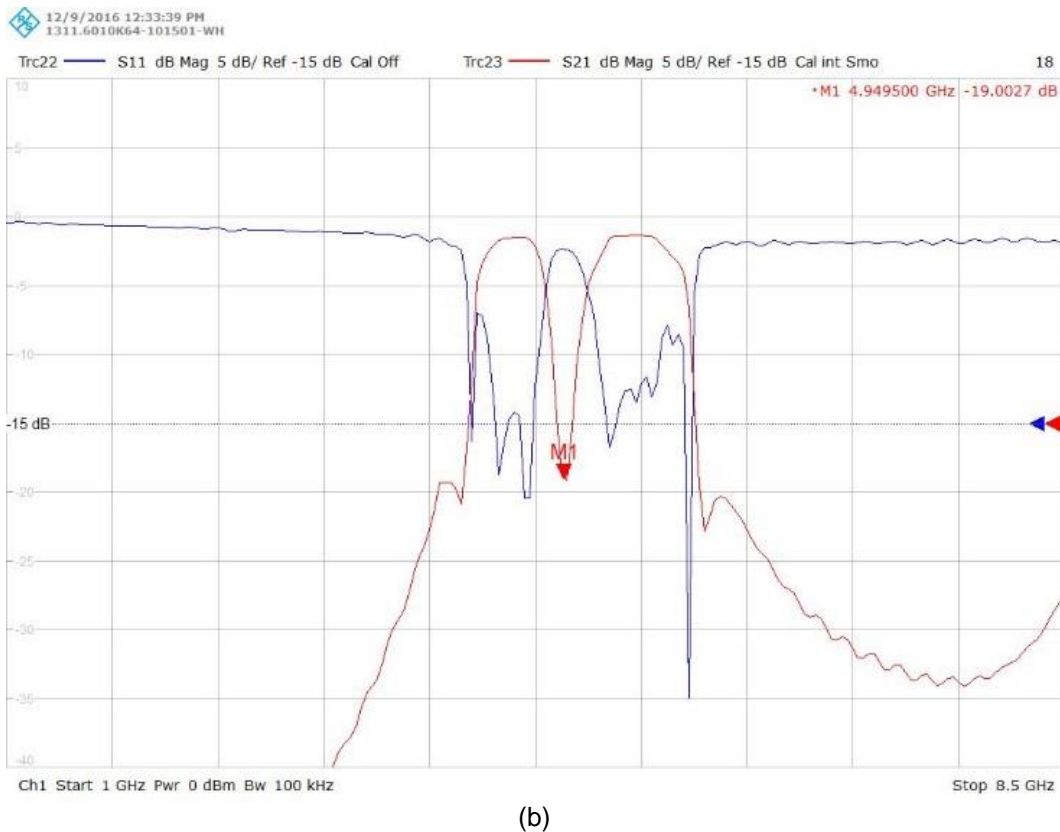
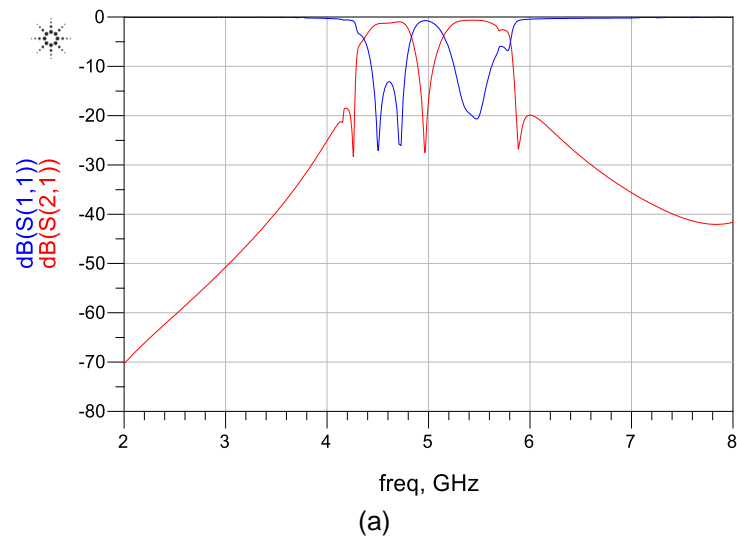


Fig. 7.7. Transmission and reflection-coefficient response of the proposed dual-band bandpass filter.

7.1.2 Simulated Results and Discussion

A parametric study was conducted to validate the filter analysis and its performance using ADS™ EM simulation software. The effect of key parameters are analysed and discussed in detail below. The effect of varying the open stub length (L_a) on frequency response is shown in Fig.7.8 and Fig. 7.9, as well as tabulated in Table 7.1. This shows the transmission zeros f_{tz1} and f_{tz2} , and the resonant mode f_{even2} can be controlled by L_a . As the length is

reduced from its optimized value 9.72 mm to 8.52 mm, the resonant mode f_{even2} changes from 5.49 GHz to 5.65 GHz, and first and second transmission zero move towards higher frequencies by 5% and 6%, respectively. L_a has a very minor effect on resonant mode f_{odd1} , which shifts towards higher frequency.

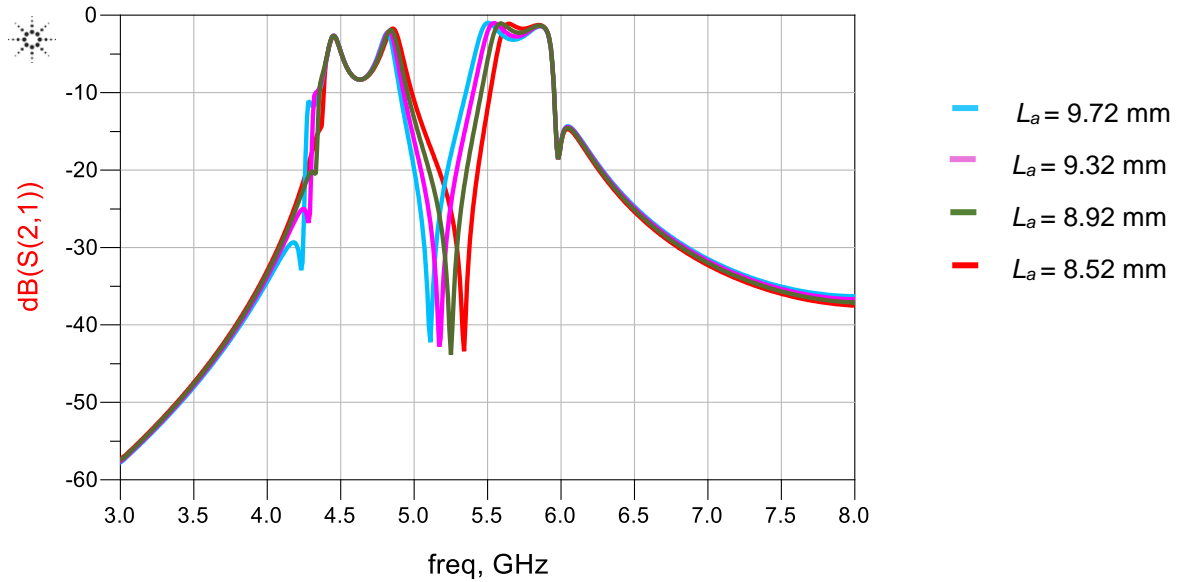


Fig. 7.8. Frequency response of the filter as a function of open stub length (L_a).

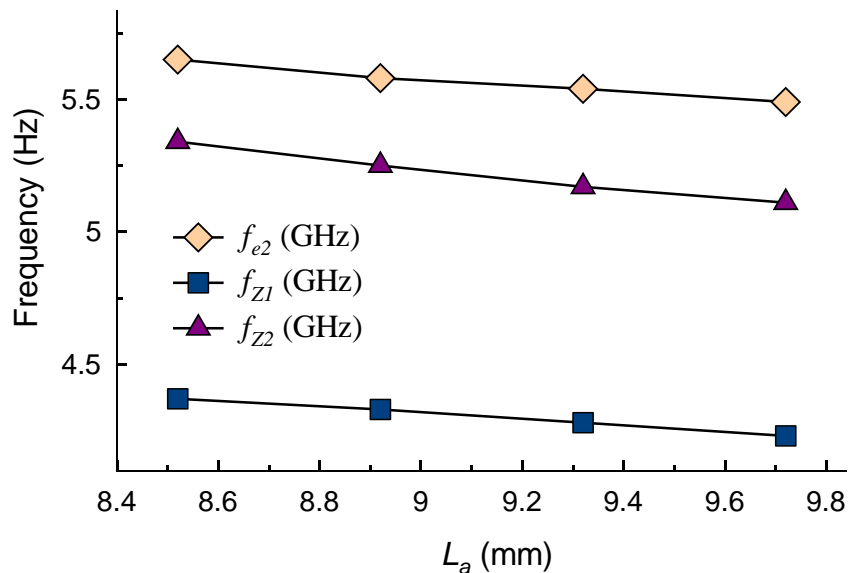


Fig. 7.9. Effect on the filter's first and second transmission zeros and second even resonant frequency as a function of open stub length (L_a).

Table 7.1. Effect of stub length on first and second transmission zeros and second even resonant frequency.

L_a (mm)	f_{even2} (GHz)	f_{tz1} (GHz)	f_{tz2} (GHz)
9.72	5.49	4.23	5.11
9.32	5.54	4.28	5.17
8.92	5.58	4.33	5.25
8.52	5.65	4.37	5.34

Fig. 7.10 and Fig. 7.11 show the performance of dual-band filter with the variation in open stub length (L_{a1}). The results are also given in Table 7.2. This simulation analysis shows when L_{a1} is reduced from its optimized value 8.24 mm to 7.04 mm the resonant mode f_{odd2} shifts from 5.86 GHz to 6.36 GHz, transmission zero f_{tz3} shifts from 5.98 GHz to 6.57 GHz, the resonant frequency f_{odd1} moves from 4.81 GHz to 4.89 GHz, and transmission zero f_{tz2} from 5.11 GHz to 5.17 GHz. However, transmission zero f_{tz3} and resonant frequencies f_{even1} and f_{even2} remain unchanged.

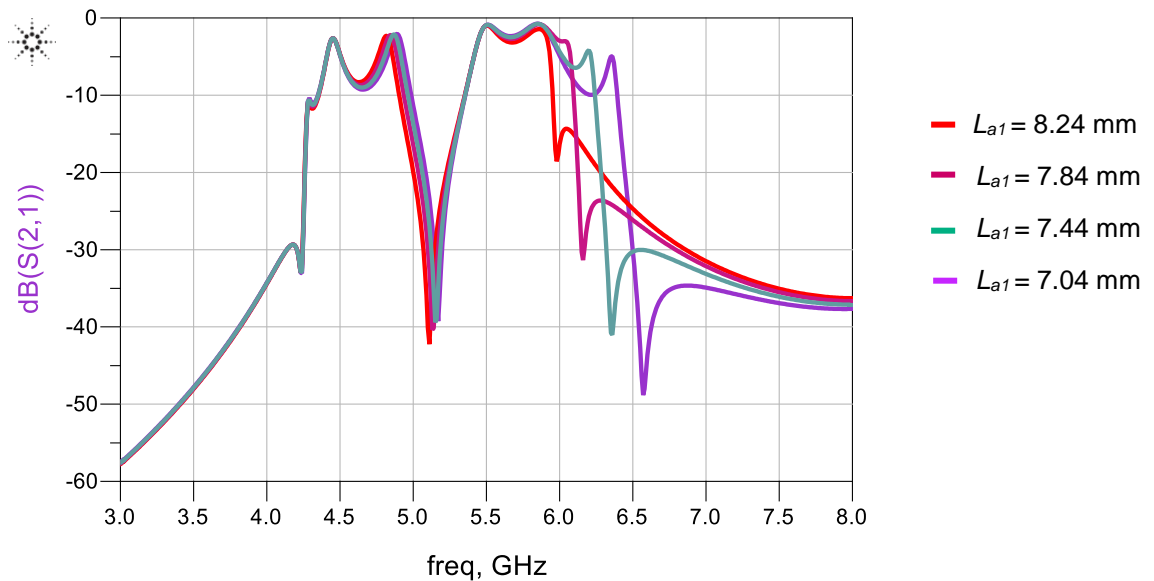


Fig. 7.10. Frequency response of the filter as a function of open stub length (L_{a1}).

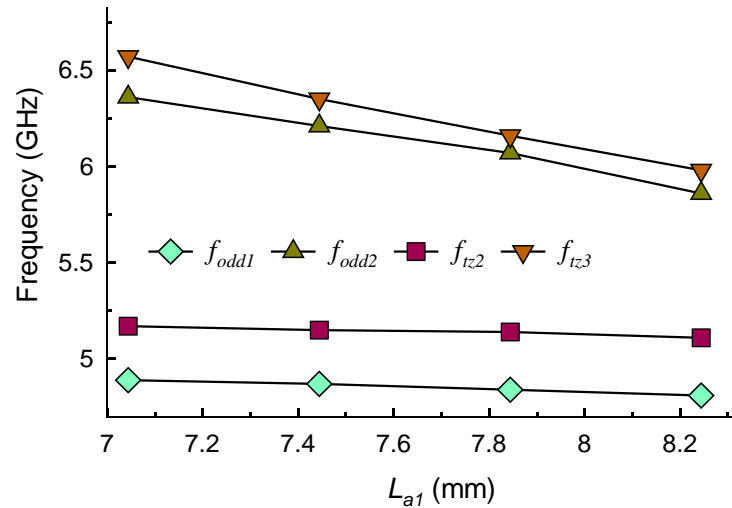


Fig. 7.11. Effect on the filter transmission zeros, even and odd resonant frequencies as a function of open stub length (L_{a1}).

Table 7.2. Effect of open stub length on second and third transmission zeros and first and second odd resonant frequencies.

L_{a1} (mm)	f_{odd1} (GHz)	f_{odd2} (GHz)	f_{tz2} (GHz)	f_{tz3} (GHz)
8.244	4.81	5.86	5.11	5.98
7.844	4.84	6.07	5.14	6.16
7.444	4.87	6.21	5.15	6.35
7.044	4.89	6.36	5.17	6.57

The effect of resonator length (L_5) on filter's performance is shown in Fig. 7.12 and Fig. 7.13, and is tabulated in Table 7.3. When L_5 is reduced from 5.44 mm to 4.54 mm the resonant frequency f_{even1} shifts from 4.46 GHz to 4.62 GHz and f_{odd1} from 4.80 GHz to 5 GHz. Transmission zeros f_{tz1} and f_{tz2} shift upward in frequency by 7% and 2%, respectively, and f_{odd2} by 2%. The upper out-of-band rejection performance of second passband deteriorates rapidly from 15 dB to 5 dB; however third transmission zero remain fixed.

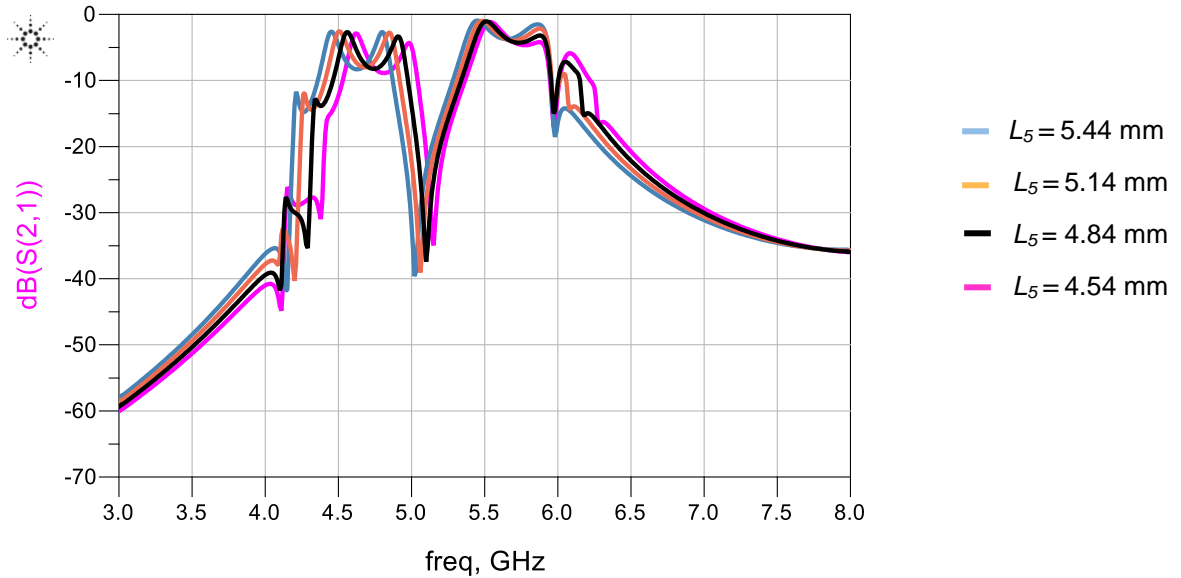


Fig. 7.12. Frequency response of the filter as a function of resonator length (L_5).

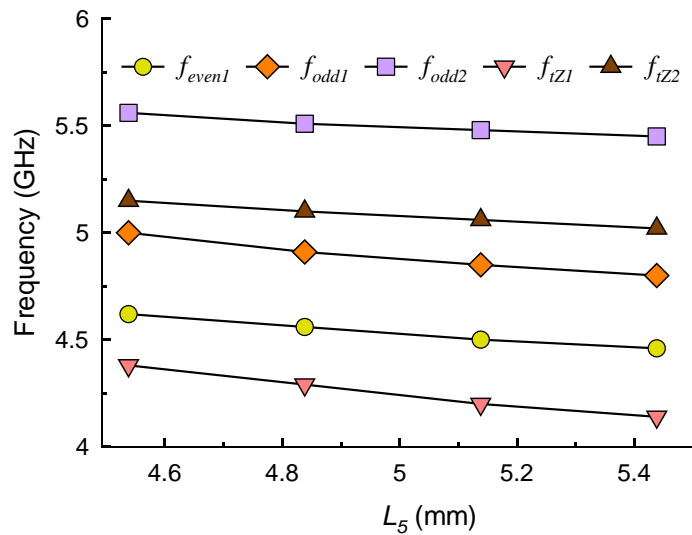


Fig. 7.13. Effect on the filter transmission zeros and even and odd resonant frequencies as a function of resonator length (L_5).

Table 7.3. Effect of resonator length (L_5) on transmission zeros, even and odd resonant frequencies.

L_5 (mm)	f_{even1} (GHz)	f_{odd1} (GHz)	f_{odd2} (GHz)	f_{tz1} (GHz)	f_{tz2} (GHz)
5.438	4.46	4.80	5.45	4.14	5.02
5.138	4.50	4.85	5.48	4.20	5.06
4.838	4.56	4.91	5.51	4.29	5.10
4.538	4.62	5.00	5.56	4.38	5.15

The effect of resonator length (L_B) on dual-band filter was assessed, when the length was varied from 4.17 mm to 2.97 mm. The results are shown in Fig. 7.14 and Fig. 7.15, as well as tabulated in Table 7.4. A moderate change is noticed in the location of resonant frequencies and transmission zeros. In fact, f_{even2} changes from 5.45 GHz to 5.57 GHz, and f_{odd1} that changes from 4.80 GHz to 4.93 GHz. The transmission zeros f_{tz1} changes from 4.14 GHz to 4.23 GHz, and f_{tz2} from 5.02 GHz to 5.57 GHz. However, the upper rejection level of second passband deteriorates rapidly from 15 dB to 7 dB. A slight change is observed in the location of resonant frequencies f_{even1} , f_{odd2} , and the lower rejection level of first passband.

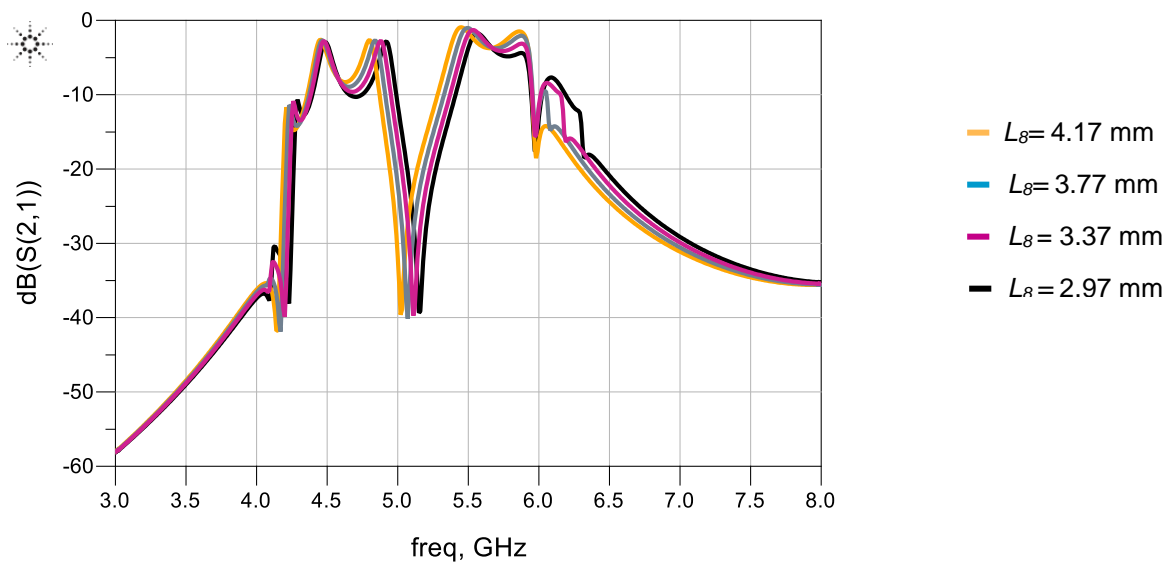


Fig. 7.14. Frequency response of the filter as a function of resonator length (L_B).

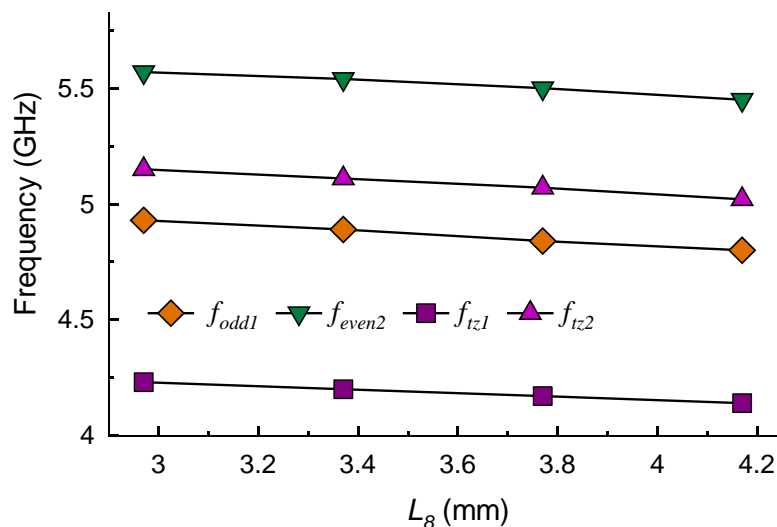


Fig. 7.15. Effect on the filter transmission zeros and even and odd resonant frequencies as a function of resonator length (L_B).

Table 7.4. Effect of resonator length (L_8) on transmission zeros, even and odd resonant frequencies.

L_8 (mm)	f_{odd1} (GHz)	f_{even2} (GHz)	f_{tz1} (GHz)	f_{tz2} (GHz)
4.17	4.80	5.45	4.14	5.02
3.77	4.84	5.50	4.17	5.07
3.37	4.89	5.54	4.20	5.11
2.97	4.93	5.57	4.23	5.15

It is evident from Fig. 7.16 and Fig. 17, the resonant modes f_{odd1} , f_{even2} and transmission zero f_{tz2} are mainly controlled by resonator length (L_7). Resonant modes f_{odd1} , f_{even2} and transmission zero f_{tz2} move upward in frequency when L_7 is changed from 3.17 mm to 4.37 mm. These results are also given in Table 7.5. The upper rejection level reduce deteriorates rapidly with the change from about 15 dB to 5 dB as compare to lower rejection level which changes from 34 dB to 28 dB. It was also observed the length of interdigital coupled line (L_{b3}) has almost the same effect on the frequency response of dual-band filter as resonator length (L_7) when it is changed from its optimized value. The effect of L_{b3} is shown in Fig. 7.18.

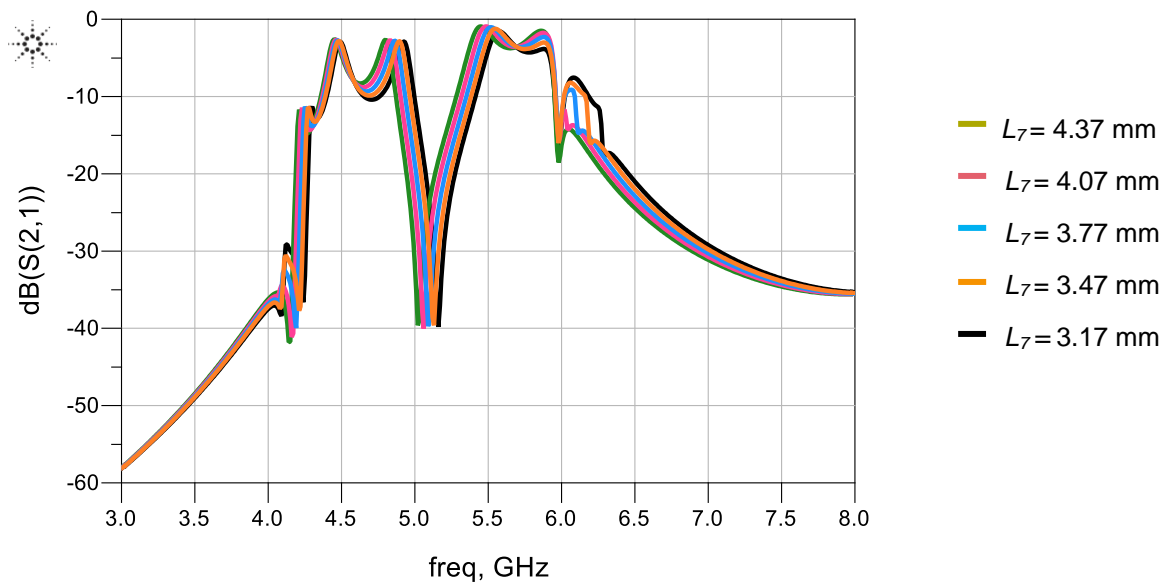


Fig. 7.16. Frequency response of the filter as a function of resonator length (L_7).

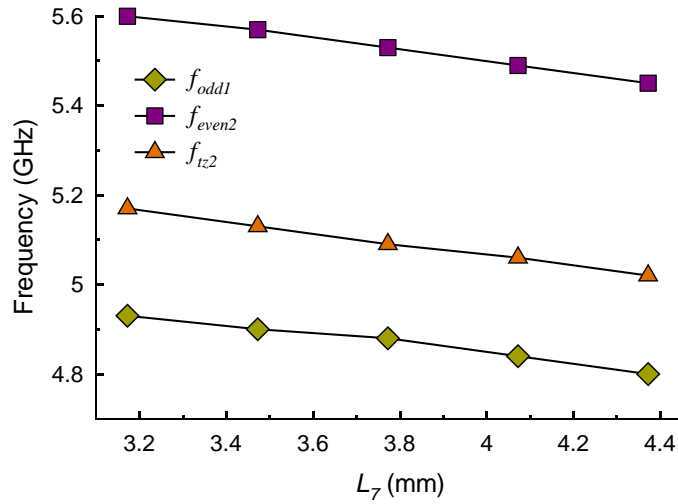


Fig. 7.17. Effect on the filter transmission zeros and even and odd resonant frequencies as a function of resonator length (L_7).

Table 7.5. Effect of resonator length (L_7) on transmission zeros, even and odd resonant frequencies.

L_7 (mm)	f_{odd1} (GHz)	f_{even2} (GHz)	f_{tz2} (GHz)
4.372	4.80	5.45	5.02
4.072	4.84	5.49	5.06
3.772	4.88	5.53	5.09
3.472	4.90	5.57	5.13
3.172	4.93	5.60	5.17

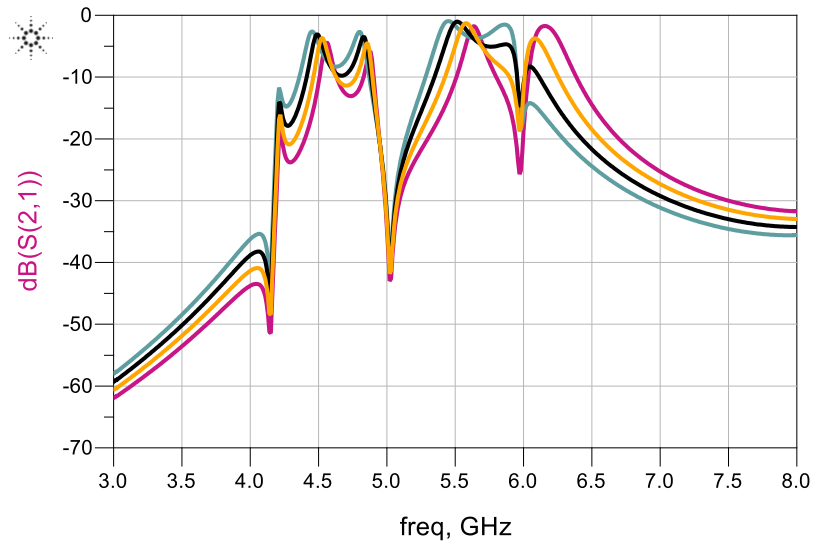


Fig. 7.18. Frequency response of the proposed filter as a function of coupled length (L_{b3}).

Fig. 7.19 depicts the effect of resonator length (W_a) on the dual-band filter's performance as it is varied from 0.30 mm to 1.20 mm. The results are shown in Fig. 7.20 and also tabulated in Table 7.6, which show the location of transmission zeros f_{tz1} and f_{tz2} can be changed by varying the dimension W_a . Change in the location of transmission zero f_{tz1} of 5% is almost linear, whereas transmission zero f_{tz2} is changed by about 2.5%.

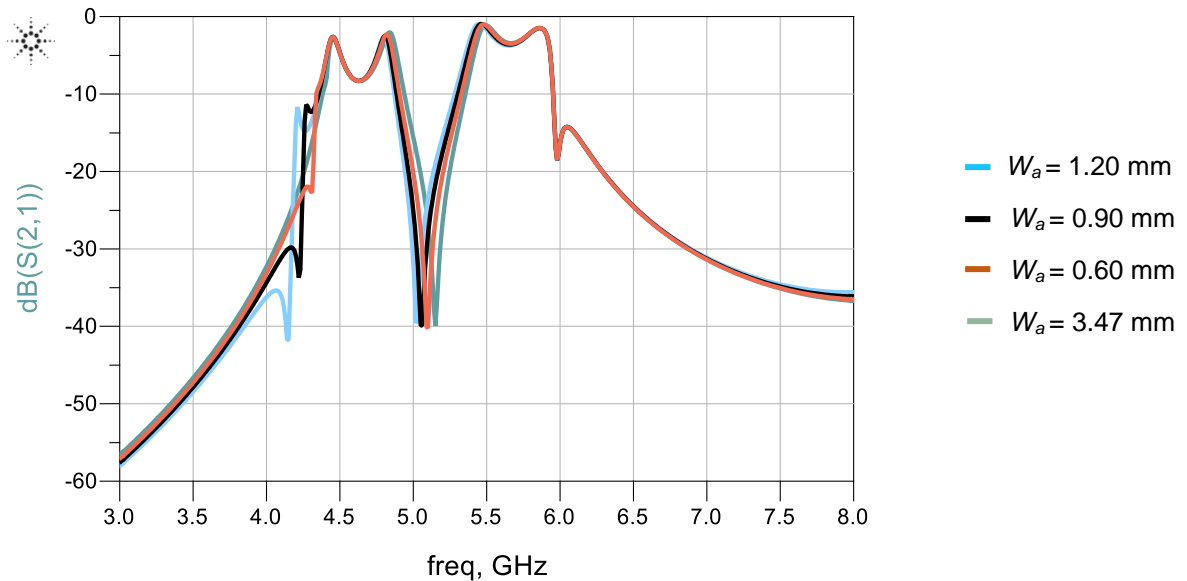


Fig. 7.19. Frequency response of the filter as a function of resonator width (W_a).

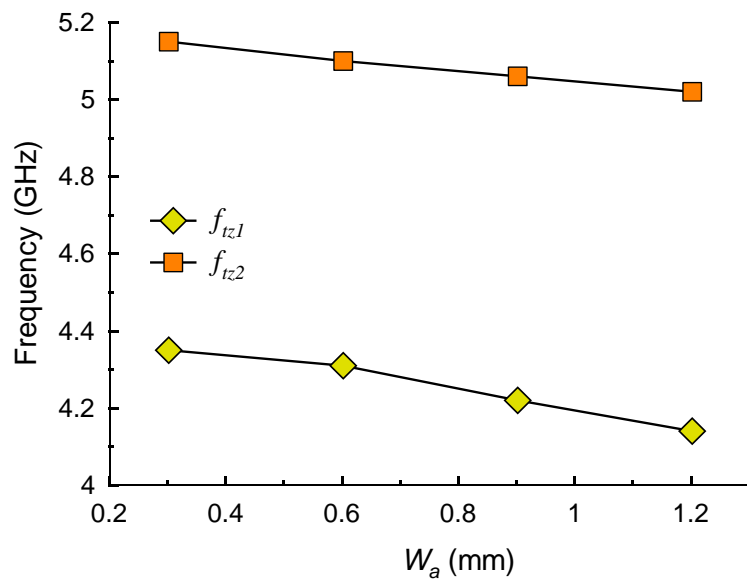
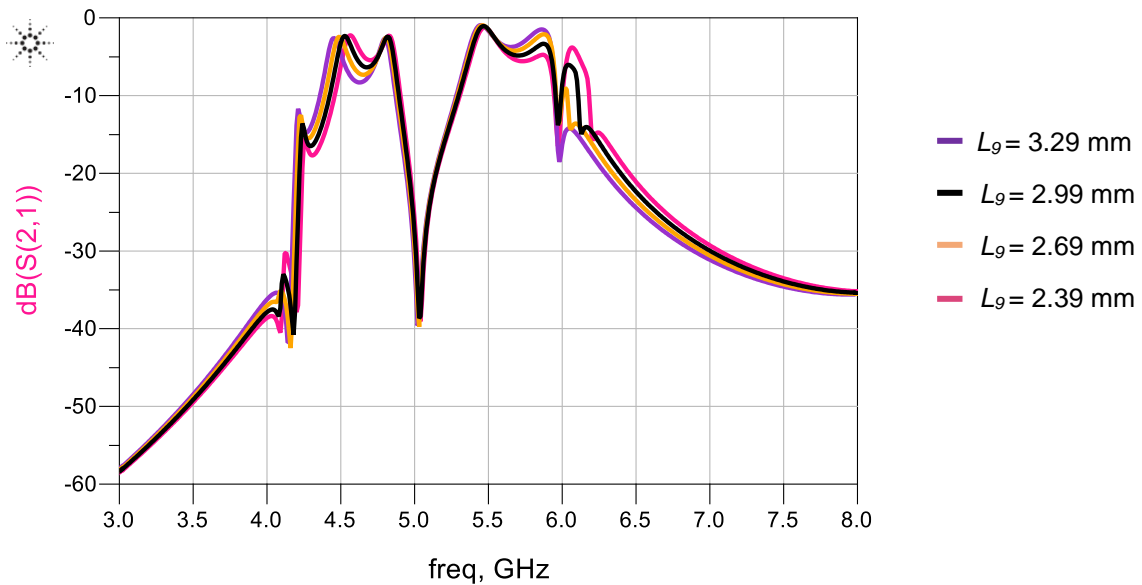


Fig. 7.20. Effect on the filter transmission zeros as a function of resonator width (W_a).

Table 7.6. Effect of resonator width (W_a) on transmission zeros.

W_a (mm)	f_{tz1} (GHz)	f_{tz2} (GHz)
1.202	4.14	5.02
0.902	4.22	5.06
0.602	4.31	5.10
0.302	4.35	5.15

The effect of resonator length (L_g) on filter's response was assessed by varying its value from 3.29 mm to 2.39 mm, as shown in Fig. 7.21. The results are plotted in Fig. 7.22 and given in Table 7.7. It is observed as the length (L_g) is reduced from 3.29 mm to 2.39 mm, the resonant mode f_{even1} shifts upward in frequency from 4.46 GHz to 4.57 GHz, and this has a minor effect on transmission zero f_{tz1} and resonant mode f_{odd2} . However, the upper rejection level is severely affected. The effect on other filter characteristics is minimal.

Fig. 7.21. Frequency response of the filter as a function of resonator length (L_g).

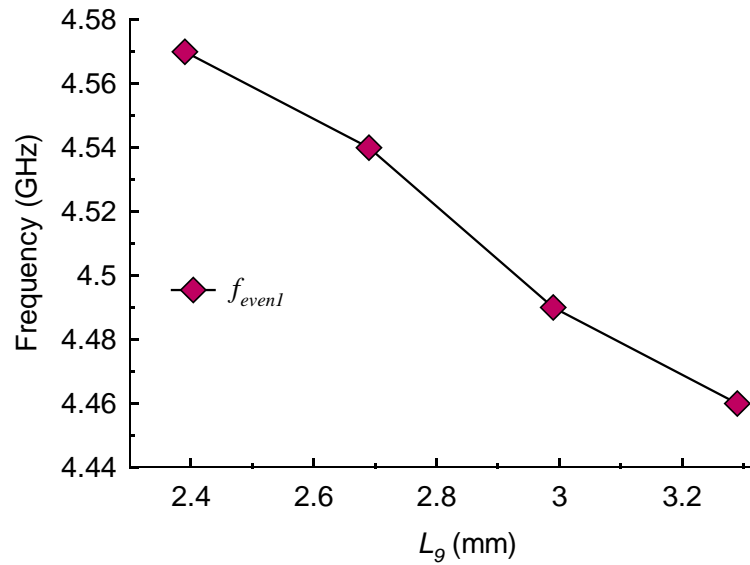


Fig. 7.22. Effect on the filter first even mode frequency as a function of resonator length (L_g).

Table 7.7. Effect of resonator length (L_g) on first even resonant mode.

L_g (mm)	f_{even1} (GHz)
3.29	4.46
2.99	4.49
2.69	4.54
2.39	4.57

Fig. 7.23 shows how the filter's performance is affected by resonator width (W_{a2}) as it's varied from 0.87 mm to 0.27 mm. The results are also plotted in Fig. 7.24 and given in Table 7.8. Study shows the resonator width controls the resonant frequency (f_{even1}) without significant affecting other characteristics of the passband. As the resonator width is reduced the resonant frequency shifts by 2%.

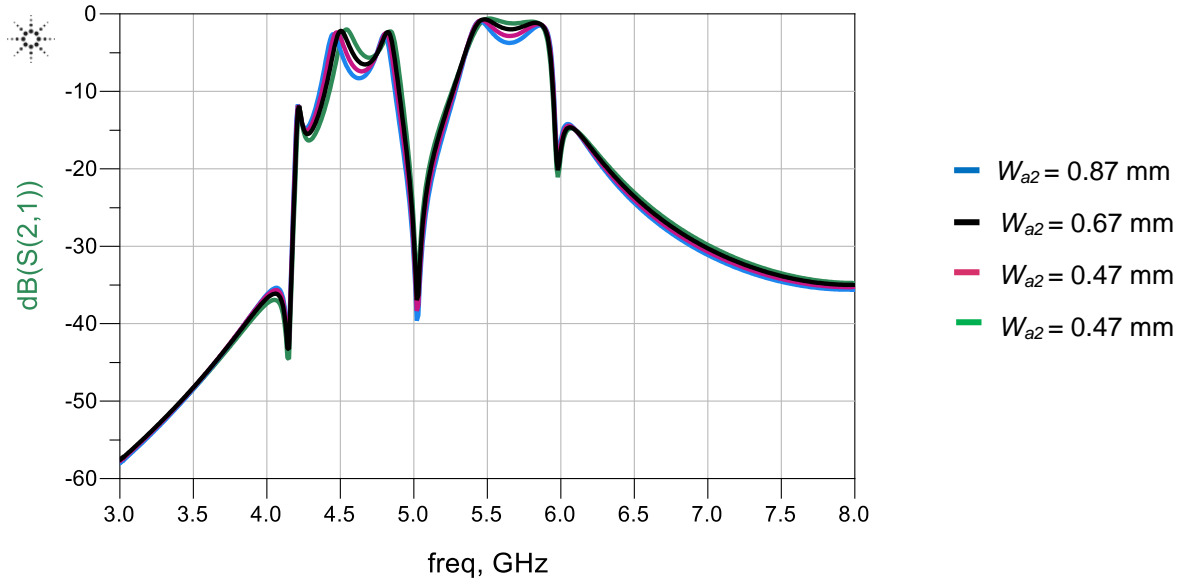


Fig. 7.23. Frequency response of the filter as a function of resonator width (W_{a2}).

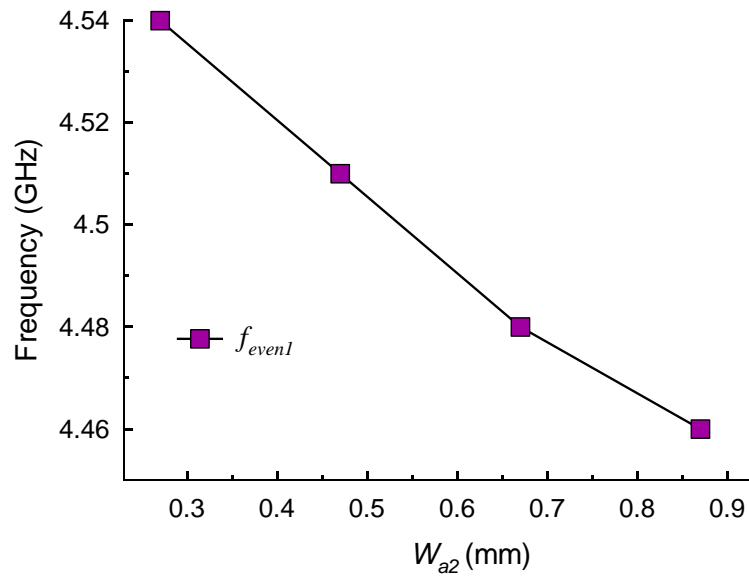


Fig. 7.24. Effect on the filter first even-mode frequency as a function of resonator width (W_{a2}).

Table 7.8. Effect of resonator width (W_{a2}) on first even-mode frequency.

W_{a2} (mm)	f_{even1} (GHz)
0.87	4.46
0.67	4.48
0.47	4.51
0.27	4.54

The effect of resonator length (L_6) on filter performance is shown in Fig. 7.25 and Fig. 7.26, and the results also given in Table 7.9. The results show as the resonator length is reduced there is a linear increase in resonant frequencies f_{odd1} and f_{even2} , and transmission zero f_{tz2} , however the out-of-band performance on upper side of the second passband deteriorates from 17 dB to 8 dB. Table 7.10 gives a comparison between this work and recent published work. Insertion-loss of the proposed dual-band filter is relatively low and unlike references [8] and [10], which has superior insertion-loss and 3-dB fractional bandwidth, the proposed filter can be implemented on just one side of the substrate plane whereas [8] and [10] required circuit implementation on both sides of the circuit board. The proposed filter is therefore easier and cheaper to fabricate.

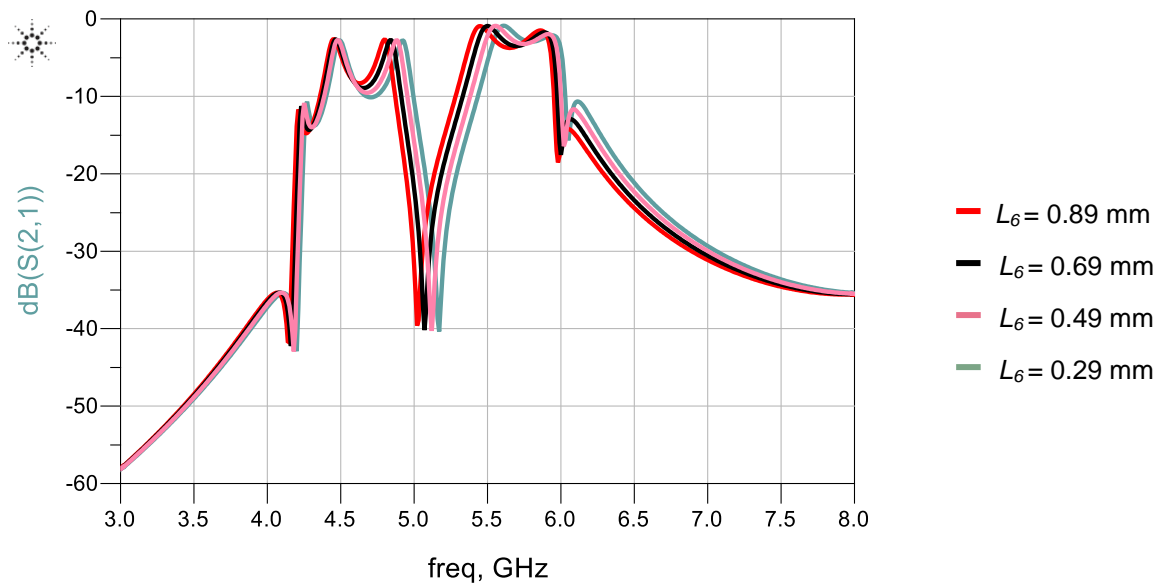


Fig. 7.25. Frequency response of the filter as a function of resonator length L_6 .

Table 7.9. Effect of resonator length (L_6) on transmission zero, even and odd resonant frequencies.

L_6 (mm)	f_{odd1} (GHz)	f_{even2} (GHz)	f_{tz2} (GHz)
0.894	4.80	5.45	5.02
0.694	4.84	5.50	5.07
0.494	4.89	5.58	5.12
0.294	4.94	5.63	5.17

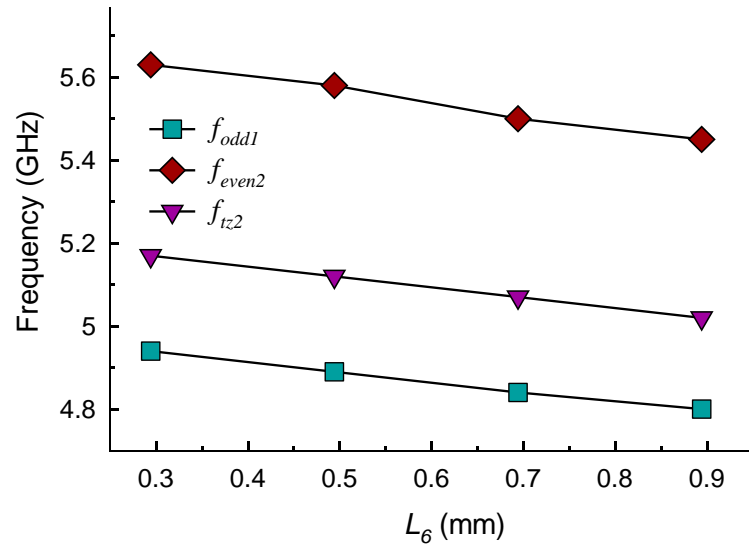


Fig. 7.26. Effect on the filter transmission zero, even and odd resonant frequencies as a function of resonator length (L_6).

Table 7.10. Comparison between this work and recently published dual-band BPF's.

Reference	Upper Stop Band (GHz)	CF (GHz)	IL (dB)	3-dB FBW (%)
This work	5.7–8.8	4.66 / 5.50	1.02 / 0.80	13 / 12
[3]	2.6–2.9	0.89 / 2.42	0.90 / 1.65	12 / 4.1
[8]	4.1–4.7	2.10 / 2.60	0.80 / 1.20	17 / 8.4
[9]	3.0–4.8	1.57 / 2.45	1.26 / 2.45	09 / 8.5
[10]	3.1–3.4	1.57 / 2.47	0.53 / 0.72	15.3 / 12.7
[11]	6.8–8.9	2.40 / 5.80	1.35 / 1.97	4.6 / 3.6

7.2 Design of Triple-Band Bandpass Filter

A triple-band filter design employs the same structure as the wideband filter in Fig. 5.61 of chapter 5, with the inclusion of a patch of length (L_9) and width (W_{a4}), which are diagonally located on the input and output SIR, as shown in Fig. 7.27. The filter was also fabricated on the same substrate. The simulated and measured S-parameter frequency response of this structure in Fig. 7.28 shows it exhibits three passbands centred at 3.4 GHz, 4.6 GHz and 5.7 GHz with 3-dB fractional bandwidth of 5.7%, 13% and 5.6%, respectively. The insertion-loss at the centre frequencies are 1.5 dB, 0.8 dB and 1.9 dB, and the return-loss is better than 18 dB, 16 dB and 11 dB, respectively. The five transmission zeros (< -27 dB) that define the passbands, which are located at 2.97 GHz, 4.13 GHz, 5.12 GHz, 5.92 GHz and 6.78 GHz, result in sharp frequency-selectivity and a good band-to-band isolation of the proposed triple-bandpass filter. There is excellent correlation between the simulated and measured results.

The optimized dimensions of the filter are: $W_a = 0.92$ mm, $W_{a1} = 0.2$ mm, $W_{a2} = 0.2$ mm, $W_{b4} = 2.4$ mm, $W_{b5} = 0.2$ mm, $W_d = 0.6$ mm, $L_a = 8.03$ mm, $L_{a1} = 8.88$ mm, $L_{b1} = 3$ mm, $L_{b2} = 1.04$ mm, $L_{b3} = 8.72$ mm, $L_1 = 5.56$ mm, $L_2 = 3.82$ mm, $L_3 = 1.76$ mm, $L_4 = 2.12$ mm, $L_5 = 5.68$ mm, $L_6 = 2.07$ mm, $L_7 = 3.67$ mm, $L_8 = 3.61$ mm, $L_9 = 1.7$ mm, $S_3 = 0.2$ mm, and $S_4 = 0.26$ mm.

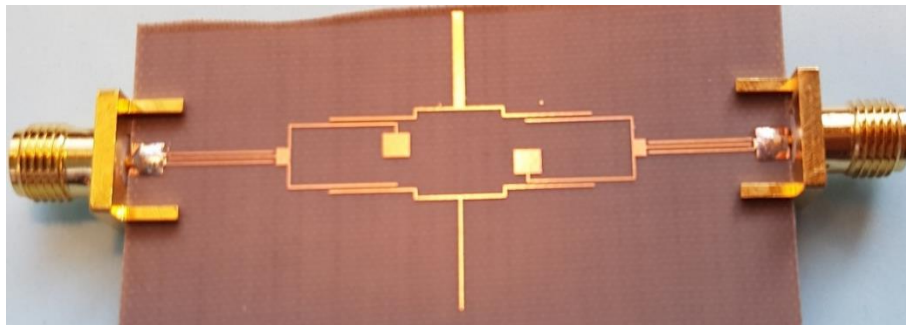
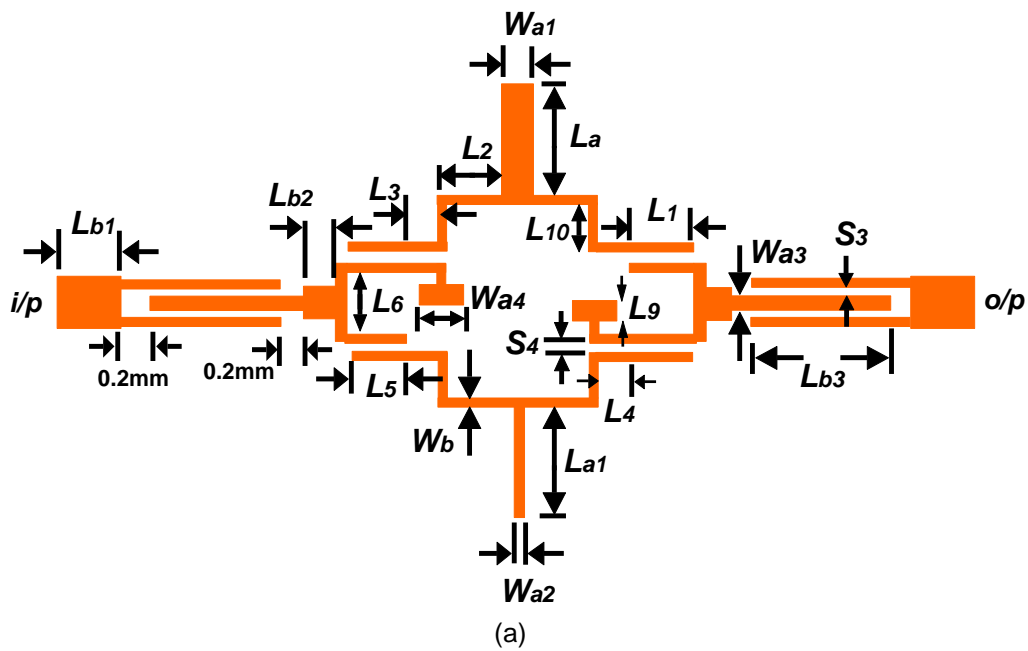
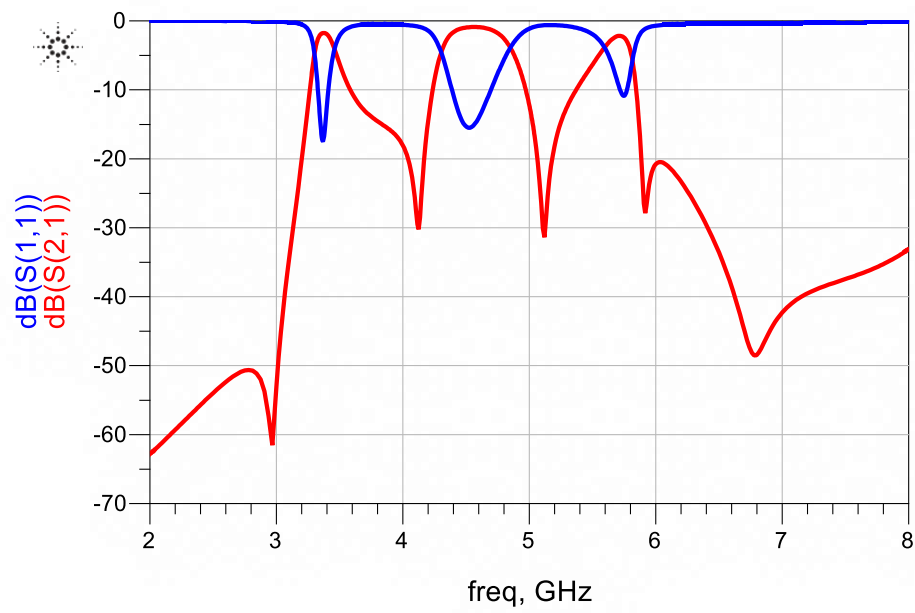


Fig. 7.27 (a) Configuration of the three finger interdigital coupled feed-line triple-band filter using stub loaded resonator, and (b) photograph of the implemented filter.



(a)



(b)

Fig. 7.28. Transmission and reflection-coefficient response of the proposed triple-band bandpass filter.

7.2.1. Simulated Results and Discussions

A thorough parametric study was conducted to investigate the influence of different filter parameters on the filter response using the ADS™ Momentum software. Although the coupled resonator length (L_{b3}) has no effect on the insertion-loss response but it affects the return-loss of the three passbands, as shown in Fig. 7.29. The results are also plotted in Fig. 7.30 and given in Table 7.11. Return-loss of passbands one and three can be changed by about 47% and 29%, respectively, and return-loss of passband two can be changed by just 16.5%.

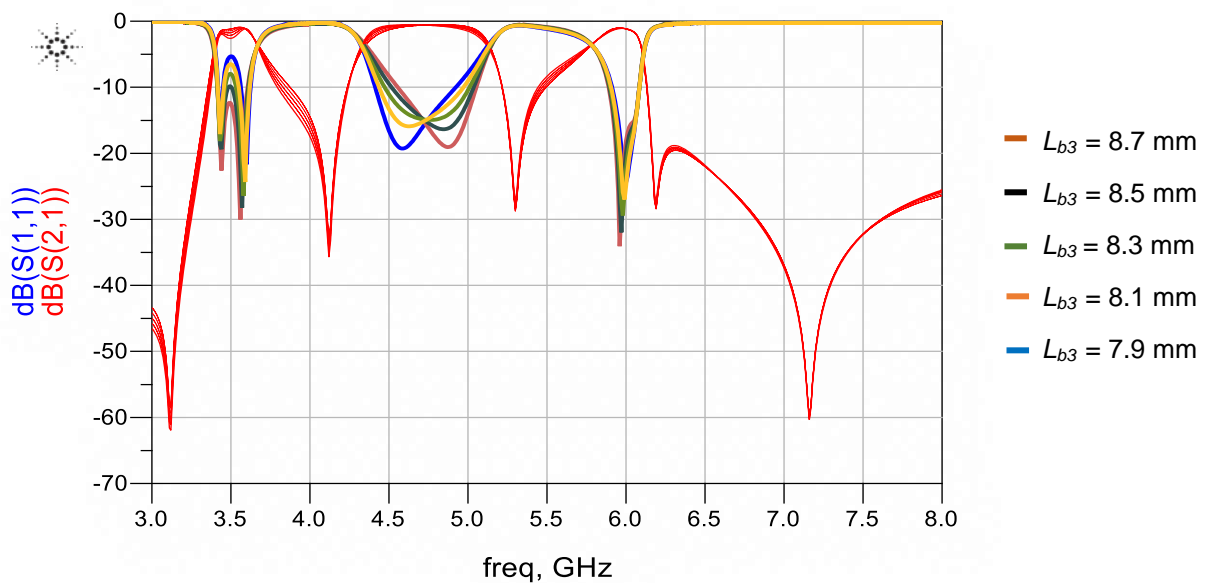


Fig. 7.29. Frequency response of the filter as a function of resonator length (L_{b3}).

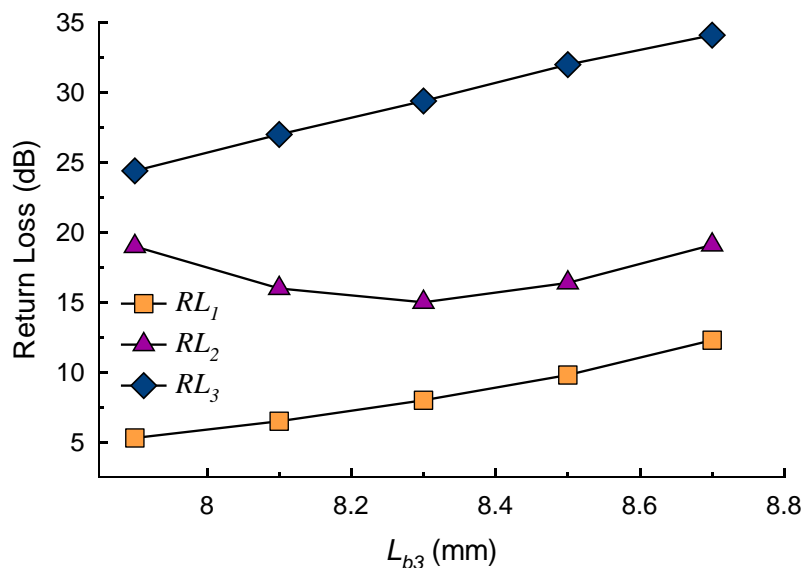
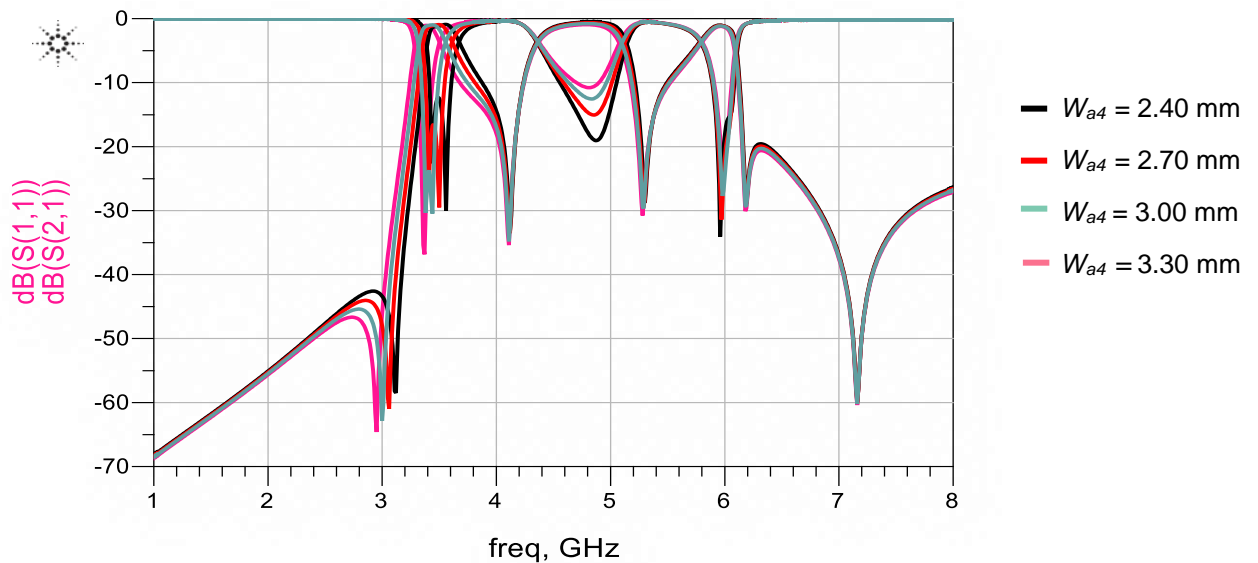


Fig. 7.30. Effect on the filter's return-loss as a function of resonator length (L_{b3}).

Table 7.11. Effect of coupled length (L_{b3}) on the filter's return-loss.

L_{b3} (mm)	RL ₁ (dB)	RL ₂ (dB)	RL ₃ (dB)
8.7	12.3	19.1	34.1
8.5	9.8	16.4	32.0
8.3	8.0	15.0	29.4
8.1	6.5	16.0	27.0
7.9	5.3	19.0	24.4

Fig. 7.31 shows the performance of a triple-band filter as a function of resonator width (W_{a4}). The results reveal W_{a4} essentially affects the first passband, the first transmission zero, and the return-loss of the second passband. The centre frequency of the first passband drops and the first transmission zero increase linearly as the width is reduced from 3.3 mm to 3.4 mm, as shown in Fig. 7.33; however, the return-loss declines from about 40 dB to 12 dB. The return-loss of the second and third passbands increases, as is evident in Fig. 7.32. The results are also tabulated in Table 7.12.

Fig. 7.31. Frequency response of the filter as a function of resonator width (W_{a4}).

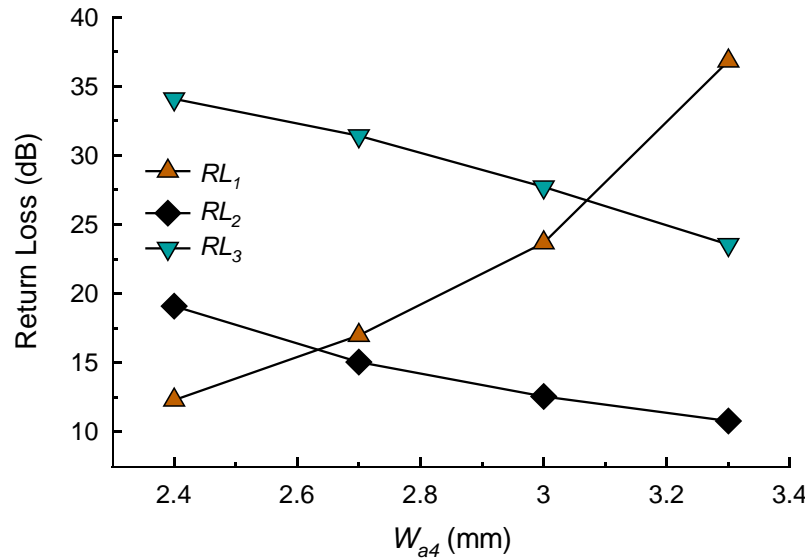


Fig. 7.32. Effect on the filter's return-loss as a function of resonator width (W_{a4}).

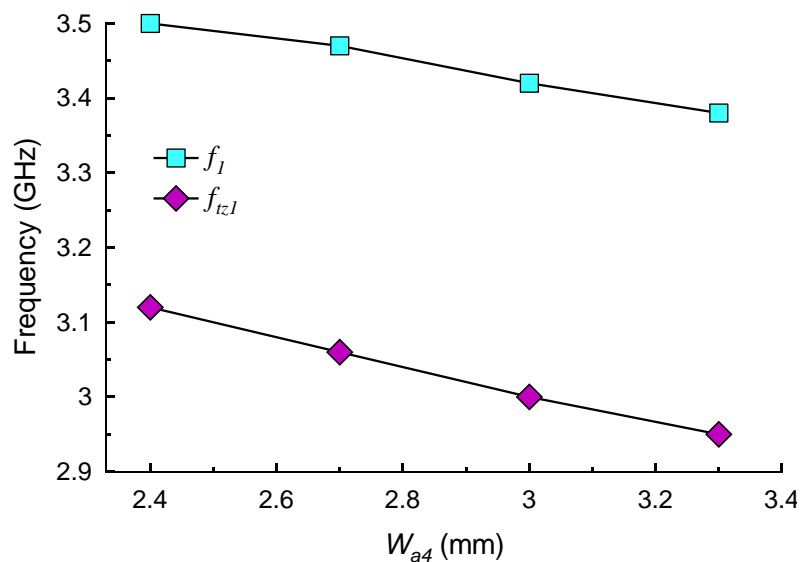


Fig. 7.33. Effect on the first passband's centre frequency and transmission zero as a function of resonator width (W_{a4}).

Table 7.12. Effect of resonator width (W_{a4}) on the filter's return-loss, transmission zero and centre frequency.

W_{a4} (mm)	RL_1 (dB)	RL_2 (dB)	RL_3 (dB)	f_1 (GHz)	f_{tz1} (GHz)
2.40	12.3	19.1	34.1	3.50	3.12
2.70	16.98	15.06	31.42	3.47	3.06
3.00	23.68	12.56	27.72	3.42	3.00
3.30	36.83	10.79	23.55	3.38	2.95

The simulated S_{21} response as a function of resonator length (L_a) is shown in Figs. 7.34 - 7.36, and tabulated in Table 7.13. It is observed that by increasing L_a from 4.01 mm to 4.61 mm, we can tune (i) the transmission zeros f_{tz3} by 5% and f_{tz5} by 7%; and (ii) the centre frequency by 7%. However, the return-loss of third passband degrades severely from 34.1 dB to 3.4 dB. It was also noticed the resonator width (W_a) and (W_{a1}) only have a minor effect on return-loss of third passband and transmission zeros f_{tz5} (GHz). In addition, the resonator length (L_{a1}) also has similar influence on the filter's performance.

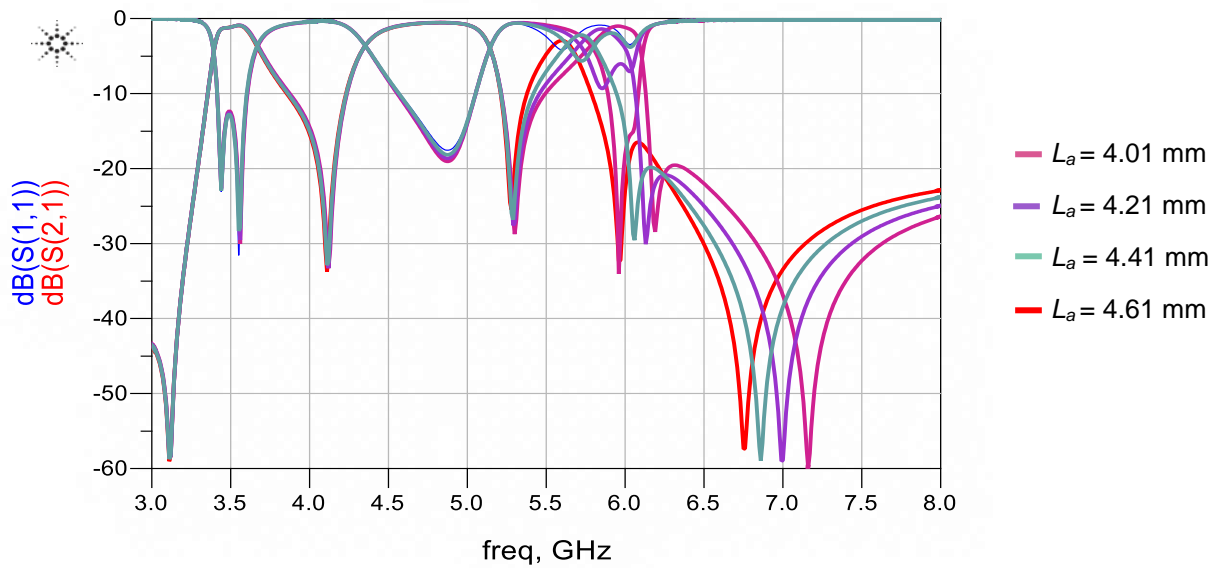


Fig. 7.34. Frequency response of the filter as a function of resonator length (L_a).

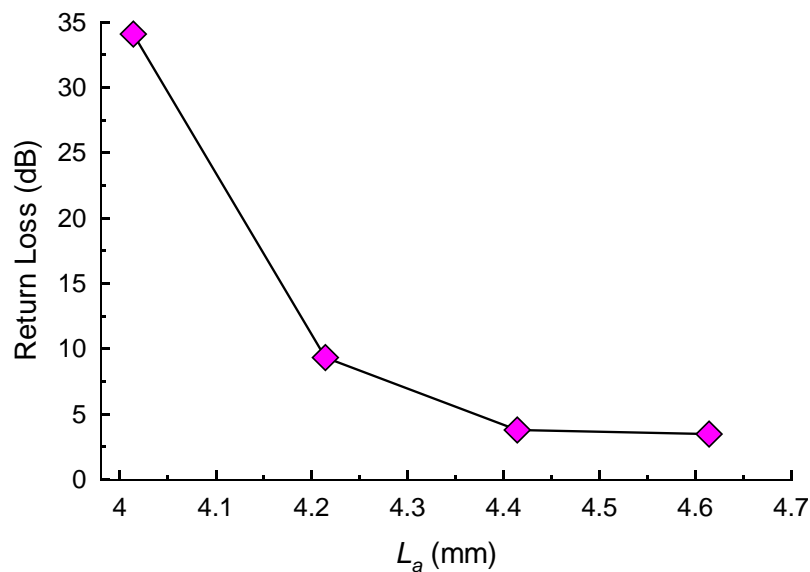


Fig. 7.35. Effect on the filter's return-loss as a function of resonator length (L_a).

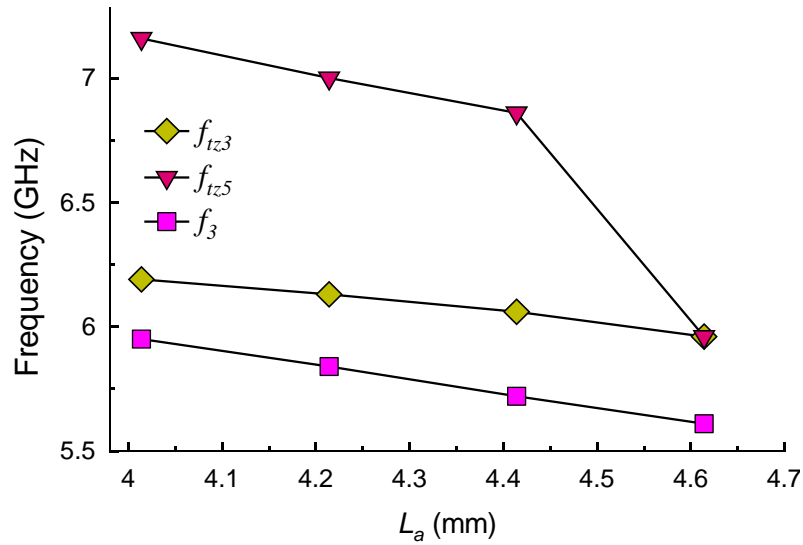


Fig. 7.36. Effect on the filter transmission zeros and centre frequency as a function of resonator length (L_a).

Table 7.13. Effect of resonator length (L_a) on the filter's return-loss, transmission zeros and centre frequency.

L_a (mm)	f_{tz3} (GHz)	f_{tz5} (GHz)	f_3 (GHz)	RL ₃ (dB)
4.014	6.19	7.16	5.95	34.1
4.214	6.13	7.00	5.84	9.33
4.414	6.06	6.86	5.72	3.79
4.614	5.96	5.96	5.61	3.48

The effect of resonator length (L_{10}) on the filter's response is shown in Figs. 7.37-7.39, and tabulated in Table 7.14. These results show L_{10} influences the transmission zeros f_{tz2} , f_{tz3} , and f_{tz4} . It is evident the third and fourth transmission zeros vary at a greater extent than the second transmission zero (f_{tz2}). The results also show centre frequency of second and third passbands can be varied. The return-loss of the three passbands are also affected by the resonator length as shown in Fig. 7.39. In fact, the return-loss of the first and third passband improve with reduction in L_{10} but the converse is true for the second passband.

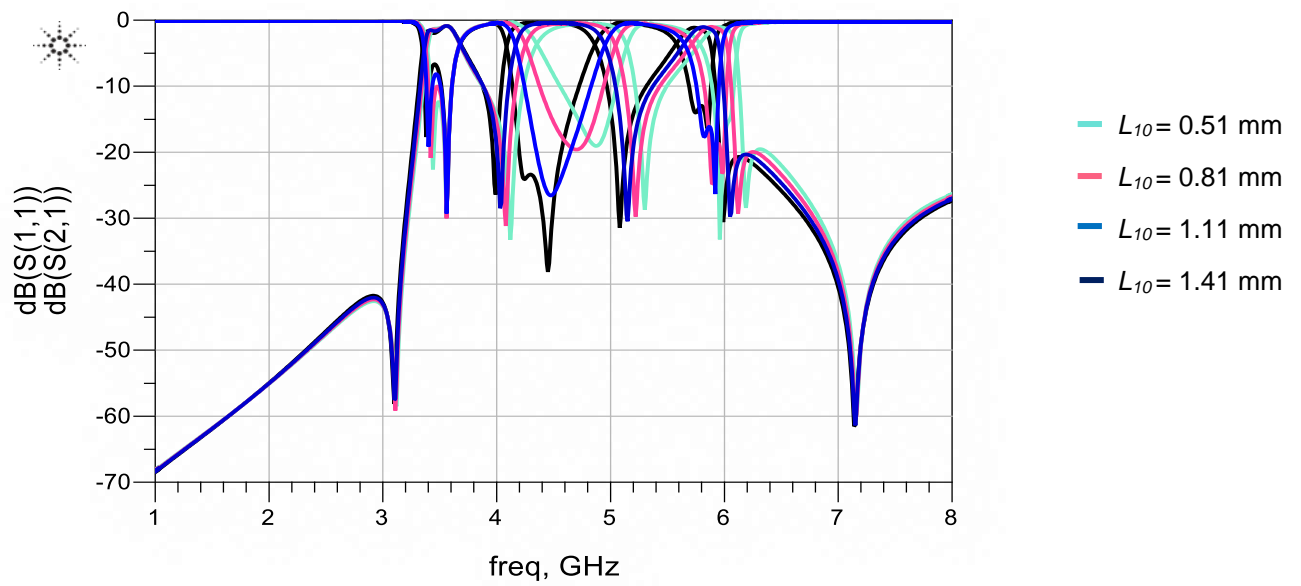


Fig. 7.37. Frequency response of the filter as a function of resonator length (L_{10}).

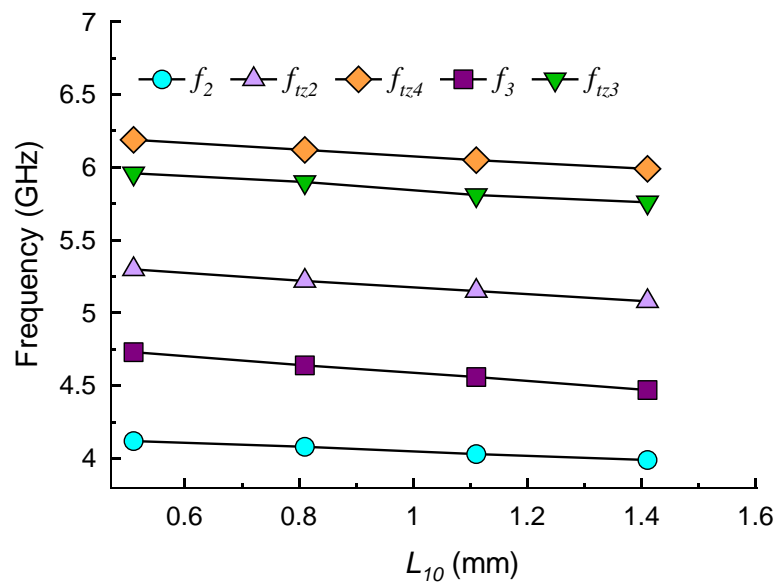


Fig. 7.38. Effect on the filter transmission zeros and centre frequencies as a function of resonator length (L_{10}).

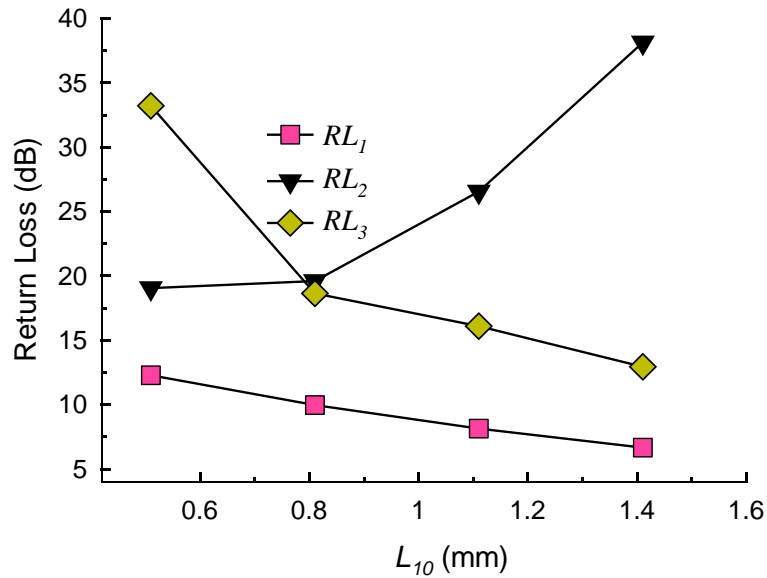


Fig. 7.39. Effect on the filter's return-loss as a function of resonator length (L_{10}).

Table 7.14. Effect of resonator length (L_{10}) on the filter's return-loss, transmission zeros and centre frequencies.

L_{10} (mm)	f_{tz2} (GHz)	f_{tz3} (GHz)	f_{tz4} (GHz)	f_1 (GHz)	f_2 (GHz)	f_3 (GHz)	RL ₁ (dB)	RL ₂ (dB)	RL ₃ (dB)
0.51	4.12	5.3	6.19	3.5	4.73	5.96	12.29	19.06	33.21
0.81	4.08	5.22	6.12	3.49	4.64	5.9	9.98	19.61	18.64
1.11	4.03	5.15	6.05	3.47	4.56	5.81	8.15	26.55	16.10
1.41	3.99	5.08	5.99	3.46	4.47	5.76	6.66	38.14	12.94

The frequency response of triple-band filter with variation in resonator length (L_5) is shown in Figs. 7.40-7.42, as well as given in Table 7.15. Frequency response shows that all transmission zeros except transmission zero (f_{tz5}), return-loss and the centre frequency of three bands can be adjusted as the resonator length is varied from 5.68 mm to 5.58 mm. Transmission zero (f_{tz2}) shows a change of about 8% and centre frequency (f_2) shifts down in frequency by 7%. Fig. 7.42 shows as the length L_5 is increased the return-loss of first and third passbands decline however the change in the return-loss of the second passband is very small.

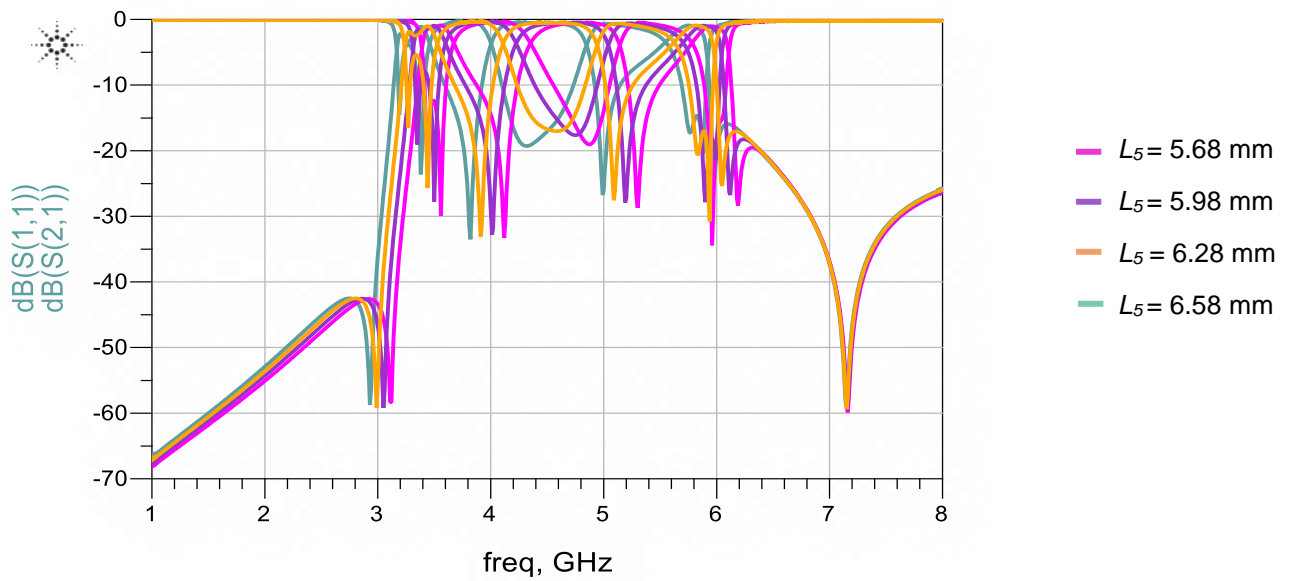


Fig. 7.40. Frequency response of the filter as a function of resonator length (L_5).

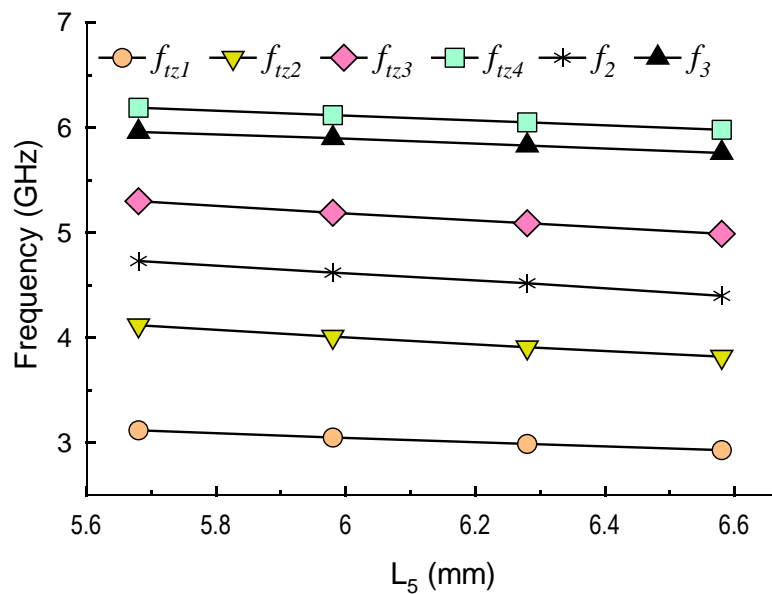


Fig. 7.41. Effect on the filter's transmission zeros and centre frequencies as a function of resonator length (L_5).

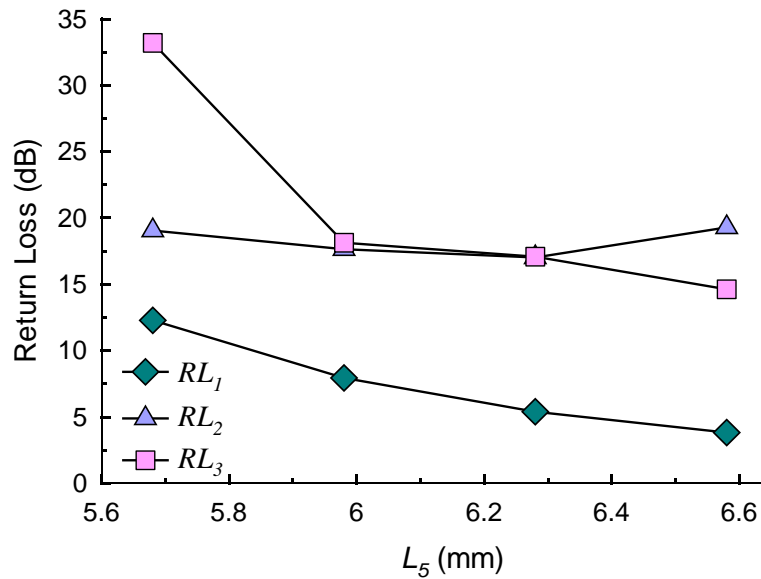


Fig. 7.42. Effect on the filter's return-loss as a function of resonator length (L_5).

Table 7.15. Effect of resonator length (L_5) on the filter's return-loss, transmission zeros and centre frequencies.

L_5 (mm)	f_{tz1} (GHz)	f_{tz2} (GHz)	f_{tz3} (GHz)	f_{tz4} (GHz)	f_1 (GHz)	f_2 (GHz)	f_3 (GHz)	RL ₁ (dB)	RL ₂ (dB)	RL ₃ (dB)
5.68	3.12	4.12	5.30	6.19	3.5	4.73	5.96	12.29	19.06	33.21
5.98	3.05	4.01	5.19	6.12	3.41	4.62	5.90	7.94	17.65	18.14
6.28	2.99	3.91	5.09	6.05	3.34	4.52	5.83	5.40	17.02	17.08
6.58	2.93	3.82	4.99	5.98	3.39	4.40	5.76	3.83	19.29	14.63

Figs. 7.43-7.45 show how the resonator length (L_6) affects the characteristics of filter's passbands. As the length is reduced from 2.07 mm to 0.87 mm, the change in the return-loss of passbands one and three are very small, however the return-loss of passband one improves from 19.06 dB to 25.68 dB. Fig. 7.44 show L_6 varies the passband's centre frequency and transmission zeros is linear fashion but the change is small.

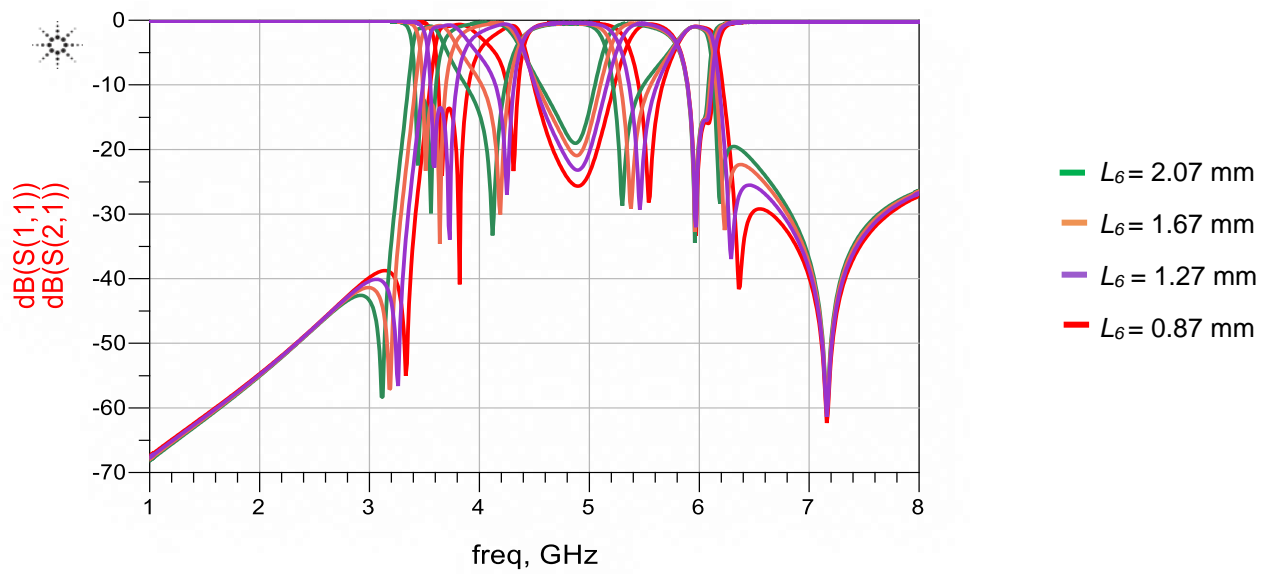


Fig. 7.43. Frequency response of the filter as a function of resonator length (L_6).

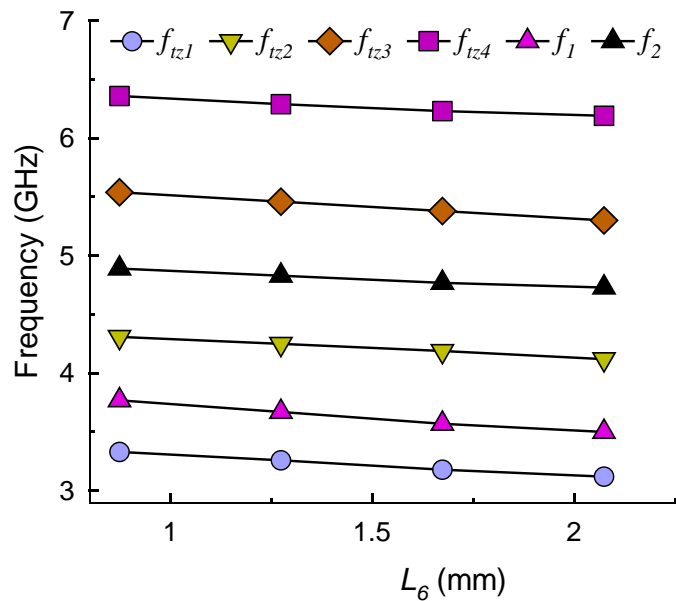


Fig. 7.44. Effect on the filter's transmission zeros and centre frequencies as a function of resonator length (L_6).

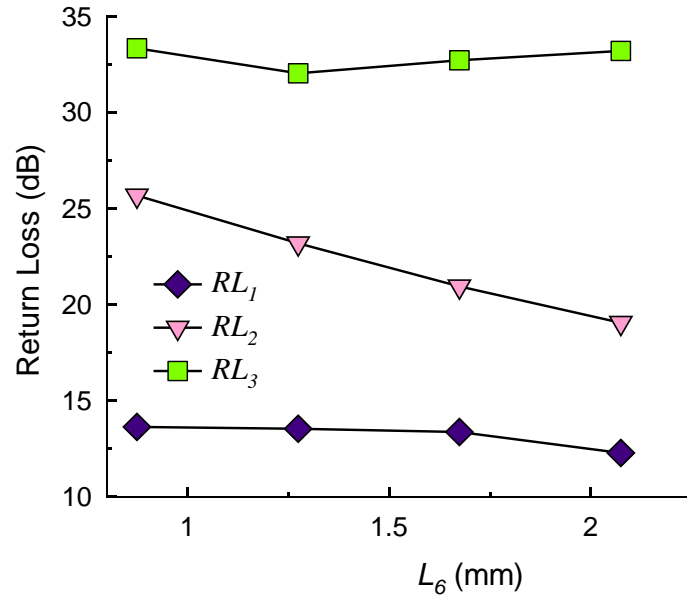


Fig. 7.45. Effect on the filter's return-loss as a function of resonator length (L_6).

Table 7.16. Effect of resonator length (L_6) on the filter's return-loss, transmission zeros and centre frequencies.

L_6 (mm)	f_{tz1} (GHz)	f_{tz2} (GHz)	f_{tz3} (GHz)	f_{tz4} (GHz)	f_1 (GHz)	f_2 (GHz)	f_3 (GHz)	RL_1 (dB)	RL_2 (dB)	RL_3 (dB)
2.074	3.12	4.12	5.30	6.19	3.50	4.73	5.96	12.29	19.06	33.21
1.674	3.18	4.19	5.38	6.23	3.57	4.77	5.98	13.38	20.95	32.72
1.274	3.26	4.25	5.46	6.29	3.67	4.83	6.00	13.55	23.20	32.05
0.874	3.33	4.31	5.54	6.36	3.77	4.89	6.02	13.64	25.68	33.35

The effect of resonator length (L_9) on the filter's response are shown in Figs. 7.46-7.48, and tabulated in Table 7.17. The results show L_9 mainly affects the transmission zero (f_{tz1}) of the first passband, and the return-loss of the three passbands. Fig. 7.47 show as the length is increased from 1.7 mm to 2.6 mm the centre frequency and transmission zero of the first passband decline linearly. Fig. 7.48 shows that as the length is increased the return-loss second and third passbands reduces whereas the return-loss of the first passband increases and then decreases with an optimum of about 22.5 dB at a length of 2.2 mm.

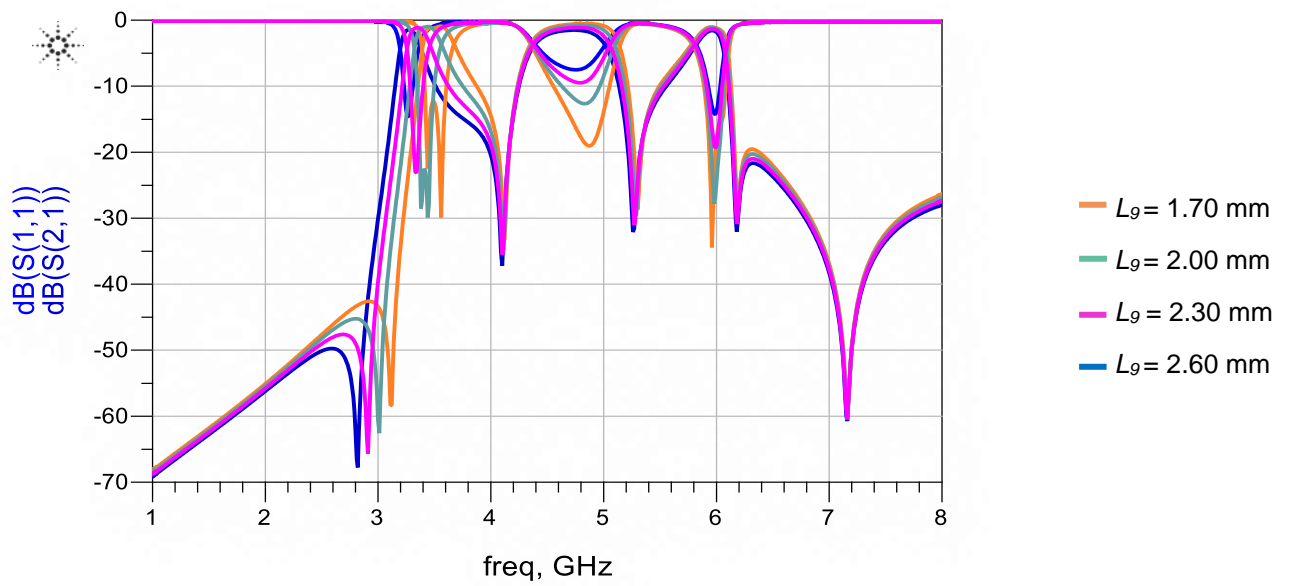


Fig. 7.46. Frequency response of the filter as a function of resonator length (L_g).

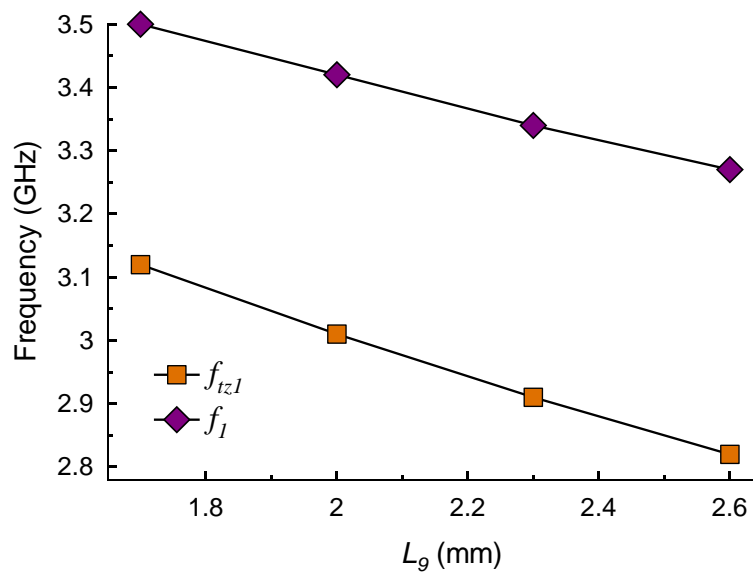


Fig. 7.47. Effect on the filter's transmission zero and centre frequency as a function of resonator length (L_g).

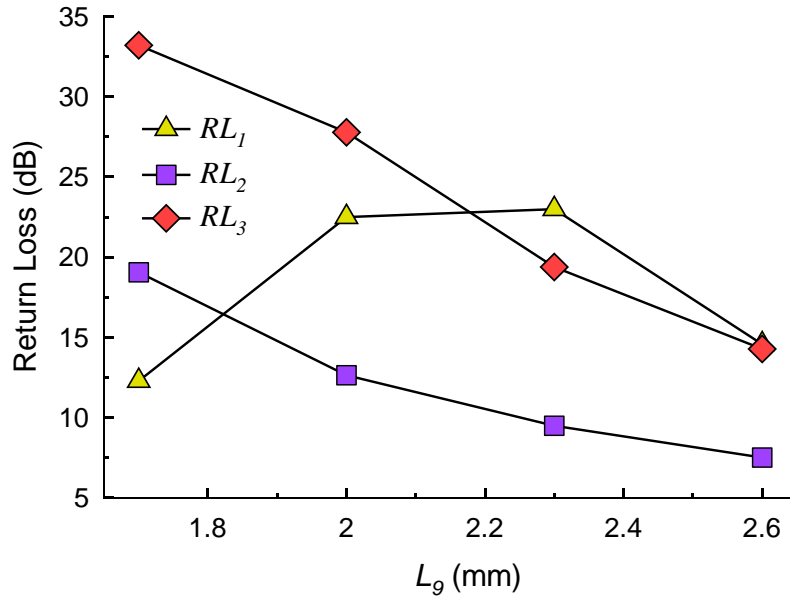


Fig. 7.48. Effect on the filter's return-loss as a function of resonator length (L_9).

Table 7.17. Effect of resonator length (L_9) on filter's return-losses, transmission zero and centre frequency.

L_9 (mm)	f_{tz1} (GHz)	f_l (GHz)	RL ₁ (dB)	RL ₂ (dB)	RL ₃ (dB)
1.70	3.12	3.50	12.29	19.06	33.21
2.00	3.01	3.42	22.50	12.65	27.79
2.30	2.91	3.34	22.99	9.49	19.39
2.60	2.82	3.27	14.58	7.52	14.28

Fig. 7.49 shows the frequency response of the filter as a function of resonator length (L_8), which only affects the passband of the first response. The return-loss first declines with increase in L_8 from 2.71 mm to 3 mm, and then increases again for larger lengths than 3 mm, as shown in Fig. 7.50. Fig. 7.51 shows the centre frequency of the first passband declines in a linear fashion with increase in L_8 from 2.71 mm to 3.61 mm. These results are also tabulated in Table 7.18.

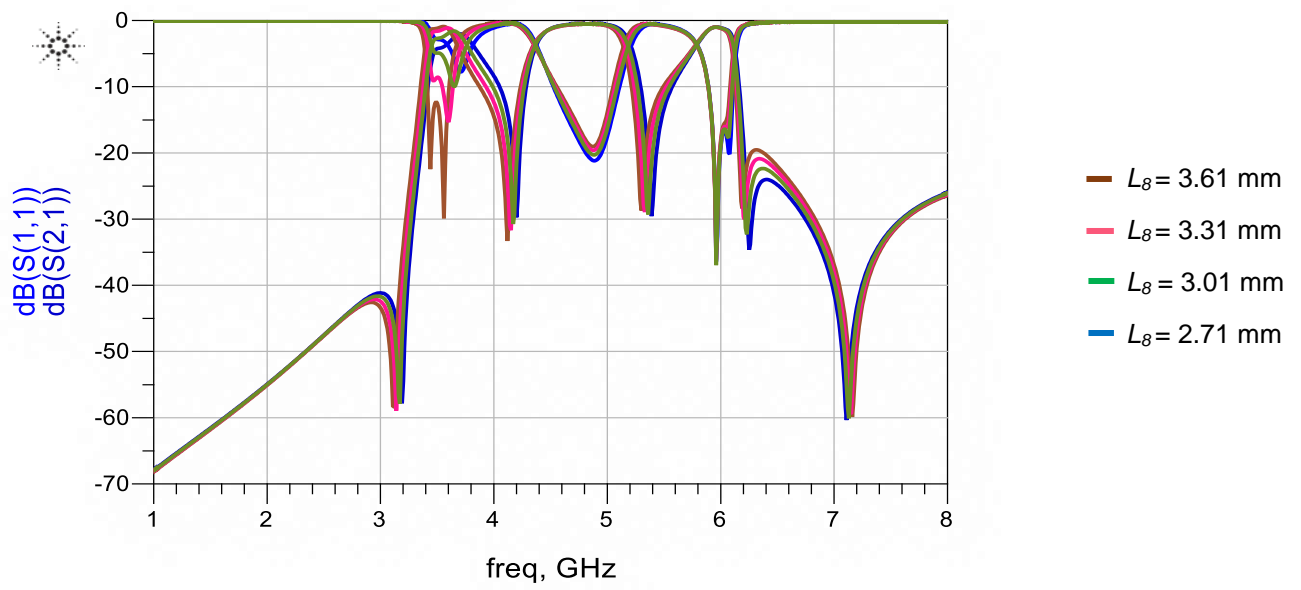


Fig. 7.49. Frequency response of the filter as a function of resonator length (L_δ).

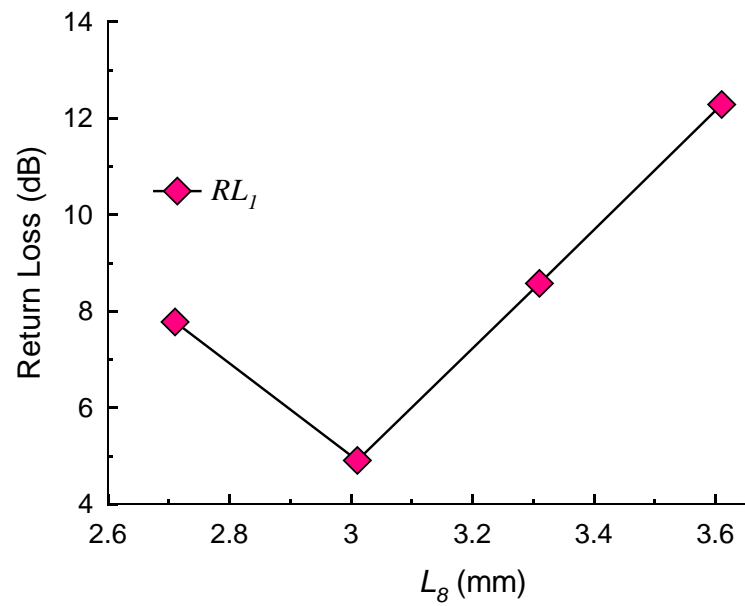


Fig. 7.50. Effect on the filter return loss as a function of resonator length (L_δ).

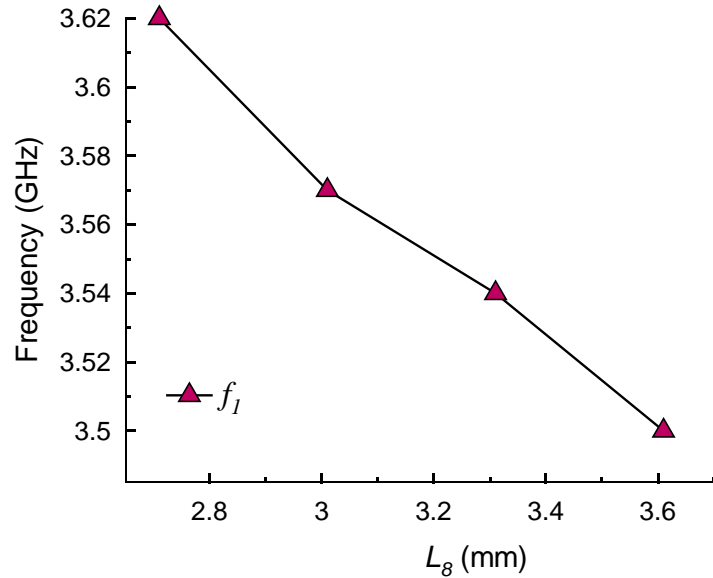


Fig. 7.51. Effect on the filter resonant frequency as a function of resonator length (L_δ).

Table 7.18. Effect of resonator length (L_δ) on the filter's transmission zero and centre frequency.

L_δ (mm)	f_1 (GHz)	RL_1 (dB)
3.61	3.50	12.29
3.31	3.54	8.58
3.01	3.57	4.91
2.71	3.62	7.78

The effect of resonator length (L_3) on the filter's performance is shown in Figs. 7.52-7.54, as well as tabulated in Table 7.19. It is evident from Fig. 7.53 that the centre frequencies of the second and third passbands, and third and fourth transmission zeros reduce marginally with increase in L_3 . Fig. 7.54 shows the return-loss of the first passband declines with increase in L_3 but the passband of the second passband increases. In the case of the third passband, the return-loss first falls with increase in L_3 then rises again for lengths greater than 2.16 mm.

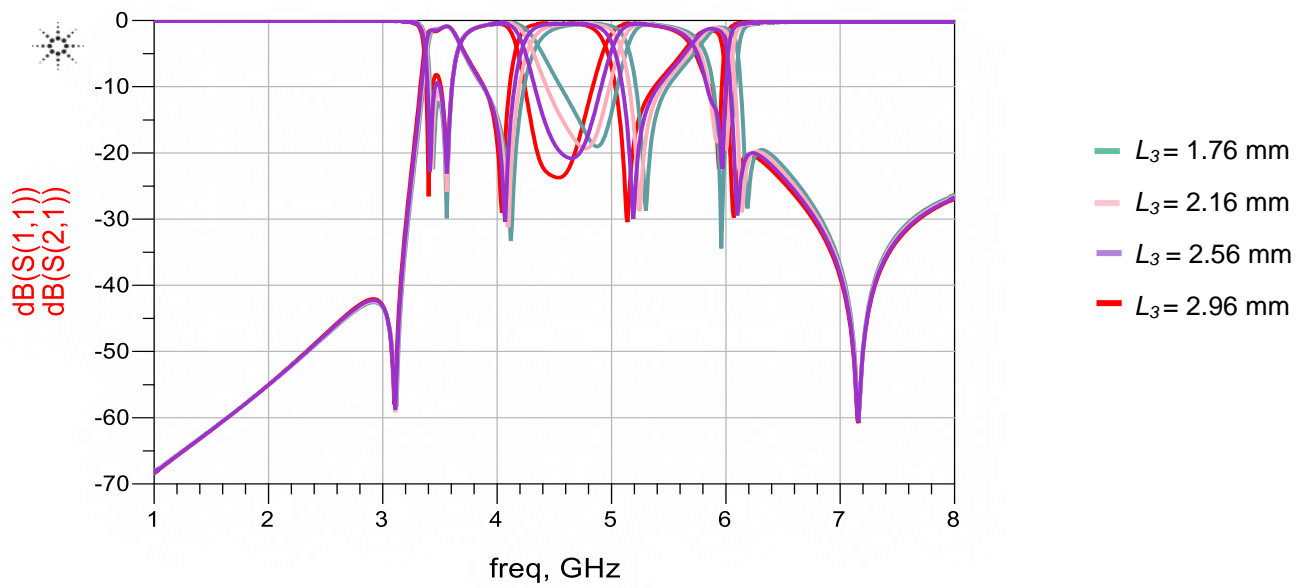


Fig. 7.52. Frequency response of the filter as a function of resonator length (L_3).

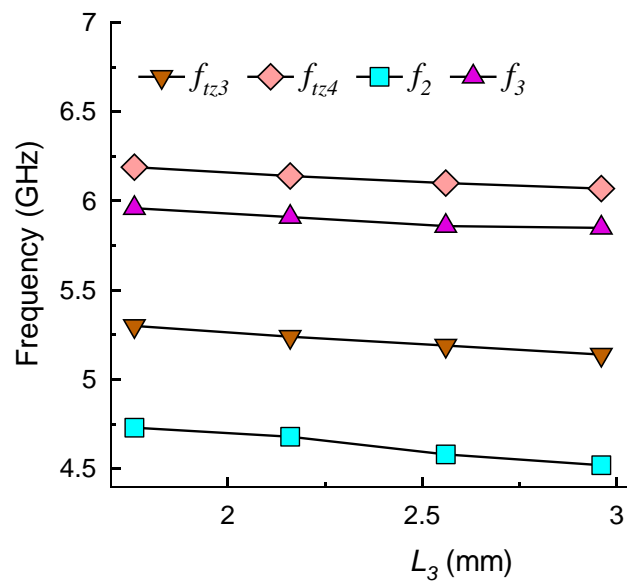


Fig. 7.53. Effect on the filter's transmission zeros and centre frequencies as a function of resonator length (L_3).

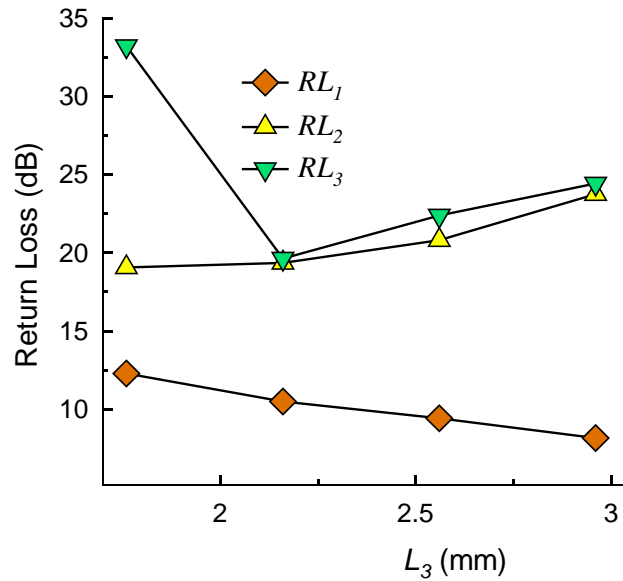


Fig. 7.54. Effect on the filter's return-loss as a function of resonator length (L_3).

Table 7.19. Effect of resonator length (L_3) on the filter's return-loss, transmission zero and centre frequencies.

L_3 (mm)	f_{tz3} (GHz)	f_{tz4} (GHz)	f_2 (GHz)	f_3 (GHz)	RL_1 (dB)	RL_2 (dB)	RL_3 (dB)
1.76	5.30	6.19	4.73	5.96	12.29	19.06	33.21
2.16	5.24	6.14	4.68	5.91	10.50	19.35	19.63
2.56	5.19	6.10	4.58	5.86	9.42	20.81	22.38
2.96	5.14	6.07	4.52	5.85	8.16	23.74	24.42

The influence of resonator length (L_2) on the filter's response is shown in Figs. 7.55-7.57, and tabulated in Table 7.20. The results show transmission zeros (f_{tz2} , f_{tz3} and f_{tz4}), centre frequencies (f_2 and f_3) and return-loss of all three passbands are affected by L_2 . In fact, Fig. 7.56 show the transmission zeros and centre frequencies are marginally affected by L_2 . Fig. 7.57 shows the return-loss of the first and second passbands decline with increase in L_2 but the return-loss of the third passband improves greatly.

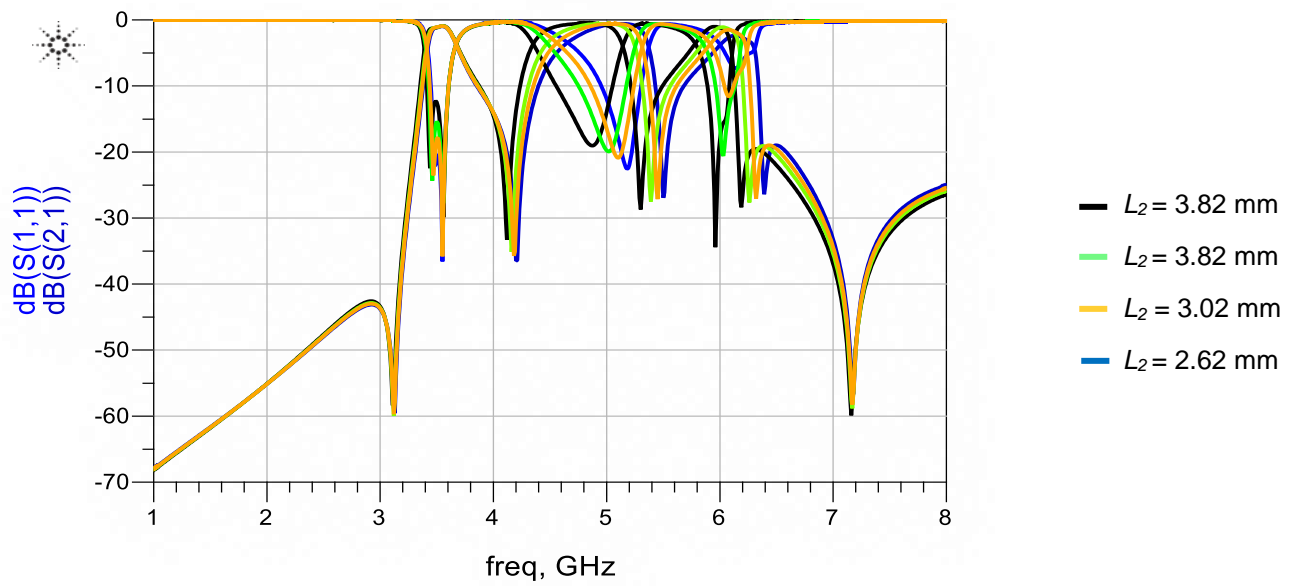


Fig. 7.55. Frequency response of the filter as a function of resonator length (L_2).

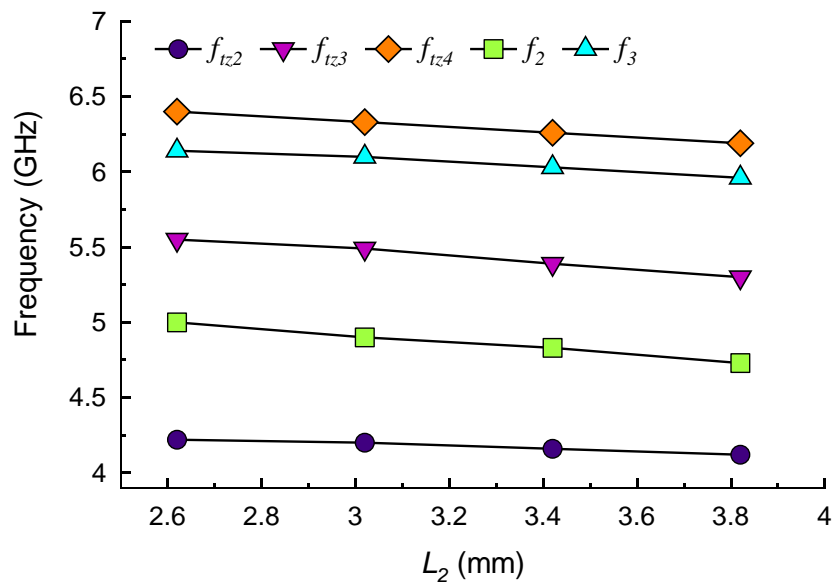


Fig. 7.56. Effect on the filter's transmission zeros and centre frequencies as a function of resonator length (L_2).

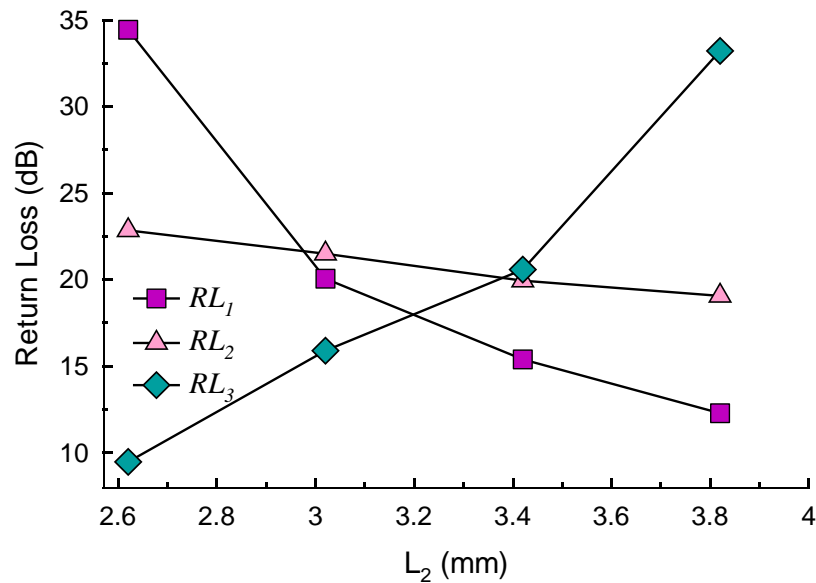


Fig. 7.57. Effect on the filter's return-loss as a function of resonator length (L_2).

Table 7.20. Effect of resonator length (L_2) on the filter's return-loss, transmission zero and centre frequencies.

L_2 (mm)	f_{tz2} (GHz)	f_{tz3} (GHz)	f_{tz4} (GHz)	f_2 (GHz)	f_3 (GHz)	RL ₁ (dB)	RL ₂ (dB)	RL ₃ (dB)
3.82	4.12	5.30	6.19	4.73	5.96	12.29	19.06	33.21
3.42	4.16	5.39	6.26	4.83	6.03	15.39	19.95	20.59
3.02	4.20	5.49	6.33	4.90	6.10	20.06	21.50	15.90
2.62	4.22	5.55	6.40	5.00	6.14	34.44	22.85	9.48

7.3 Summary

In this chapter two miniature microstrip dual-band and triple-band BPFs were proposed. Detailed parametric studies were conducted to fully understand how the geometric parameters affect the filters. The filters were optimised and fabricated. Measured results were used to validate their performance. In the case of the dual-band filter, it has passbands centred at 4.66 GHz and 5.5 GHz with 3-dB fractional bandwidth of 13% and 12%, respectively. The insertion-loss at the centre frequencies are 1.02 and 0.8 dB, and the return-loss better than 13 and 21 dB, respectively. Study shows even and odd resonant modes and three transmission zeros can be tuned independently to some extent without degrading the passbands. In the case of the triple-band filter, it had centre frequencies of at 3.4 GHz, 4.6 GHz and 5.7 GHz with 3-dB fractional bandwidths of 5.7%, 13% and 5.6%, respectively. The insertion-loss at the centre frequencies are 1.5 dB, 0.8 dB and 2.0 dB, and their corresponding return-loss better than 18 dB, 16 dB and 11 dB, respectively. The

five transmission zeros are located close to the passband edges resulted in sharp selectivity and a good band-to-band isolation.

References

1. Advances in Multi-Band Microstrip Filters, by Vesna Crnojević-Bengin.
2. Sovuthy Cheab, Peng Wen Wong, and Xiao Yan Chew, "Parallel connected dual-mode filter," *IEEE Microwave and Wireless Components Letters*, vol. 25, no. 9, Sept 2015, pp. 582 - 584
3. Jin Xu, Wen Wu, and Gao Wei, "Compact multi-band bandpass filters with mixed electric and magnetic coupling using multiple-mode resonator," *IEEE Transaction on Microwave Theory and Techniques*, vol. 63, no. 12, Dec 2015, pp. 3909 - 3919
4. Zhi-Chong Zhang, Qing-Xin Chu, and Fu-Chang Chen, "Compact Dual-band bandpass filters using open-/short-circuited $\lambda/4$ stub-loaded resonators," *IEEE Microwave and Wireless Components Letters*, vol. 25, no. 10, Oct. 2015, pp. 657 - 659
5. Chin, K.-S., Yeh, J.-H., "Dual-wideband bandpass filter using short circuited stepped-impedance resonators," *IEEE Microw. Wirel. Compon. Lett.*, 2009, vol. 19, no. 3, pp. 155–157
6. Mo, Y., Song, K.-J., Tao, P., and Fan, Y., "Miniaturized dual-band bandpass filter using modified SIR," *Electron. Letter*, 2013, vol. 49, no. 14, pp. 888–890.
7. Wenqing He; Zhewang Ma; Chun-Ping Chen; Tetsuo Anada; Yoshio Kobayashi, "A novel dual-band bandpass filter using microstrip stub-loaded two-mode resonators with source and load coupling," *Microwave Conference, APMC 2008*, pp. 1 - 4
8. Dong Chen, Lei Zhu, Chonghu Cheng, "A novel dual band bandpass filter with closely spaced passbands," *IEEE Microwave & Wireless Compon. Lett.*, vol. 24, no. 1, Jan. 2014, pp. 38 - 40
9. Yatao Peng, Lijun Zhang, Jun Fu, Yudong Wang and Yongqing Leng, "Compact Dual-band bandpass filter using coupled lines multimode resonators," *IEEE Microwave and wireless Components Letters*, vol. 25, no. 4, April 2015, pp. 235 - 237
10. Feng Wei, Pei-Yuan Qin, Jay Guo, "Compact Balance dual and Tri-band BPFs based on coupled complementary split-ring resonators (C-CSRR)," *IEEE Microwave and wireless Components Letters*, vol. 26, no. 2, Feb. 2016, pp. 107 - 109
11. Zhi-Chong Zhang, Qing-Xin Chu, and Fu-Chang Chen, "Compact dual-band bandpass filters using open/short-circuited stub-loaded $\lambda/4$ resonators," *IEEE Microwave and wireless Components Letters*, vol. 25, no. 10, Oct. 2015, pp. 657 - 659

Conclusion and Future Work

8.0 Conclusion

Planar filters play an irreplaceable role in virtually any type of RF/Microwave system today. However, modern wireless communications systems demand compact wideband filters with sharp passband skirts, low insertion-loss and high return-loss properties, and a wide stopband with high rejection level. It is necessary to have highly sharp passband skirts to efficiently utilise the EM spectrum, and a wide stopband is necessary to suppress/eliminate undesired spurious responses that would otherwise interfere with other systems. Planar filters implemented with printed circuit technology are particularly attractive as they are easy to fabricate. However, conventional filter designs that are based on distributed components usually suffer from unwanted spurious responses due to their higher order resonances. The occurrence of out-of-band spurious responses can degrade the system performance. In addition, despite of many advances, miniaturization of microstrip filters still remains challenging because their dimensions are determined by the wavelength.

In chapter three a quasi-elliptic function bandpass filter was presented. The filter structure consists of two mixed (electric and magnetic) coupled open-ring resonators where the input/output feed-lines are inductively loaded with a pair of open stub in the shape of spirals. The open stubs were spiralled to keep the structure compact in size. The open stubs were used to suppress harmonics generated by the filter across a wide bandwidth on both sides of the passband thus ensuring broad harmonic rejection characteristics are achieved without any degradation in the filter's characteristics. Further improvement in frequency-selectivity and stopband were achieved by interdigitally coupling the resonators to the input/output feed-lines. The interdigital feed-lines create a pair of transmission zeros above and below the filter's passband to provide highly sharp roll-off and steep skirt with high rejection. It was shown the coupling scheme employed controlled the filter's 3-dB bandwidth. With the proposed filter structure, the minimum and maximum 3-dB fractional bandwidth achievable was 5.52% and 17%, respectively. The filter can be easily configured for narrowband and wideband applications.

In chapter four, various coupling schemes were initially theoretically analysed. Based on this analysis two filter structures were explored. The first design was a highly compact where the resonant structure was parallel coupled to the input/output feed-lines using high impedance lines. The feed-lines were loaded with inductive stubs to eliminate/spurious

higher order harmonics and spurious generated by the filter. Parametric study was carried out to understand how the geometric parameters of the filter structure affect its response. The second filter investigated was to realise a wide passband which was achieved by using coupled open-loop resonators that were loaded with an open-circuited inductive stub, and where the feed-lines were interdigitally coupled to the resonators. It is shown the 3-dB fractional bandwidth of the filter can be controlled by manipulating its geometric parameters from 9.8% to 16.8%. Both filters designs investigated are: (i) compact in size when fabricated on a low dielectric constant substrate; (ii) possess a sharp quasi-elliptic function bandpass response with low passband insertion-loss; and exhibits a wide stopband performance. These results were validated with measurements.

In chapter five, a novel wideband quasi-elliptic function bandpass filter structure was analyzed that exhibits a sharper roll-off and steep skirt selectivity. The quasi-elliptic function filter comprises open-loop resonators that are coupled to each other using a stub loaded resonator (SLR), which was analyzed in odd and even-modes. The result of this analysis reveals that the length of SLR can be reduced by increasing the impedance of the stub in relation to the resonator, i.e. reducing the impedance ratio. Also, the spacing between the fundamental and spurious responses generated by the SLR can be increased by reducing the impedance ratio. The filter was shown to achieve a 3-dB fractional bandwidth of 23%, which was verified through measurement.

This chapter presented a miniature microstrip UWB and wideband BPF designs. Multimode resonator structure was used to design a UWB bandpass filter, where open stubs were employed to generate even and odd modes to provide UWB performance. Analysis on the proposed structure revealed that even mode frequencies can be mainly controlled by adjusting the dimensions of the central loaded stepped impedance stub, and the odd mode frequencies can be affected by the dimensions of the horizontal resonator and the length of the interdigital coupled lines. The compact filter exhibited a sharp quasi-elliptic function bandpass response with low passband insertion-loss, and ultra-wide stopband performance. The design of the wideband filter with a sharp roll off skirt involved exciting four resonant modes, and two transmission zeros at the cut off frequencies enabled. Analysis shows that both even and odd modes can be relocated within the passband by tuning the geometric parameters of the proposed structure. The measured results were used to validate the UWB and wideband filters.

In chapter seven two miniature microstrip dual and triple-band BPF filters were proposed. A detailed parametric study on the dual-band filter structure was undertaken to fully understand how the filter's performance was influenced. Study revealed that even and odd resonant modes and three transmission zeros can be tuned independently to some

extent without degrading the filter's two passbands measured centred at 4.66 GHz and 5.5 GHz with 3-dB fractional bandwidth of 13% and 12%, respectively. The insertion-loss at the two centre frequencies are 1.02 and 0.8 dB, and return-loss better than 13 and 21 dB. The quasi elliptic triple-bandpass filter was realised by planting five transmission zeros to yield sharp frequency-selectivity and a good band-to-band isolation. Parametric study shows the characteristics of triple-band bandpass filter can be controlled by tuning the dimensions of the filter structure. The measured centre frequencies of the three bands are 3.4 GHz, 4.6 GHz and 5.7 GHz with 3-dB fractional bandwidths of 5.7%, 13% and 5.6%, respectively. The insertion-loss at the centre frequencies are 1.5 dB, 0.8 dB and 2.0 dB whereas the return-loss are better than 18 dB, 16 dB and 11 dB, respectively.

8.1 Future Work

In this dissertation, several compact and novel cross coupled microwave filter structures were proposed that exhibit quasi-elliptic function response and wide stopband with desirable characteristics of: (i) sharp quasi-elliptical response, (ii) low passband insertion-loss, and (iii) an extremely wide out-of-band rejection. These characteristics are normally achieved with high temperature superconductors (HTS), which are significantly larger and require cryocooler to maintain the 77 K operating temperature and cryopackaging. Hence, HTS filters are expensive to implement and maintain. The sharper skirts of the proposed filters minimize the signals lost due to crossover interference and also give increased bandwidth which translates into providing greater system capacity by enabling more channels. The filters developed are much smaller than conventional filters, which facilitates miniaturization of RF/microwave transceivers. The filter structures were theoretically modeled and analyzed using advanced electromagnetic simulation tools. Performance of the filters was validated with compared results. To extend the work further the following can be explored:

1. Electronic tuning to enable remote reconfiguration of the filter specifications without degrading the passband and stopband performance. This should enable systems to be quickly and dynamically modified according to a particular application. This flexibility would save tremendous cost to the systems operator who will not need to replace transceivers every time there is amendment to the communication standards.
2. A methodology for designing any of the proposed filters needs to be developed to enable the design for a given filter specification.

3. Filter structures proposed in this thesis were designed on Arlon CuClad217LX substrate with thickness of $h = 0.794$ mm and dielectric constant $\epsilon_r = 2.17$. Latest substrate materials should be investigated to further reduce the filters loss performance resulting from ohmic and dielectric loss, reduce its size, and increase its power handling capability.

Papers Produced on the Research Work

Journals

1. "Compact Quasi-Elliptic Function Wideband Bandpass Filter with Wide Stopband Characteristics," submitted to *IEEE Transactions on Microwave Theory and Techniques*.
2. "Miniature Quasi UWB Bandpass Filter with Ultra-Wide Stopband," submitted to *IEEE Transactions on Microwave Theory and Techniques*.
3. "High-Selectivity Quasi-Elliptical Dual-Band Bandpass Filter with Wide Stopband Rejection," submitted to *IEEE Transactions on Microwave Theory and Techniques*.

Conference

"Compact Quad-Band Bandpass Filter Based on Stub-Loaded Resonators," *IEEE IMS International Conference*, Hawai'i USA, 6th of May 2017 (Accepted)